Metal-induced aggregation of β-peptides on membrane surfaces

Dissertation
zur Erlangung des mathematisch-naturwissenschaftlichen
Doktorgrades
"Doctor rerum naturalium"
der Georg-August-Universität Göttingen

im Promotionsprogramm Chemie
der Georg-August University School of Science (GAUSS)

vorgelegt von
Markus Wiegand
aus Hann. Münden

Göttingen 2022

Thesis Committee

Prof. Dr. Ulf Diederichsen	Institute of Organic und Biomolecular Chemistry, Georg-August-University Göttingen
Prof. Dr. Manuel Alcarazo	Institute of Organic und Biomolecular Chemistry, Georg-August-University Göttingen
Prof. Dr. Claudia Steinem	Institute of Organic und Biomolecular Chemistry, Georg-August-University Göttingen

Members of the Examination Commission

Reviewer	
Prof. Dr. Manuel Alcarazo	Institute of Organic und Biomolecular Chemistry, Georg-August-University Göttingen
Reviewer	
Prof. Dr. Claudia Steinem	Institute of Organic und Biomolecular Chemistry, Georg-August-University Göttingen

Additional Members of the Examination Commission

Prof. Dr. Jörg Enderlein	III. Physical Institute, Georg-August-University Göttingen
Prof. Dr. Kai Tittmann	Institute of Molecular Enzymology, Georg-August-University Göttingen
Prof. Dr. Konrad Koszinowski	Institute of Organic und Biomolecular Chemistry, Georg-August-University Göttingen
Prof. Dr. Marina Bennati	Max Planck Institute for Electron Paramagnetic Resonance, Göttingen

Day of oral examination: March 3rd, 2022

The present work was carried out from October 2015 to December 2019 at the Institute of Organic and Biomolecular Chemistry, Georg-August-University Göttingen, Germany, under the guidance and supervision of Prof. Dr. Ulf Diederichsen.

Zwei Dinge sind unendlich, das Universum und die menschliche Dummheit,
aber bei dem Universum bin ich mir noch nicht ganz sicher.

Albert Einstein

Contents

Part I

Introduction

As macromolecules, biopolymers form the backbone on which a large number of complex biological systems, such as genetic information (DNA, RNA) or a cell, are based.[1] By far the most important biopolymers are the proteins (from the Greek "proteios" "the first"), which consist of one or more relatively long chains of amino acids. Chain lengths of less than 100 amino acids are called peptides and chain lengths of more than 100 amino acids are considered proteins.[2] The sequence of amino acids is described as amino acid sequence, which forms the primary structure. Together with the peptide backbone, the primary structure forms the secondary structure, which is used to describe the conformation of individual sections of a peptide chain relative to one another. The secondary structure forms the superordinate tertiary structure, which finally forms the quaternary structure.[2] The complex form of the peptides results in the complex functions of the peptides. For example, the interaction of peptides with lipids or (lipid) membranes is responsible for many important biologic functions, including tasks such as enzyme catalysis, signal transduction, protein-protein binding, and the flexibility and stability of the membranes themselves.[3–8] Many of these processes are still difficult to understand or to study, so attempts are being made to simulate the biological system with simpler model systems. Various peptidomimetics have been developed for such an application, including the two α-helix peptides WALP and KALP.[9–11] Both peptides are well known and widely used in the literature.[12, 13] Through this model, it is possible to study the behavior of other similar α-helical peptides in a simple and controlled environment to better understand the biological processes.[9–11, 14]

The aim of this thesis was to develop the design, synthesis and analysis of artificial model systems for metal-induced aggregation at the surface of simple model membranes. With this model system the possibility should be created to mimic higher organized structures in or on a model membrane. As a basic concept for the peptides, β-peptides were chosen. β-peptides were chosen because β-peptides are proteolytically stable and form a stable secondary structure even with very short primary structures.[15, 16] In recent years, the 14-helix, which is also very well known and well characterized in the literature, has proved to be particularly remarkable. The success of the 14-helix is mainly due to the fact that the secondary structure formed is extremely stable and independent of the solvent used.[5, 17] The 14-helix is char-

acterized by its regular pattern, so each peptide turn consists of three amino acids, resulting in a three-sided secondary structure.[18, 19] The design of the peptides was chosen in such a way that the peptides have a hydrophobic character for binding to the membrane surface as well as a hydrophilic character to improve the solubility in aqueous media and at the same time to inhibit the incorporation of the peptides transmembrane. To form higher aggregates, the peptides were modified with recognition units based on BiPy derivatives. The BiPy motif is known to form complexes with a whole range of transition metals.[20, 21] This property was exploited to trigger aggregation between the peptides by targeted addition of metal ions. The interaction or complex formation is non-specific.

Based on previous work, it could be assumed that one or two membrane anchors and at least two recognition units should be present in a peptide. The design was adapted to use cholesterol as a hydrophobic moiety to bind the peptides to the membrane surface. Cholesterol is known to avoid a hydrophilic environment and prefer a hydrophobic environment as in a membrane.[22–24] Thus, it can be assumed that the peptides automatically bind to the model membrane. The other two sides were designed to be hydrophilic to prevent binding to the membrane surface, and care was generally taken to ensure that all amino acids used had a certain steric requirement to support the formation of the 14-helix. The original solid phase peptide synthesis (SPPS) was optimized in terms of time, temperature, equivalents used and synthesis sequence. In particular, the synthesis sequence could be optimized, resulting in the development of a “toolbox” that could significantly accelerate the synthesis of several similar peptides.

The behavior or properties of the peptides were analyzed by different methods. These include CD, UV/Vis, ESI-MS and FRET measurements. To confirm the secondary structure of the peptides in solution, the peptides were analyzed by CD spectroscopy. The property of metal induced aggregation was performed and evaluated in UV/Vis titrations of peptide solutions with metal salt solutions of known concentration. Furthermore, the binding of the peptides to the membrane surface was considered by FRET measurements. FRET is very advantageous in this respect, since by FRET, measurements of two components spatially close to each other can be performed.[25, 26]

Part II

Basics

In this part all the necessary background information should be given. Topics like the difference between biological and model membranes will be discussed. Furthermore, it will be described the influence of amino acids and their side chain residues on the secondary structure of peptides and therefore their influence on the function of the peptide. In which way will be the function of the peptide determined by the structure, how can be the function to structure relationship be manipulated and which consequences could this have for example on the interaction of the peptides with a membrane.

1 Biological Membranes and Model membranes and their Interaction with Peptides

1.1 Biological Membranes and Model Membranes

1.1.1 Biological Membranes

Biological membranes or cell membranes separate a cell. On the one hand, the cell is separated from the outside, e.g. from the cytoplasm or other cells, and on the other hand, the various cell components are separated from the inside. Cell membranes are not simple and rigid barriers that let nothing and no one through. Membranes are subject to constant change and alteration. Membranes are affected by biophysical processes such as diffusion, segregation or by interaction with membrane proteins. One can consider membranes as a non-equilibrium system whose components are in constant exchange due to membrane traffic. This results in a continuous change of shape and reorganization of the membrane, which can lead to the formation of "lipid domains".[27]

Our current understanding of the function and structure of a natural membrane was largely shaped in 1972 by the liquid mosaic model published by Singer and Nicolson.[28] This model combines thermodynamic considerations with experimental results and forms the idea that natural membranes adopt a mosaic-like structure (Fig. 1.1). This means that integral proteins interact with and permeate the lipid

bilayer. The interaction is characterized by hydrophobic interactions between the hydrophobic phospholipids and the hydrophobic part of the proteins.[29]

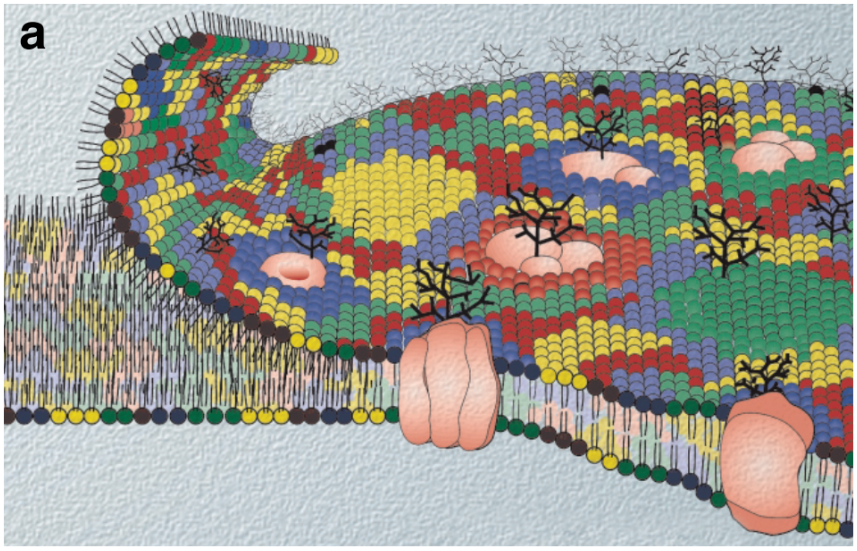

Figure 1.1: The image describes the heterogeneous composition of the cell membrane according to the liquid mosaic model of Singer and Nicolson.[29]

The image describes the heterogeneous composition of the cell membrane according to the liquid mosaic model of Singer and Nicolson. It is important that the peripheral and integral proteins can be distinguished.[28, 30] The biggest difference between the two is the amount of effort required to remove the proteins from the membrane. Peripheral proteins can be solubilized under mild conditions such as a solution with high ionic strength. These peptides can be extracted free of any lipid material and in their free state peripheral peptides are highly soluble in buffers.[28] Integral peptides are represented with more than 70 % share in a membrane. Integral peptides are clearly more difficult to separate from their environment. Thus, much more drastic conditions are required to separate integral peptides from their membrane environment. For integral peptides, detergents, bile acids, organic solvents or even protein denaturants are needed. Once the integral peptides have finally been extracted, the peptides are often not without lipid material and in their free state the integral peptides are often no longer soluble in buffers and form aggregates.[28, 31]

A strict distinction is made between these two types of peptides, because it is as-

sumed that it is primarily the integral peptides that are responsible for the structural integrity of a membrane. It has been shown that the integral peptides are not only very heterogeneously distributed in the membrane, but that the integral peptides also differ widely among themselves. Thus, the integral peptides span a wide range of different molecular masses.[32–35] Furthermore, there is no specific structure-stabilizing peptide, it seems that the heterogeneous distribution of the peptides has a large influence on the stability of the membrane.[28] The integral peptides themselves take a right-handed α-helix as a stable form in a membrane, like it was shown by Ke[36], Wallach and Zahler[37], and Lenard and Singer[38].

The description of the peripheral and integral peptides is of great importance, because the peptides in interaction with the membrane create the functional space in or at which many of the important tasks and functions of a membrane take place.[39, 40] In order to be able to predict the behavior and functioning of a membrane. Singer and Nicolson have extended their mosaic model by a "liquid" part. While, as described above, the lipid bilayer is crossed by peptides, as in a mosaic, the lipids are in their fluid state. This fluidity extends the model and allows further predictions of functions and the mechanisms behind them. Thus, it is now possible that the composition of a membrane can be partially influenced by lateral or transversal diffusion. It can occur a completely new interactions between lipids and peptides.[28]

Today, however, we know that the liquid mosaic model of Singer and Nicolson is no longer up-to-date and has been disproved by other models and hypotheses. The lipid raft concept also belongs to these models and hypotheses.[41]

Shortly after Singer and Nicolson published their paper on the liquid mosaic model, the first insights were gained that the membrane must be much more complex than first assumed by Singer and Nicolson. It was shown that the components of a membrane can be divided into those that are stable to detergents and those that are not stable to detergents.[42] This in turn led to the assumption that a (biological) membrane must be laterally inhomogeneous.[43–47] The question was now how the lateral heterogeneity can be explained. One approach is the observation that specific lipids, such as cholesterol, saturated lipids or glycolated lipids, can

form ordered structures along the membrane plane. These structures are important functional spaces and they are attracting other lipids and proteins.[48, 49] This observation is supported by biomimetic model membranes, that show that some lipids preferentially interact with certain other lipids, leading to an area-wide effect in which lateral domains are formed as a consequence of liquid-liquid phase separation.[50] Based on these observations and assumptions, the hypothesis about lipid rafts emerged.[51]

Some of the core properties of lipid rafts cannot be clearly determined to this day. For example, no clear evidence can be found for the lifetime, size or area covered by a lipid raft.[52] So far, computer models have shown that the formation of temporally and spatially restricted micro-domains are essential for the function of a membrane.[53] It is precisely the properties such as size or lifespan that make it so difficult to gather direct experimental evidence in vivo for the existence and impact of raft domains. Moreover, due to the high complexity of a biological membrane, raft-like domains have been shown to exist in addition to lipid rafts.[52, 54] Distinguishing lipid rafts and raft-like domains from each other is difficult, making it difficult to determine individual properties of the lipid rafts or raft-like domains. Due to the high complexity of a biological membrane, the question arises how the domains are distributed in the membrane and how large the area covered by the domains is. In a first assumption of the lipid raft hypothesis, it was assumed that the majority of the membrane is in a non-ordered (non-raft) state and is punctuated by ordered (raft) domains.[55, 56] This assumption has been contradicted by recent results, it seems that the ratio has been reversed. It is assumed that a large part of the membrane surface is ordered and that there may be occasional disordered regions.[57] The area ratio of both states or their lifetime is meanwhile also dependent on certain cell processes.[51, 58]

1.1.2 Model Membranes

In 1965 Bagham et. al.[59] showed for the first time that hydrated dispersions of phopholipids are able to form closed structures. The special feature of these so-called liposomes is their impermeability to trapped ions and other molecules.[60] Li-

posomes, also called vesicles, have worked their way up to become a most commonly used tool due to their outstanding properties. Thus, liposomes can[60]

1. be used for the transport of drugs, due to their size and amphiphilic character.[61]
2. enclose an aqueous phase within them due to their impenetrable lipid bilayer. With this aqueous phase, everything that has dissolved in the aqueous phase is also enclosed[60]
3. and their characteristic morphology can be specifically manipulated[60]
4. be bio-compatible[60]
5. be non-toxic[60]
6. be non-immunogenic[60]

On the other side liposomes have also their disadvantages[62]:

1. The production of liposomes is very expensive.
2. Liposomes can undergo a fusion or leakage of the enclosed drug/molecules.
3. The half-life of a liposome is very short.

Liposomes are small artificial spherical vesicles that can consist of both natural phospholipids and cholesterol. The spherical structure of the vesicles can take a size between 20 nm and more than 1000 nm. In this case, the shell of the vesicles is not limited to a single lipid bilayer, with the hydrophilic head groups facing the inner or outer aqueous phase, while the hydrophobic lipid components always face away from the aqueous phase.[63] The formation of liposomes is defined by the amphiphilic character of the lipids used. Due to the amphiphilic character, the thermodynamic driving force is such that the lipids spontaneously self-aggregate, forming spherical bilayers.[61, 64] The choice of the composition of lipids has a decisive influence on the properties of the Liposome. Thus, the “rigidity”, the “fluidity”, the size or surface charge is significantly determined by the lipids used. While unsaturated lipids increase fluidity and decrease rigidity, saturated lipids have the opposite effect.[65–67]

Besides the composition of the lipid bilayer, the size or diameter of the liposomes plays a role on the lifetime and thus on the stability of the vesicles. Based on the number of lipid bilayers, vesicles can be divided into two categories (Fig. 1.2)[68]

1. multilamellar vesicles (MLV)
2. unilamellar vesicles (GUVs, LUVs or SUVs)

MLVs differ from GUVs, LUVs and SUVs in that, like an onion, MLVs have multiple lipid bilayers that are separated from each other by the inclusion of aqueous phases. GUVs, LUV and SUV, on the other hand, often have only a single or double lipid layer to separate an aqueous phase encapsulated inside to the outside. Unilamellar vesicles are very versatile in regard of their possible ways to be used in the lab or in regard of their properties.[69, 70]

Starting from MLVs, unilamellar vesicles of different sizes can be prepared depending on the chosen preparation method. Thus, unilamellar vesicles can be divided into three distinct size classes (Fig. 1.2).

1. giant unilamellar vesicles (GUV), size: $\geq$ 1000 nm
2. large unilamellar vesicles (LUV), size: 100 - 1000 nm
3. small unilamellar vesicles (SUV), size: 20 - 40 nm

SUVs and LUVs are obtained by sonification or by extrusion, while GUVs are treated by electroformation or by hydration at temperatures above their liquid phase transition temperatures.[69, 70]

One of the most distinctive properties of all membranes, whether artificial or natural, is to form a boundary between two vesicles or between two cells in an organism. Cells or cell-like structures are separated from each other by their membranes, but a regulated exchange and communication between the individual components is of extraordinary importance. This means that a membrane separates, but must also allow or promote a certain exchange. In order to perform these important tasks, biological membranes are extremely complex and versatile in their composition.[9, 10, 14, 71] In order to better understand and investigate this complexity, one relies on the model membranes with a simpler and known composition. By simplifying

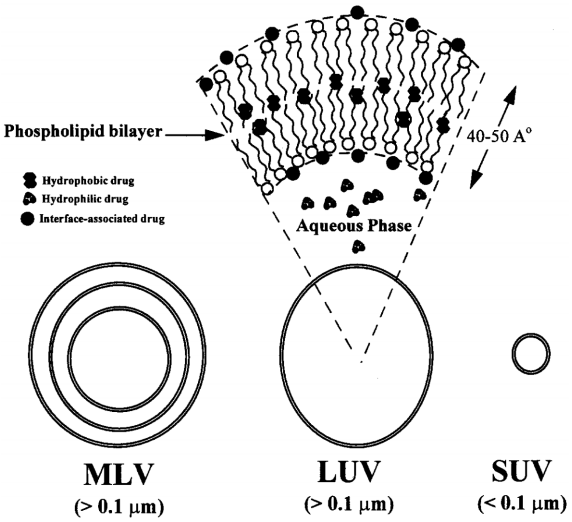

Figure 1.2: Schematic representation of MLVs, LUVs and SUVs (from left to right). MLVs are characterized by their multilamellar structure, while LUVs and SUVs are unilamellar in structure and differ in size and manufacture.[68]

the system under study, the influence of individual key components can be investigated.[71] Thus, model systems can be used to simulate some properties of biological membranes such as ion-discrimination, osmotic swelling, or the response to physiological or pharmacological stimuli. Under certain circumstances, model membranes can differentiate between different ions in their diffusion behavior.[59] For example, cations can hardly pass through the membrane, while the membrane is permeable for anions. This ion-discrimination is based on the net charge of membrane surface and can therefore manipulated on this way. Also, model membranes behave similarly to biological membranes in terms of their swelling properties as well as the tendency to be stabilized or destabilized by introducing detergents, hormones or other substances.[72] The swelling properties are primarily defined by the lipids used and their composition. Other factors are the ionic strength, ionic valence and the pH value of the surrounding solution.[73, 74]

For this work, only LUVs formed by extrusion from MLVs were used. LUVs are characterized by having a spherical structure and a strong curvature of the surface. The advantages[75] of using LUVs are

1. Homogeneous size distribution and structure.

2. They resemble the structure of a biological cell, as they are also unilamellar.
3. Inside LUVs can hold a large volume of solution or dissolved ions.
4. LUVs are easily and quickly accessible.
5. LUVs are relatively stable, as they are produced free of detergents or organic solvents.

The use or production of LUVs also has its limitations. For example, LUVs with an asymmetric lipid distribution cannot be produced and the loss of lipid material during the extrusion of the lipid material cannot be determined either. Nevertheless, LUVs are an effective tool to simulate natural membranes. LUVs are suitable especially for the investigation of transport along the membrane (lateral diffusion) or across the membrane, the investigation of membrane fusion, the investigation of peptide-membrane interaction or the loading of the inside of a LUV with a substance that is released during a certain event.[69, 75, 76]

1.2 Peptide-Membrane Interaction

The peptide-lipid or peptide-membrane interaction is required for a variety of essential biological and physicochemical processes and operations.[77] These include defense mechanisms based on antimicrobial peptides, viral translocation, membrane protein functionality, membrane fusion, and membrane integrity disruption.[78]

Due to the peptide-lipid interaction and the mutual influence of both sides, there is a change in the structural properties on both sides. Therefore, it is of great importance to identify a link between the structure of a peptide and its biological mode of action. Thus, it is possible to synthesize new tailor-made peptides with specific functionalities, which can fulfill new tasks or purposes.[58, 78]

In general, we can speak of membrane active peptides, which are responsible for important roles in some cellular processes. For example, protein trafficking[79], exocytosis and endocytosis[80], and virus entry and exit[81, 82] are among the

key functions. Other special membrane active peptides are the antimicrobial peptides (AMP)[83] and the cell penetrating peptides (CPP)[84]. AMPs serve to kill pathogens and are often found as components of natural immune systems.[85] CPPs can translocate across the membrane alone or in conjunction with molecular transport. This opens the possibility that CPPs may be suitable for delivering drug products into the cell.[78]

AMPs and also CPP are pharmaceutically relevant due to their properties and are therefore the focus of research. AMPs give new hope for alternative treatments in view of the growing number of germs that are resistant to antibiotics. The fact that AMPs are able to perturbate the membrane and still show a high specificity against microorganisms is used. Therefore, the structure and associated properties of an AMP are of great importance.[78, 86, 87] Furthermore, CPPs are also of great interest as they are involved in drug transport and drug transport systems. CPPs are therefore used to study the cellular uptake or transport of drugs in a biophysical way, which in turn will attempt to imply and optimize an artificial drug transport system.[88] To simplify these studies, model membranes are often used, and the results of these experiments can be used to draw conclusions about drug-lipid interaction, drug pharmacokinetics, biodistribution and tissue accumulation.[89–91]

For translocation of CPPs or penetration of AMPs through membranes, interaction with the membrane is mandatory. However, the interaction and the effect of this interaction depends on some factors. For example, the peptide concentration determines the behavior of the peptide[92], i.e., whether the peptide reacts as an AMP or as a CPP. At high concentrations, peptides can react as CPPs and permeabilize the membrane, whereas at low concentrations AMPs are more likely to reach a cytotoxic limit before membrane permeabilization can begin.[58, 78] Other factors that influence the peptide-lipid interaction are the membrane affinity of the peptide and the capacity to destabilize the membrane. Both factors also determine the extent to which the peptides can penetrate the membrane or cell. In the first step of the interaction of CPPs with a membrane, electrostatic attraction exists between the membrane surface and the peptide itself, usually triggering an endocytotic uptake of the peptide into the cell.[58] A change in conformation leads to a change in the peptide/lipid interaction, thereby modulating the strength of the interaction as well.

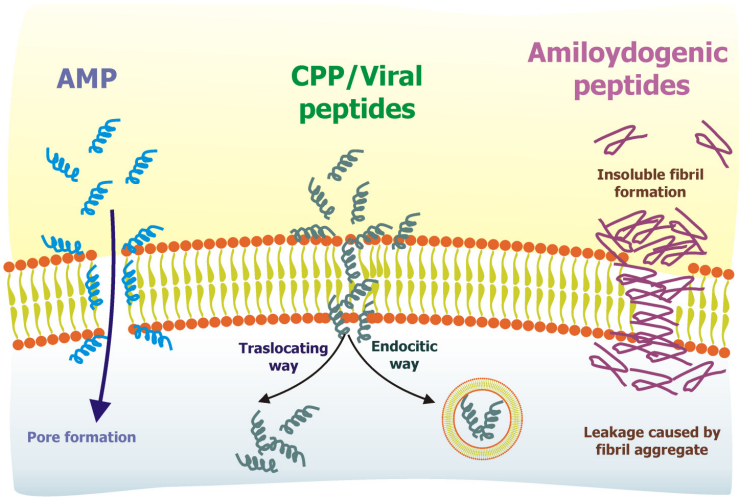

Figure 1.3: Schematic representation of the mechanisms for interaction of membrane-active peptides, such as AMPs, CPPs, and amyloidogenic peptides with the membrane. AMPs penetrate the membrane and form pores, thereby permanently disrupting membrane integrity. CPPs and amyloidogenic peptides, on the other hand, can enter the cell by endocytosis and direct translocation, respectively. The route via endocytosis is preferred by CPPs, whereas amyloidogenic peptides prefer direct translocation through the membrane.[78]

The strength of the interaction in turn determines the further course of uptake of the peptide. Either the peptide remains trapped in the plasma membrane or not, or the peptide causes increased disorder in the membrane, which in turn causes translocation of the peptide.[78]

The interaction of AMPs can be further described by three different mechanisms.[93] These mechanisms include the carpet model, toroidal pore model, and barrel-stave model (Fig. 1.4). All three mechanisms are based on the initial binding between the peptide and the membrane surface, which can only occur when the critical Peptid:Lipid ratio is reached. This initial binding is based on electrostatic and/or hydrophobic interactions. Based on the different binding affinities between peptides and membrane surface and depending on the membrane composition, different sensitivities and selectivities result.[58, 78] The initial binding of the peptides to the membrane surface usually occurs via an electrostatic attraction which is supported or even replaced by a hydrophobic interaction in the further course. The respective proportion of the two interactions is difficult to determine, since the binding of the peptide to the surface of the membrane can lead to a change in the conformation

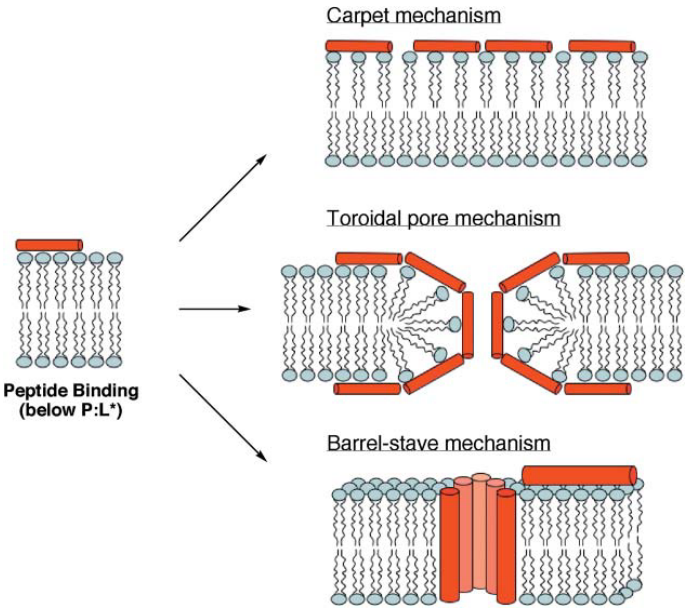

Figure 1.4: Schematic representation of the pore-forming mechanisms of antimicrobial peptides (AMP).[58]

of the peptide. Hydrophilic or hydrophobic peptide residues are shifted in such a way that the best possible binding can occur. After initial binding, the behavior of peptides divides into the three possible mechanisms.[94]

Carpet mechanism[58] In the carpet mechanism, the peptides lay parallel on the surface of the membrane similar to a "carpet". It is not possible to distinguish whether the peptides bind to the surface or are slightly immersed in the membrane. Due to the interaction between the peptides and the membrane, a destructive force acts on the membrane, causing the lipids in the membrane to be arranged differently, resulting in higher surface tension and rupture of the membrane.

Toroidal pore mechanism[58] Similar to the carpet mechanism, peptides bind to the membrane surface in this mechanism. Thus, using the example of magainin, it could be shown that the peptides immerse into the headgroup region of the lipids. This leads to a disturbance of the lipid-lipid interaction, which results in a narrowing of the membrane thickness and finally in a positive surface tension. When the P:L ratio exceeds a certain point, the peptides begin to behave similarly to a transmembrane peptide, causing the membrane struc-

ture to break down and a pore to form that is lined with peptide from the inside.

Barrel-stave mechanism[58] The barrel-stave mechanism works in a similar way to the toroidal mechanism. The peptide monomers accumulate on the membrane surface and align to the membrane according to their amphipathicity. Once the critical concentration is reached, the peptides begin to aggregate and deposit into the membrane, forming a pore together with lipid material. The size and properties of such a pore are very dynamic and are controlled by the local concentration of peptide. Thus, the pore is able to absorb further peptide material or to release it again, and the size of the pore varies as a result.

One of the most important aspects in the discussion about the interaction of peptides and membranes is the analysis of the interactions, because on the basis of established analytical methods, conclusions can be drawn about biological processes and thus the established hypotheses and mechanisms can be tested or proven.

A variety of different methods can be used to measure the binding, localization and orientation of peptides to a membrane or lipid, as well as the rearrangement of lipids by interaction with a peptide (Fig. 1.5).[78] Some of the methods such as electron microscopy (EM), atomic force microscopy (AFM) and more generally fluorescence imaging can be used to clearly visualize the morphology and change in structures[95–98]. Especially the two methods EM and AFM have shown their great benefit in the analysis of biological systems due to the great spatial resolution, both methods have the disadvantage that the sample preparation can generate artifacts which can lead to wrong results.[78] An AFM measurement also has the disadvantage of not providing chemical information about the system under investigation. This disadvantage can be circumvented by combining AFM with fluorescence measurements.[95] For EM often, the fluorescence of dyes is used, which gives a high sensitivity, the disadvantage here is that the influence of the dyes on the peptide-lipid interaction is not known and can disturb the measurement. The use of dyes offers further advantages, such as the ability to determine the kinetics of binding of the peptides to the membrane surface.[78] Calorimetry, solid-state nuclear magnetic resonance (NMR) or X-ray analysis provide detailed information about global phase changes.[99] Especially solid-state NMR takes a special position, because only NMR analysis is able

to resolve the topological as well as the 3D structure of peptides in membranes. Due to the resonances and couplings of the protons among each other, distances through space can also be observed and evaluated.[99–101]

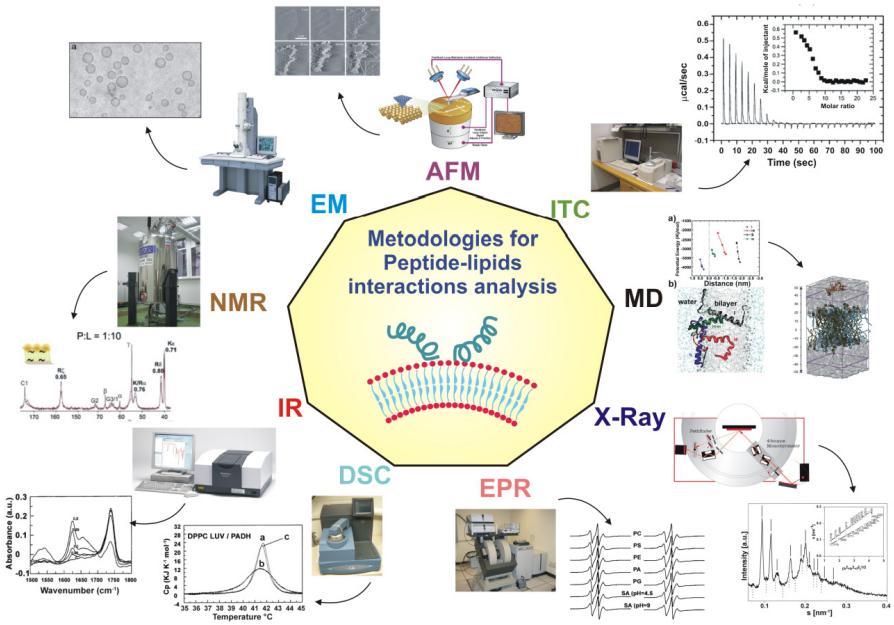

Figure 1.5: The figure shows schematically the multitude of different methods for the investigation of biochemical processes. The methods shown include nuclear magnetic resonance (NMR), electron microscopy (EM) and X-ray crystallography (X-ray).[78]

2 The Structure and Function of beta-Peptides

In its evolution over millions of years, nature has created an incredible correlation between biological function and structure. Molecules that are relevant for biological processes and regulate them have a precisely defined and stable structure. Commonly known and widespread is the image of the structure of human DNA.[1, 2] In this context, the question arises whether it is possible to imitate similar biologically relevant molecules with a stable structure under controlled conditions in the laboratory.[102] This subfield, which deals with the reproduction of biological systems under synthetic conditions, is called "protein mimetics". One part of the field of protein mimetics deals with β^3-amino acids[103] and the resulting β-peptides.[9, 104]

2.1 Principles of beta-Amino Acids and beta-Peptides

There is a direct relationship between the function of a peptide or protein and its (spatial) structure. It is known that peptides from alpha-amino acids can only form stable secondary structures from a chain length of about 100 amino acids. It is not practical to artificially produce similar systems with 100 or more amino acids in the laboratory [105]; one solution could now be to truncate the target peptide to its interesting core aspects. Shorter peptide sequences can be produced well on a laboratory scale, but the problem remains that shorter sequences generally do not form stable secondary structures.[105] Thus, an alternative is needed that can be readily

implemented in the laboratory with respect to its chain length and that can form a stable secondary structure even with shorter sequences. One possibility is the aforementioned β-peptide consisting of β-amino acids.[105]

β^3-amino acid have long been known to be present as building blocks in many biological cell components, whereas β-peptide are not present in biological systems.[2] The great advantage of β-peptide is that these peptides form a stable secondary structure from a length of six amino acids and that β-peptides are stable against proteases.[106] This advantage makes it much easier to mimic natural systems and their secondary structure on a laboratory scale.

The difference between β-amino acids and its α-analogs lies in the additional methylene unit ($-CH_2-$) between the amino and carboxy function (Fig. 2.1).[107]

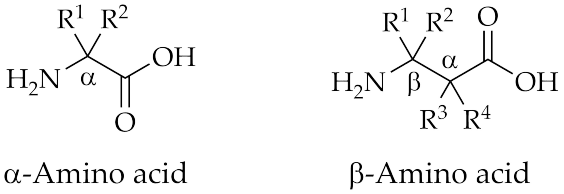

Figure 2.1: Comparison between a α and β amino acid.[103]

The additional methylene unit dramatically increases the structural variance . There are more positions for additional substituents and more possibilities for different configurations (Fig. 2.2). On the most used ways to synthesis β-amino acids is the so-called Arndt–Eistert homologation.[108] In addition, the introduction of heteroatoms into the peptide backbone becomes possible, as well as cyclic derivatives that prevent rotation around the C(2)-C(3) bond.[103]

Another factor influenced by the additional methylene unit is the number of torsion angles per β-amino acid, which has a direct influence on the conformation of β-peptides. Due to the additional unit, there is another C-C bond that is free to rotate. Via the torsion angles ϕ, θ and ψ (Fig. 2.3), the conformations of β-peptides can be analyzed, where the torsion angle θ, between C_α-C_β, is crucial for the formation of the secondary structure of β-peptides.[107, 109]

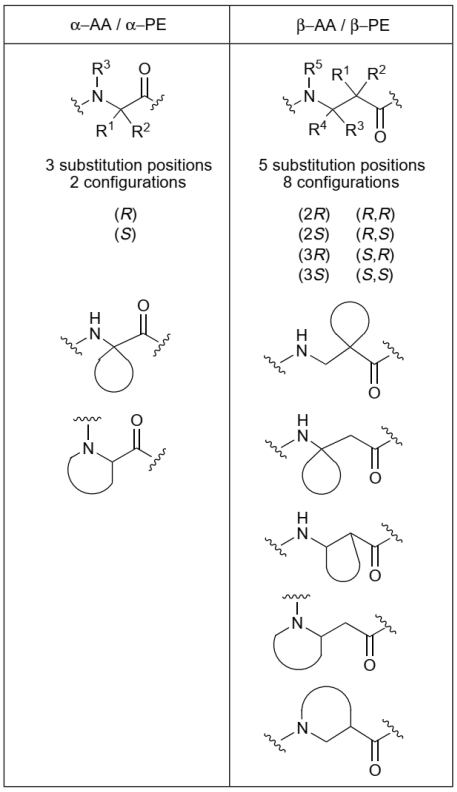

Figure 2.2: Comparison of the different substitution patterns and configurations in α-amino acids and β^3-amino acids.[107]

If the β-peptides adopt a helical or loop-like structure, this requires a *gauche* conformation over the θ angle. A significant role is played by the substitution pattern of the β^3-amino acid. Thus, the different substitution patterns and their effects on the conformation, have been the target of numerous experimental studies and molecular dynamic calculations.[109]

Unsubstituted β^3-amino acids, such as β-alanine or its α-analogue glycine, are very flexible and show high free rotatability over all torsional angles. Much more restricted systems are obtained by substituents on $C(2)$ and $C(3)$; these systems prefer a *gauche* arrangement.[107, 112] If a β^3-amino acid is doubly substituted at positions two and three, respectively, the β-amino acid is even more severely restricted in its rotatability. Provided that the substituents adopt a *anti* conformation, a *gauche* conformer is preferentially generated. If the substituents at positions two and three are linked to each other via a cyclic alkyl residue, as in

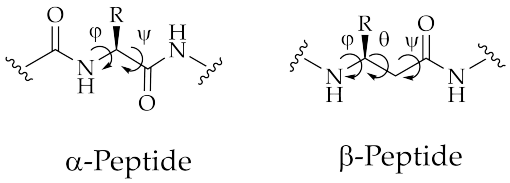

Figure 2.3: Schematic representation of torsion angles in α- and β-peptides according to the convention of Balaram.[110, 111]

trans-2-aminocyclohexanecarboxylic acid (ACHC), the torsion angles for a *gauche* conformation formally "forced". In this process, the ring size can be used to control the torsion angle and thus indirectly the formed helix that the β-peptide occupies.[109] As can be seen from the figure (Fig. 2.4), a *strand* or leaflet structure

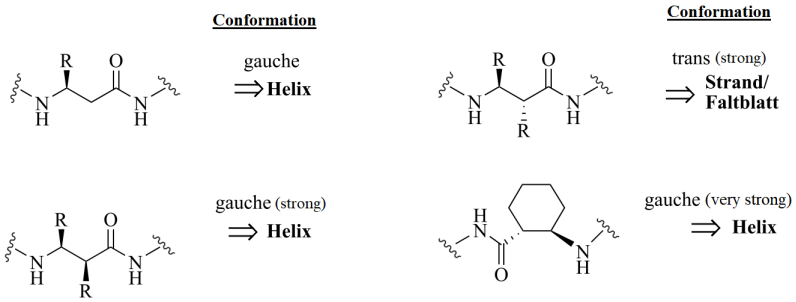

Figure 2.4: Conformational preference for different substituted β-peptides.[2]

can only form when the substituents are syn, resulting in a *trans* conformation.[109, 113]

2.2 Different Types of Secondary Structures

The large structural diversity of β^3-amino acids and β-peptide already mentioned leads to a large variety of possible secondary structures.[2] In this context, the respective leading authors have introduced their own different nomenclature for the secondary structures.[113–116] In the context of this work the nomenclature of Gellmann[112] will be used. In this nomenclature the atoms involved in the formation

of a ring formed by hydrogen bonds are counted. Among the best-known representatives of their kind are the 8-, 10-, 10/12-, 12- and 14-helix (Fig. 2.5). Each helix has its own characteristic features and properties, they differ in diameter, number of amino acids per turn or torsion angle (Fig. 2.6).[109]

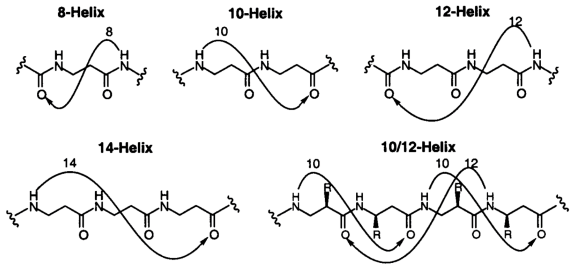

Figure 2.5: Representation of the different helix types, depending on the respective intramolecular hydrogen bonds formed. The helix structure is named for the number of atoms located within the forming hydrogen bond.[109]

If the structures of the α-helix[117] are compared with the structures of the two β-helixes, it becomes obvious that the structures differ drastically in some characteristic points. For example, all three examples have a different diameter, as well as a different shape and arrangement of the amino acid residues.[107] They also differ in their orientation of polarity with respect to their respective *C*- and *N*-termini, and in the two β-helices there is the possibility that the secondary structure is stabilized by hydrophobic interactions through overlapping side chains.[109]

In regard of this work, the 14-helix will be focused on in the following, since it can be compared most closely to that of a α-helix in terms of its properties and regular distance.[109] Early measurements on simple poly(α-isobutyl-L-aspartate)[115] showed that β-peptides adopt a helix-like structure. The assignment of the measured signals and the conclusions drawn were not clear and different conformations were proposed and discussed.[118, 119] By introducing cyclic β-amino acids that are strongly sterically hindered, such as *trans*-2-aminocyclohexanecarboxylic acid, the resulting secondary structures became more uniform and more predictable. This, allowed the peptides to be studied by NMR and crystallography, respectively, and to provide an accurate indication of the secondary structure.[113, 120]

For example, by Seebach *et. al.*, it was shown that in addition to cyclic β-amino

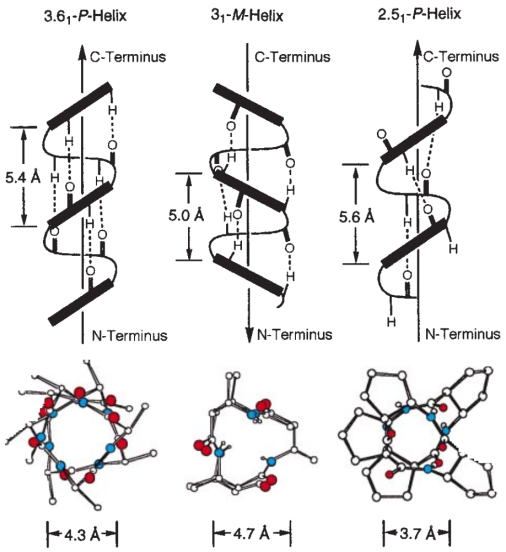

Figure 2.6: Comparison shows a α-helix (left, 3.6$_1$-*P*-helix) versus two β-helix represented by a 14-helix (middle, 3$_1$-*M*-helix) and a 12-helix (right, 2.5$_1$-*P*-helix). The different diameter, the different distribution of amino acid residues and the opposite polarity (α-helix vs 14-helix) can be seen.[107]

acids, a large number of acyclic amino acids also form a 14-helix in organic solvents as well as in the solid state.[113, 121, 122]

The turn or the direction of the turn of the helix is determined by the stereocenter of the amino acid used. Thus, the L forms give rise to a left-handed helix and the D form to a right-handed helix. The helix is stabilized by hydrogen bonds between the amide proton at the *i* position and the carbonyl function at the *i+2* position, resulting in a 14-membered ring. If the 14-helix, is compared with the 12-helix and a α-helix, the 14-helix and the α-helix are still most similar. Both have a similar number of amino acids per turn and a comparable pitch per amino acid (Tab. 2.1). Thus, a 14-helix has a pitch of three amino acids per turn, and the α-helix has 3.6 amino acids per turn. Due to the uniform rise of the 14-helix, every third amino acid or its side chain comes to lie on top of each other.[112, 113, 121, 123] This results in a very even distribution of the side chains, which makes it very easy to manipulate the position of each side chain. In terms of radius, the 14-helix is 0.5 Ã... larger than a α-helix, also the torsion angles differs from each other.[114, 124, 125]

Table 2.1: Comparison between the 14-, 12- and α-helix. Shown are the torsion angles and different helical parameters.[114, 124, 125]

Characteristic	14-helix	α-helix	12-helix
ϕ (°)	-134.3	-57	95.0
θ (°)	60		-94.3
ψ (°)	-139.9	-47	103
ω (°)	180.0	180	-180
radius (Å)	2.7	2.2	2.3
residue/turn	3.0	3.6	2.5
rise/residue (Å)	1.56	1.5	2.1

3 The Bipyridine unit

The term molecular recognition include the interaction between two or more molecules through non-covalent bonds. These non-covalent bonds include hydrogen bonding, coordination of metals or metal ions, hydrophobic forces (hydrophobic effect)[126, 127], VAN-DER-WAALS interaction, π-π interaction, and electrostatic and electromagnetic[128] effects. Here, molecular recognition follows the principle of "keyhole and key" and is intended to understand and mimic specific binding as exemplified by nature.[129]

First over all we will discuss the general mechanics of metal coordination and there use in chemical synthesis. Selected examples are used to demonstrate the benefits of metal complexes, especially with regard to the bipyridine derivative used for the metal coordination. In the ongoing discussion selected examples are presented to show the connection between metal coordination and protein folding.

3.1 Molecular Recognition

Enzymes are Nature answer to the question how molecular recognition and the catalysis of a reaction can be efficiently combined. Reactions catalyzed by an enzyme-substrate complex are much faster than comparable bimolecular reactions. The degree of regio- and stereoselectivity is very high and is achieved by a favored and precise orientation of the reactive position towards the catalytic center of the enzyme.[130] ŠMEJKAL *et al.* is inspired by the precise regio- and stereoselectivity, they have established a system that works on the same principle and is expected to significantly increase the regioselectivity of the catalyzed hydroformylation of unsaturated

carboxylic acids. Their system is based on the principle of a temporarily bound directing group(s). As a directing group, *ortho*-diphenylphosphinobenzoate (*o*-dppb) has been used with a rhodium catalyst (Fig. 3.1).[130] The *o*-dppb ligand can bind

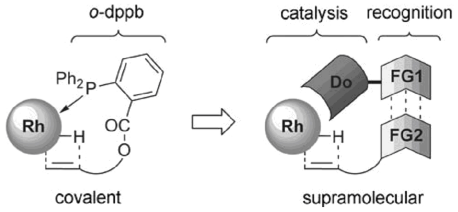

Figure 3.1: Schematic representation of the concepts of covalent and supramolecular catalysts directing group. Do = donor, FG1,2 = complementary functional groups.[130]

the substrates but cannot provide sufficient orientation of the substrate. A guanidinium moiety has been added to the ligand, which should make it possible to recognize carboxylic acids as a recognition unit (Fig. 3.2).[130]

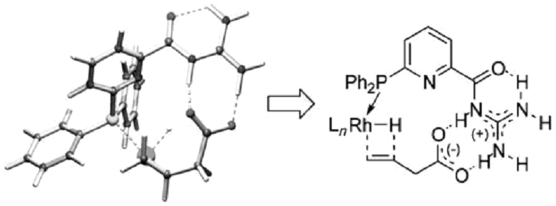

Figure 3.2: Schematic representation of the non-covalent bond between catalyst and recognition unit. Ligands not involved in the reaction are not shown.[130]

Another approach which also based on the recognition of carboxylic acids is provided by De Santis *et al.*[131] In the system presented, the aim was not to selectively bind a substrate in order to perform a catalytic reaction with a highest possible regioselectivity, but to detect the binding of an anion or carboxylic acid by changing the fluorescence behavior of anthracene. They have synthesized a zinc(II)-anthrylamine complex with a four-coordinated zinc(II) and thus still has an open binding site for a trigonal-bipyramidal geometry (Fig. 3.3). The open binding site results in a high binding affinity to carboxylic acids. The binding of carboxylic acids can result in electron transfer (ET) from the residue on the carboxylic acid to the anthracene, quenching the fluorescence (Fig. 3.3). Almost complete quenching of fluorescence

occurs even at a 1:1 ratio between the zinc(II)-anthrylamine complex and the carboxylic acid.[131]

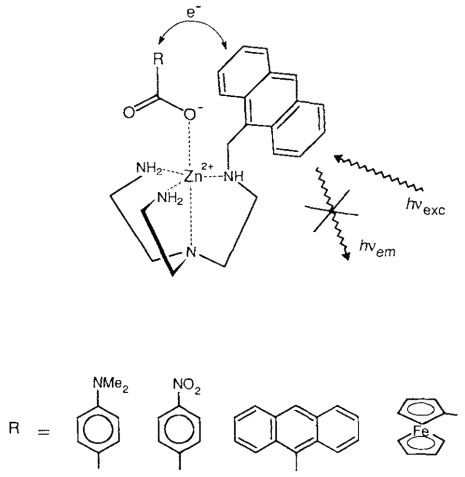

Figure 3.3: Chemical illustration of electron transfer responsible for quenching fluorescence.[131]

De Santis *et al.* have been able to develop a basis for molecular sensors. These sensors are designed to selectively bind an analyte, changing the optical properties of the sensor. In the same type of sensors chromophores are often covalently bound to the recognition moiety, if the analyte is bound to the recognition moiety, the microenvironment around the chromophore changes, resulting in a change of the optical properties.[132] For chemosensors, their optical properties change and it comes to a change in the absorption of the UV/VIS spectrum (shift of λ_{max}) or the emission wavelength is shifted.[133] The specific binding of analytes and the associated effects make chemosensors perfect candidates in many different tasks in chemistry, biology and especially medicine.[134] Main group metals such as lead(II) can be bound via the oxygen atoms of the amide bond. In this case, a fluorescence of the pyrene units occurs, based on a reverse photoinduced electron transfer. In this process, the pyrene units act as donors for the carbonyl groups. Furthermore, an intramolecular conformational change occurs as the carbonyl groups turn from the outside to the inside to coordinate the lead(II) ion. Due to this conformational change, a parallel arrangement of the two pyrene units and the associated π-*stacking* is no longer possible. Due to this change in the structure of the molecule the absorption and emission properties are changed.[134]

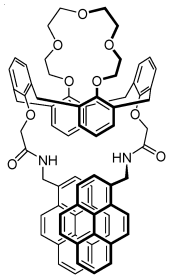

Figure 3.4: Illustration of modular 1,3-alternating calix[5]crown ether.[134]

As mentioned at the beginning, the presented molecule has two recognition units for cations. The second recognition unit is the [13]crown-5 unit at the top of the molecule. This unit shows a great affinity for cations from the first main group and in particular for potassium. The affinity for the coordination of potassium is so high that a already coordinated lead(II) is displaced from its coordination. This metal exchange will restore the fluorescence that was quenched by the coordination of lead(II).[134]

As shown by the example of Kim *et al.*, molecular recognition plays a major role in supramolecular chemistry. This importance is also given to molecular recognition in supramolecular catalysis. In the next system presented by Bassani *et al.* in 2000, it is shown how the photodimerization of cinnamic acid derivatives is significantly accelerated in solution. Cinnamic acid is known to undergo topochemical[i] photodimerization. The ester derivatives of the cinnamic acid undergo the same reaction only under catalysis by a Lewis acid [136] or in solid phase.[137] To address this problem Bassani *et al.* have covalently attached to the methyl ester of cinnamic acid **1** a diaminotriazine unit as intermolecular recognition units (Fig. 3.5).[138] The hydrogen bonding patterns of **1** and **2** are complementary to each other allowing dimers and trimers to form. In the trimers, the cinnamic acid esters can adopt a parallel arrangement (Fig. 3.5b), favoring cyclodimerization. The formation of trimers shifts the reaction products toward the templates due to the template effect that occurs. The products obtained and their regioselectivity is shown in **(b)** (Fig. 3.5b).[138]

[i]Topochemistry is a field of physical chemistry that describes reactions that occur on or in solid phase.[135]

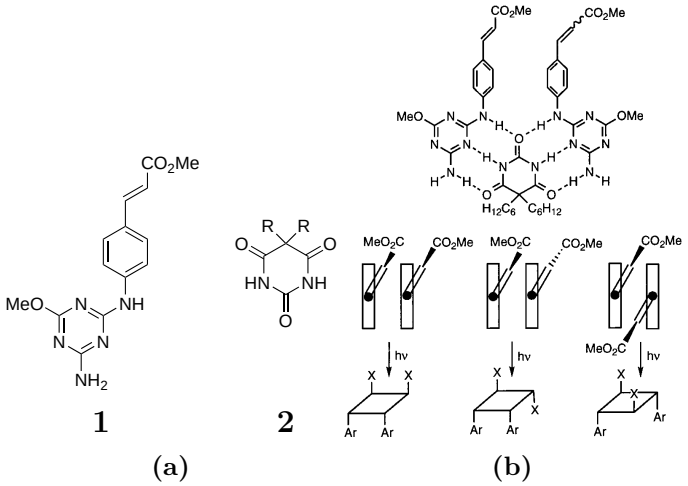

Figure 3.5: **(a)** Left: Representation of the cinnamic acid derivative with the diaminotriazine moiety **3**, Right: Representation of the barbiturate derivative (R = hexyl) **2**; **(b)**: In the upper section, the arrangement of a trimer of **1** and **2** can be seen, and below, the observed regioselectivity of photodimerization.[138]

3.2 The BiPy-Unit and their Derivatives

Starting with the discovery of bipyridine and its derivatives in the nineteen century the use of this ligand has been drastically increased due to the superior properties.[139] It is possible to coordinate metal ions to form charged complexes, the bipyridines are stable against redox active substances and the compounds are easy to modify. In general the bipyrindines can be classified as symmetric isomers (2,2', 3,3' and 4,4') and asymmetric (2,3', 2,4' and 3,4') (Fig. 3.6).[20] The focus is particularly on the two isomers 2,2'- and 4,4'-bipyridine based on their possibilities to be modified and their positioning of the two nitrogen atoms. Especially the 2,2'-bipyridine is of particular interest. Based on the 2,2' position of the nitrogen atoms a (direct) coordination of metal ions is favored. The class of the smallest representatives are two 2,2'-bipyridine units which are covalently bound to each other and therefore they cannot be classified as oligopyridines. Ligand systems that use more than two 2,2'-bipyridine units can bridge multiple metal centers to interconnect them. With these assemblies it is possible to construct well-defined spatial layout which can be func-

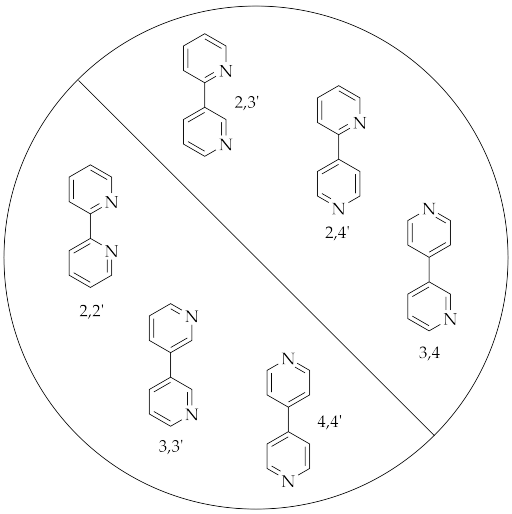

Figure 3.6: Symmetric und asymmetric isomers of bipyridine.[20]

tionalist to form helices or luminescent compounds.[20]

With the possibility to coordinate a lot of different metals and metal ions[21] the use of bipyridines provides a broad spectra of different key features. By coordination of a metal ion by bipyridine groups α-helical or collagenous structures can be assembled.

Furthermore, by coordination of metal ions the general spatial structure of peptides can be controlled or functional peptides can be designed.[140–142] This means, among other things, that two or more amino acids can be brought into spatial proximity to each other, which can lead to new artificial properties (Fig. 3.7).[143] As shown in the picture each of the three 4,4'-bipyridine units is flanked on both sides by the same pattern of amino acid: GGA$-$5 Bpy$-$FGP. By the coordination of the Ru^{2+} ion the peptide is folded into an artificial motif[143] and shows some interesting photochemical properties like emission of longer wavelength after absorption of light, photoinduced electron or energy transfer and it can undergo photosensitive reactions.[144]

The example before clearly shows the influence of the coordination of metal ions to the secondary structure of peptides. This dependence is no one-way, the coordination or binding affinities of the metal ions by the incorporated ligands can

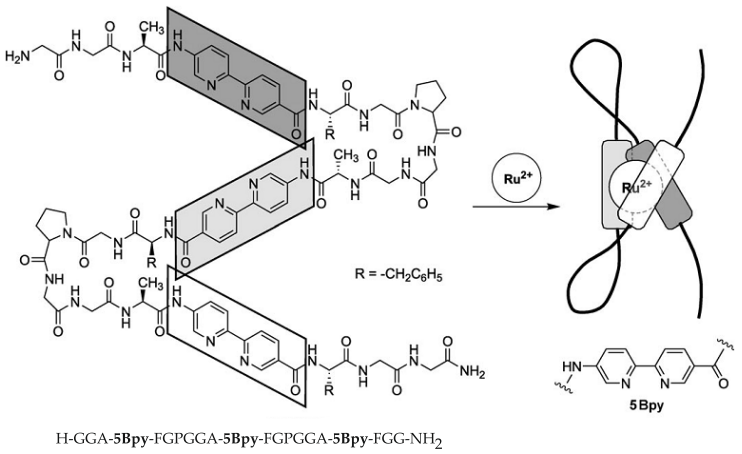

Figure 3.7: Molecular design of an artificial metalloprotein with a Ru(II) tris(bipyridine) complex as the core.[143]

be influenced by the coordinating groups and be changed by electron withdrawing or electron donating groups, which decrease or increase the electron density or the sterical demand can be varied by addition or removing of sterically demanding groups.[145]

Beside this it is possible to control/modify the coordination of a bipyridine ligand by its neighbor groups. The properties of the ligand are indirectly controlled by remote substituents if the ligand is incorporated in a peptide dendrimer[ii]. In the group of Uhlich was observed that the influence on the ligand in dendrimers depends on the amino acids which are up to ten bonds away from the coordinating atoms and these amino acids are consequently called remote amino acids.

Uhlich *et al.* generated a library of different peptide dendrimers, which can be classified in charged (negative or positive), in aromatic and hydrophobic amino acids in the close proximity of the bipyridine ligand. The results were that dendrimers which consists of (more) negative charged amino acids can bind the metal ions stronger, than dendrimers with (more) positive charged amino acids. The same dendrimers without the bipyridine unit does not show any metal ion capacities. That means that a binding of the metal ion based on interactions between charges can be excluded.[145]

[ii]Donald A. Tomala is known as the inventor of what is called today a dendrimer. A dentrimer is a synthetic polymer which growth branched like a tree around a trunk in the middle of the dendrimer. A dendrimer is typically only a few nanometer in size.[146]

The remote control of the coordination of metal ions shows the potential of creating new functional macromolecules. A well-known motif in where the peptide or macromolecules obtain their function/structure by coordination of a metal ion are the finger proteins.[145]

One of the most prominent example of the finger proteins is the classical Cys_2His_2 zinc-finger motif. More than 300 enzymes are known which uses zinc as a crucial part in catalytic reactions. Furthermore, it was elaborated that zinc is an important cofactor for hundreds of proteins which consist of one or more zinc-stabilized structural elements.[147, 148] The simplicity and nature of the classical zinc-finger motif makes it a perfect and useful model system to study the relation between metal binding and protein folding. By CD measurements Section 7.2 could be shown that the secondary structure is dependent on the influence of bound metal ions. The "naked" no bound metal peptide has no defined secondary structure, which is changed by the addition of metal ions.[149] After the addition of the metal ions the peptides are starting to fold, which is supported by formation of a hydrophobic core. NMR studies have proven that with lager finger proteins the role of hydrophobic interactions and forming a hydrophobic core are more and more important and are supporting the folding of the peptide.[150, 151]

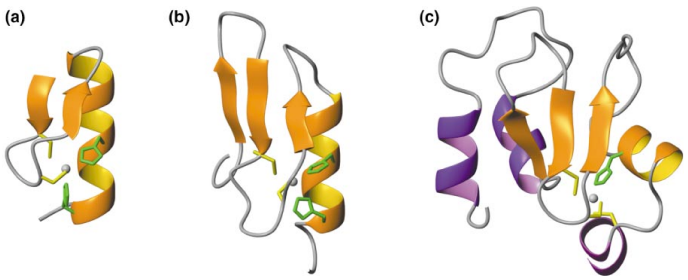

Figure 3.8: Depiction of the classical Cys_2His_2 zinc-finger motif. **a)** TFIIIA-type zinc-finger, **b)** *N*-terminal zinc-finger of SWI5 and **c)** BIR2 domain of XIAP. In orange are colored the α-helices and β-sheets, in magenta are shown all additional α-helices of BIR2.[152]

Saski[153] and Lieberman[140] showed with their work, that it is possible to use rigid molecules as a template structure to assemble secondary structure motifs in simple proteins. In particular, Saski was able to introduce to a 15 amino acid long peptide a well-defined secondary structure. The peptide them self-showed a random

coil structure, by addition of Fe^{2+} the peptides started to assemble to helix bundles. That was possible because it was incorporated a 2,2'-bipyridine-4,4'-dicarboxylic acid unit at the *N*-terminus of each peptide. These 2,2'-bipyridine-4,4'-dicarboxylic acid units coordinated the added Fe^{2+} and the single peptide strings get closer to each other and formed the mentioned α-helical structures (Fig. 3.9). Induced by

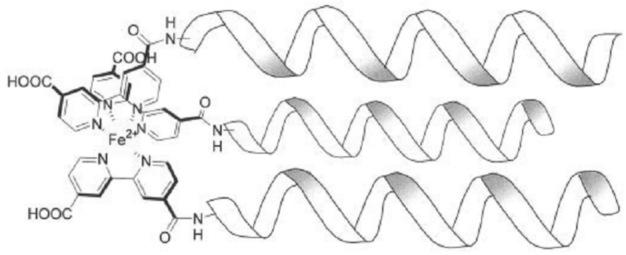

Figure 3.9: Metal induced aggregation of three peptides. At each of the *N*-termini there is a bipyridine unit, which coordinates the Fe^{2+} ion octahedrally.[140, 153]

the addition of the metal ions analysis showed that the content of aggregation is increased to 35 % - 85 %.[21] By the coordination of the metal ions by the peptides is not only the content of aggregation increased, also the stability of the peptides is increased. In temperature dependent CD measurements could be shown that the stability of the formed aggregates was raised from $T_m = 33$ °C (without any metal ion) to $T_m = 46$ °C (with metal ion).[21]

4 Fundamentals of fluorescence

4.1 Introduction

The emission of light from a given compound, from an excited state, is called luminescence. The excited state is obtained by applying energy from an external source.[154] Many different types of luminescence can be described which can be distinguished by the type of excitation. Among others, there is electroluminescence (known from diodes or OLEDs), chemiluminescence (reaction between luminol and blood), bioluminescence (oxidation of luciferin in fireflies) and photoluminescence. Within photoluminescence, further different types can be distinguished on the basis of the transition state. Among the known types are fluorescence, phosphorescence and also the special case of the Mößbauer effect. In the following, only the phenomenon of fluorescence will be considered in more detail.[155]

In 1852 the phenomenon of fluorescence was described more precisely for the first time by Stokes.[156] In 1845 Herschel has already described a similar phenomenon namely the emitting of blue light from Quinine (Fig. 4.1a) in Tonic Water.[157]. The phenomenon that both scientists observed is called fluorescence and is typically introduced by large aromatic compounds, two examples of fluorescent dyes are shown in the following picture (Fig. 4.1).[158] The fluorescence is in contrast to the phosphorescence by the factor 10^5-10^8 faster. The speed of the fluorescence is 10^8 s^{-1} and for the phosphorescence the speed is between 10^3 and 10^0 s^{-1}. The lifetime of the excited state τ of a fluorescent dye is described by the average time between its excitation and the return to the ground state. The time of the emission is thereby

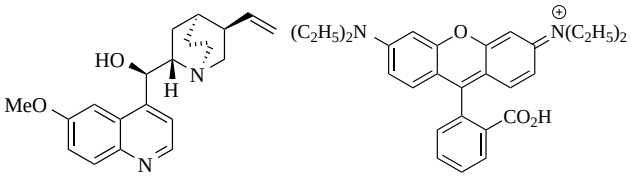

(a) Chinin **(b)** Rhodamin B

Figure 4.1: Exemplary representation of the two fluorescent dyes quinine **(a)** and rhodamine B **(b)**.[158]

decisively determined by the kind of emission: is observed a fluorescence or phosphorescence phenomenon? Which emission is observed is based on the kind of the excited state. If an electron is excited to a excited singlet state with an opposite spin to the spin of the second electron in the ground state, the transition to the ground state is allowed. Consequently, the transition is spin-allowed and very fast by emission of a photon which results in a very low lifetime.[158]

In the opposite case if the spin of the excited electron has the same spin than the second electron in the ground state, the transition is forbidden. Resulting in very low emission rates, that means that the observed phosphorescence has lifetimes typically of milliseconds to seconds. Despite the forbidden transition it is observed a emission of a electron. This transition occurs not a direct transition from the excited state to the ground state. The excited electron falls down in a triplet excited state and from there the electron falls down to the ground state by emission of light.[158] These complex relationships are best illustrated by a Jabłoński-diagram (Fig. 4.2).[159] The Jabłoński-diagram illustrates the complex relationships between the different electronic states of a molecule. S_1 and S_2 are the excited single states. Electrons are excited in these states after absorption of a defined amount of energy ($h\nu_A$). By an internal conversion the electrons can convert from S_2 to S_1 and from there the electrons can undergo a transition to the ground state S_0 ($h\nu_F$). It is also possible that an electron undergoes a intersystem crossing into the triplet excited state T_1, from where it is possible to fall back to the ground state by emission of light ($h\nu_P$). It can be seen, that the energy of the emission of light is lower and the wavelength is higher than the energy and wavelength of the light for the irradiation of the molecule. This observation was done in 1852 by Stokes, til today this phenomenon is called *Stokes shift*.[158]

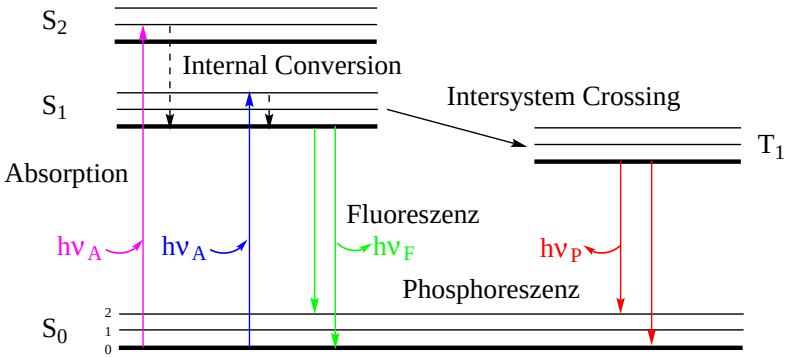

Figure 4.2: Schematic representation of a JABŁOŃSKI-diagram to illustrate the relationships of possible transitions of electrons into the various excited states when light is irradiated.[158]

4.2 Resonance energy transfer (RET)

The Resonance Energy Transfer (RET) is the general term for all processes that involve any kind of energy transfer. That means, that the RET-effect is a very important process which is directly associated with the excited state(s) of an atom or molecule. Therefore, RET describes the process that occurs when the emission spectrum of a fluorophore (donor) overlaps with the absorption spectrum of any other molecule (acceptor).[25] The acceptor does not have to be a fluorophore, but if it is, the term FRET is used. In the case of (F)RET it is essential to understand that the energy transfer does not depend on the emission of light from the donor and its absorption by the acceptor, it is a dipole-dipole interaction.[158, 160]

Many biological phenomena or functions in cells are based on physicochemical processes such as molecular binding, aggregation, conformational changes, diffusion, and catalysis of reactions.[26] In order to visualize these phenomena, a non-inversive method would be appropriate for studying these biological systems.[161] To address this issue, (F)RET the so called (Förster) Resonance Energy Transfer, from among many different methods of fluorescence microscopy, is an obvious choice. (F)RET is sensitive, selective, offers high spatial resolution to detect intra- or intermolecular distances in the range of 1 – 10 nm, and is capable of resolving interactions

and conformational changes well above the inherent diffraction limit ($\approx \frac{\lambda}{2}$).[26, 162]

The FRET process is mechanistically a two-step process that occurs simultaneously. An electron is transferred from the ground state to the excited state of the donor. From this excited state, the non-radiative energy transfer from the donor to the acceptor takes place through a dipole-dipole interaction of the FRET pair through space.[26, 163] In this process, the non-radiative energy transfer represents a relaxation of the excited state of the donor, which is in competition with other quenching processes, such as fluorescence.[164] The energy transfer can be described by the energy transfer rate k_t, where k_t shows an inverse dependence on r^{-6}, where r is the distance between donor and acceptor. Furthermore, k_t depends on three other factors [26]

1. The overlap integral J from the overlap of the emission spectrum of the donor and the absorption spectrum of the acceptor.
2. The relative orientation κ^2 of the dipole moments of donor and acceptor.
3. The refractive index n^{-4} of the solution in which the measurement is carried out.

In 1948 Förster was able to describe these relations quantitatively and to link them with formulas for k_t, J, the lifetime τ, the "Förster constant" R_0 and the energy transfer efficiency E[26].

$$k_\mathrm{t} = \frac{1}{\tau_\mathrm{o}} \left(\frac{R_\mathrm{o}}{r} \right)^6 \tag{4.1}$$

$$R_\mathrm{o}^6 = c_\mathrm{o} \kappa^2 J n^{-4} Q_\mathrm{o} \tag{4.2}$$

$$= c_\mathrm{o} \kappa^2 J n^{-4} \left(k_\mathrm{f} \tau_\mathrm{o} \right) \tag{4.3}$$

$$E = k_\mathrm{t}\tau \tag{4.4}$$

$$= \frac{\left(\frac{R_\mathrm{o}}{r}\right)^6}{1+\left(\frac{R_\mathrm{o}}{r}\right)^6} \tag{4.5}$$

$$\tau_\mathrm{o}^{-1} = k_\mathrm{f} + k_\mathrm{nr} + k_\mathrm{isc} + k_\mathrm{pb} \tag{4.6}$$

$$J = 10^{17} \int q_{\mathrm{d},\lambda}\epsilon_{\mathrm{a},\lambda}\lambda^4 \mathrm{d}\lambda \tag{4.7}$$

where $c_\mathrm{o} = 8.8 \cdot 10^{-28}$ nm, Q_o is the quantum yield, and $q_{\mathrm{d},\lambda}$ is the normalized donor emission spectrum. It appears from the equations that the fundamental relation between k_t and k_f that FÖRSTER reveals does not provide a necessary relation to the donor lifetime τ_o or the quantum yield Q_o. It can be concluded that the inclusion of τ_o and Q_o in the definition of R_o is arbitrary. The justification of this definition is based on the determination of the energy transfer efficiency E from the comparison with the properties of the unperturbed donor.[26]

FRET is widely used as a *Spectroscopic Nano-Ruler* to measure distances in the nano and subnano range.[165] As mentioned, the energy transfer efficiency E does not depend solely on the distance between the two fluorophores, but also on the relative orientation of the dipole moments. This property makes it possible to follow conformational changes and other similar transitions during a reaction also in biological systems. In addition, protein-protein and protein-DNA interactions can be studied.[163] Other potential applications can be found in materials science, polymer chemistry, and drug and ligand screening. Another major field of application is clinical in the form of spectrofluorimetry, flow cytometry, *Photobleaching FRET Digital Imaging Microscopy*, and the study of cell surface distribution of hematopoietic cluster Differentiation (CD) Molecules.[163, 166]

Part III

Design and Synthesis

In this part the design and the synthesis of the used β-peptides and building blocks are elucidated. At the beginning the synthesis of the β^3-homoanalogs of the Fmoc-α-amino acids (**SOP 13.1.2**) is presented. Followed by the synthesis of the commercially not available cholesterol derivatives and the cholesterol modified β-amino acids (Section 14.3) for the hydrophobic binding site. Furthermore it is presented the synthesis of the cyclic amino acid *trans*-2-((((9*H*-fluoren-9-yl)methoxy)carbonyl)amino)cyclohexane-1-carboxylic acid (*trans*-Fmoc-ACHC-OH) and the synthesis of the β^3-amino acid (*R*)-3-((((9*H*-fluoren-9-yl)methoxy)carbonyl)amino)-6-(allyloxy)-6-oxohexanoic acid (Fmoc-β^3-D-Glu(OAllyl)-OH) as a binding site for the modification with a cholesterol derivative.
The general design idea of the β-peptides, their synthesis and functionalizations will be shown. The design and modification of the β-peptides should guarantee, that their interaction with the membrane to construct a metal induced aggregation network on top of the membrane surface. The synthesis of the β-peptides was simplified to a modular synthesis to gain a faster access to a greater diversity of β-peptides.

5 Building Blocks

This chapter gives a detailed insight in the synthesis and purification of the used building blocks. It will be shown the synthesis of the used β^3-amino acids, including the synthesis of the β^3-amino acids, which were used as binding sites for the different peptide modifications. Additionally, the synthesis of the lipid anchors and the complex synthesis of *trans*-Fmoc-ACHC-OH will be discussed.

5.1 Fmoc-d-β^3-amino acid

The synthesis of all used β-peptides is based on the use of commercially not available Fmoc-D-β^3-amino acids. As the starting material for the β^3-amino acids the respective Fmoc-α-amino acids were used. A well-established method to produce β^3-amino acids is the so called Arndt-Eistert reaction (Fig. 5.1). The Arndt-Eistert reaction is a three step reaction to convert carbon acids and carbon acids derivatives to their corresponding homologue. In the first step the carbon acid is activated by the reaction with $^{i}BuCO_2Cl$ to form an acid chloride, which reacts, in the second step, with an excess of diazomethane to give a diazoketone, which can be used without further purification. The last step is a Wolff-Rearrangement, where the intermediate diazoketone is transformed to the homologated carbon acid by metal catalysis (Ag_2O) in the presence of a nucleophile (e. g. water, alcohols or amines).[167–171]

The Wolff-Rearrangement was carried out in the presence of water to yield the carbon acid and for the rearrangement two synthetic routes were established. For the reaction of the diazoketone to the desired β^3-amino acid were used two different methods. In the first method the diazoketone was dissolved in a mixture

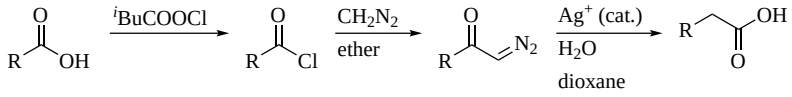

Figure 5.1: Three step Arndt-Eistert reaction. Starting from a Fmoc-α-amino acid to synthesize the corresponding β-amino acid.

of THF/water and treated in an ultrasonic bath. The other method described the processes of the Wolff-Rearrangement in a domestic microwave. Therefore, the diazoketone was dissolved in a mixture of 1,4-dioxane/water and heated in the microwave.[172] Independent of the synthetic method, the final β³-amino acids for this project were precipitated in cold *n*-pentane and collected by filtration in excellent yields (Tab. 5.1).

Table 5.1: Overview over the synthesized β³-amino acids, their corresponding abbreviations and yields.

β³-amino acid	Abbreviation	yield in %
Fmoc-D-β³-Lys(Boc)-OH (**4**)	^{h}Lys(Boc)	75
Fmoc-D-β³-Lys(Mtt)-OH (**5**)	^{h}Lys(Mtt)	89
Fmoc-D-β³-Val-OH (**6**)	^{h}Val	80
Fmoc-D-β³-Glu(OAllyl)-OH (**7**)	^{h}Glu	70

5.2 Synthesis of Fmoc-β³-Dap(Mtt)-OH (8)

Along with the shown β³-amino acids one more β³-amino acid was tried to synthesize without success. The amino acid Fmoc-β³-Dap(Mtt)-OH (**8**) (^{h}Dap(Mtt)) should be synthesized as an alternative for ^{h}Lys(Mtt). To obtain **8** two synthetic pathways were carried out (Fig. 5.2).

The starting material to obtain **8** is Fmoc-D-Asn-OH **9**, which is transformed by a Hofmann rearrangement with iodosobenzene diacetate (PIDA) to Fmoc-D-α-Dap-OH **10**. With **10** was introduced Mtt as a new protecting group to obtain Fmoc-D-

α-Dap(Mtt)-OH **11**. With this in hands the Arndt-Eistert reaction was performed without success. However, the obtained product **12** was a result of an intramolecular ring closing reaction between the diazoketone and the Mtt protected amine, with an elimination of the Mtt group.

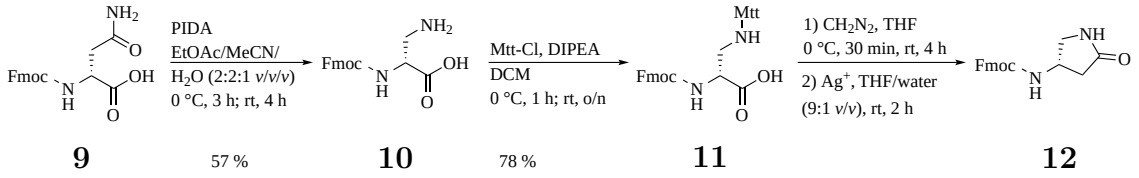

(a) Reaction pathway A. Starting from **9** to obtain **12** in a four-step reaction.

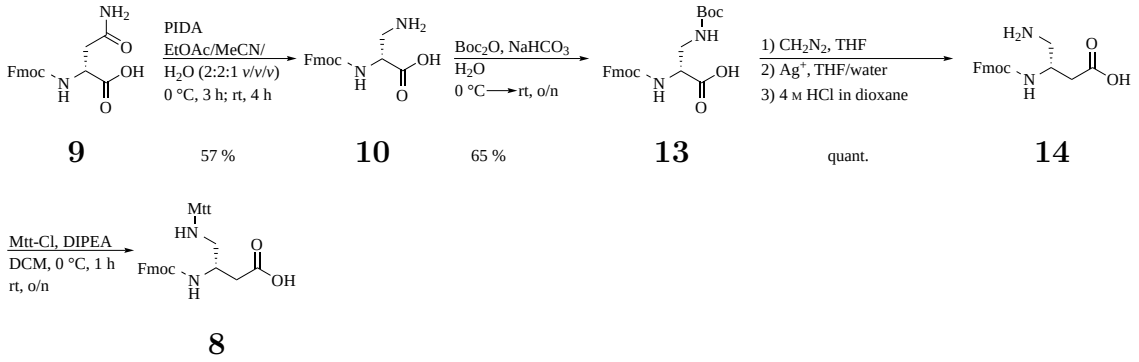

(b) Reaction pathway B. Starting from **9** to obtain **8** in a five step-reaction.

Figure 5.2: Schematic drawing of pathway A and B to obtain **8**

In the second pathway, **10** was Boc-protected to obtain **13** and then the Arndt-Eistert reaction was performed. The resulting β³-amino acid was successively deprotected by HCl (4 M in 1,4-dioxane) (**14**) and the deprotected amine was protected with Mtt-Cl in DCM (+ DIPEA). However, the final product ^{h}Dap(Mtt) **8** could not be isolated or detected by MS analysis.

^{h}Dap(Mtt) **8** (Fig. 5.3) should be synthesized, because the side chain is reduced by three $-CH_2-$ units, in comparison with a ^{h}Lys. The application of **8** would result in a shorter (covalent) bond between its side chain and the recognition unit, which could have a big advantage the design and function of β-peptides. The reduced length should prevent, that two recognition units of one β-peptide undergo a intramolecular metal coordination.

5.3 ^{h}Glu 7 as a binding site

To incorporate cholestamine **15** (subsection 5.4.2) in the β-peptides ^{h}Glu was used as a binding site. The ^{h}Glu unit was synthesized starting from the unprotected D-α-Glu (**16**), which was converted in a four step synthesis to Fmoc-D-β^{3}-Glu(OAllyl)-OH (**7**) (Fig. 5.3). The unprotected amino acid **16** was selectivly protected as an allyl-

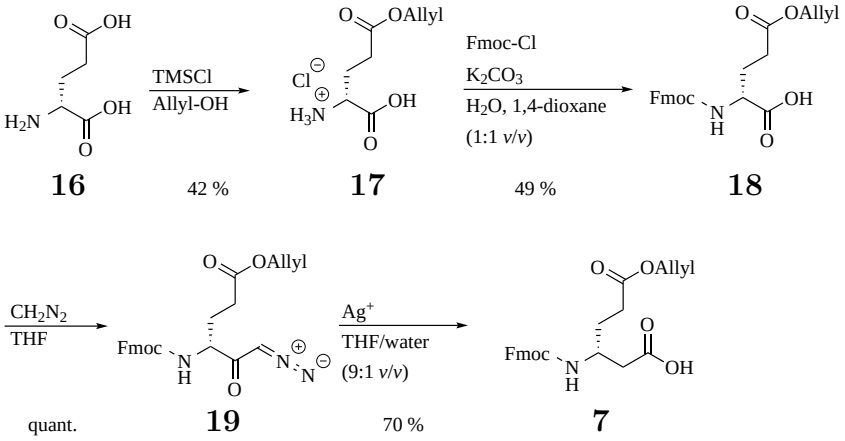

Figure 5.3: Synthesis pathway for ^{h}Glu **7**. Starting from **16** over four steps with a yield of 14 %.

ester at the ϵ-carboxylic acid using TMSCl. The crude product was precipitated with cold ether as the chloride salt of the amine to obtain **17**. Compound **17** was deprotonated by K_2CO_3 and subsequently protected with a Fmoc-Cl at the primary amine to yield the product **18**. **18** was converted by the Arndt-Eistert reaction into the acid **7**.

5.4 Cholesterol (20) and Cholestamine (15) as lipid anchor

5.4.1 Synthesis of the Cholesterol derivative (20)

The first approach to incorporate cholesterol (**21**), in the β-peptides was to synthesize a modified β^3-amino acid, which should be linked the cholesterol via its side chain. Therefore, one synthesis pathway was to modify the *C*-terminus of Fmoc-L-Asp(O*t*Bu)-OH (**22**) (Fig. 5.4). The use this amino acid had the advantage, that it is not necessary to perform the Arndt-Eistert reaction, because the *C*-terminus is modified with the cholesterol moiety and the γ-carbon acid is deprotected. It is possible to incorporate the amino acid in the primary structure through coupling with the γ-carbon acid, because of that reason the amino acid is tilted and the initial *C*-terminus becomes the side chain and pseudo converts the stereo information. In the

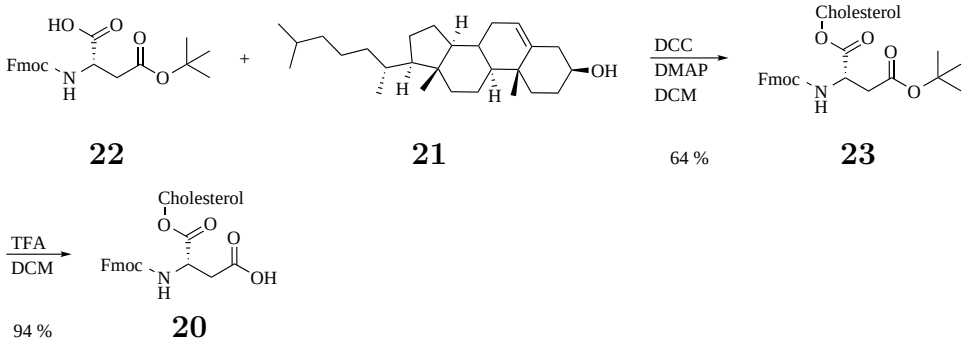

Figure 5.4: Scheme of the two-step synthesis of **20** starting from **22** and **21**.

first step L-Asp **22** reacts with DCC (dicyclohexylcarbodiimide), DMAP (4-*N*,*N*-dimethylaminopyridine) and cholesterol **21** in a STEGLICH-esterification. In this reaction the amino acid was activated with DCC by forming an *O*-acylisourea intermediate following by the addition of the alcohol to form dicyclohexylurea (DHU) and the product **23**. By adding DMAP the reaction speed is increased, because DMAP reacts faster with the *O*-acylisourea leading to a "active ester", which can react very fast with an alcohol.[173] In the last step, the *t*Bu protecting group was

removed by treatment with TFA (trifluoroacetic acid) and TES (Triethylsilane) in DCM to obtain the final product **20**. The reaction was done with an overall yield of 60 %.

5.4.2 Synthesis of Cholestamine (15)

The cholesterol derivative **15** was synthesized with the purpose to enable the β-peptides to bind on the surface of a model membrane. The synthesis was carried out after a modified three-step procedure from Sun *et al.* (Fig. 5.5).[174] Starting from

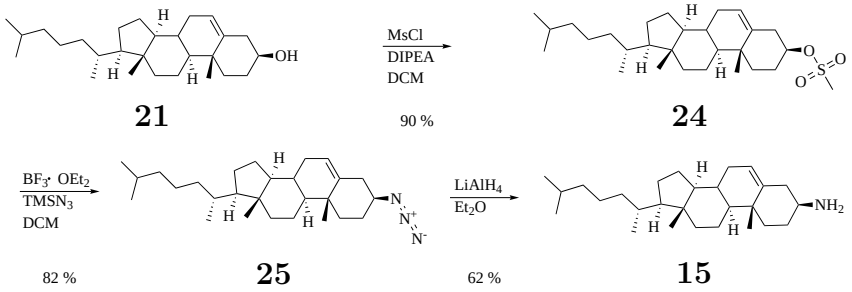

Figure 5.5: Synthesis pathway for **15**. Starting from **21** to the cholesterol OMs derivative **24** and under retention of the stereo information to the azide **25**. The last step was the subsequent reduction of **25** with $LiAlH_4$ to the final product **15**. The yield over three steps was 46 %.

cholesterol **21** the OH-group was transformed by MsCl and DIPEA in DCM, into a better leaving group (mesylate group), to obtain compound **24**. In the second step, the OMs group was converted by a nucleophilic substitution with $TMSN_3$ and the use of $BF_3 \cdot OEt_2$ as a Lewis-acid. After the nucleophilic substitution was performed the subsequent reduction of **25** with $LiAlH_4$ in diethyl ether to yield the final product **15**.

Sun *et al.*[174] pointed out, that a solvolysis reaction during a group-assisted glycosylation reaction with the use of $TMSN_3$ and a Lewis-acid will undergo the retention of the stereo information at the three position during the reaction.[174–176] The assumption of Sun *et al.* was supported by the reports from Shopee[177] and Winstein[178, 179], Shopee and Winstein could show that cholesterol and their reactive derivatives undergo a solvolysis with retention of the configuration at the

three position. During the reaction a nonclassical carbocation (Chol2) is formed by using the neighboring homoallylic alkene (Fig. 5.6).

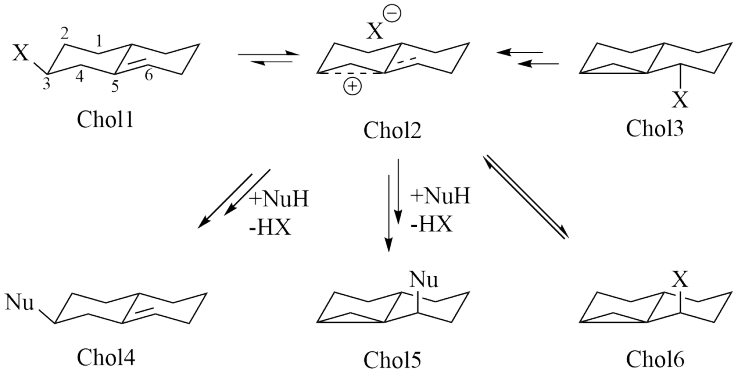

Figure 5.6: The CholX compounds are simplified representations of the cholesterol motif. Starting from Chol1, dissociation gives rise to the ion pair Chol2, which is stabilized by its proximity to the alkene, Chol2 being in equilibrium with Chol1. Chol2 can then react further to form various products. The 6α substituted product (Chol3) or the 6β substituted product (Chol6) can be formed while a ring closure occurs between the 3- and 5-position. The 6α substituted product tends to react back to Chol2 and there is an equilibrium reaction between Chol2 and Chol6. The other two favored reactions are the reaction products Chol4 and Chol5. Chol4 represents the 3β substituted product and Chol5 represents the 3,5-cyclocholestan-6β substituted product.[178]

The formed cation (Mech2) reacts fast at the six position forming the 6β-substituted cyclosteroid in a so called *i*-steroid rearrangement (Mech4). The same cation will undergo a slower reaction at the three position to obtain the 3β-substituted cyclosteroid (Mech3). It was shown by experimental results that the presence of $TMSN_3$ and two eq. of $BF_3 \cdot OEt_2$ are necessary to promote the formation of the desired 3β-substituted product (Fig. 5.7).

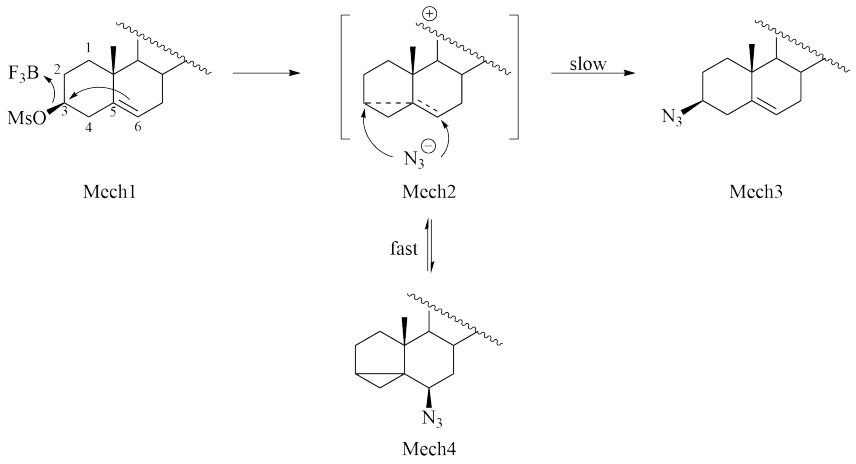

Figure 5.7: The tosylate compound (Mech1) undergoes the formation of a non-classical carbocation due to the influence of $BF_3 \cdot OEt_2$ as shown in the figure before and which is stabilized by the neighboring alkene unit (Mech2). The attack of N_3^- can now occur rapidly by a *i*-steroid rearrangement at position 6 or slowly at position 3. Compound Mech4 and Mech2 are in equilibrium, which is repeatedly shifted by the reaction of Mech2 to Mech3.[174]

5.5 Recognition unit for metal induced aggregation

The recognition units **26** and **27** were synthesized for the metal induced aggregation of the β-peptides on the model membranes. The units were coupled to the β-peptides after the synthesis of the peptide backbone onto a lysine side chain (subsection 13.2.4). The lysine side chain offers, after deprotection, a primary amine, which is suitable for crosslinking with other amino acids or peptide fragments.[180, 181] The recognition units were synthesized with a carbon acid suitable for a coupling reaction at a primary amine of a lysine side chain. During the coupling reactions were treated the recognition units as amino acids. The reactions conditions for all coupling steps were the same. In order to investigate the effect of chains of different lengths, several units were manufactured. Therefore, two of four possible recognition units were successfully synthesized.

5.5.1 5-(4'-methyl-[2,2'-bipyridin]-4-yl)pentanoic acid (26)

The recognition unit **26** was synthesized in a two-step synthesis (Fig. 5.8). Starting from 4,4'-dimethyl-2,2'-dipyridyl (**28**) and 4-Bromobutyronitrile (**29**) the nitrile **30** was synthesized in a nucleophilic substitution. LDA deprotonated the methyl-group to give a lithiated carbon anion, whichs undergoes a substitution reaction with the 4-Bromobutyronitrile under elimination of lithium bromide. The difficult purification of the nitrile **30** was possible by the use of deactivated silica gel[i]. In the second step, the nitrile **30** was hydrolysed with conc. aq. HCl to obtain the final product **26**. The overall yield was 66 %.

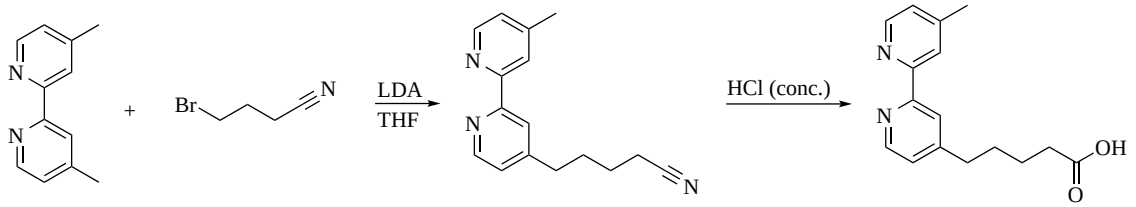

28 **29** **30** **26**

Figure 5.8: Schematic representation of the synthesis of compound **26**. The two-step synthesis starts from the bipyridine derivative **28** and the bromonitrile **29** to obtain the nitrile **30**. In the last step the nitrile **30** was hydrolysed to obtain the final product **26**. The yield over two steps was 66 %.

5.5.2 2-(4'-methyl-[2,2'-bipyridin]-4-yl)acetic acid (27)

The compound **27** (Fig. 5.9) represents a recognition unit with a shorter carbon acid chain in comparison with the other recognition units. The synthesis was done in one step, by deprotonating one of the methyl-groups of **28** to generate a lithiated carbon anion, which was directly converted with $CO_{2(s)}$ to obtain the final product **27**.

[i]TLC plates and silica gel were stores over night in 10 % NEt_3 in *n*-pentane. Before use the plates were dried and the silica gel was washed with *n*-pentane.

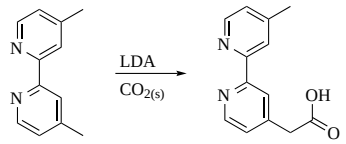

28 70 % **27**

Figure 5.9: One-pot synthesis of compound **27**. **28** is converted in a one-pot synthesis to **27** by reaction between a carbon anion, which attacks CO_2(s). The yield was 70 %.

5.6 *trans*-2-((((9*H*-fluoren-9-yl)methoxy)-carbonyl)amino)cyclohexane-1-carboxylic acid (31)

The cyclic amino acid *trans*-Fmoc-ACHC-OH (*trans*-2-((((9*H*-fluoren-9-yl)methoxy)-carbonyl)amino)cyclohexane-1-carboxylic acid) **31** was used because it is known to induce and stabilize the 14-helix. It could be shown that a peptide consisting of six ACHC moieties already have a stable secondary structure.[120] These advantageous characteristics makes **31** to an excellent candidate for the synthesis of the desired β-peptides. In the following figures ((Fig. 5.10) and (Fig. 5.11)) two different synthetic pathways are presented to synthesize *trans*-Fmoc-ACHC-OH (**31**).

In the first synthetic pathway (Fig. 5.10) cyclohexen **32** reacts with chlorosulfonyl isocyanate (CSI) in DCM to the lactam **33**, which is cleaved by conc. aq. HCl to yield the cis-ACHC-OH **34**. **34** is proctected by Boc (**35**), afterwards esterified (**36**) and converted to the *trans*-isomer **37**. The ester **37** is cleaved (**38**) and the Boc protecting group is removed by HCl (4 M in 1,4-dioxane) (**39**) to yield the final product **31** after Fmoc protection with Fmoc-OSu in 1,4-dioxane/water. The total yield was 10 % over 8 steps.[182–185]

The second synthesis pathway (Fig. 5.11) follows a different approach. Starting from **40** the stereoinformation is introduced by the amine **41** as a chiral auxiliary. The double bond of **42** is reduced by $NaBH_4$ and isobutyric acid in toluene to yield the racemate **43**. Compound **44** is obtained by racemic resolution of **43** by

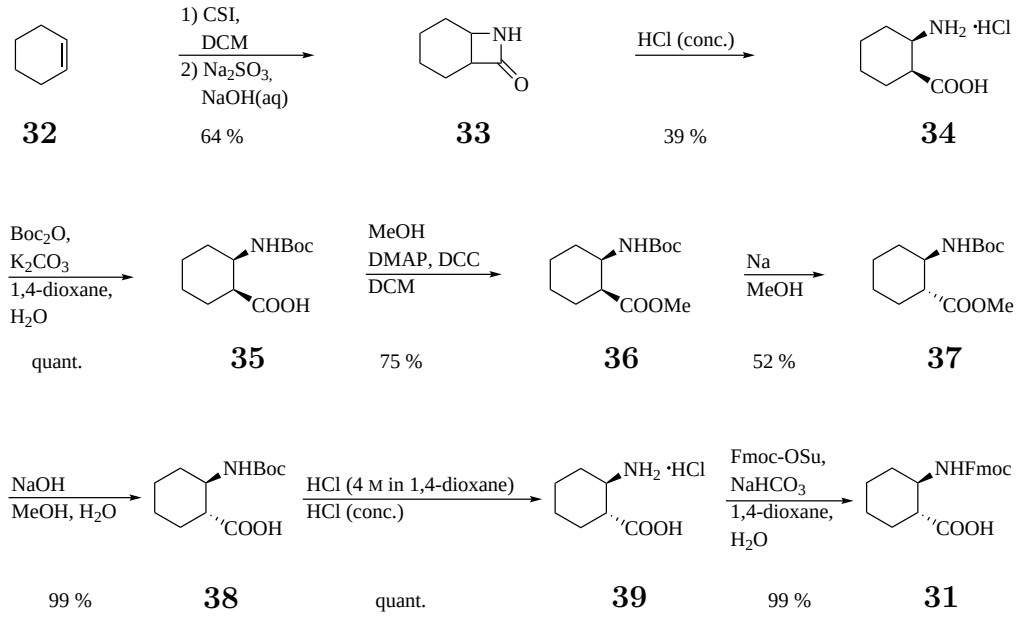

Figure 5.10: Synthesis of compound **31** (Path A). The yield was 10 % over 8 steps.[182–185]

precipitation with a HBr solution in acetic acid. After removal of the bromide salt with $NaHCO_3$ (**45**) an other racemate is created at the carbon attached to the ester group (**46**). The isomers are seperated by precipitation of the *trans*-isomer **47** with HCl (4 M in 1,4-dioxane). Cleavage of the ester (**48**) and the chiral auxiliary yield the unprotected amino acid **16**. In the final step, the target product could not be obtained. The total yield (excluding the final step) was 7 % over 8 steps.[120, 186, 187]

If both options are compared, it is noticeable that both have similar number of steps (8 vs 9) and have a similar outcome in respect of the total yield of 10 vs 7 %. However, only the first shown synthetic pathway delivered the target product. On the one side this fact is a clear advantage, one the other side it should be discussed the stereochemical purity or outcome in the first synthetic pathway. In the first synthetic pathway, the stereoinformation is generated upon a regio- and stereoselective[188] ring opening, accordingling to the Markovnikov rule[189], to the compound **34** and the mandatory stereoselectivity is obtained by base catalyzed epimerization to **37**. Purification of **37** is achieved by recrystallization from *n*-hexane.[182, 183] This synthetic pathway completely lacks an auxiliary that provides the stereo information,

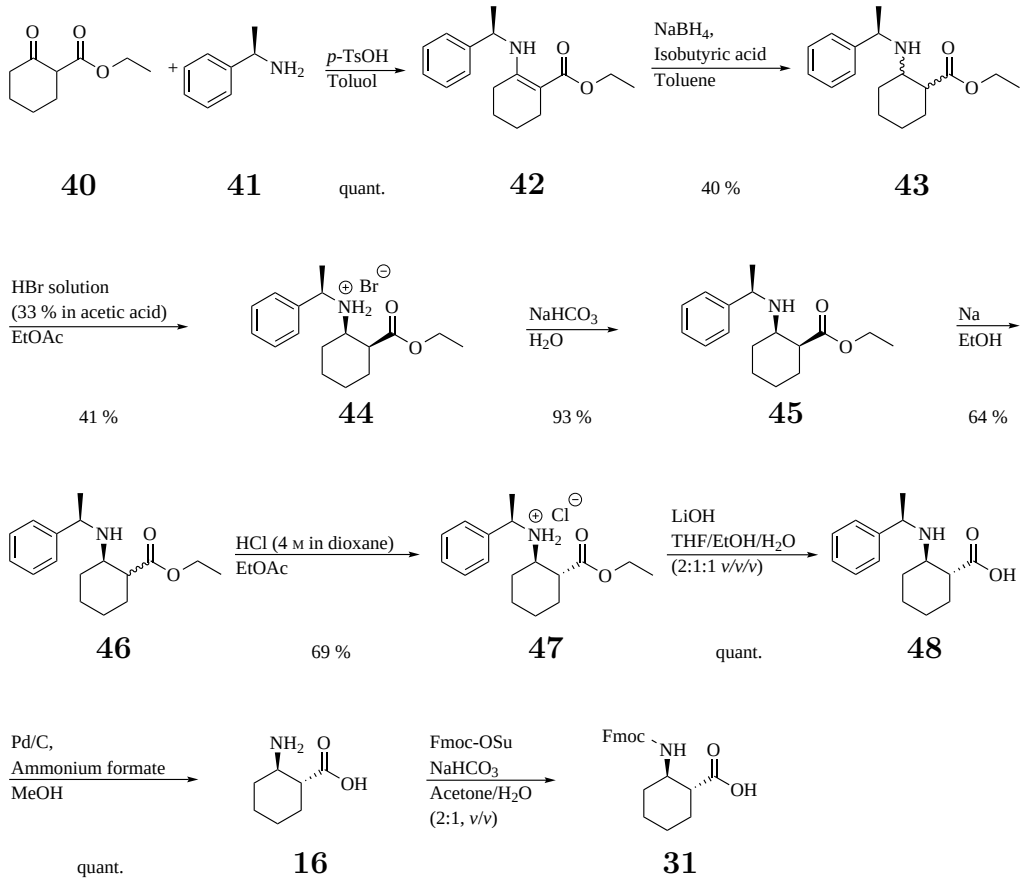

Figure 5.11: Synthesis of compound **31** (Path B). The yield was 7 % over 8 steps.[120, 186, 187]

as is the case in the synthetic pathway B. Despite this "drawback", it has been shown by Gellman[190] experimentally that synthesis via path A can successfully present the target molecule. Combined with the higher yield and the smaller number of stages makes the first pathway to the favorite.

6 Design and Synthesis of the β-peptides

The next chapter describes the process of finding the right design, to fulfill the necessary tasks and properties, which are demanded by the β-peptides. The tasks and properties of the β-peptides are given and serve as the starting point to find a design that fits all purposes.

6.1 Design of the β-peptides

The summarized tasks of the β-peptides are the metal induced aggregation of the β-peptides, the interaction with the surface of a model membrane and the β-peptides should show a good solubility in organic and aqueous media. To fulfill all these tasks a reliable model system with predictable properties is needed. Such a model system e. g. to mimic α-peptides can be found in the β-peptides. As mentioned earlier β-peptides can occupy different secondary structures, which are all well-known and well-predictable. The chosen secondary structure was the 14-helix with their superior properties, for example the fact that one turn consists of three amino acids. This results in a stacking effect of every third amino acid and makes it possible to divide the outside of the peptide helix in three helical interfaces (Fig. 6.1). The helical interfaces can be modified to introduce peptide modifications to influence the properties of a given β-peptide. Two of the helical interfaces were modified with the bipyridine derivative **26**, which serves as a recognition unit for the metal induced aggregation of the β-peptides. The last helical interface was modified with side chain-bound cholestamines, which act as a lipid anchor to induce

the interaction between a β-peptide and the surface of a model membrane. The two recognition units are distributed at different helical interfaces and at least divided by three turns from each other. The lipid anchor(s) are placed on the same interface, but are also divided by multiple turns of the helix. The recognition unit is bound to the side chain of a ^{h}Lys(Mtt) and the cholestamine is bound to the side chain of ^{h}Glu.

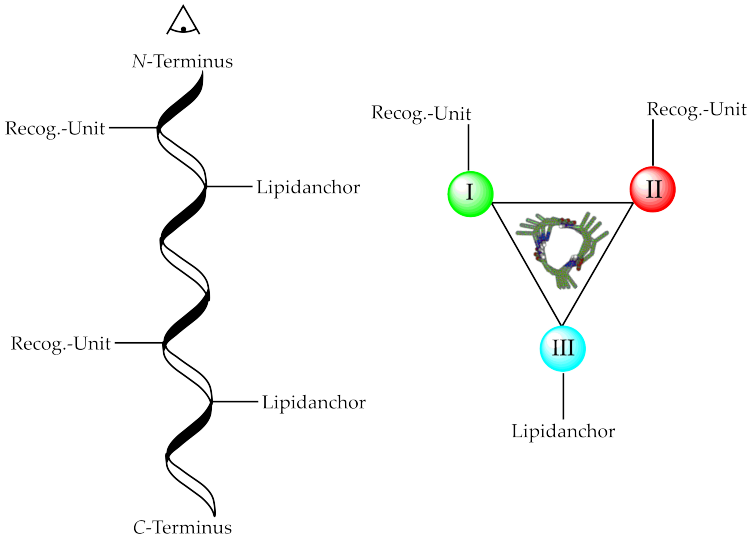

Figure 6.1: Schematic depiction of the three helical interfaces and the distribution of the recognition units and lipid anchors.

Regarding the length of the β-peptides, all synthesized β-peptides should be as short as possible. The designed sequences contained a combination of *trans*-Fmoc-ACHC-OH, ^{h}Lys(Mtt), ^{h}Lys(Boc), ^{h}Val, ^{h}Glu and/or β-glycine. The used β^3-amino acids are known to promote and stabilize the wanted 14-helix. Especially *trans*-Fmoc-ACHC-OH is known for this fact. The used ^{h}Lys(Boc) has the additional property to make the β-peptides more hydrophilic and increases the solubility. The positive charge at the side chain of the lysine should prevent that the β-peptides completely dip into the model membrane. Additionally, the helical interfaces should have an alternating sequence of polar and non-polar amino acids.

The exact position of the used β^3-amino acids changed and evolved from peptide generation to peptide generation. The first generation of synthesized β-peptides was **P-49** (Fig. 6.2), which contained a combination of *trans*-Fmoc-ACHC-OH, ^{h}Lys(Mtt),

^{h}Lys(Boc) and ^{h}Glu. The ^{h}Lys moieties were not evenly distributed among the three helical interfaces. The interface of the lipid anchor should be hydrophobic to promote and ensure, that the β-peptides are immersed in the model membrane. To comply with all requirements a larger number of ACHC was incorporated in the β-peptides. That results in a dipolar-like structure within the β-peptide, with two helical interfaces, that are more hydrophilic and one helical interface, which is very hydrophobic. As *N*-terminal modification was used Oregon Green 488 (OG488) as fluorescence probe for further measurements. To introduce the other peptide modifications the *N*-terminus must be temporarily protected. The terminal Fmoc-group of the last amino acid does not fit all conditions during the synthesis, it was observed that the open primary amine after the Mtt deprotection is able to remove the Fmoc-group. The idea was to introduce as first step the fluorophore followed by the other modifications. OG488 showed, that it is not fully compatible with the conditions during the other peptide modifications, what made it necessary to introduce another protecting group which is orthogonal to the existing PGs. To solve this problem the *p*-Nitrobenzyloxycarbonyl (pNZ) PG was introduced. That means, that the last β^3-amino acid was pNZ-β-Gly-OH. The deprotection of the pNZ PG is fully orthogonal to Mtt, Fmoc, Boc as well as OAllyl and vice versa.

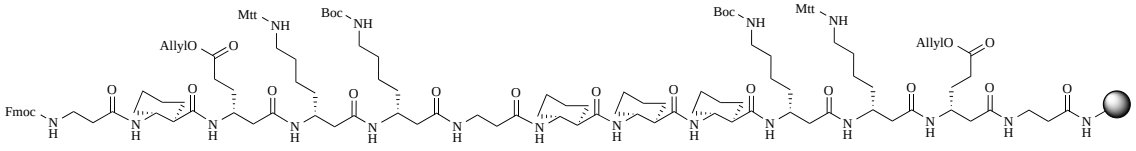

49a

Figure 6.2: Structure of the solid-support bound precoursor β-peptide **P-49a** for the final β-peptide **P-49**.

In the next generations of β-peptides, the peptides were elongated and the primary structure was refined (Fig. 6.3). One big problem was that the previous β-peptides were overall to hydrophobic. The influence of the cholestamine moieties and the ACHC could not be compensated by the few lysines. The strong hydrophobic character of the β-peptides (**P-50**, **51**, **52**, **53** and **54**) promoted an outstanding behavior in regards to the interaction with the surface of the model membrane, but the downside was that these β-peptides disturb the membrane integrity. To overcome this

problem the β-peptides had a greater number of β^3-amino acids and the content of polar β^3-amino acids were increased. This second generation of β-peptides evolved in the right direction, but still showed a very hydrophobic character in all measurements. It was decided to further increase the content of hydrophilic amino acids. At two positions in the primary structure of the β-peptide **P-55** were incorporated two aspartic acids. With the negative charge at the side chain, the hydrophobic character of the β-peptide should be countered, the hydrophilic character should be increased, which should lead to a better solubility. The interaction between the negative charge of the aspartic acid and the positive charge of the lysines results in a salt bridge, which should stabilize the secondary structure. The solubility was increased, but the β-peptide stopt working in the way they should. It could be shown, that the β-peptides did not bind any longer to the surface of the model membrane and with no interaction between the β-peptides and the model membrane, the β-peptides did not disturb the membrane integrity any longer.

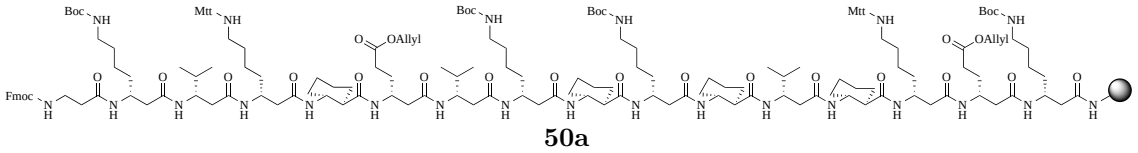

50a

Figure 6.3: Structure of the solid-support bound precoursor β-peptide **P-50a** for the final β-peptides **P-50**, **51**, **52**, **53** and **54**.

For the last generation of synthesized β-peptides (**P-56**, **57**, **58** and **59**), the previously introduced aspartic acid and ACHC moieties were removed and exchanged for more ^{h}Lys and ^{h}Val moieties, respectively (Fig. 6.4). Additionally, the ^{h}Lys moieties were distributed evenly over all three helical interfaces. These β-peptides showed the wanted behavior in regards to the solubility, the interaction with the model membrane and less tendency to disturb the membrane integrity.

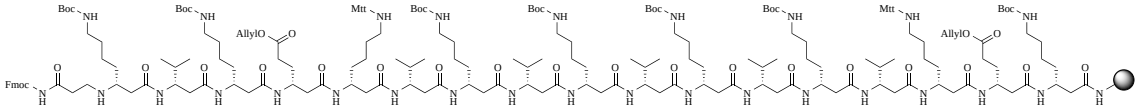

56a

(a) Structure of the solid-support bound precoursor β-peptide **P-56a** for the final β-peptides **P-56** and **58**.

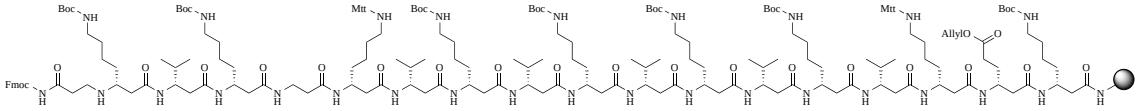

57a

(b) Structure of the solid-support bound precursor β-peptide **P-57a** for the final β-peptides **P-57** and **59**.

Figure 6.4: Overview of the design for the β-peptides **P-56**, **57**, **58** and **59**

6.2 Synthesis & Purification of the β-peptides

All β-peptides were synthesized after the solid-phase peptide synthesis (SPPS) as described by Marrifield.[191, 192] The Fmoc/Boc-protocol for SPPS was first published in 1978 by Meierhofer and Shepard and though previous works in our group the Fmoc-based synthesis of α-peptides and β-peptides already has been established and refined.[193–195] The synthesis of peptides has some advantages over the peptide synthesis in solution. While the peptide chain will be elongated the peptide is bound to the solid-support and the excess of all reagents can be very easily washed away. During the final cleavage of the peptide from the solid-support can cause the removal of the side chain protecting groups. In the Fmoc-SPPS the standard side chain protecting groups are the acid-labile *tert*-butyloxycarbonyl (Boc) or 4-methyltrityl (Mtt) group. Both groups will be removed during the acidic conditions in the cleavage process. For the cleavage a mixture of TFA/water/TIS (95:2.5:2.5 *v*/*v*/*v*) is used.

The synthesis were carried out under semi-automatically standard microwave-assisted procedures in a BD-syringe equipped with a PE-frit. The synthetic procedure for all synthesized β-peptides is depicted in the following figure (Fig. 6.5) (for experimental details see Section 14.7). For the synthesis of β-peptide **P- 49**, a

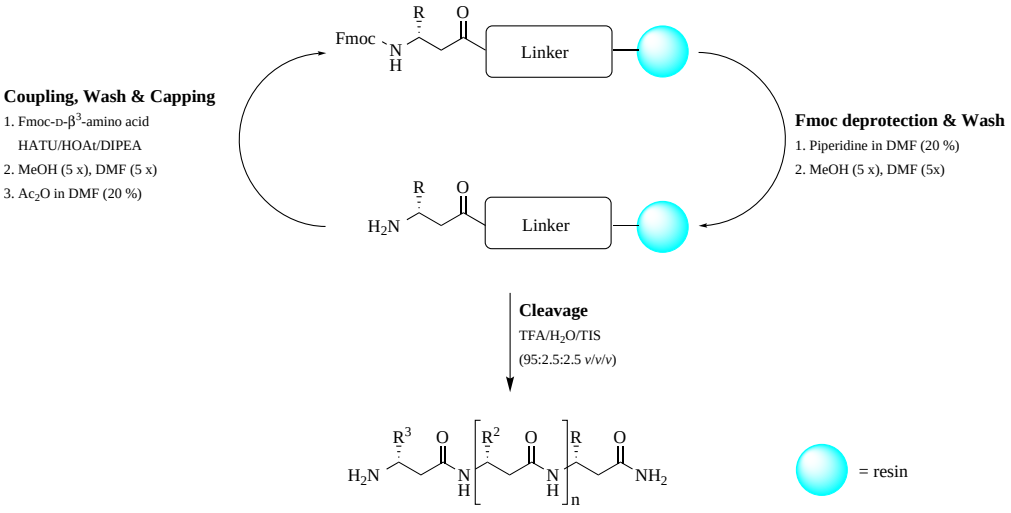

Figure 6.5: Synthesis of the β-peptide backbone using Fmoc/Boc-SPPS.

rink amide MBHA resin with a relativ high loading of 0.57 mmol g^{-1} was used. For the synthesis was used amongst other β^3-amino acids (3*S*)-3-((((9*H*-fluoren-9-yl)methoxy)carbonyl)amino)-4-cholesterol-4-oxobutanoic acid (**20**). Test cleavages and mass spectrometric analysis showed formation of the β-peptide, but without the mentioned building block **20**. It seems that, the coupling is aborted after the first β^3-amino acid so the loading of the resin was checked. The first check was done with the stock resin, the second check was done after the coupling of the first β^3-amino acid and than after the coupling of the building block **20**. The check of the loading showed, that the coupling of the building block **20** was almost incomplete. It was tried to improve the coupling step by variations of the conditions (Tab. 6.1). It was tried to use different coupling reagents, different coupling times and temperatures during the coupling step and a NovaPEG Rink amind resin as a low loaded resin. It is known from literature, that low loaded resins are prior to use for hydrophobic peptides. Overall the coupling efficiency could be improved by varying the coupling reagents and particularly through the use of a low loaded resin, but the coupling efficiency, was not satisfactory.

Table 6.1: A selection of different conditions during the coupling step and the resulting coupling efficiency.

Coupling Reagents	Coupling efficiency [%]
HATU/DIC	~10
HOAt/DIC	~10
PyBob/DIPEA	~33
PyBrBob/DIPEA	~44
COMU/DIPEA	49–52

With these results a change in the strategy for the synthesis of the β-peptides was needed. The idea was to incorporate the recognition unit and the lipid anchor after the synthesis of the β-peptide backbone. With this said a total new protecting group strategy became necessary. The protection group strategy had to fulfill different general conditions:

- Use of the Fmoc chemistry for the synthesis of the backbone
- All other protection groups have to be orthogonal to the Fmoc chemistry
- The used side chain protecting groups have to be orthogonal to each other to selectively deprotect the different side chains in the backbone

To meet all conditions, it was chosen the Fmoc group as protecting group for the α-*N* position, Boc and Mtt for the side chain of the lysines and the OAllyl group for the binding spot of the lipid anchor. The conditions during the synthesis of the β-peptide backbone are orthogonal to all chosen protecting groups. Boc and Mtt are cleaved under acidic conditions, while OAllyl is cleaved under Pd(0) catalysis. Boc and Mtt are pseudo orthogonal to each other. Mtt can be cleaved under mild acidic conditions (~1 % TFA in DCM) in presence of a Boc group, but not vice versa. The same restriction have to be made for the combination of the Fmoc and OAllyl group. The Fmoc group is cleaved under basic conditions (20 % piperidine in DMF) in presence of a OAllyl group, while the conditions for the cleavage of a OAllyl group, in presence of a Fmoc group, causes an uncontrolled lost of the Fmoc group.

As mentioned earlier, the recognition unit and the lipid anchor should be incorporated in the β-peptides after the synthesis of the peptide backbone. The recognition unit should be attached to the lysine with the Mtt protected side chain and the lipid anchor to the OAllyl modified side chain of a glutamic acid (**7**). To divide the attachment points by their functional groups provides an additional orthogonality and a higher flexibility. The used glutamic acid has a second advantage with the elongated side chain, in comparison with the Asp building block. The elongated side chain offers more space between the β-peptide backbone and the lipid anchor.

The order of deprotection and introduction of the modifications is determined by your own selection. You only have to keep in mind, that the OAllyl group can not be deprotected without the uncontrolled lost of the *N*-terminal Fmoc group. To overcome this problem the *N*-terminus either way was deprotected and modified with NBD, the *N*-terminus was capped with acetic anhydride (20 % in DMF) or the last amino acid was *p*NZ-Gly-OH. The Mtt group was cleaved with HFIP/DCM/TFE/TIS (6.5:2:1:0.5, *v*/*v*/*v*/*v*) within an hour. The OAllyl group was cleaved under microwave irradiation for 2 × 5 min at 38 °C in DCM with $Pd(PPh_3)_4$ (0.25 eq) and $PhSiH_3$ (15.0 eq).

After the deprotection of the Mtt- respectively OAllyl group. The peptide modifications could be incorporated. Both peptide modifications are introduced by forming an amide bond between the peptide backbone and the modification itself. The amid bond was chosen because, this bond is known to be very stable even against the very harsh conditions during the final cleavage. Alternative, a ester or ether bond would be possible too, but these bonds are less stable against some of the used conditions during the synthesis. The recognition unit was treated and coupled like any other β^3-amino acid during the coupling steps. The recognition unit was dissolved in DMF, preactivated with HATU/HOAt and DIPEA and heated (65 °C) under microwave irradiation. The recognition unit was double coupled to ensure a complete saturation of all attachment points. The lipid anchor was dissolved in as little as possible DCM and mixed with an excess of DMF without any participation of the cholestamine. The open carboxylic acid on the resin was preactivated with COMU/DIPEA in DMF till a deep red color occurred (~3–5 min). The dissolved lipid anchor was added to the resin and shaken for one hour at rt. All

deprotection and modification steps were controlled and monitored by UHPLC and HR-MS.

The β-peptides were purified by semipreparative RP-HPLC. For all β-peptides without a cholestamine was used a C-18 column with MeCN in different gradients as organic phase. First, the β-peptides with cholestamine were also tried to purify with a C-18 column, but the peptides could not be recovered after the purification step. It was assumed that the β-peptides with the cholestamine, were to hydrophobic, they stick to the column and are not eluted or highly diluted, while eluted by the organic phase. The change to a C-8 column lowered the interactions between the column material and the β-peptides. With this improvement it was possible to elute the β-peptides with a high gradient of the organic phase. The HPLC chromatograms show for each β-peptide sharp peaks with an good till excellent peak separation. For detailed information please see the experimental part Section 14.7.

Part IV

Analysis

The following part deals with the analysis and interpretation of the performed investigations of the synthesized β-peptidesȦfter the discussion about the "Design and Synthesis" (see chapter 6) of the used β-peptides we are going to have a closer look on the properties and functionalities of the synthesized β-peptides. As discussed in the chapter "Design and Synthesis", the secondary structure is very important and forms the basis for the further analysis. CD spectroscopy was used to determine the secondary structure in solution. Afterwards, the metal induced aggregation of the β-peptides was measured by UV/Vis titrations. In addition, the interaction between the β-peptides and the surface of model membranes was examined via different FRET-based fluorescence measurements.

7 CD-Spectroscopic characterization of the synthesized β-peptides

7.1 Introduction

In order to investigate the secondary structure of peptides and proteins in solution or lipid bilayers, different methods like X-ray crystallography, molecular dynamic simulation studies as well as NMR- or CD-spectroscopy were used.[5, 112, 122, 196–199] Especially the CD-spectroscopy is a well-known, established and a common method.[200] This method is based on the differential absorption of right- and left-handed circularly polarized light by optically active molecules like peptides (or β-peptides) and proteins. One can imagine that planar polarized light consists of two circularly polarized components of the same order of magnitude. One component moves clockwise (R) while the other component moves counterclockwise (L). If the light now moves through a medium with a chiral center, the two components L and R are absorbed to different extents, this is called circular dichronism. The light is elliptically polarized after passing through the chiral medium.[201] For more details please see the next section (Section 7.2).

The interest of Seebach *et al.* was aroused by experimental results, that show a replacement of α-amino acids in α-peptides at a specific position with β-amino acids can improve the stability against certain peptidase and shows an improvement of the biological activity.[112, 202–206] With this background Seebach *et al.* started to investigate the influence of β-amino acids in β-peptides on the structure of the

peptides. The group around Seebach used a set of α- and β-peptides with the generel pattern of $(Val\text{-}Ala\text{-}Leu)_2$ for their analysis.[112]

Seebach received from the CD measurements of the analyzed β-peptide a different and unexpected CD pattern in comparison to the CD pattern of α-hexapeptide. The β-peptide shows a maximum at 198 nm and a minimum at 216 nm, where against the α-hexapeptides show no further defined secondary structure (Fig. 7.1). To verify the characteristic signals from the CD measurements Seebach *et al.* performed several structural analyses to compare the results from the CD measurements with the measurements from NMR and X-ray crystal structure analysis.[112] From X-

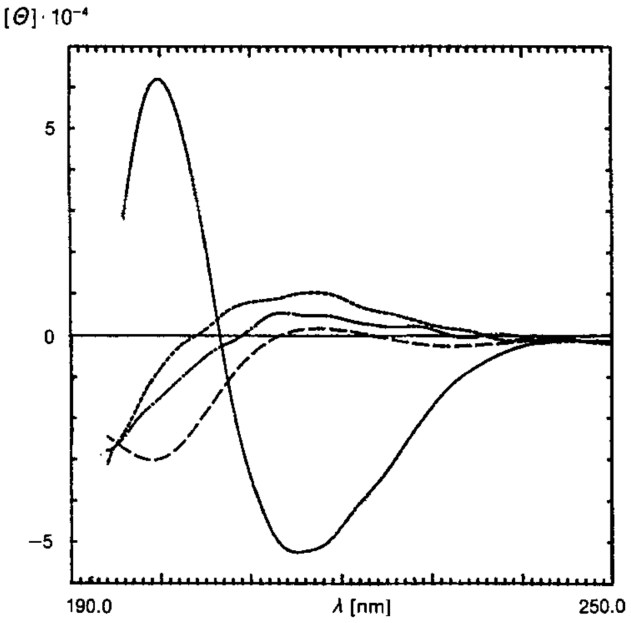

Figure 7.1: Comparison of the CD spectra of different β-peptides with a defined set of α-peptides. The black solid line shows the mentioned β-hexapeptide and the dashed line represents the corresponding α-hexapeptide.[112]

ray crystal structure analysis was found that α-peptides prefer to occupy a β-sheet conformation.[23] The group of Seebach found that their β-hexapeptides form 14-membered rings and that the β-peptides tend to form turns like spirals or helices. In further analysis, this assumption was confirmed by NMR using various NMR techniques ((Fig. 7.2)). These measurements confirmed the 14-membered ring and that the analyzed β-peptides occupy helical structures.[112] With this and the further work of Seebach *et al.* it could be shown that β-hexapeptide form stable and

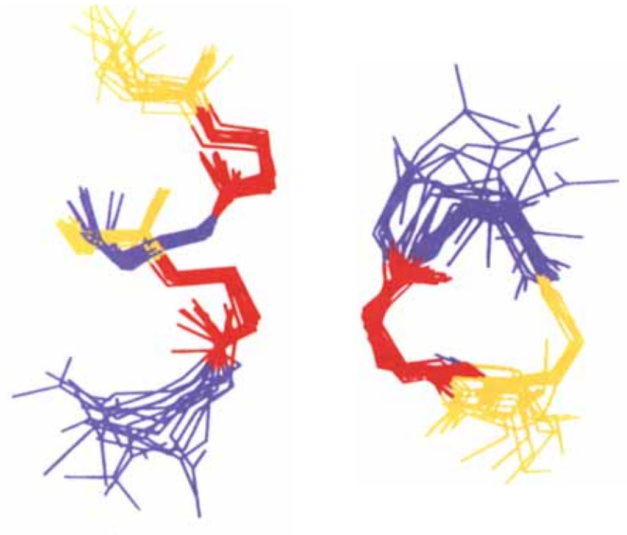

Figure 7.2: Depicted is the side- and top-view of the formed 14-membered ring of the β-hexapeptide from SEEBACH *et al.* The colors represent each of the used β^3-amino acid, yellow = Val, red = Ala and purple = Leu. The side chain residues are omitted.[112]

well defined left-handed 14-membered helices. Based on this work from SEEBACH *et al.*[121] the secondary structure can be analyzed and characterized by their typical CD pattern which differs significantly from the CD pattern of similar α-peptide even if these peptides consist of more amino acids.[112, 123]

7.2 Basics of CD spectroscopy

A growing demand of the structural biology is a fast and reliable method to determine the structure of proteins. Often is used the X-ray crystallography to describe the structure, therefore crystals of the peptides/proteins were needed. A big drawback is that crystals of these biomolecules often does not represent their active state neither their natural environment.[200] Under these circumstances the CD spectroscopy gained more and more interest, because it is possible to measure the structure and even rates of structural changes of proteins due to changes in the temperature, mutation or denaturation.[207] These measurements can be carried out in solution or under conditions in which proteins operate.[200] This opportunity gives the chance to analyze all kind of different proteins or peptides. The chromophores of

the amid bond of these polypeptide backbones results in an optical absorption due to the fact that the proteins are aligned and are forming their specific secondary structure. As a result, it can be observed that different structures are resulting in characteristic CD spectra (Fig. 7.3).[207] For example, peptides which occupy

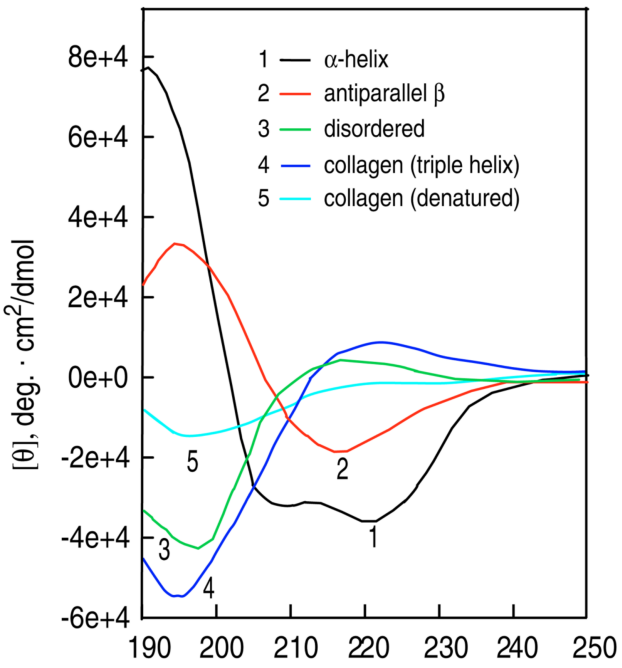

Figure 7.3: Overview of different secondary structures of poly-L-Lysine shown in black (pH =11.1, α-helical), red (anti-parallel β-sheet) and green (pH = 5.7 extended conformation). For comparison two other secondary structures of collagen are shown in blue (triple-helix) and cyan (denauturated).[207]

a β-helical structure (antiparallel β-pleated sheets) show characteristic absorptions bands at 218 nm (negative band) and 195 nm (positive band). Another example are the α-helical proteins which show their absorptions bands at 222 nm, 208 nm (both negative) and 193 nm (positive).[207]

The origin of these observations is the so-called CD-effect, the CD-effect describes the property of a (bio)molecule to absorb right and left polarized light to a different extent. Plane polarized light is viewed consisting of two circularly components with the same magnitude (Fig. 7.4).[201] One component is rotating clockwise (R) and the other one is rotating counter-clockwise (L). An CD signal can be observed if the R or L part of the circular polarized light is absorbed to a dif-

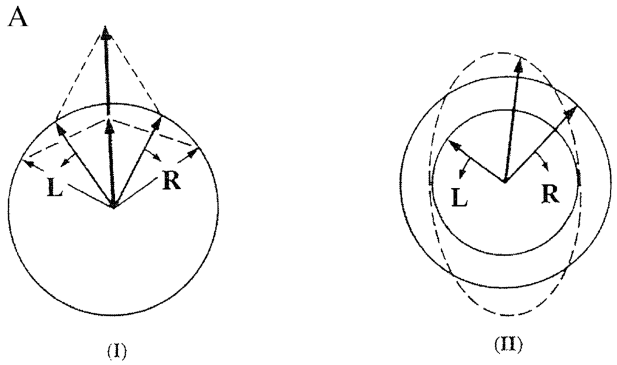

Figure 7.4: Depiction of the origin of the CD-effect, with the left (L) and right (R) polarized components of the plane polarized light. On the left half of the picture is shown, that both components have the same amplitude and when both components are combined they result in a plane polarized radiation. On the other half the same components have a different amplitude, when both components are combined they result in an elliptically polarized radiation.[201]

ferent extent after passing through the sample. To absorb one of the two components in a different extent the chromophore has to be chiral. This can be achieved through[200]:

1. the chromophore is chiral based on its structure
2. the chromophore is directly linked to a chiral center
3. the chromophore has a position in an asymmetric environment due to the spatial structure of the molecule

After the light has passed the sample both components would recombine and in case of an CD-effect the light would be elliptically polarized (Fig. 7.4). In practice, a CD instrument would detect R and L independently from each other in dependence from the wavelength. The difference between R and L can be viewed as difference in the absorption of R and L ($\Delta A = A_{\mathrm{L}} - A_{\mathrm{R}}$). In the most cases the difference is depicted as the ellipticity (θ) as a function of the wavelength.[200, 201]

7.3 Experimental setup for the CD-Spectroscopy

With the CD-spectroscopy the secondary structure of all synthesized β-peptides was examined in different solvent systems, both in organic and aqueous media. The solvents were selected for each β-peptide in dependence of the solubility of the respective β-peptide. For example, **P-49** was soluble only in organic solvents, whereas the β-peptides **P-56**, **P-57**, **P-58** and **P-59** were soluble in organic and aqueous media. The solvent plays an important role for the CD-spectroscopy, interactions between the helix and the solvent can stabilizes the secondary structure, as it is known for methanol and TFE.[208–210] Furthermore, Hamuro *et al.* have shown that a micellar environment strongly stabilizes the secondary structure, too.[211]

The experimental details are given in the chapter 12 and in the Tab. 12.4. If not other stated the β-peptides were measured with a concentration of 30 μM.

7.4 Results of the CD-Spectroscopy

The CD-spectra of all synthesized β-peptides show a comparable curve to the results from Seebach *et al.* indicating, that all β-peptides occupy a right-handed 14-helix in solution. For a better overview only, the CD-spectra of **P-56**–**59** are discussed as an example. The CD-spectra of the other β-peptides are shown in the appendix, there maxima and minima are summarized and compared in the following table (Tab. 7.1).

The CD-spectra of the synthesized β-peptides **P-56**–**59** (30 μM) were recorded in solutions of MeOH, TFE, water and PBS-buffer. The respective spectra show a pattern with the minima in a range from 195–200 nm, the maxima at ~215 nm and a zero-crossing at ~203 nm. The deviations between the used solvents for each

β-peptide are minimal. The intensities of the CD signals are highest for all four β-peptides in the organic solvents.

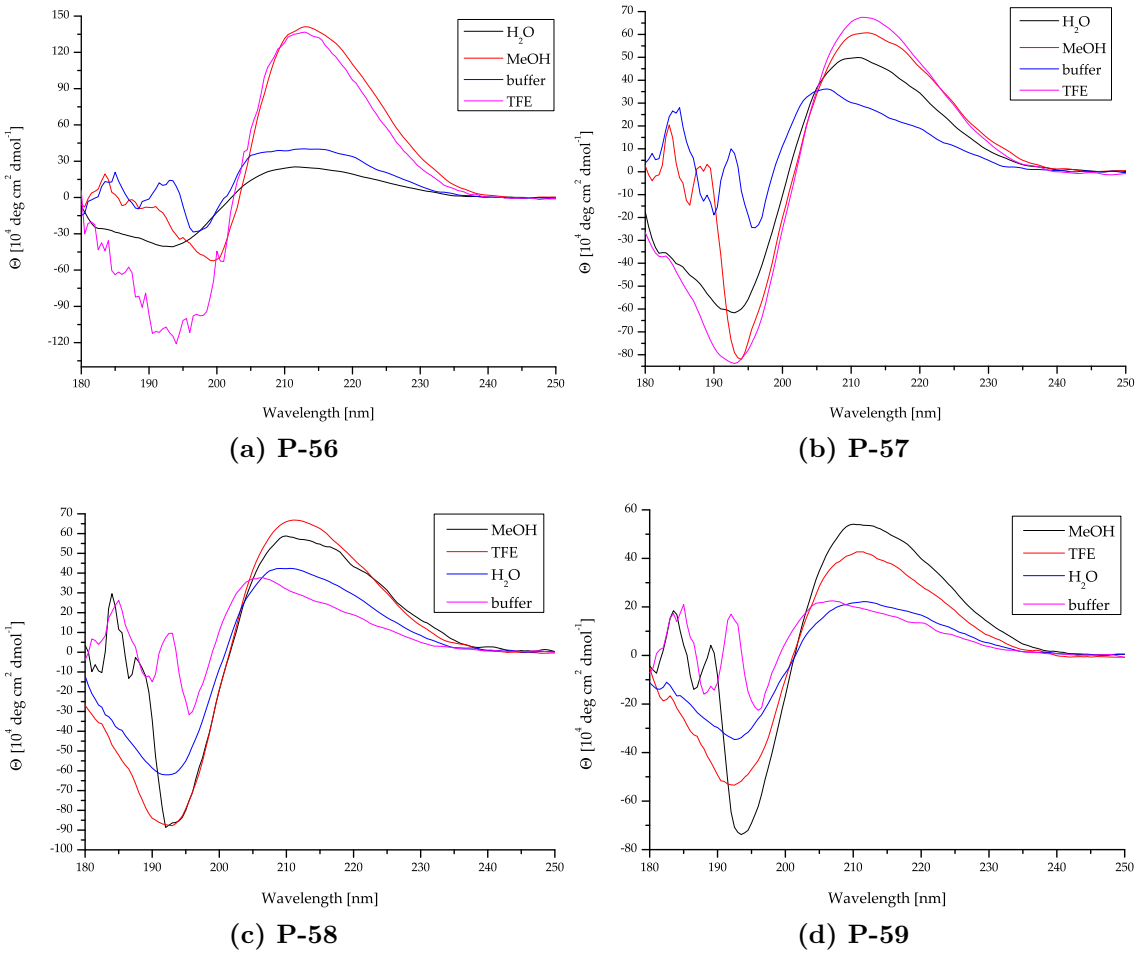

(a) P-56 **(b) P-57**

(c) P-58 **(d) P-59**

Figure 7.5: Overview of the CD-spectra for the β-peptides **P-56**, **57**, **58** and **59** (each 30 μM) in different solvent systems.

Table 7.1: Analytical data of the CD measurements from the synthesized β-peptides in different solvent systems. The CD spectra are shown in the appendix.

β-peptide **P-** \ Solvent system		MeCN	MeOH	TFE	H_2O	buffer
49	Maximum	215	\	\	\	\
	Minimum	195				
60	Maximum	\	215	\	209	\
	Minimum		193		190	
61	Maximum	\	211	\	213	\
	Minimum		192		193	
50	Maximum	\	214	212	\	\
	Minimum		196	190		
51	Maximum	\	214	211	\	\
	Minimum		195	193		
52	Maximum	\	214	212	\	\
	Minimum		194	190		
55	Maximum	\	205	203	214	\
	Minimum		195	190	195	
62	Maximum	\	204	202	215	\
	Minimum		194	190	193	
56	Maximum	\	213	213	212	212
	Minimum		200	194	194	197
57	Maximum	\	212	212	211	206
	Minimum		195	193	193	196
58	Maximum	\	210	211	210	207
	Minimum		193	193	192	196
59	Maximum	\	211	211	211	206
	Minimum		194	193	193	196

8 Metal induced aggregation

8.1 Introduction

The analysis and verification of the assumption with regard to the secondary structure was discussed. The correct secondary structure forms the basis of the following metal induced aggregation of the β-peptides. The aggregation was examined by UV/Vis titrations and for this purpose, the synthesized β-peptides were modified with the recognition unit **26**. The usage of **26** has two advantages: first, the bipy-derivative can be used as a binding unit between the β-peptides due to the aggregation. **26** is a derivative from the well-known 2,2'-dimethyl-4,4'-biprydine, which is prone to form very stable complexes with different transition metal ions like $Fe^{2+/3+}$, Cu^{2+} and Ru^{2+}.[20, 212–214] The high stabilities and binding affinities of the metal ligand complexes afforded by nitrogen containing multidentate ligands is caused by the chelating effect and the π-acceptor character of the ligands.[215]

The second advantage is, that the unit **26** induce the aggregation and is simultaneously able to me monitored by UV/Vis. This leads to a deeper insight into the degree of complexation between the unit(s) **26** and the metal ions. This can be implemented, because **26** is sensitive in the presence of metal ions. To be more precise, this means that the UV/Vis absorption properties change with the degree of metal complexation. Therefore, the metal complexation results in a distinct red-shift of the main absorption band due to a $\pi - \pi^*$ transition.[216]

To investigate the metal ion complexation ability of the engineered β-peptides and the stoichiometry between the β-peptides and the metal ions, UV/Vis measurements were applied. To analyze the molar ratio of the metal ions to β-peptides, UV/Vis

titrations were performed in organic or aqueous solvent systems. The change of the absorption profile in presence of various metal ion concentrations was measured. The used metal ions were Fe^{3+}, Cu^{2+} and Zn^{2+}, which were added in distinct amounts to a known concentration of the β-peptide. By continuously changing the concentration of the added metal ions and constant concentration of the β-peptide during the titrations could the change of the UV/Vis absorption bands be observed. Introduced by the presence of metal ions, the original absorption band of the recognition unit **26** moved from 280 nm to over 300 nm by decreasing the intensity at 280 nm and increasing the intensity of the two new maxima. Subsequently, the obtained data was plotted as a function of the wavelength with dependence of the metal concentration and the obtained data was converted into a Job-Plot.

8.2 The Job-Plot

The Job-Plot, often called "'method of continuous variations"', is a method, which is often applied in the organometallic chemistry. This technique provides an insight into the stoichiometries of associations between m molecules of L and n molecules of M. The simplest way to illustrate this, is the following equation:

$$m\mathrm{L} + n\mathrm{M} \overset{K}{\rightleftharpoons} \mathrm{L}_m\mathrm{M}_n \tag{8.1}$$

The complexation can be probed by holding the concentration one component, i. e. L, constant and varying the concentration of the other component while monitoring a physical property, as a substitute (here the wavelength λ). When all molecules of L are consumed by M, it is called saturation.[217, 218]

Another way to set up a Job-Plot, is to keep the total concentration or the amount of substance constant and varying L and M relative to each other. In such a Job-Plot is not any longer the concentration of L or M plotted against a physical property, the concentration is transformed into the mole fraction of L or M (χ_L). The physical property could be any observable effect, which correlates linearly with the concentration of $\mathrm{L}_m\mathrm{M}_n$. This could be an NMR resonance signal[219] , conductivity[220]

, a specific signal in the circular dichroism[221] and/or with special regards to this topic, a UV/Vis[222] absorption.

The Job-Plot provides an easy and powerful tool to extend the interpretation of already existing analytical data. As a result, the Job-Plot gives a graphical answer to the question of the relative stoichiometries of the formed metal-β-peptide L_mM_n-complex. Furthermore, the shape of the curve provides an insight into the binding constant K. Is $K \gg 1$ the curvature is more like a perfect triangle, that means that the formation of the L_mM_n-complex is fast. Is $K \ll 1$ takes the curvature a gentler trend, the formation of the L_mM_n-complex is slower. With all the advantages provided by the Job-Plot, some aspects have to be kept in mind. For example, there is no consistent method for the calculations and fittings behind the Job-Plot, there is always some room to interpret the results in anyone's favor. Furthermore, the Job-Plot gives no insight into the exact stoichiometries of the L_mM_n-complex. It cannot be distinguished between LM, L_2M_2 nor L_3M_3, this means all three complexes would yield the same Job-Plot.

8.3 UV/Vis-measurements

First, the metal binding for **P-49** was examined. For the measurements, four different metal salts were used, two zinc and two copper salts: $ZnBr_2$, $Zn(NO_3)_2$, $CuCl_2$ and $Cu(ClO_4)_2$. Zinc and copper were used because they are known to form very stable complexes with the recognition unit **26** and because of their important role in biological systems. Furthermore, the usage of metal salts with different counterions enables the observation of their respective upon complexation.

P-49 and all salts were individually dissolved in MeOH. The concentration of **P-49** was 8 µM, and 250 µM for each salt. The sample volume was 500 µL and the added volume of the salt solution (1 µL) was calculated to correspond to 0.5 µM in the final solution. The added volume was so small, that the measurements of each data point could be done with one sample. It was assumed that any dilution effect can

be neglected. The associated UV/Vis spectra were recorded between 250 – 350 nm (Fig. 8.1).

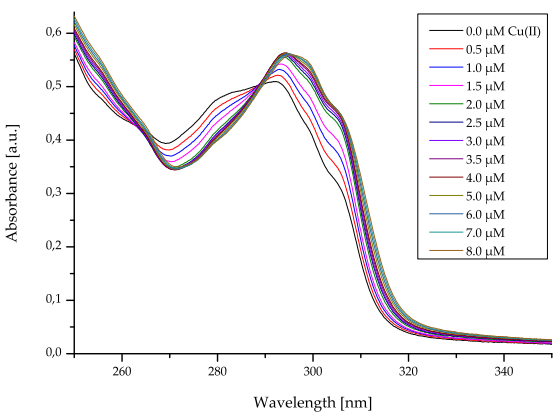

(a) Plot of the change in the absorption of **P-49** (8 µM) during the metal titration of $CuCl_2$ (250 µM) in MeOH.

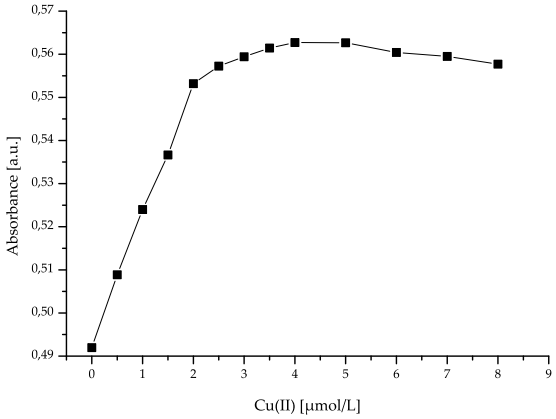

(b) Plot of the absorption values at 295 nm against their corresponding Cu(II) concentration.

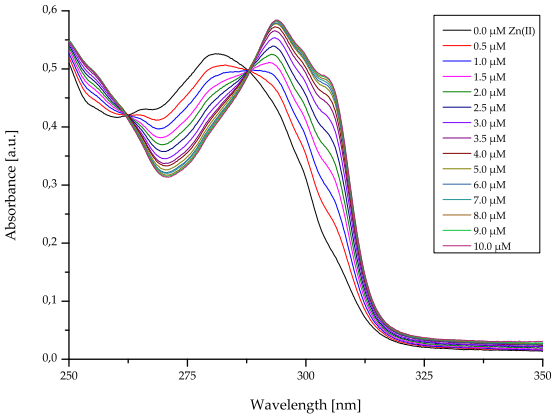

(c) Plot of the change in the absorption of **P-49** (8 µM) during the metal titration of $Zn(NO_3)_2$ (250 µM) in MeOH.

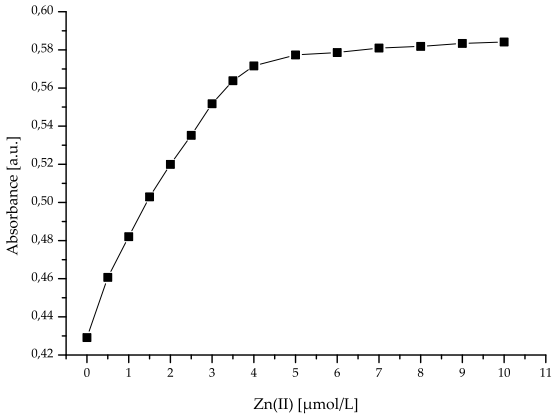

(d) Plot of the absorption values at 294 nm against their corresponding Zn(II) concentration.

Figure 8.1: UV/Vis analysis of **P-49** (8 µM) in MeOH with $CuCl_2$ and $Zn(NO_3)_2$.

The undisturbed system (**P-49** black lines) shows a maximum at 281 nm for the titration with $Zn(NO_3)_2$ (Fig. 8.1c), $Cu(ClO_4)_2$ (Fig. B.1a) as well as $ZnBr_2$ (Fig. B.2a) and at 292 nm for the titration with $CuCl_2$ (Fig. 8.1a). With increasing metal concentration different trends in the absorption curves are occurring. The intensity of the absorption at small wavelength is increasing, until an isobestic point is crossed. After this point, the former maximum from the undisturbed system is decreasing and a second isobestic point is crossed. After that point is crossed, the intensity

increases again to form two new maxima (red-shift of the old maximum) between 290 – 310 nm. At higher wavelength the intensity is near zero. The titrations were done until a saturation of the β-peptide was observed. The saturations were indicated by a consistent absorption signal and were reached with concentrations higher than 8 µM. AS the peptide concentration was also 8 µM, this indicates a 1:1 metal-β-peptide complex.

Two different metal cations with two different counterions each were tested. It was checked if the different metal ions and counterions show any difference in their ability to form complexes. The recognition unit has to replace the counterion in the coordination sphere at the metal center to form a stable metal-β-peptide complex. From the literature it is known, that some counterions are described as "noncoordinating" or "weakly coordinating anion" (WCA) and one of these WCAs is the used $[ClO_4]^-$-anion.[223] The idea was, that the WCAs show a weaker coordination and therefore it should be easier for the recognition unit to replace the counterion.

However, between the two metals no difference could be measured. In all measurements with Cu(II) and Zn(II) the saturation is reached with a concentration of 8 µM. With the variation of the counterion, no difference could be measured, what is similar to the variation of Cu and Zn. To summarize, the analyzed metal ion and the counterions do not have an impact of the metal-β-peptide complexation.

With the previews set of β-peptides, the principle of the metal-β-peptide complexation was tested and the differences in dependence of the chosen metal center and the counterion evaluated. In the next generation of β-peptides the analysis was refined and expanded by the application of a Job-Plot. In the UV/Vis analysis of the metal complexation (Fig. 8.2a), it is shown that the β-peptide **P-60** (30 µM in MeOH) aggregates with $CuCl_2$ (50 µM in MeOH).

Like in the first generation of β-peptides, the saturation of the complexation is reached at 30 µM. With concentrations higher than 30 µM the intensity starts to decrease, because through the addition of the metal solution the sample solution is getting diluted and the concentration of **P-60** is reduced.

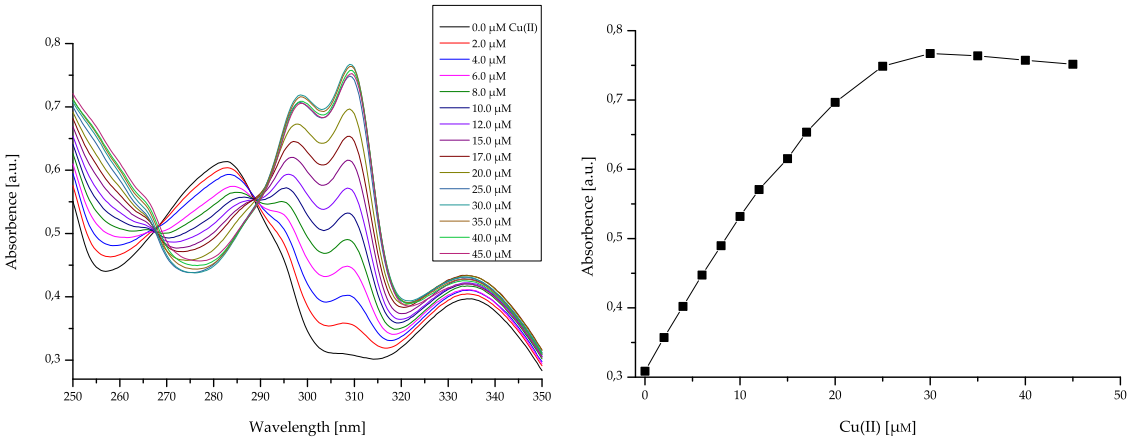

(a) Plot of the change in the absorption of **P-60** (30 µM) during the metal titration of $CuCl_2$ (50 µM) in MeOH.

(b) Plot of the absorption values at 309 nm against their corresponding Cu(II) concentration.

Figure 8.2: UV/Vis analysis of **P-60** (30 µM) in MeOH with $CuCl_2$.

To extend the analysis of the binding situation and to get an insight into the stoichiometry of the formed complex, two Job-Plots were evaluated (Fig. 8.3). The first Job-Plot (Fig. 8.3a), is made out of the already existing data from the UV/Vis titration and for the second Job-Plot (Fig. 8.3b) new data were recorded. While the concentration of **P-60** changed over time during the metal titration, the total concentration (**P-60** + Cu^{2+}) for each data point was held constant for the new data series. This means that the amount of added β-peptide and metal solution was varied at the same time.

In both Job-Plots, the product of the change of the absorption at one of the maxima relative to the undisturbed system and the mole fraction of **P-60** against the mole fraction of **P-60** were plotted. The tip of the triangle suggests the ratio of the stoichiometry from the formed complex. In the left Job-Plot (Fig. 8.3a) both lines cross at a mole fraction of ~0.6, which indicates a ratio of L_2M (2:1). On the opposite, the Job-Plot on the right side (Fig. 8.3b) indicates a ratio of LM (1:1) with a crossing at a mole fraction of ~0.4.

The analysis of **P-60** is compared with the analysis of **P-61**. Both β-peptides have the a very similar backbone, but differ in the amount of recognition units. While **P-60** has one unit, **P-61** has two units. Similarities and differences in the analytic results are discussed below.

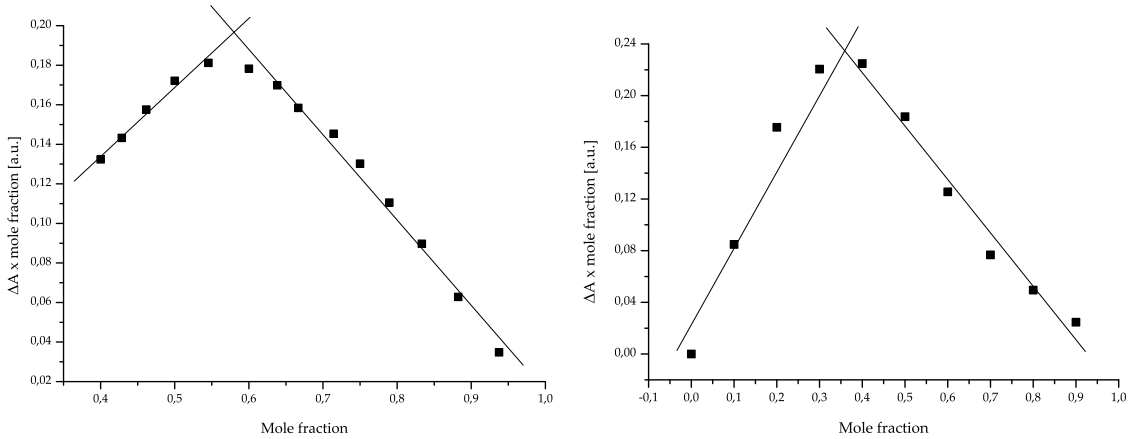

(a) Job-Plot made out of the already existing data from the titration of **P-60** (30 μM) with $CuCl_2$ (50 μM) in MeOH.

(b) Job-Plot made out a new series of samples, while the total concentration was held constant and the concentration of **P-60** and $CuCl_2$ was varied.

Figure 8.3: Comparison of the Job-Plots of **P-60** (30 μM) with $CuCl_2$ (50 μM) in MeOH.

P-61 (30 μM in MeOH) was titrated like **P-60** with $CuCl_2$ (50 μM in MeOH). The shown trend of the absorption spectrum is the same like before with the exception, that the absorption values in general are getting lower with higher metal ($\gg$ 20 μM) concentrations (Fig. 8.4a). This effect is clearly visible in the plot of the absorption values at 308 nm against their Cu(II) concentrations (Fig. 8.4b).

The absorption values reach their maximum at 20 μM and afterwards, the values start to decrease. This trend can be explained by the dilution effect mentioned in the discussion of **P-60**, but the observed effect can be seen more clearly than before. The extended analysis of **P-61** via the Job-Plots (Fig. 8.5) shows no significant differences to the analysis of **P-60**. The Job-Plot based on the metal titration (Fig. 8.5a) results in a crossing point at a mole fraction ~0.6 and the Job-Plot made out of the new series of data points (Fig. 8.5b) gives a value around 0.4 just like before. The results seem to be comparable, but it has to be kept in mind, that the Job-Plot makes no difference between the pairs L_2M and L_4M_2 or LM and L_2M_2. It is possible that **P-61** has a higher aggregation (based on the two recognition units), but it cannot be finally distinguished by the Job-Plot.

It can be summarized, that between **P-60** and **P-61**, there is no difference in regard of the metal-β-peptide complexation, that can be evaluated by the Job-Plot.

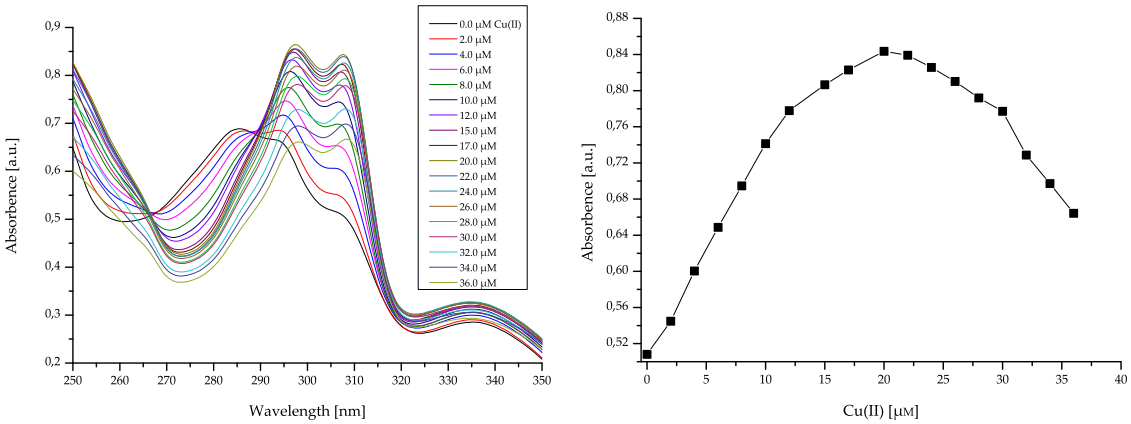

(a) Plot of the change in the absorption of **P-61** (30 µM) during the metal titration of $CuCl_2$ (50 µM) in MeOH.

(b) Plot of the absorption values at 308 nm against their corresponding Cu(II) concentration.

Figure 8.4: UV/Vis analysis of **P-61** (30 µM) in MeOH with $CuCl_2$.

Both β-peptides show in the analysis a very similar behavior and both β-peptides aggregate with a metal ion independent of the used counterion. Also, both β-peptides seem to form complexes with a L_2M-ratio, with the exception, that **P-61** could have higher aggregates, that correspond to a multiple of the 2:1 (L:M) ratio.

The last set of synthesized β-peptides were refined and optimized to fit the needs of this thesis. To mimic any natural system and for all measurements evolving biological or artificial membranes the used β-peptides should have a good solubility in aqueous media. Previous sets of β-peptides were not or insufficient soluble in aqueous media and had to be analyzed in organic solvents or were added as a solution in an organic solvent. The use of organic solvents, especially for measurements with membranes, could have a significant impact on the membrane. were analyzed, like the β-peptides before by UV/Vis-measurements and evaluated by Job-Plots. For the Job-Plots, no new data series were recorded, because it will be expected to gain no new information out of the additional measurement(s).

The β-peptides **P-56**, **57**, **58** and **59** (each 30 µM in water) were titrated with $CuCl_2$ (5 mM in water), all other experimental details were taken from the previous measurements without change. The pair **P-56** and **P-58** correspond to each other. They only differ in the presence of the cholestamine moieties. Beside the metal-β-

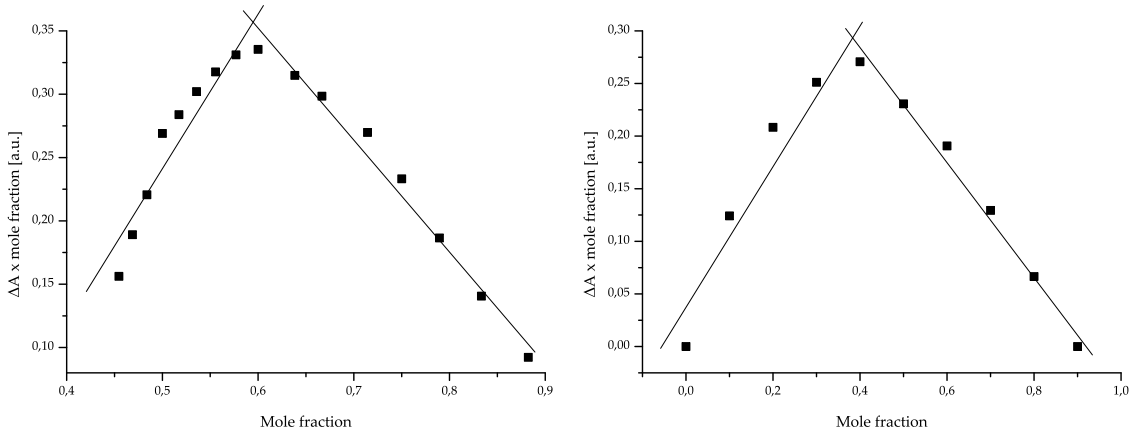

(a) Job-Plot made out of the already existing data from the titration of **P-61** (30 μM) with $CuCl_2$ (50 μM) in MeOH.

(b) Job-Plot made out a new series of samples, while the total concentration was held constant and the concentration of **P-61** and $CuCl_2$ was varied.

Figure 8.5: Comparison of the Job-Plots of **P-61** (30 μM) with $CuCl_2$ (50 μM) in MeOH.

peptide complexation, the influence of the cholestamine on the aggregation behavior was analyzed, because the measurements were carried out in water and cholesterol is known to self-aggregate in aqueous media.[22–24]

In (Fig. 8.6a) can be seen, that the β-peptide **P-56** has a very different behavior in the metal titrations. In comparison to the other measurements, **P-56** shows the prominent isobestic points and the different trends of increasing and decreasing of the intensity in dependence of the wavelength. The most notable difference is that in the titration of **P-56**, no distinct red-shift of the absorption maximum can be seen. The absorption maximum of the undisturbed system is already shifted to higher wavelength even without any influence of metal ions. On the opposite shows the corresponding β-peptide **P-58**, which comes without any cholestamine moieties, a clear difference to the titration of **P-56**. The titration of **P-58** is comparable with the other titrations (in comparison to **P-57** and **P-59**) and shows no deviation in its behavior to the other β-peptides. The comparison of the titration of **P-56** and **P-58** leads to the conclusion, that the cholestamine moieties must have an influence on the aggregation. It seems that **P-56** is already preorganized in aqueous media, introduced by the hydrophobic properties of the cholestamine moieties.

The saturation curves show a similar picture compared to the preview's measurements, **P-56** reaches a saturation at 25 µM (Fig. 8.6b), which is less than one equivalent and at concentration higher than 30 µM the intensity starts to decrease. For the β-peptide **P-58** the saturation is reached at 35 µM (Fig. 8.6d), which is slightly more than one equivalent. With higher concentrations the measured intensity stays nearly constant.

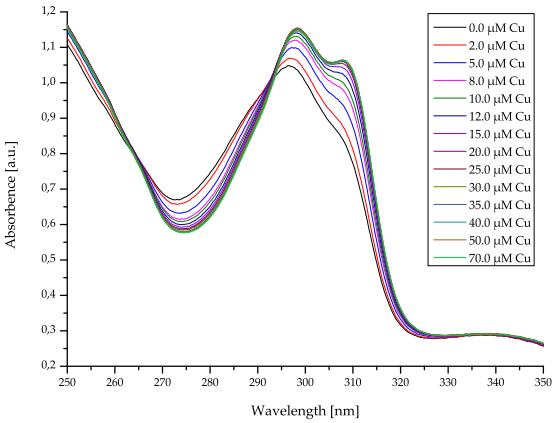

(a) Plot of the change in the absorption of **P-56** (30 µM) during the metal titration with $CuCl_2$ (5 mM) in water.

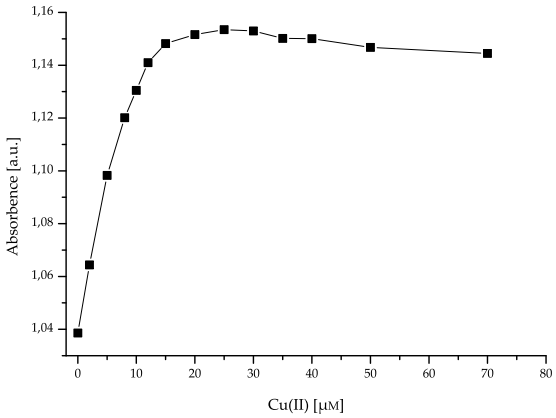

(b) Plot of the absorption values at 298 nm against their corresponding Cu(II) concentration.

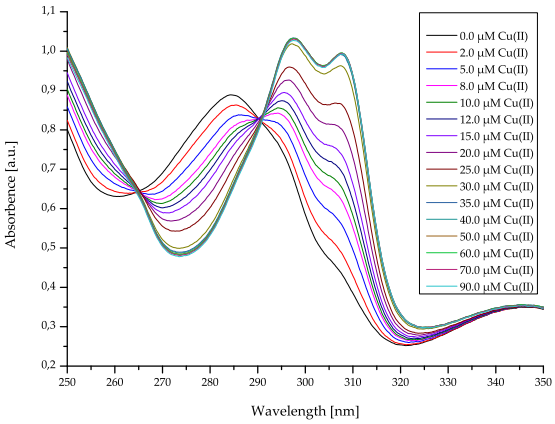

(c) Plot of the change in the absorption of **P-58** (30 µM) during the metal titration with $CuCl_2$ (5 mM) in water.

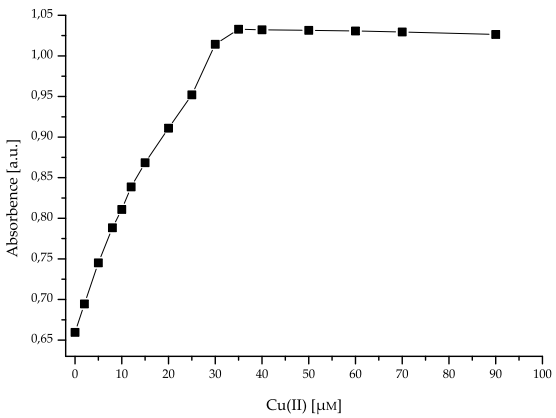

(d) Plot of the absorption values at 298 nm against their corresponding Cu(II) concentration.

Figure 8.6: UV/Vis analysis of **P-56** (30 µM) and the corresponding blank β-peptide **P-58** (30 µM) with $CuCl_2$ (5 mM) in water.

The corresponding pair, β-peptides **P-57** and **P-59**, was analyzed to identify any dependence from the number of cholestamine moieties. **P-56** was modified with

two cholestamine moieties and **P-57** was modified with just one moiety. The second binding site for the cholestamine was substituted against a β-Alanine. **P-59** was synthesized as a blank sample to **P-57** and was modified without any cholestamine moiety.

Both β-peptides, **P-57** (Fig. 8.7a) and **P-59** (Fig. 8.7c), show an identical behavior to the preview's measurements. The trends of the wavelength and metal concentration dependent increasing and decreasing of the intensity and the distinct red-shift are notable. Interesting is the saturation curve, for both β-peptides the saturation is shifted to higher concentrations. For **P-57** (Fig. 8.7b) and **P-58** (Fig. 8.7d) the saturation is reached at 70 µM (2.3 eq). The intensity stays at a constant level even with higher concentrations. This observation supports the previously made assumption, that the number of cholestamine moieties has in impact of the aggregation abilities of the β-peptides.

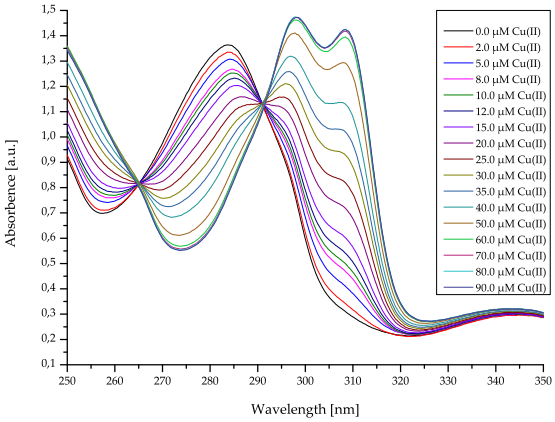

(a) Plot of the change in the absorption of **P-57** (30 µM) during the metal titration with $CuCl_2$ (5 mM) in water.

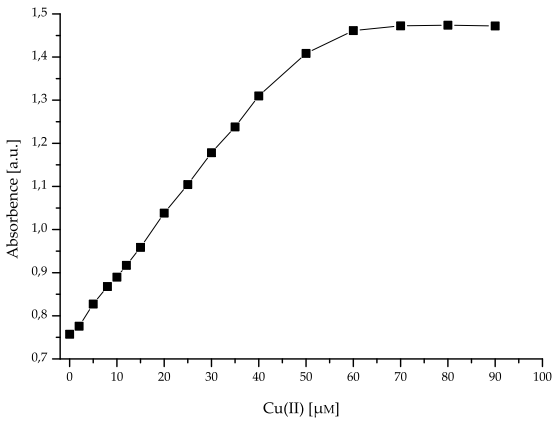

(b) Plot of the absorption values at 298 nm against their corresponding Cu(II) concentration.

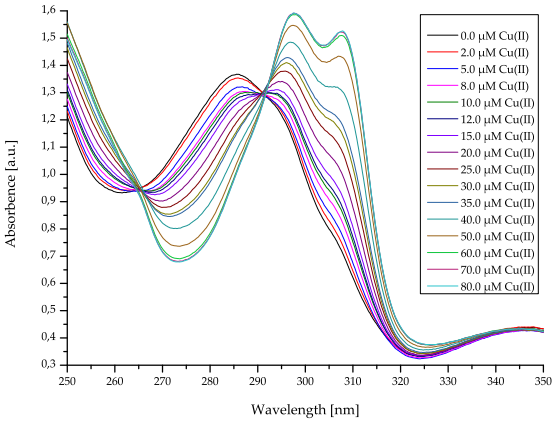

(c) Plot of the change in the absorption of **P-59** (30 µM) during the metal titration with $CuCl_2$ (5 mM) in water.

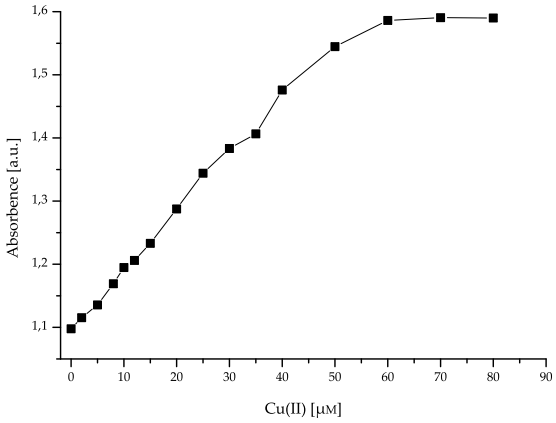

(d) Plot of the absorption values at 298 nm against their corresponding Cu(II) concentration.

Figure 8.7: UV/Vis analysis of **P-57** (30 µM) and the corresponding blank β-peptide **P-59** (30 µM) with $CuCl_2$ (5 mM) in water.

9 Interrogation of the binding on the surface of model membranes

As the second part of my topic the binding event of the synthesized β-peptides was analyzed. The secondary structure resulting from the primary structure and the chosen lipidanchors were designed to enable the β-peptides to bind to the surface of a model membrane. With the design (chapter 6) of the β-peptides should be ensured, that the β-peptides bind to the surface and not to be incorporated in the membrane, like transmembrane peptides.

9.1 Binding Studies

9.1.1 Introduction to the binding assay of the β-peptideson model membranes

To study the binding event between the β-peptides and the surface of the model membranes a measurable signal or property is needed. Additionally, this signal or property has to be dependent of the binding event and should have a high sensitivity for changes in the system. One way to study the binding event would be an optical signal, which produces a quantitative feedback. If the β-peptide binds to the membrane an optical signal can be observed (positive result) and if there is no signal, then the result for the binding event is negative. To produce an optical signal the β-peptides and/or the membrane must be labelled with an optically active

molecule. The response of optically active molecules could be a change in absorption properties or the optically active molecule is emitting light, what is known as phosphorescence and fluorescence.

If the β-peptide side, of a two-component system, is labeled many different options can be chosen. One option would be to use the fluorescence from specific aromatic residues, like the intrinsic fluorescence emissions of a tryptophan residue. Tryptophan is known to have a solvatochromic effect, that means the emission of the tryptophan can change with its microenvironment. The typical emission wavelength of tryptophan is at 280 nm and can be red-shifted to 300–350 nm depending on the polarity of the local environment. The use of tryptophan in this situation is less preferred, because it would be an additional amino acid that has be incorporated, which would increase the complexity of the design and synthesis of the β-peptide. Another important aspect is, it has to be ensured, that the tryptophan will be incorporated into the membrane and that the observed red-shift of the tryptophan emission is caused by the hydrophobic environment of the inner leaf of the membrane. Tryptophan is known to have a preferred interaction with the membrane interfaces[224, 225], therefore tryptophan is often used to support the anchoring abilities of transmembrane peptides like WALP[226] or the transmembrane β-peptides from our own group[227, 228]. For this thesis a preferred or supportive influence of a tryptophan residue could not be strong enough to attach the β-peptides on the surface of a membrane. To ensure a strong binding of the β-peptides the well-known cholesterol motive was used as primary lipid anchor.[229–231]

A more preferred way to achieve the same results is to use extrinsic fluorophores. Many fluorophores can be covalently bound to peptides, to obtain fluorescent protein conjugates. These tags represent an important, valuable and versatile tool for studying structures and changes in the microenvironment of the peptides. Some fluorophores show similar to tryptophan a solvatochromic effect, but often these effects are less notable or non-existent. To overcome this problem, it is possible to combine two different fluorophores, which correspond to each other as a Förster or Fluorescence resonance energy transfer (FRET) pair. With a FRET pair, each side of a two-component system can be labeled. The so-called FRET measurements have many advantages and one of these is, the high sensitivity regarding the distance between the donor and acceptor dipoles in a range of 1–10 nm. This property makes it

a perfect method to analyze any changes in the molecular proximity, like the binding of a β-peptide on the surface of a model membrane.

9.1.2 Experimental setup of the binding assay

To investigate the binding event between the synthesized β-peptides and the surface of a model membrane, the FRET effect between the FRET pair NBD and 1,2-dimyristoyl-*sn*-glycero-3-phosphoethanolamine-*N*-(lissamine rhodamine B sulfonyl) (Lissamine rhodamine B DOPE) was used. For this method vesicles were made consisting of 1,2-dioleoyl-*sn*-glycero-3-phosphocholine (DOPC), and were labeled with Lissamine rhodamine B DOPE (0.75 mol-%). The β-peptides (4 μM in PBS buffer) were modified with NBD (Fig. 9.1) (the rest of the experimental details can be found in subsection 13.3.1).

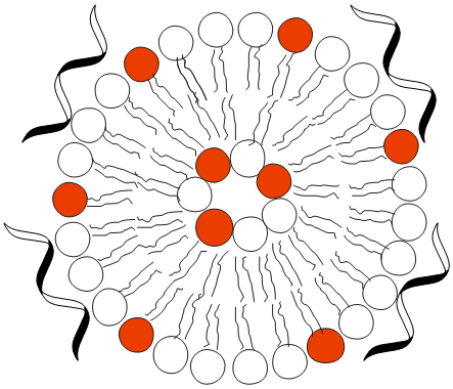

Figure 9.1: Systematic drawing of the interrogation for the binding event of β-peptides on the surface of a DMPC model membrane.

9.1.3 Results of the binding assay

The first generation of synthesized β-peptides **P-49** showed, that the β-peptides are capable to bind metal ions. One step further it was tried to investigate the binding abilities of the β-peptides on model membranes. For **P-49** was chosen a slightly different system consisting of DOPC vesicles, that were labeled with Texas

Red™ 1,2-Dihexadecanoyl-*sn*-glycero-3-phosphoethanolamine (Texas Red™ DHPE, 0.75 mol-%). The combination with OG488 at **P-49** and Texas Red™ DHPE containing vesicles resulting in another suitable FRET pair. For the preparation of the vesicles, **P-49** was extruded together with the rehydrated lipid material, which did not work as planned. A check of the membrane filters insight the extruder revealed, that all the lipid and peptide material stuck in the filters. It was not possible to generate any vesicles, even after lowering the peptide-lipid ration to 1:1000. It was suggested, that the concentration of **P-49** was incorrect, because the intensity of the absorption and emission of OG488 shows a strong pH dependence and **P-49** was to hydrophobic to be soluble in aqueous media. Based on the strong hydrophobic character of **P-49** it could be possible, that no vesicles could be formed, because **P-49** prevented the formation. To address these problems two changes were made: first, the fluorophore OG488 was exchanged with NBD and the primary structure was refined (please see chapter 6).

With the second generation of synthesized β-peptides (**P-50**) the measurements were repeated. The fluorophore at the β-peptide was changed, what made it also necessary to adjust the opposite fluorophore at the membrane surface. A suitable counterpart to NBD is the already mentioned Lissamine rhodamine B DOPE. The measurements were carried out with three different peptide-lipid ratios 1:300, 1:500 and 1:1000 and the peptide-lipid films were rehydrated in PBS-buffer. With the β-peptide **P-50** was done a feasibility study and to see if all suggestions are correct (proof of concept). For the measurements with **P-50**, the binding event was recorded time-independent. Therefore, NBD was excited at 464 nm and the resulting emission of the Lissamine rhodamine B DOPE was recorded between 475–700 nm (Fig. 9.2).

The figure above shows the intensity in dependence of the wavelength and at 590 nm a strong maximum is depicted of the emission of the Lissamine rhodamine B DOPE, and in addition a FRET effect. It can be concluded, that **P-50** binds at all three peptide-lipid ratios to the surface of the membrane. The difference between the measurements at 1:300 and 1:500/1:1000 are comparable and the difference between 1:500 and 1:1000 is nearly zero regarding to the intensity. This simple method represents the starting point for all the further measurements. Overall, it could be shown,

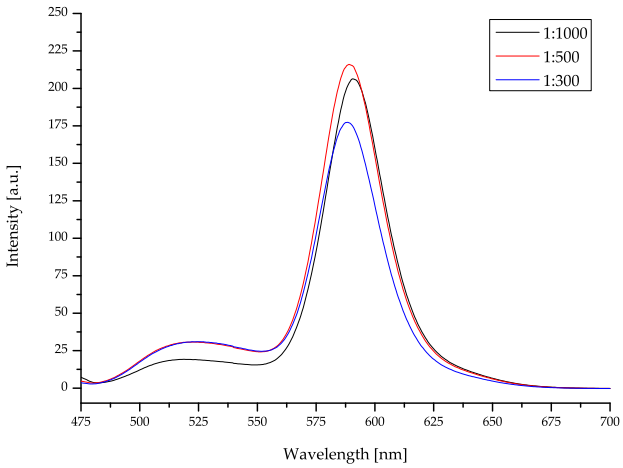

Figure 9.2: Comparison of the binding events of **P-50** (4 μM) at 1:300, 1:500 and 1:1000 in PBS-buffer.

that the β-peptide is binding to the surface of a model membrane, however all other aspects of the binding event will be later addressed.

To gather more information about the binding event itself, it was switched from a time independent to a time dependent measurement. The basic principle and settings for measurement stays the same. The only difference that was made is the time when the β-peptide was added to see if the fluorescence is directly influenced by the β-peptide. After 10 min of background measurement **P-51** (4 μM, 1.0 ml, peptide-lipid-ratio 1:300) in TFE and PBS-buffer (1:1, v/v) (Fig. 9.3). After the addition the fluorescence signal from Lissamine rhodamine B DOPE is increased directly from ~0.8 to ~1.1. This increase is a clear indication, that **P-50** binds very fast to the surface of the membrane. This measurement was repeated three times and two of the three curves show a similar trend. In all three repetitions correlates the increase of the Lissamine rhodamine B DOPE emission directly with the addition of **P-50**. In two of three measurements the curve passes a maximum and then starts to decrease again. Only in one measurement the intensity of the signal stays constant. The deviation of the decrease was analyzed later with a Leakage assay in Section 9.3.

To verify the obtained results, control measurements were implemented to show the difference between different binding events. The control measurements should show a miscellaneous behavior with regard to binding event and the observed fluores-

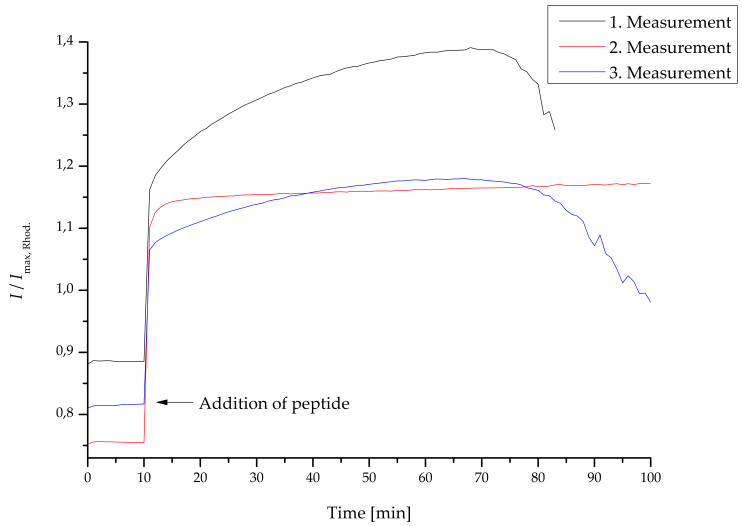

Figure 9.3: Overview of the binding event of **P-51** (4 µM) at a peptide-lipid-ratio of 1:300 in PBS-buffer.

cence intensity. For this purpose, three different β-peptides, **P-52**, **P-53** and **P-54** were synthesized, which differ in their modifications attached to the side chains (Fig. 9.4). The backbone of all synthesized β-peptides were the same to guarantee the comparability during the measurements and later on in the analysis of the results. The β-peptides for the control measurements are modified in that way, that the different influences of all modifications, like an attached recognition unit or a protected/unprotected carbon acid side chain can be analyzed. For example, **P-52** is modified with recognition units, but the lipid anchor (cholesterol moiety) is missing. To replace the lipid anchor the protected carbon acid side chain is left at this position. **P-53** is very similar to **P-52**, but the carbon acid side chain is unprotected. In **P-54** the carbon acid side chain is still protected, but the recognition unit is replaced by a –Ac group. With this set of β-peptides it was possible to evaluated the different influences and to give a statement, about the binding event of the various β-peptides. In first place it will be described the comparison of the control measurements with **P-52**, **P-53** and **P-54** and the differences between them (Fig. 9.4). Afterward, the results from this comparison will be discussed together with the results from the β-peptide **P-50** (Fig. 9.5).

The graph shows big differences between the various β-peptides. It was expected that all control measurements would show a similar picture, with the intensity of

the fluorescence signal being small or smaller than the signal of the β-peptide with a FRET-effect. But it was observed that the two β-peptides **P-52** and **P-54** show a clear and distinct FRET signal, whereas **P-53** shows the expected lower signal intensity. The behavior of **P-52** and **P-54** was unexpected especially in regard, that in both β-peptides the lipid anchor moiety is missing. As a replacement both β-peptide have an −OAllyl-group which is a left over from the synthesis and this group should also prevent a negative charge at the binding side of each β-peptide (chapter 6). It seems that the −OAllyl-group has a big impact on the binding affinity, because the β-peptide **P-54** shows no significant fluorescence signal and has no −OAllyl-group. In contrast to the other two β-peptides, the β-peptide has a negative charge, where the other two β-peptides have located the lipid anchor or the −OAllyl-group. The recognition unit seems not to play any bigger role, the β-peptides **P-52** and **P-53** where modified with the recognition unit and as it can been seen **P-52** has the highest intensity fluorescence signal, while **P-53** has the lowest intensity. This assumption is supported by the comparison between **P-52** and **P-54**. Both β-peptides have a similar fluorescence intensity and differ only in the presence or absence of the recognition unit. The different trends of the single graphs are interesting, because the graph of **P-53** is constant, the intensity of **P-52** is decreasing over time and the intensity of **P-54** is increasing.

In the following, the negative controls will be compared with the positive results. The control measurements are plotted together in a graph (Fig. 9.5) to be able to view and analyze them in relation to each other. The obtained result is surprising, because the β-peptide **P-50** does not show the highest intensity. This was not expected, especially when the design and the modifications of the β-peptide are taken into account. The β-peptide was modified with two cholesterol moieties and should therefore bind very well to the membrane surface. It was observed a FRET-effect which is constant over time, but with a slightly higher intensity than **P-53** and drastically lower than **P-50** and **P-52**. An explanation is still under discussion. It could be possible that **P-50** is not able to bind quantitatively to the membrane due to its strong hydrophobic properties. Which means, **P-50** forms micelles-like aggregates in aqueous solution to avoid a hydrophilic environment. The building of micelles-like aggregates is preferred by the β-peptide over the binding to membrane surface and just a little part of the added β-peptide is binding on the membrane

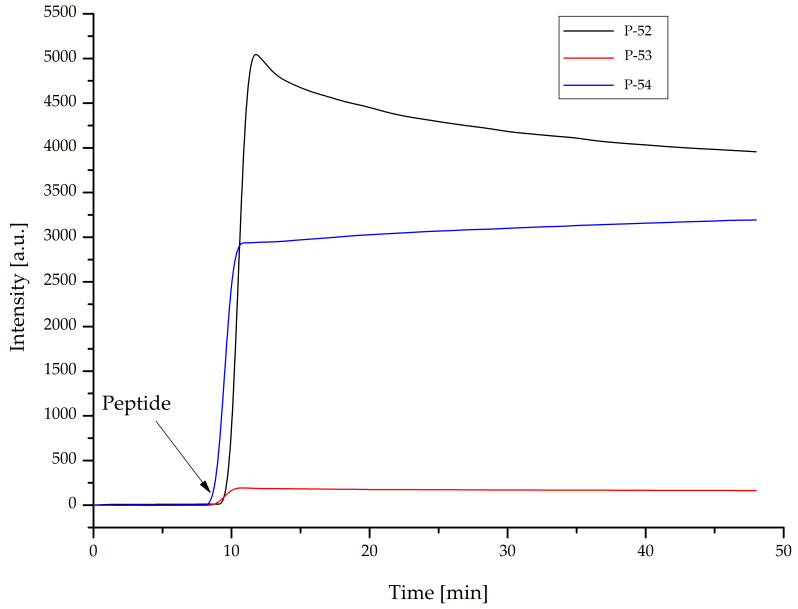

(a) Comparison of the control measurements **P-52**, **P-53** and **P-54**.

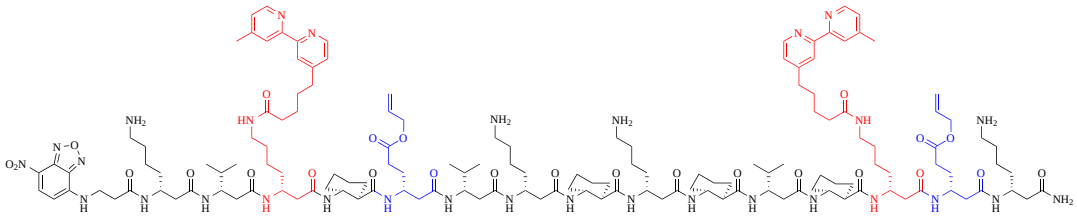

(b) β-peptide **P-52**

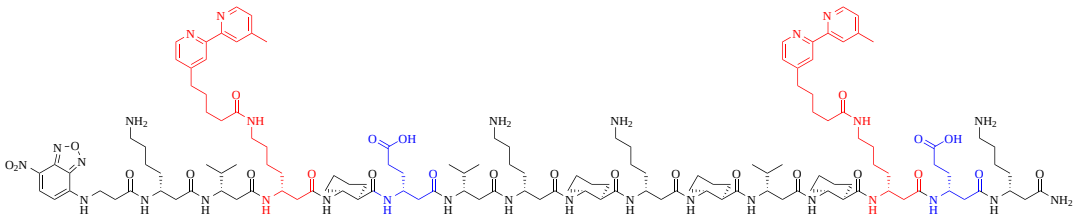

(c) β-peptide **P-53**

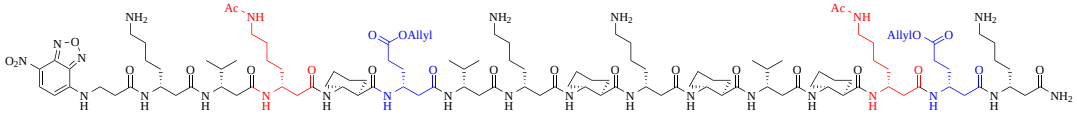

(d) β-peptide **P-54**

Figure 9.4: Comparison of different control measurements **(a)** for the binding studies of **P-52 (b)**, **P-53 (c)** and **P-54 (d)**. The positions that are varied between the β-peptides are shown in red and blue.

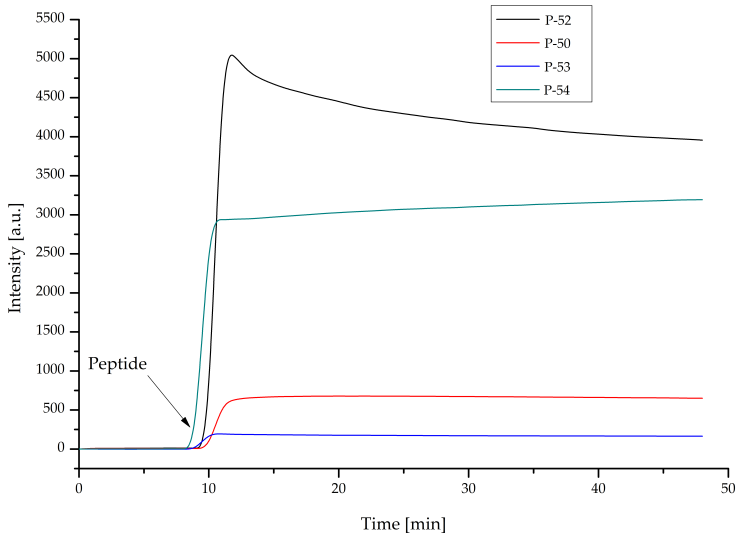

Figure 9.5: Comparison of the negative control measurements with the β-peptides **P-52**, **P-53** and **P-54** together with the positive control β-peptide **P-50**.

surface.

The results showed on the one side that the synthesized β-peptide **P-50** binds to the surface of a membrane, but on the other side **P-50** has a very strong hydrophobic character, which make it nearly impossible to measure the β-peptide near to a membrane at a constant level. Another downside was the measurement and the comparison with the control β-peptides. It was shown that the control β-peptides showed partly better results. To overcame this problem the next generation of β-peptides were introduced. For a detailed discussion please see chapter 6.

The next generation of β-peptides were represented by **P-55** and **P-62**, which were designed to be less hydrophobic. With an increased hydrophilic character **P-55** and **P-62** were better soluble in water and they should be less membrane active. In the following the binding properties to the membrane surface are analyzed, and afterwards the influence towards the membrane integrity. **P-55** and **P-62** are a corresponding β-peptide pair, consisting of the main β-peptide (**P-55**), that was analyzed and a control measurement (**P-62**). The analysis of **P-55** (Fig. 9.6) was repeated three times, with relative different graphs. After a short equilibration time, **P-55** was added as indicated in the figure. The intensity of the observed fluorescence

signal started to decrease after the start of the measurement, due to the addition of **P-55** the signal intensity increased over time and the measuring signal exceeded the initial value in all three measurements, without reaching a maximum of the signal. The individual measurements show strong differences in the initial starting values and in the slope of the measurement signal after the addition of the **P-55**. Overall

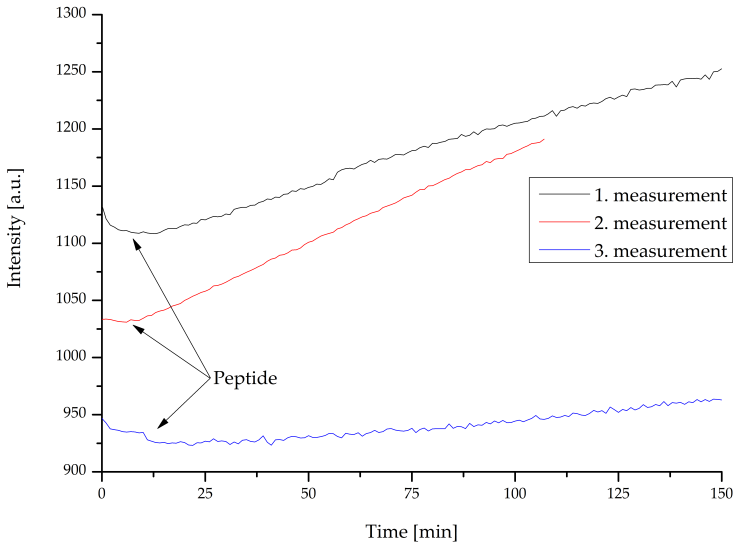

Figure 9.6: Overview of the three repetitions of the FRET analysis for β-peptides **P-55**.

in all three measurements a FRET-effect could be observed. The absolute values are not very high, but higher than their initial values and the increase is linked directly to the addition of **P-55**. It was observed a FRET-effect, but the effect was not very intensive.

To verify the positive results from the measurements of **P-55**, the corresponding control measurement with **P-62** was also measured under the same conditions (Fig. 9.7). All three measurements are comparable to each other, which means that they have comparable initial values of the fluorescence signals and the course of the graphs are identical. At the start of each measurement the intensity drops and then takes on a constant value. After 10 min, **P-62** was added (as indicated in the figure), whereby the intensity of the signal increased strongly, but then decreased again. The trend of the graphs became weaker over time, yielding of almost constant values. The three measurements are shifted in their absolute intensity: the first and second measurement show the highest intensity of the initial values, where the third

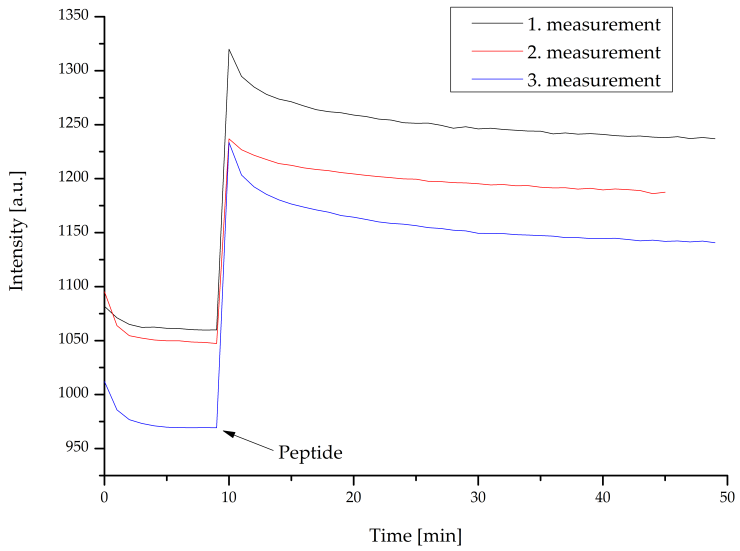

Figure 9.7: Overview of the three repetitions of the FRET analysis for β-peptides **P-62** as a control for the measurement of **P-55**.

measurement shows clearly lower values. The second measurement does not reach the signal intensity of the first measurement after the addition of **P-62**. In contrast shows the third measurement the same intensity of the signal after the addition of **P-62**, although the first and second measurement showed higher initial values. This observation could have many reasons, for example small variations in added amount of **P-62** or small fluctuations in the binding of **P-62** on the membrane surface.

The two measurements are compared with each other, it was found that a clearly different behavior was measured for the binding of **P-55** (Fig. 9.6) and **P-62** (Fig. 9.7) to the model membrane. While **P-55** shows a slow and continuous binding behavior, the control β-peptide **P-62** binds much faster and also quantitatively. The measurements for **P-55** were stopped for time reasons and it is not possible to show where the absolute maximum could be. It can be assumed that the first two measurements of **P-55** could reach a higher absolute intensity value than measured in the control measurement for **P-62**.

As already discussed in chapter 6, the next and last generation of β-peptides has to be introduced. The second last generation made two steps in the right direction, but one step to far. The β-peptides **P-55** and **P-62** were to hydrophilic,

whereby the binding speed of **P-55** seems to be too low, that no quantitative binding of the **P-55** to the membrane surface has occurred within a reasonable time.

The last generation of β-peptides that were synthesized and analyzed were the β-peptides **P-56**, **P-57**, **P-58** and **P-59**. The design strategy combines the ideas of **P-50** and **P-55** to combine the best properties from both generations. The results of the binding studies and the leakage assays will be discussed in the following part.

Under the same conditions as in the previous measurements **P-56** was also measured and compared with its corresponding control β-peptide **P-58** (Fig. 9.8). After 10 min equilibration **P-56** or **P-58** was added to the solution and a corresponding change of the measurement signal was recorded. When measuring **P-56**, a slow but steady increase was observed. All three repetitions are comparable with each other, showing the same course with slight differences in intensity. A maximum of the intensity for **P-56** could not be measured due to time reasons. The control measurement on the other hand shows a fast and direct increase in intensity after the addition of **P-58**. After reaching the maximum, the intensity starts to decrease slightly. The control measurement reaches a higher value after a significantly shorter time than **P-56** at the same time, but **P-56** reaches significantly higher intensity values with a longer measuring time. Overall it can be stated that **P-56** shows a FRET-effect and binds well to the surface of a model membrane. The control measurement shows also an increase in the signal intensity, but the increase is less prominent.

The β-peptides **P-57** and **P-59** were synthesized to corresponding pairwise to **P-56** and **P-58**. The permutation was that **P-57** was modified with just one lipid anchor and **P-59** is the appropriate control β-peptide. The same experiments with the identical condition were repeated and the results are shown below (Fig. 9.9). The β-peptide **P-57** and **P-59** show over three measurements the same pattern. After 10 min equilibration **P-57** or **P-59** was added to the solution and a corresponding change of the measurement signal was recorded. For **P-57** the increase of the fluorescence signal is immediately and spontaneously like for the control measurement. The difference is, that the increase for **P-57** is significantly higher: the

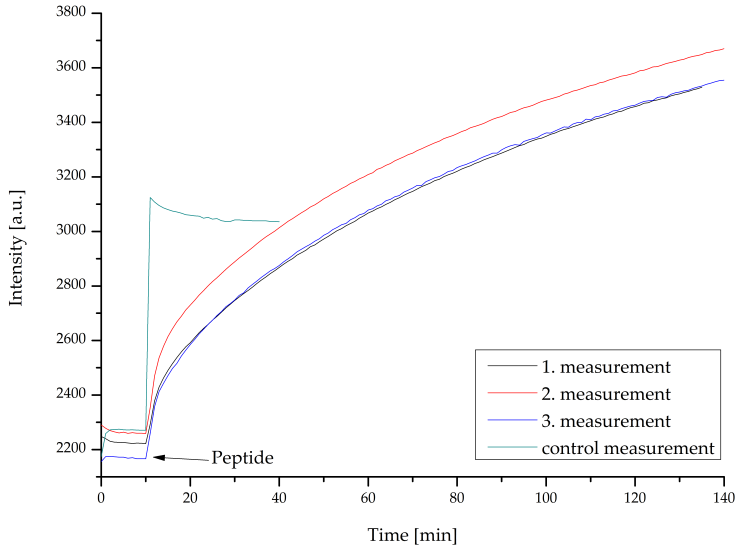

Figure 9.8: Overview of the three repetitions of the FRET analysis for β-peptides **P-56** with the corresponding control measurement with **P-58**.

intensity rises from 2200 a.u. to nearly 7000 a.u. for the first measurement. In the following two measurements the increase is still high but not to the same extent as before. The control measurement shows the same pattern with an immediately and spontaneously increase of the intensity, but less dominant. Between the three measurements of **P-57** can be seen that the initial values are more or less the same, but the increase of the signal is getting smaller with the number of repetitions. In addition to this trend, it can be said that after the increase of the intensity, the intensity begins to slightly decrease again. The decrease in intensity does not stop during the measurement and never reaches a constant value. For the control β-peptide, the decrease in intensity is smaller and the intensity remains constant over the rest of the measurement time.

The measurement for **P-57** shows a FRET-effect and thus a clear binding of the β-peptide to the surface of the membrane. Matching this, **P-59** with its control shows the corresponding opposite course. The intensity of **P-59** is clearly lower than for **P-57**.

When the β-peptides **P-56** and **P-57** are compared two very different pattern of the binding event can be seen. On the one side the course of **P-56** is slowly increasing over time and even after more than 130 min the maximum of the intensity is not

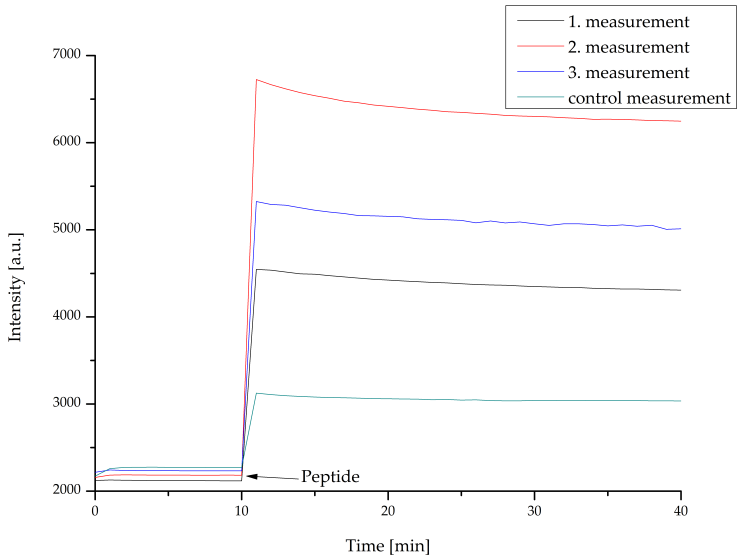

Figure 9.9: Overview of the three repetitions of the FRET analysis for β-peptides **P-57** with the corresponding control measurement with **P-59**.

detected. On the other side **P-57** shows a sharp increase to the maximum followed by a slowly decrease of the intensity. In both cases it can be assumed, that the β-peptides are binding successfully to the surface of the membrane, but with different binding affinities. That means that **P-56** is binding slower to the membrane than **P-57**. To find an explanation for this difference, the slightly different modification of the two β-peptides must be taken into account. **P-56** has two lipid anchors compared to **P-57** with just one lipid anchor, which has a significant effect on the hydrophobicity, which means **P-56** is much more hydrophobic. This difference in hydrophobicity also has a direct influence on the solubility of the β-peptide in aqueous media. In retrospect, **P-56** shows a better solubility than the β-peptides of the other generations, but is still less soluble than **P-57**. These differences are a clear indication for the explanation of the different binding properties of the two β-peptides. It is assumed that **P-56** dissolves in aqueous media, but is still present in a kind of micelle-like aggregates. The hydrophobic cholesterol units try to evade the hydrophilic medium (hydrophobic effect) and thus the β-peptides join together to form aggregates similar to micelles. **P-57** is not able to show the same behavior because its hydrophobic properties are less pronounced. As a result, there is more "free" β-peptide, which can then bind faster to the surface of a membrane. **P-56**, on the other hand, must first be released from its micelle-like aggregates. This

process takes some time, which explains the slow but significant increase in the curve.

9.2 Peptide coordination between two model membrane systems

9.2.1 Introduction

With the two previous measurements and with the associated results, the foundation for the following measurements were created. The previous results showed that on one side the synthesized β-peptides are capable to aggregate induced by metal ions and on the other side that the β-peptides are binding to the surface of a model membrane. In this section the question should be addressed, if it is possible to combine both methods to gather information about the metal induced aggregation of β-peptides on model membranes.

The first idea was to utilize the UV/Vis measurements, which are sensitive to the metal induced aggregation (see Section 8.3) , easy to prepare and time-efficient. The experimental setup would be a vesicle suspension with a defined concentration of β-peptide and peptide-lipid-ratio. This suspension would be titrated like in the measurements for the metal induced aggregation study Section 8.3. The characteristic change would be an increase in the absorption between 290 – 300 nm, while the former absorption maximum at 280 nm is decreasing. With the change in the UV/Vis spectra we would see a clear indication for the aggregation of the β-peptides on the surface of the vesicles. This means, that this method would only be a cross-section over all vesicles, so to say an average over all aggregation events. A deeper look in a few single events of aggregation would be of greater interest. Nevertheless, this experimental setup could combine the facts of aggregated peptides on a vesicles surface. The major disadvantage with this setup is, that it is not possible to do any UV/Vis measurements with vesicles, because of the strong light scattering caused by the vesicles themselves. That means that the light scattering

would prevent a correct and precise measurement. To overcome this problem, another method has to be used, which is not disturbed by any light scattering effects of the vesicles.

9.2.2 Experimental setup for the peptide coordination

As mentioned above further measurements require a method which is not disturbed by any light scattering effect caused by vesicles. For this further fluorescence measurements were used to make use of the FRET-effect. The question was how to determine aggregation events between two or more β-peptides, the following setup was used:

The experimental setup consisted of two β-peptides (**P-51**) which were attached to two different model membrane systems. The model membrane systems were of the same lipid material, with the same peptide-lipid-ratio, same vesicle diameter, the same concentration of labeling and the same preparation. The vesicle systems differ in the point, that one part is labeled with Oregon Green™ 488 DHPE (1,2-Dihexadecanoyl-*sn*-Glycero-3-Phosphoethanolamine) and the other part is labeled with Texas Red™ DHPE. Following this setup, the advantages of both dyes can be implemented perfectly: The dyes are very sensitive, which means each of them can be incorporated in small mole-% from 0.2 to 1.5 (each), they result in a FRET pair and their observation would not be disturbed by light scattering and/or the influence is so small, that it could not be detected. The following figure (Fig. 9.10) depicts the schematic setup of the experiment.

Both kinds of vesicles were labeled with a fluorescence marker and β-peptide and mixed in equal parts. After a short equilibration time, a defined volume of metal solution was added, which should promote the aggregation between the β-peptides.

To get a deeper insight in the behavior of the analyzed β-peptide, different key features of the experiment were permuted like the lipid material, the peptide-lipid-

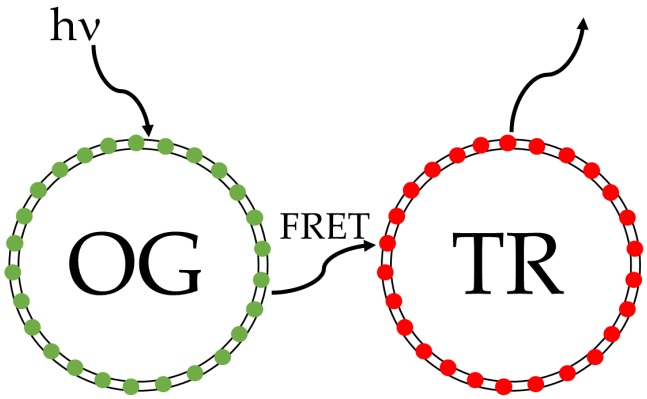

Figure 9.10: Experimental setup for the peptide coordination between two model membrane systems. Depicted in green (left side) the Oregon Green™ 488 DHPE marked vesicles and in red (right side) the Texas Red™ DHPE marked vesicles.

ratio or the concentration of the fluorescence label. The permutations are listed in the following table Tab. 9.1.

Table 9.1: Summary of the used permutations for the fluorescence analysis of the synthesized β-peptides (**P-51**). The vesicles are prepared after Section 13.3 and the β-peptides are added after Method I or Method E. Method I describes the addition of the β-peptides before the extrusion of the peptide/vesicle suspension. Method E describes the addition of the β-peptide after the extrusion of the vesicle suspension.

Parameter	Permutation
Lipid material	DOPC
	DMPC
Concentration of the fluorescence label	0.2 mole-%
	1.5 mole-%
peptide-lipid-ratio	1:50
	1:150
Vesicle diameter	100 nm
	200 nm
	400 nm
	1000 nm
Peptide concentration	4 µmol/L
Addition of the peptide	Method I
	Method E

The different permutations were used to determine single parameter influences in regard of the experiment. All analyzed variations are shown in the table (Tab. 9.2). Some of the experimental results are shown and discussed here in detail. All other results and spectra are shown in the Appendix.

Table 9.2: Used permutations for the fluorescence analysis of the synthesized β-peptide (**P-51**). Addition of the β-peptide by Incorporation (I) and after the extrusion (E). Results that are marked **bold** are described and shown in detail in this section. All other results and spectra are depicted in the Appendix.

peptide-lipid-ratio	Lipid material	Vesicle diameter	Conc. of the fluorescence label	Addition of the peptide
1:50	DOPC	100 nm	1.5 mole-%	I
1:50	DOPC	100 nm	0.2 mole-%	I
1:50	DOPC	200 nm	1.5 mole-%	I
1:50	**DOPC**	**200 nm**	**0.2 mole-%**	**I**
1:50	DOPC	400 nm	1.5 mole-%	I
1:50	DOPC	400 nm	0.2 mole-%	I
1:50	DOPC	100 nm	1.5 mole-%	E
1:50	**DOPC**	**100 nm**	**0.2 mole-%**	**E**
1:50	DOPC	200 nm	1.5 mole-%	E
1:50	**DOPC**	**200 nm**	**0.2 mole-%**	**E**
1:50	DOPC	400 nm	1.5 mole-%	E
1:50	DOPC	400 nm	0.2 mole-%	E
1:50	**DMPC**	**200 nm**	**1.5 mole-%**	**E**
1:50	DMPC	200 nm	1.5 mole-%	E + 20 % TFE
1:50	DOPC	200 nm	0.2 mole-%	E
1:50	DOPC	200 nm	0.2 mole-%	E + 20 % TFE
1:50	DOPC	100 nm	0.2 mole-%	E
1:50	**DOPC**	**400 nm**	**0.2 mole-%**	**E**
1:50	**DOPC**	**1000 nm**	**0.2 mole-%**	**E**
1:50	DOPC	200 nm	0.5 mole-%	E
1:150	**DOPC**	**200 nm**	**0.5 mole-%**	**E**

It could be shown in preliminary tests, that with a peptide-lipid-ratio $\geq$ 1:100 under comparable conditions no FRET-effect could be observed ((Fig. C.1) – (Fig. C.6)). The conclusion was to lower the peptide-lipid-ratio to get better results, that leads to a FRET-effect. Therefore, the majority of the experiments were carried out with

a peptide-lipid-ratio of 1:50. To make sure that higher peptide-lipid-ratios do not lead to satisfying results, the peptide-lipid-ratio of 1:150 was tested once. For all used peptide-lipid-ratios the vesicle diameter was varied between 100 and 400 nm, leading to a modulation of surface tension in the vesicles. Based on the Laplace-equation (Eq. 9.1) the surface tension is related to the radius and the pressure. This means if the radius is getting smaller the pressure is getting higher and the vesicle surface has a stronger curvature. This fact could have a negative influence on the outcome of experiments, because the stronger curvature could prevent or disturb a stable aggregation of the β-peptides. Smaller diameters of the vesicles could have the advantage, that these vesicles could get closer to each other, which should increase the probability of observing a FRET-effect.

$$\Delta p = \frac{2\gamma}{r} \tag{9.1}$$

Also, different lipid materials were tested. The used DOPC and DMPC have different transition temperatures (-16.5 vs. 41.3 °C, respective), that means that DOPC is at room temperature in a fluid-like liquid crystalline state (L_β), whereas DMPC with his higher transition temperature is in a solid-like gel state at room temperature. Different lipid states can influence the membrane functionality significantly. Therefore, DOPC and DMPC were chosen to represent two of the main lipid states. Furthermore, these two lipids provide different thickness of the vesicle membrane, which has an effect on the interaction between the β-peptide and the vesicle surface. With different interactions between the β-peptides and the membrane surface, different outcomes of the experiment could be observed.

The second last parameter that should be discussed is the concentration of the fluorescence label. TR and OG488 are known from the literature to be very sensitive, but also, they are known to be prone to self-quenching at higher concentrations. To overcome this problem the experiments were carried at two different concentrations (0.2 vs 1.5 mole-%). With 0.2 mole-% the lower limit was tested and with a concentration of 1.5 mole-% the upper limit was investigated. With a concentration of 1.5 mole-% the probability to observe a FRET-effect should be higher, but also the probability of self-quenching is increased. At 0.2 mole-% the probability

of self-quenching is reduced, but also the probability to observe a FRET-effect is decreased.

The last parameter that has to be taken into account is the timing of the addition of the β-peptides. Two possibilities were evaluated:

I The β-peptides were incorporated onto the vesicles membrane after Section 13.3

E The β-peptides were added to the vesicles suspension during the analysis

In item **I** the β-peptides were incorporated onto the vesicle membrane during the manufacturing process of the vesicles, that means that the β-peptides were also extruded with the multilamellar vesicle suspension. In item **E** the β-peptides were added after the manufacturing process of the vesicles, during the analysis at certain time points. In method **I** the β-peptides are definitely incorporated with the vesicles. The downside could be that the β-peptide is not only incorporated onto the surface of the vesicles but also incorporated into the membrane in a transmembrane-like fashion. To overcome this disadvantage method E was used. If the peptides were added after extrusion, the β-peptides can only attach themselves to the surface of the membrane. For this purpose, it was tested if the property of the β-peptides to incorporate themselves (subsection 9.1.3) onto the membrane surface is strong enough to ensure a positive test result. The results from these experiments lead to the conclusion, that the β-peptides tend to attach themselves to the surface of a membrane.

9.2.3 Result for the peptide coordination

The first result that should be discussed, is measured with a peptide-lipid-ratio of 1:50, 200 nm vesicle diameter, a fluorescence label of 0.2 mole-% and the peptide was directly incorporated after **I**. In the figure (Fig. 9.11) the intensity of the fluorescence signal of TexasRed against the time t is depicted. It was observed that the intensity is slightly decreasing with small up and down deflections. It can be stated, that after around 240 min the intensity started to increase and reaches a value of around

1525 a.u. and stays constant until the metal solution is added. After 260 min the next increase of the intensity can be observed due to the addition of metal ions. With the addition of the metal solution the intensity reached a constant higher level in regard of the starting value. Overall it could be summarized that based

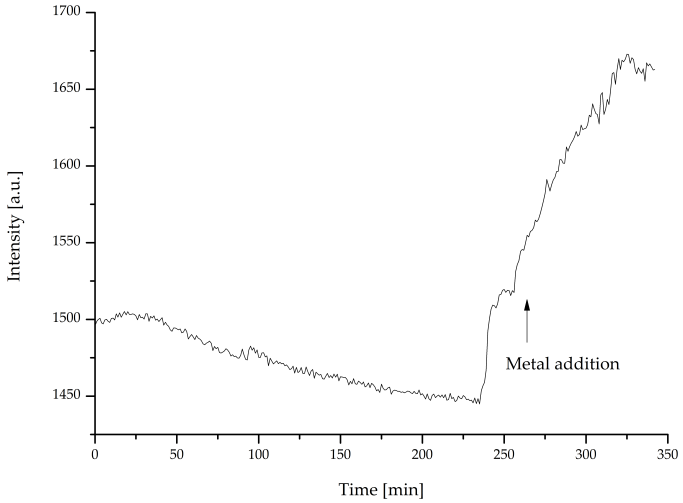

Figure 9.11: Peptide coordination with a peptide-lipid-ratio of 1:50, 200 nm vesicle diameter, a fluorescence label of 0.2 mole-% and the peptide was directly incorporated after **I**.

on this first measurement the experiment worked out as planned. The intensity showed an increasing of the signal before the addition of the metal ions and after the addition the intensity increased again. A conclusion can be drawn in which a FRET-effect was observed, but also the first increasing of the signal cannot be explained.

For the second analysis (Fig. 9.12) the vesicle size was decreased to 100 nm and the β-peptide was incorporated after method I before the extrusion of the vesicle suspension. The rest of the conditions were the same. In the first 30 min of the analysis the intensity of the signal started to decrease and then fluctuated between two values, 3150 and 3450 a.u. After a total time of 50 min the metal solution was added without any apparent change. After additional 10 min the experiment was aborted.

In comparison with the first experiment it was assumed, that the diameter of the vesicles and the method of the addition of the β-peptide are two essential key el-

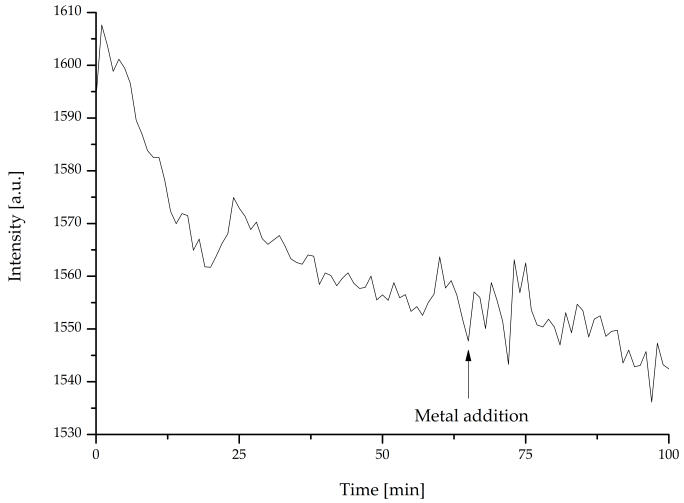

Figure 9.12: Peptide coordination with a peptide-lipid-ratio of 1:50, 100 nm DOPC vesicles, a fluorescence label of 0.2 mole-% and **P-51** was incorporated after method **I**.

ements. By reducing the vesicle diameter from 200 to 100 nm and changing the method of addition (from **I** to **E**) the result of the experiment changed from a positive to a negative ending. To differ between the impact of the method of addition and the vesicle diameter, a third measurement was performed. In the third measurement, vesicles with a diameter of 200 nm were used, also a degree of 0.2 mole-% of labeling and the method **E** of β-peptide addition.

In the figure (Fig. 9.13) a nearly linear intensity with small up and down deflections was observed. After 53 min, metal ions in form of zincbromide solution were added and as a result, the intensity of the fluorescence signal increased spontaneously. The intensity kept constant for about 20 min. During the measurement the intensity starts to decrease after 70 min. At 90 min and 115 min the solution was shaken in addition to the constant stirring. These shaking movements increased the intensity of the fluorescence signal drastically and in the same manner the intensity started to decrease again. At 115 min this procedure was once again repeated with the same result like before. The reason why this shaking movement has such a big impact is still unknown. It could be possible that the vesicles and their aggregates are so heavy that the constant stirring in the cuvette is not enough to spread the vesicles evenly in the solution. This question will be addressed later on in the section "'Leakage assay"' (Section 9.3)

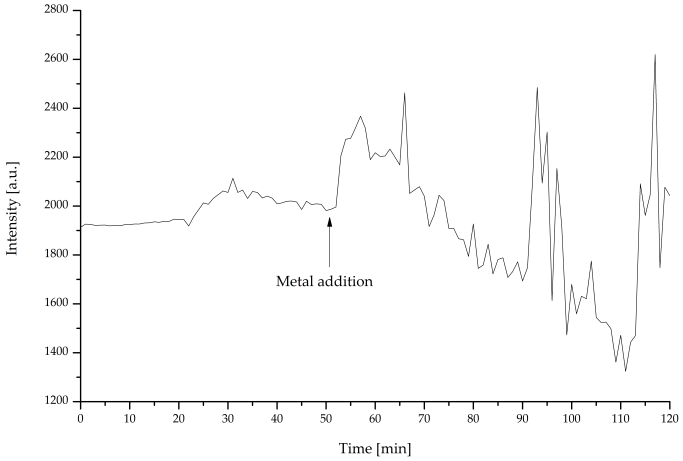

Figure 9.13: Peptide coordination with a peptide-lipid-ratio of 1:50, 200 nm vesicle diameter, a fluorescence label of 0.2 mole-% and the peptide was directly incorporated after **E**.

Both measurements with the 200 nm vesicles showed a positive impact on the FRET-effect and therefore on the results of the experiments. To investigate the influence of the vesicle size more measurements with even bigger vesicles were performed. Among others, vesicles with a diameter of 400 (Fig. 9.14) and 1000 nm (Fig. 9.15) were analyzed. Two exemplary measurements will be discussed in more detail. The first example will be the measurement with 400 nm vesicles under the same conditions like in the measurements before. It can be seen that the intensity is constant at the beginning of the analysis, but after 30 min the intensity starts to decrease again. After a total time of 75 min the metal solution was added, which causes a spontaneous increase of the intensity. However, the intensity did not increase above the starting intensity and is decreasing again after several minutes. All these trends were already observed in the previous measurements with a similar conclusion: Caused by the addition of metal solution a small increase in the intensity was observed. That means, that a corresponding FRET-effect was observed, even when the overall trend of the intensity is decreasing. It seems that a bigger diameter of the vesicles has a positive effect on the results of the measurements. To analyze this hypothesis, vesicles with a diameter of 1000 nm were also tested. (Fig. 9.15). However, the hypothesis could not be proven. The overall trend is that the intensity of the signal starts immediately to decrease, even the addition of the metal solution could not change this process. The small increase after the addition could

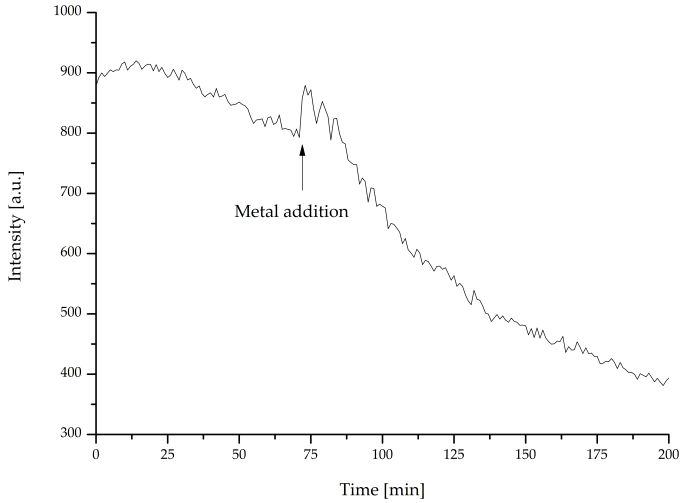

Figure 9.14: Peptide coordination with a peptide-lipid-ratio of 1:50, 400 nm vesicle diameter, a fluorescence label of 1.5 mole-% and the peptide was incorporated after method **E**.

be a sign for a FRET-effect, but it could also be a random deflection. If LUVs with a diameter of 1000 nm are used that were manufactured according to the SOP Section 13.3, it is possible that the LUVs are no longer unilamellar or that the vesicles are to some extent no longer unilamellar. For LUVs of this size the probability of polydispersity increases.[232] This fact can lead to significant disturbances in the measurements, since a polydisperse membrane behaves very differently to a unilamellar layer.

It can be summarized that the size of vesicles plays an important role for the output of the measurement, with an increasing diameter (from 100 to 400 nm) the results were getting better, but with even bigger vesicles, like the vesicles with a 1000 nm diameter, the results are not repeatable. Which is no surprise, when the fact is taken into account, that vesicles with a diameter of 1000 nm are prone to be polydisperse.[232] The content of fluorescence marker also seems to have an impact. With a higher content the noise in the spectra is more present, than with a content of 0.2 mole-%. Also, the method of incorporation of the β-peptide can be compared and it seems, that different methods have in impact on the results. In general, for the measurement with method **I** the initial trend of the intensity is decreasing like for the measurements with method **E**. In both cases a FRET-effect was observed induced by the addition of metal solution. After the addition, the intensity is in-

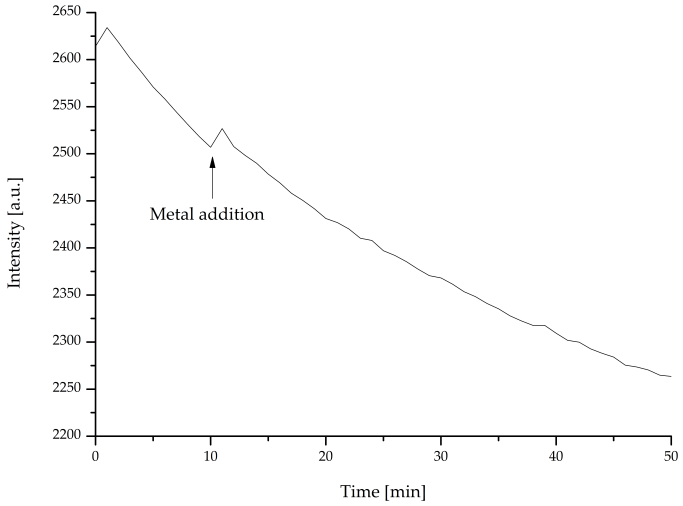

Figure 9.15: Peptide coordination with a peptide-lipid-ratio of 1:50, 1000 nm vesicle diameter, a fluorescence label of 0.2 mole-% and the peptide was incorporated after method **E**.

creased and remains constant for method **I** and is decreasing for method **E**. It could be assumed that method **I** is to be preferred to method **E**, since no decrease in intensity can be observed when measuring with method **I**. From the view of the results this assumption could be agreed, unfortunately there were big problems to get a consistent vesicle solution when preparing samples according to method **I**. Some of the results and the sample preparation for method **I** have suggested, that there is something wrong with the obtained sample solutions. Like mentioned earlier, a certain amount of the lipid material was found to stuck on the membrane filter of the extruder. For that reason, the sample solution for the measurements were analyzed in regard of their size distribution. It was found, that no LUVs with a defined size distribution could be produced and therefore the further use of method **I** was abandoned.

The influence of a further parameter should be considered, as up to now all vesicles have only be analyzed with DOPC. As already described in the introduction, DMPC was chosen as the second lipid material, in contrast to DOPC. A peptide-lipid-ratio of 1:50, a vesicles diameter of 200 nm, a content of fluorescence marker of 0.2 mole-% were chosen and the β-peptide was added after method **E**. In the following figure (Fig. 9.16), it can be seen that the initial intensity is decreasing and after the addition of the metal solution after 20 min the intensity is drastically

reduced. The measurement was aborted after 66 min. The usage of DMPC seems

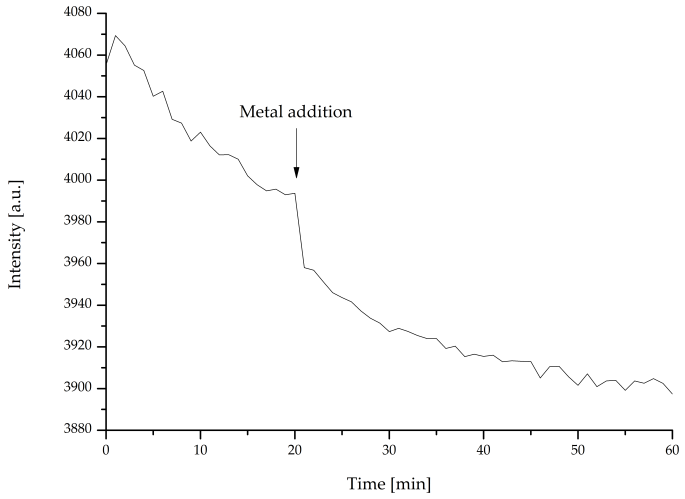

Figure 9.16: Peptide coordination with a peptide-lipid-ratio of 1:50, 200 nm DMPC vesicles, a fluorescence label of 0.2 mole-% and the peptide was incorporated after method **E**.

not very promising, that is why all further measurements were carried out using DOPC.

As a last parameter, the peptide-lipid-ratio and their impact on the results should be taken into consideration. A possible positive influence on the peptide/membrane interaction with a low peptide-lipid-ratio was studied, to analyze if a low whether a peptide-lipid-ratio can counteract the negative influence of the membrane activity. Therefore, a measurement with a peptide-lipid-ratio of 1:150 was performed, vesicles with a diameter of 200 nm were used, a fluorescence marker content of 0.2 mole-% and the β-peptide was incorporated after method **E** (Fig. 9.17).

As can be seen from the graph, the intensity drops immediately after the start of the measurement. The addition of the metal solution does not change the general course of the intensity. The intensity continues to drop after the addition until the measurement was finished after 220 min.

In summary, it can be said about all measurements carried out (measurements which are not discussed can be found in the Appendix) that the measurement results are not clear. The majority of the measurements (13 out of 21) show a course

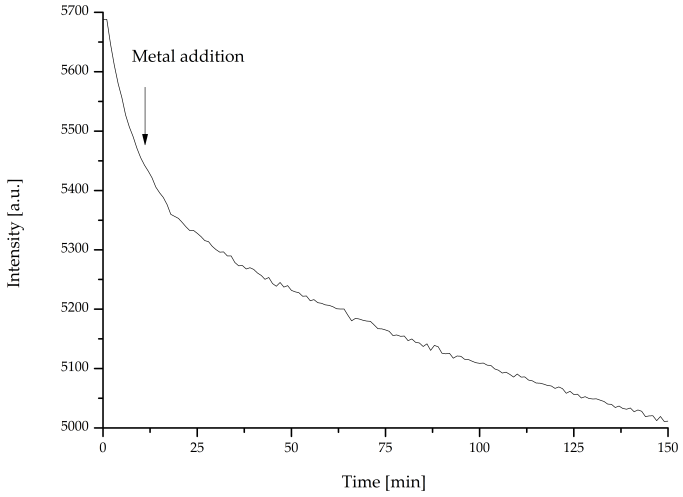

Figure 9.17: Peptide coordination with a peptide-lipid-ratio of 1:50, 200 nm DMPC vesicles, a fluorescence label of 0.2 mole-% and the peptide was incorporated after method **E**.

that deviates from expectations. In these cases no FRET-effect could be observed. The remaining 8 measurements show an increase in intensity after the addition of metal solution, which however, begins to fall again after a short time. In the following part the reason why, the intensity tends to fall in all measurements will be discussed.

All measurements had one thing in common: after the long measuring times the vesicle solution showed a strong opacity and the vesicles stuck together at the inner side of the cuvette by forming a kind of aggregates. By mechanical shaking of the solution these aggregates were detached and distributed in the solution. This effect would explain why the intensity is decreased over time and increased again after shaking the cuvette. The intensity drops, because the local concentration of the vesicles, that are available for the measurement based on the sticking effect is diminished. Shaking of the cuvette distributes the vesicles again in the solution and causes the increase in the intensity. The other phenomenon with the problem during the sample preparation after method **I** could also be explained with this effect. If the β-peptide causes such aggregates with the vesicles, then the same can happen with the MLVs before the extrusion. The MLVs will stick together and could not pass the filter inside of the extruder and that would prevent forming of the LUVs.

There must be a property of the β-peptides, that make this phenomenon possible and can explain the observations. The interaction of the β-peptides and the surface of a membrane has to be more diverse than assumed, even though a simplified model system was used for all experiments. One explanation could be, that the β-peptides are membrane active, that means that the β-peptides are disturbing the membrane integrity and cause unstable membrane structures. The exact motif of disturbing the membrane integrity in this case is unknown, but there are several possibilities, that could explain the above described observations. Some of the possible models are the barrel-stave, the toroidal pore and the carpet model (Fig. 9.18).

For the barrel-stave model pore consisting of peptides is formed, while the hydrophobic parts of the peptides show in the direction of the membrane and the hydrophilic parts forms the inner side of the pore. Like the carpet on the floor are aligned the peptides in the carpet model on the surface of a membrane, which is characterized by a parallel lining of the peptides to the surface of the membrane. The pore formation is caused by a detergent-like behavior of the peptides. The toroidal pore model is very similar to the barrel-stave model, in both models pores are formed caused by the peptides. In the toroidal pore model the pore not only consists of the peptide, it also consists of inward curved lipid material. Cationic peptides can cause an electrical potential difference across the membrane and the pores are formed by electroporation. This effect is summarized under the molecular electroporation model. In the last model, the sinking raft model the amphipathic peptides cause a mass imbalance, what increases the curvature of the membrane surface. The peptides start to self-aggregate, while sinking into the membrane, what causes transient pores. Due to the transient pores the peptides are distributed on both leaflets of the membrane.

Comparing the models A, B and C with the model during the measurement, it can be concluded that these models fit the most to describe and explain the already mentioned observations. Especially in regard to the design of the used β-peptide it is not unlikely that a membrane active β-peptide was generated and subsequently analyzed. To prove this hypothesis a leakage assay was performed to analyze if or if not the used β-peptide is membrane active.

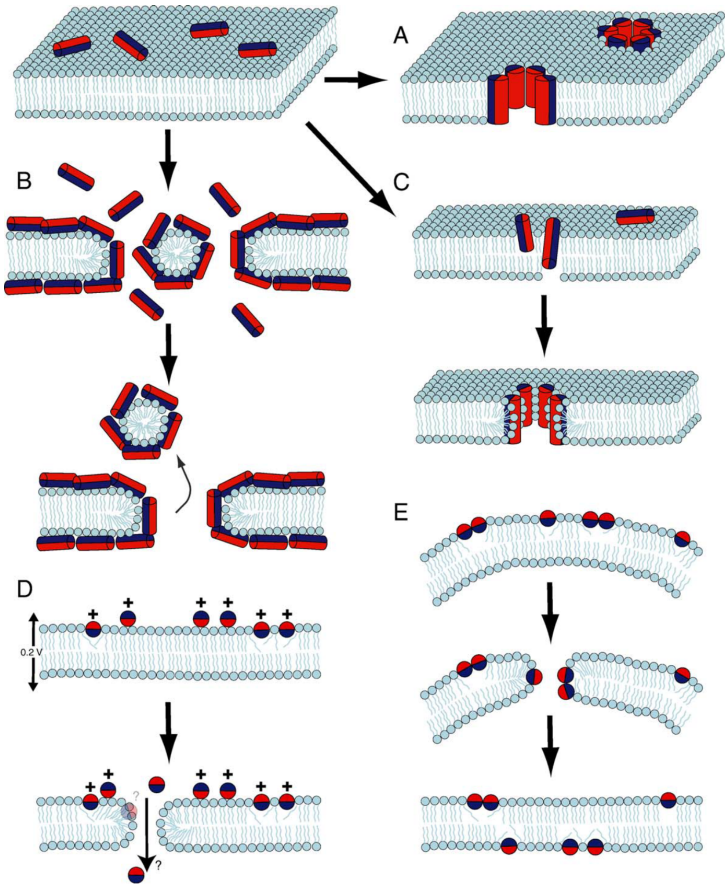

Figure 9.18: Five different possibilities of peptides, that could act as a membrane active peptide. The hydrophobic parts are shown blue and the hydrophilic parts are shown in red. A, B and C starts from the interaction of the peptide with the surface of a membrane. A) barrel stave model, B) carpet model, C) toroidal pore model, D) molecular electroporation model and E) sinking raft model.

9.3 Leakage assay

9.3.1 Introduction

The previous measurements have shown, that a FRET-effect between two different vesicles can be established, but due to a steady decrease of the fluorescence intensity the majority of measurements failed. It is reasonable to assume that the used β-peptides are membrane active and therefore disturbing the membrane integrity and preventing as a direct result the measurement. In order to prove the hypothesis and the membrane activity of the β-peptides a leakage assay was performed. The membrane stability and permeability were investigated by adding a defined amount of β-peptide.

9.3.2 Experimental setup for the leakage assay

The vesicles were prepared following the procedure from Section 13.3, subsection 13.3.2 and separated as described in **SOP 11**. Afterwards, the prepared vesicles were filled with a 20 mM solution of PBS-buffer with sulforhodamine B. Sulforhodamine B is known for self-quenching at concentrations higher than 20 mM. If the concentration of the sulforhodamine B is decreased the intensity of the fluorescence is increased, because the self-quenching effect is reduced. Sulforhodamine B trapped inside a vesicle with a concentration $\geq$ 20 mM and the membrane integrity is disturbed by any effect that causes a loss of vesicle content to the surrounding solution, an increase of the intensity of the fluorescence can be observed. With this method the membrane activity of the synthesized β-peptides can be analyzed.

Three different peptide-lipid-ratios were investigated: 1:50, 1:300 and 1:500. The larger the ratio, the smaller the negative effect of the membrane activity of the peptides should be. All measurements were performed three times for each peptide-lipid-ratio and the intensity maximum I_{max} of sulforhodamine B was determined by adding Triton X-100 (0.1-%ig in solution). While adding Triton X-100 all vesicles in the solution are destroyed and the sulforhodamine B is completely released. All

measurements are normalized according to equation Eq. 9.2 with the respective maximum intensity I_{max} of sulforhodamine B. Analogous to this procedure, blank samples were measured. Different β-peptides were used for the measurements and in case of the blank measurements the solvent mixture (TFE/buffer, 4:1 v/v) or a corresponding control β-peptide was used.

$$\frac{I(t) - I(0)}{I_{max} - I(0)} = L(t) \tag{9.2}$$

9.3.3 Results of the leakage assay

Figure (Fig. 9.19) shows the first example of a leakage assay with β-peptide **P-51**. After a short time of equilibration to measure the background diffusion, **P-51** was added after 11 min and the intensity increased by 0.6. After another 5 min the value was stabilized and after a total time of 39.5 min Triton X-100 was added to measure the maximum fluorescence intensity of sulforhodamine B. The measurements clearly

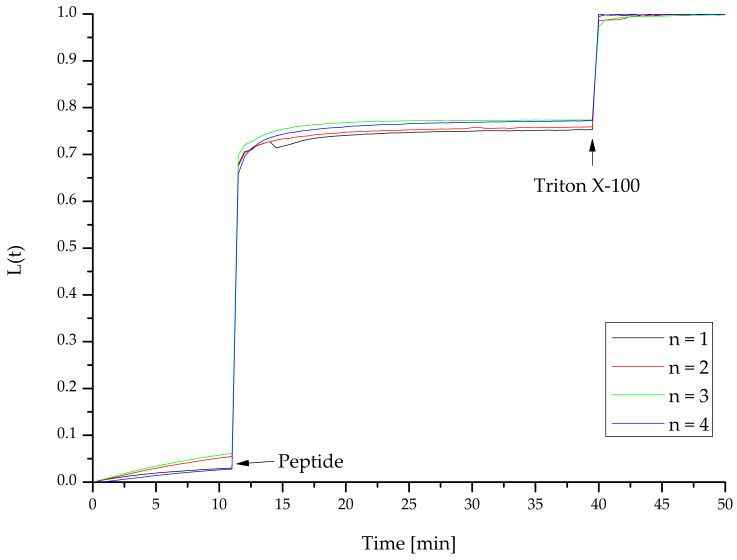

Figure 9.19: Leakage-assay with a peptide-lipid-ratio of 1:50, the β-peptide **P-51** is solved in TFE/buffer (25 µL, 4:1, v/v). The β-peptide is added after 11 min and Triton X-100 is added after 39.5 min.

show, that **P-51** strongly disturbs the membrane integrity. Most of the content inside the vesicles is released by adding the β-peptide. By addition of Triton X-100

the last vesicles are destroyed and the fluorescence intensity reaches their maximum. As already mentioned, the β-peptide has to be dissolved in a combination of TFE and buffer. TFE was chosen because it has less influence on the membrane integrity and, in addition, the stress on the membrane while mixing with the buffer should be reduced (Fig. 9.20).

Figure (Fig. 9.20) shows the results of the blank measurements. The intensity increased to 0.2 which means, that the pure solvent mixture has an influence on the membrane but in comparison to the influence of **P-51** at a peptide-lipid-ratio of 1:50 it is less pronounced.

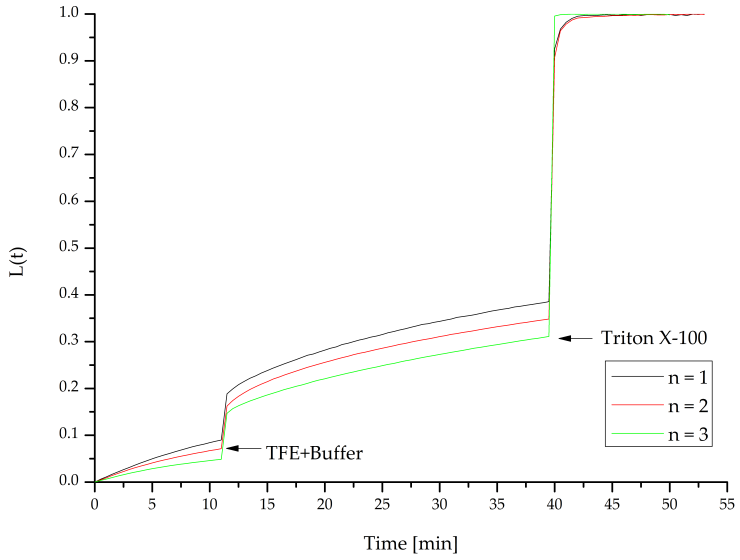

Figure 9.20: Leakage-assay - blank measurement with TFE/buffer (25 µL, 4:1, v/v). The mixture is added after 11 min and Triton X-100 is added after 39.5 min.

The peptide-lipid ratios 1:300 (Fig. D.2) and 1:500 (Fig. D.2) were measured in the same manner and are depicted in the Appendix (chapter D). In Figure (Fig. 9.21) all three peptide-lipid-ratios and the blank measurement are shown together (the single measurements were accumulated).

Figure (Fig. 9.21) demonstrates, that with a chance of the peptide-lipid-ratio the influence on the membrane integrity changes, too. The influence correlates directly with the peptide-lipid-ratio, which means, that with the biggest ratio (1:50) the influence is the strongest. The intensity is increased by 0.8 after the addition of the β-peptide. When the ratio is lowered to 1:300 the intensity is increased by 0.6 and

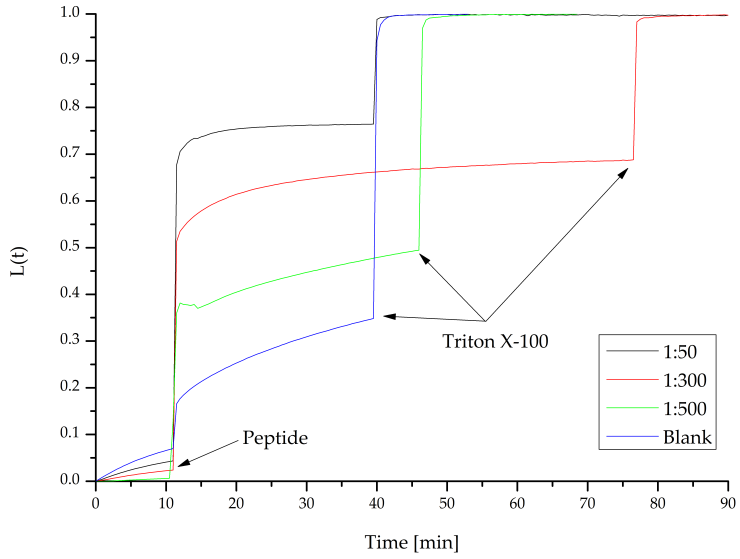

Figure 9.21: Leakage-assay - Comparison of all three peptide-lipid ratios and the corresponding blank measurement. The β-peptide **P-51** was added after 11 min and Triton X-100 was added after a variable time.

by lowering the ratio to 1:500 the increase in the intensity is 0.4. The influence of the solvent mixture increased the intensity by 0.2. It can therefore be concluded that the greater the difference in intensity, the more membrane-active the β-peptide and consequently the membrane integrity is disturbed. The trend within the peptide-lipid ratios was thus expected. As the ratio decreases, the influence of membrane activity decreases. Even at a ratio of 1:500, a change in the intensity to 0.4 can still be observed, whereby the influence of the pure solvent mixture can no longer be neglected.

These results provided the necessary explanation for the previously made observations during the peptide coordination (see subsection 9.2.3). With the knowledge about the ability to disturb the membrane integrity the general trend in the results (decreasing intensity) for the peptide coordination can be explained. Another observation during previous studies was, that after the long measuring times during the experiments for the peptide coordination, the vesicles stick together. To prevent the problem with the sticking of the lipid material in the filters, the incorporation of the β-peptides using method **E** was introduced, which allowed the preparation of LUVs. Unfortunately, after addition of the β-peptides the vesicles start to aggregate

and forms bigger vesicles-peptide formations. These aggregates stick to glass and were not longer present for the analysis, that could be a reason why the intensity is constantly decreasing.

It was mentioned, that it some cases the solution with the MLVs and the directly incorporated β-peptides (method **I**) could not be extruded and that the lipid material stuck to the filter. This observation could be due to the membrane activity of the β-peptide. It seems that in case of a direct incubation of the β-peptide with the lipid material, the extrusion of this suspension will not succeed as the β-peptides prevent the formation of stable LUVs. Furthermore, the MLVs will stick together and get caught in the filter.

In order to solve the previously described problems, the next generation of β-peptides represented by **P-55** and **P-62** were introduced. During the studies for the binding of the different β-peptides (subsection 9.1.3) it could be shown that the two new β-peptides are an improvement in peptide design. The results of the binding studies (subsection 9.1.3) were inconclusive, because the behavior to each other of **P-55** and **P-62** showed big differences. To further analyze the two β-peptides **P-55** and **P-62**, their membrane activity was determined. The same conditions like before were chosen and applied for these measurements. The measurement for **P-55** were repeated four times and for **P-62** three repetitions were made. **P-62** was also used as a control β-peptide to **P-55**. The measurements for **P-55** (Fig. 9.22) show a clear result: **P-55** is not membrane-active. After 10 min **P-55** is added to the test solution, but there is no change in the fluorescence signal. Only when Triton X-100 is added after 38 min, a significant increase in the fluorescence is observed as expected.

The same measurement was done with three repetitions for the control β-peptide **P-62** (Fig. 9.23). Between 10 and 15 min the β-peptide was added and a small increase in the fluorescence was observed. This small increase showed more membrane activity of the control β-peptide, than for the regular β-peptide and this case was not expected. To measure the maximum fluorescence once again Triton X-100 was added after 38 min. These measurements lead to the conclusion, that the β-peptides **P-55** and **P-62** have a good solubility in aqueous media, but have no or just a very bad ability to bind the surface of a membrane. This is indicated by the relative weak

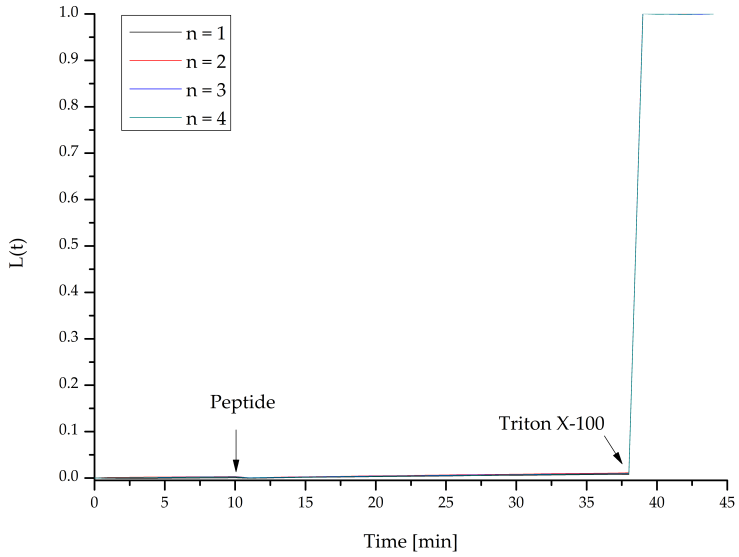

Figure 9.22: Leakage-assay - Comparison of all four repetitions of the measurement for **P-55**. The β-peptide **P-55** was added after 10 min and Triton X-100 was added after 38 min.

signal during the binding studies (Fig. 9.6) and was confirmed with the leakage-assay. Both β-peptides caused no or just a little leakage, which means that the β-peptides do not interact with the surface of the membrane.

With the last two generations of shown β-peptides two extreme cases were shown and analyzed. On the one hand, the β-peptides were too hydrophobic, hardly soluble in aqueous media and had a strong negative impact on membrane integrity. On the other hand, the other extreme case: the β-peptides were well soluble, significantly more hydrophilic, but did not interact with the membrane. The last generation of synthesized β-peptides **P-56**–**59** tried to combine the best properties from both extreme cases. These β-peptides were designed to find the "golden mean". The β-peptides should be hydrophobic enough to bind on the surface of a membrane, but should also have a hydrophilic character to ensure a good solubility in aqueous media.

Under the conditions like before the β-peptides **P-56**–**59** were also analyzed and their results are shown here. The measurements of **P-56** and **P-57** were always shown and compared to their respective control β-peptide **P-58** and **P-59**. The measurements for **P-56** and **P-57** were repeated three times (each), whereas **P-58**

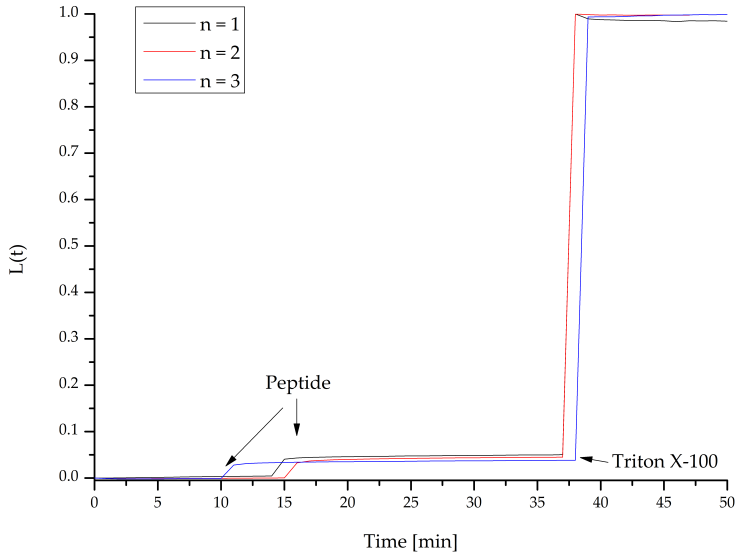

Figure 9.23: Leakage-assay - Comparison of all three repetitions of the measurement for the control β-peptide **P-62**. The β-peptide **P-62** was added between 10 and 15 min and Triton X-100 was added after 37 and 38 min.

and **P-59** were measured just one time.

The analysis of **P-56** together with the comparison of the control measurement with **P-58** are shown in Fig. 9.24. An equilibrium of 10 min was recorded before the β-peptide was added and the resulting change in the fluorescence signal was measured. The intensity of the signal was increased of 0.3 and after 50 min Triton X-100 was added to measure the intensity maximum. By addition of Triton X-100 the intensity raised from 0.3 to 1. All three repetitions are comparable and differ only in a small range. The intensity maximum was also determined for the control β-peptide which means that **P-56** is membrane active and causes a leakage that is in comparison to the control β-peptide less intensive.

In case of **P-58** and **P-59** a stronger influence of the β-peptides on the membrane integrity is shown in Fig. 9.25. After around 10 min the β-peptides were added and the caused change in the fluorescence signal is measured. For **P-58** an increase in the intensity of around 0.8 is observed. After 50 min Triton X-100 was added to measure the absolute maximum for the leakage-assay. It should be noted that the measurements of **P-58** shows strong fluctuations, which were not observed for **P-56** and for the two control measurements. The reasons for these fluctuations are

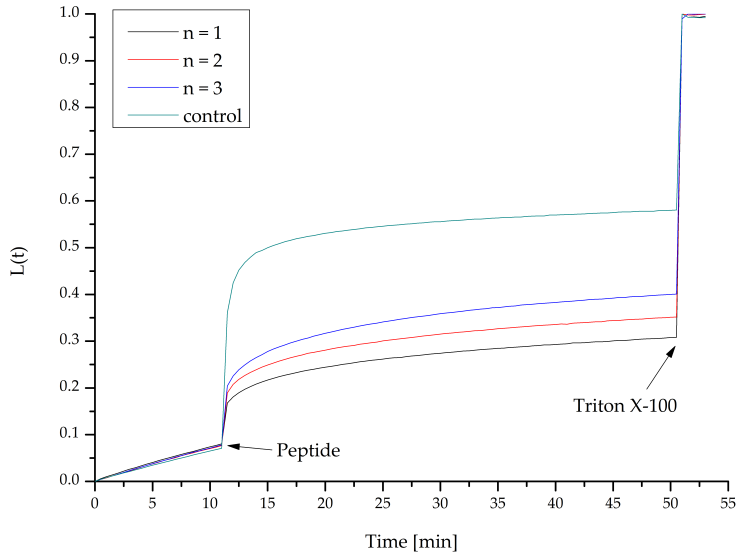

Figure 9.24: Analysis and comparison of the leakage-assay of **P-56** and **P-57**.

not known, but it seems to be a systematic cause, since all three repetitions show the same effect. Also, the general course and the effect on the membrane is comparable in all three repetitions. The corresponding control (**P-59**) shows a lower influence on the membrane, the intensity of the fluorescence increases by 0.45, which is about the half of the intensity of **P-58**. The intensity distribution of **P-58** and **P-59** is more in line with expectations than of **P-56** and **P-57**. In **P-58**/**P-59** the main β-peptide shows a higher activity than its control. However, while the intensity of **P-58** suggests a better interaction with the membrane, the stronger interaction with the membrane also leads to a greater disruption of membrane integrity.

The comparison of all four β-peptides (Fig. 9.26) will also be discussed to illustrate the different influences of the β-peptides on a membrane and to link the results from the leakage-assay with the analysis from the binding study between the β-peptides and the surface of a membrane. The two corresponding pairs **P-56**/**P-58** (black/green lines) and **P-57**/**P-59** (red/blue lines) are illustrated. **P-56** and **P-58** show the lowest intensities, where **P-56** has the lowest intensity of all four samples. The next sample is the control β-peptide **P-59** for the main β-peptide **P-57**. That means that **P-56** shows the lowest influence on the membrane integrity and **P-57** shows the opponent effect, with the highest influence. This is kind of unexpected

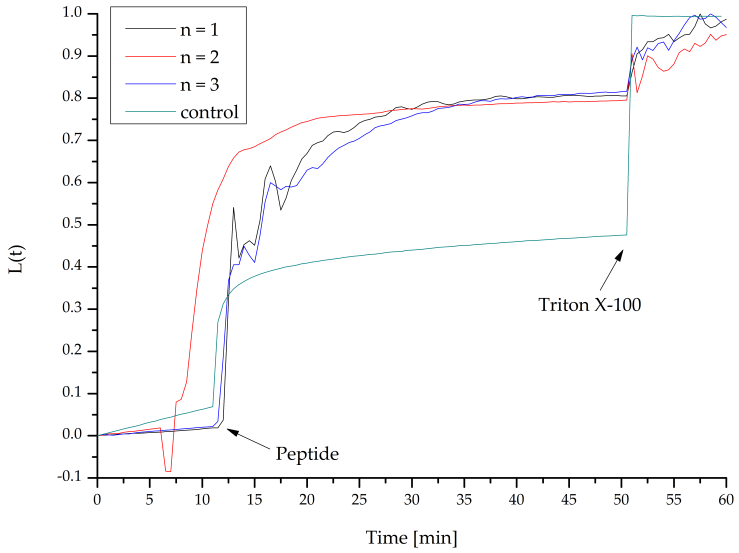

Figure 9.25: Analysis and comparison of the leakage-assay of **P-58** and **P-59**.

because **P-56** was modified with two membrane anchors and **P-57** was modified with just one lipid anchor. Both controls are sorted between **P-56**/**P-57**, despite both controls do not have any lipid anchor. These results are in line with the results from the subsection 9.2.3: In the analysis of the binding studies **P-56** showed a lower binding affinity than **P-57** and this is reflected in the results of the leakage-assay. With a lower binding affinity of the β-peptides, the membrane activity of the β-peptides is also reduced. The result of the two controls are interesting too, as **P-58** shows a lower activity than **P-59** even though both β-peptides have no lipid anchor at all. That means that the backbone of the β-peptide and the involved side chains of the amino acids play an important role in the interaction with surface of a membrane. Overall the results of all four β-peptides together show the influence of two lipid anchors up to the absence of any lipid anchors.

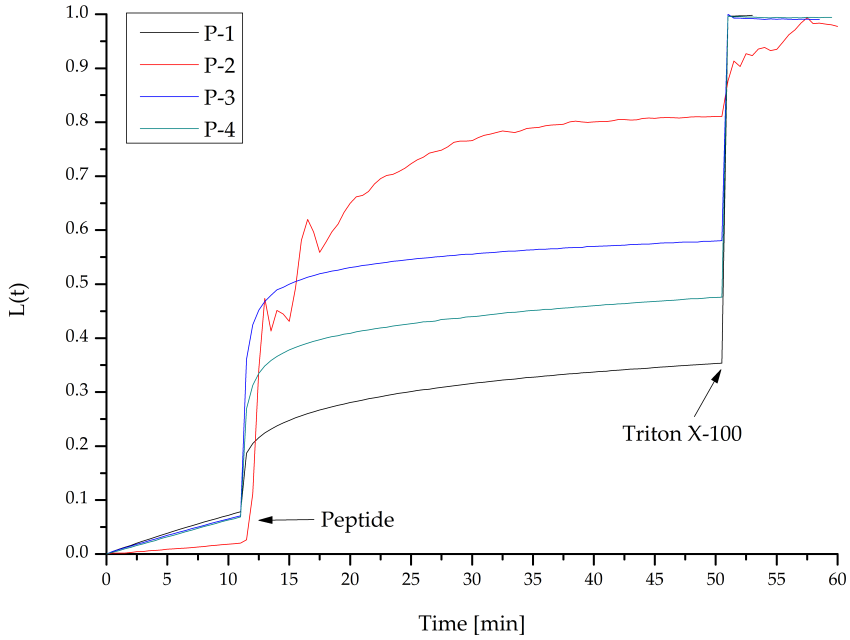

Figure 9.26: Analysis and comparison of the leakage-assay of all four β-peptides **P-56** – **P-59**.

Part V

Conclusion

According to the liquid mosaic model of Singer and Nicolson, the cell membrane defines the boundaries of a cell to the inside and outside and describes a two-dimensional lipid bilayer. Integrated into this lipid bilayer are various membrane proteins that are involved in a large number of vital processes and tasks. These tasks include signal transduction as well as transport into and out of the cell. These biomolecules can interact at the membrane surface or as a transmembrane domain with the membrane.

In contrast to the hypothesis according to the liquid mosaic model, the peptides and proteins in a membrane are not completely unrestricted in their mobility along the membrane. In order to perform all membrane functions, a long-range molecular and structural organization is required. In order to ensure a long-range structural organization and stability, the so-called membrane skeleton (MSK) is involved as part of the cytoskeleton. The MSK forms and stabilizes domains in the membrane, provides the membrane with increased mechanical stability and provides important anchor points for various other cytoskeletal components.

In order to explain the mechanical stabilization of the membrane by the MSK, the anchored protein picket model was established. According to this model, the MSK forms a kind of "net" that holds the components of a membrane together on one side and prevents them from diffusing freely through the membrane on the other side. It is still unclear how the MSK controls the domain formation and differentiates between the individual membrane components. An important aspect here is to improve the understanding of the interaction between the membrane (surface) and the membrane components with a main focus on the membrane-peptide interaction. In order to bring this highly complex issue to a more comprehensible level, various model systems have been developed and introduced. To reduce the complexity of the investigated system the peptidomimetics were developed. With the peptidomimetics it is possible to reduce the function of the used peptides and to analyse the basic properties and functions of this system.

In the presented thesis β-peptides with their well defined secondary structure was used to mimic natural peptides that interact with the surface of a membrane to manipulate the composition of the membrane or to introduce a peptide network. Both aims should lead to a deeper insight in the lipid-peptide interaction and how lipid

domains are formed. The model β-peptides were synthesized by using the Fmoc/tBu based solid-phase peptide synthesis (SPPS) with multiple instances of orthogonal protective groups. With this flexibility during the synthesis it was possible to get access to a toolbox-like synthetic strategy, what lead to an easy and fast way of synthesising different β-peptides. With this toolbox one peptide backbone was synthesized, which could be modified at the end with different recognition units or lipid anchors. Even the access to blind β-peptides as a negative control during the versatile analysis was simplified. Multiple generations of β-peptides were synthesized and with each generation the properties and functions were further optimized. The first generation of β-peptides **P-49** (Fig. 6.2) was very hydrophobic and showed a strong tendency to be membrane active and therefore to disturb the membrane integrity and therefore the analysis. The advantage of this system was, that the binding abilities were very pronounced and **P-49** bind very well to the surface of a membrane. In the following generations it was tried to optimize the binding abilities without the down side of disturbing the membrane integrity. The further β-peptides, like **P-55**, were modified so that they had a much more hydrophilic character. By introducing additional Asp amino acids, additional net charges were introduced into the β-peptide, which made the β-peptide much more soluble, especially in aqueous media, but the β-peptide also stopped binding to the membrane surface. Some of the more hydrophilic character was removed for the following generation (**P-56**, **57**, **58** and **59**). With this generation a good compromise could be found between the hydrophilic component to ensure solubility and the hydrophobic component so that the β-peptides can bind to the membrane.

The first property analyzed property of the synthesized β-peptides was the secondary structure by CD-spectroscopy. The secondary structure is an important component of the whole thesis, without a well defined and known secondary structure the design and the corresponding analysis of the β-peptides would be worthless. For all analyzed β-peptides could be shown, that the β-peptides, no matter from which generation they come, all have a right-handed 14-helix as planned. Like expected their are differences in the intensity of the signals. In organic solvents the secondary structure is more pronounced, than in aqueous media. The organic solvents support the secondary structure and therefore an increased intensity could be observed.

A main focus of this work was the analysis of the β-peptides with respect to the ability of a metal induced aggregation and to form a kind of peptide network on the surface, similar to the MSK or lipid domains in the membrane. To answer this question, first it was investigated the binding of metal ions by the β-peptides and their recognition unit(s) and then it was tried to transfer these results to the metal induced aggregation on model membranes.

The coordination of metal ions by the β-peptides was investigated by UV/Vis titrations. This was done using the property of the recognition unit that the metal coordination significantly changes the absorption spectrum. Three different metal ions were analyzed and it could be shown that the β-peptides quantitatively coordinate the metal ions in solution. To get a deeper insight in the coordination itself, the Job-plot analysis was performed. It allowed to draw conclusions about the coordination number between the β-peptides and the metal ions. For some β-peptides higher aggregates, which indicate a network-like coordination, were found. It has to keep in mind, that the Job-plot method is not undisputed. For example, this method cannot differentiate between aggregates with the ratio 1:1, 2:2 or 3:3. All ratios that represent an integer multiple always give the same result. With these positive results in hand, the next step was tried. It should be tested, if a metal induced aggregation on a model membrane can be demonstrated. Before this can be done, it has to be checked, if the β-peptides bind to the surface of a model membrane. For this purpose a binding study was performed, where fluorescence labeled β-peptides should bind to a membrane, which were also labeled. If a FRET-effect could be observed the β-peptides are binding to the membrane. This experiment was performed with all synthesized β-peptides and the summary of these experiments is, that the β-peptides show different binding affinities on the surface of a membrane. The generation of β-peptides around **P-50** show a strong affinity to bind to the surface. The next generation of β-peptides (**P-55**/**P-62**) showed no binding at all and the last generation represented by **P-56**, **57**, **58** and **59** showed a combination of the two further mentioned generations. **P-56**, **57**, **58** and **59** showed a good binding ability, the affinity was lower than for **P-50**, but higher than for **P-56**, **57**, **58** and **59**.

Up to this point it could be shown that the β-peptides take on a defined secondary structure, that the β-peptides successfully bind metal ions in solution and also bind

to the surface of membrane. The aim is to bring together these partial results in a further analysis. For this purpose the following experiment was constructed and carried out (Fig. 9.27). With this experiment, the previous experiments and their results should be combined with each other. Two labeled vesicle systems with unlabeled β-peptides were combined. During the experiments, a defined amount of metal salt solution was added and it was observed whether the β-peptides coordinate the metals accordingly, thus bringing the two vesicle systems in close proximity to each other to cause and observe a FRET-effect. Different variations of the vesicle diameter (100 – 400 nm) or different concentrations of lipid labeling (0.2 and 1.5 mol%) were tested for the experiments. For some combinations, a corresponding FRET-effect was observed after the metal salt solution was added. Also, for many of the experiments no FRET-effect could be observed, but a decrease in the intensity was always observed during the measurements. This observation could not be explained

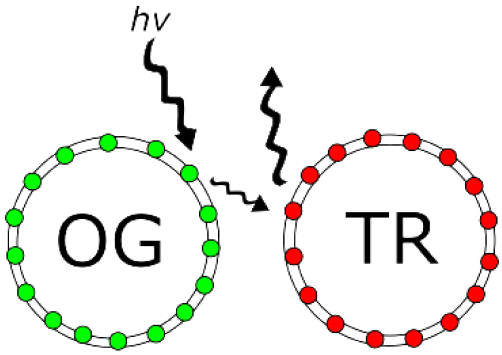

Figure 9.27: Experimental setup for the peptide coordination between two model membrane systems. Depicted in green (left side) the Oregon Green™488 DHPE marked vesicles and in red (right side) the Texas Red™DHPE marked vesicles.

directly and was therefore not to be expected in this context. A literature search confirmed the assumption that the β-peptides are membrane active and thus have disturbed the membrane integrity. To support this assumption with experimental results, a leakage assay was performed to determine the level of membrane activity and to compare the β-peptidesṪhis analysis showed, for example, that the first generation of β-peptides disturbs the membrane integrity very strong and thus causes a very strong leakage. In the following generations, this behaviour was reduced, but partly at the expense of the interaction with the membrane. For example, the

β-peptides **P-50** no longer disturbed the membrane integrity, but also the β-peptides did not longer bound to the membrane. The last generation of β-peptides then showed a moderate behaviour. These β-peptides still attempted a leakage, which was significantly lower compared to the β-peptides of the first generation and they bound to the surface of the membrane.

With this thesis, the first promising foundations for further research have been made. Metal coordination by the β-peptides in solution was successfully demonstrated, and it could also be shown that the β-peptides bind to the surface of a membrane. In further experiments it should now be shown that the β-peptides can bind the metal ions on a membrane surface and thus form a network-like system on the surface. A suitable method would be for example the atomic force microscopy.

Part VI

Experimental Part

10 General Equipment and Methods

Solvents and Reagents All solvents used during syntheses were *pro analysis* (p.a) grade, those with technical grade were purified by distillation. For all other uses HPLC grade was used. For water-based solutions like buffers or HPLC, ultra-pure water was obtained by filtration of demineralized water by an *arium mini* lab system by Sartorius (Göttingen, Germany). The commercially available reagents had the highest possible quality and were purchased from different suppliers. The NBD, Oregon Green 488 and Texas Red labeled lipids were purchased from Molecular Probes (Eugene, USA) and all other lipids were supplied by Avanti Polar Lipids, Inc. (Alabaster, USA). The used Amino acids were purchased from GL Biochem Ltd. (Shanghai, China) or IRIS Biotech GmbH (Marktredwitz, Germany) and the resin for the solid-phase peptide synthesis was from Novabiochem (Merck KGaA, Darmstadt, Germany).

Freeze Drying Aqueous samples were frozen with liquid nitrogen and the solvent was removed under reduced pressure (<1 mbar) with a *Alpha-2-4-LD plus* benchtop freeze-dryer manufactured by Christ (Osterode am Harz, Germany). If the volume of the sample was less than 2 mL, the sample was placed and dried in a *RVC 2-18* vacuum centrifuge by Christ.

Software Each time it is indicated which software was used for the data acquisition. All chemical structures were drawn and molecular masses were calculated by *ChemDraw Professional* (version 16, PerkinElmer Inc., Massachusetts USA). NMR spectra were analyzed by *MestReNova* (version 8.0.0, MESTRELAB RESEARCH, S.L,

Santiago de Compostela Spain). All shown spectra were plotted with *OriginPro* (version 8.5G, OriginLab Corporation, Northampton, MA 01060).

Mass Spectrometry All mass spectra were measured with a *maXis* spectrometer by Bruker Daltonik GmbH (Bremen, Germany). All samples were analyzed by using an electrospray ionization (ESI) method. For the sample preparation, all probes were dissolved in methanol (HPLC grade) and acidified with 10 % formic acid. The analysis of the spectra was performed by *Compass DataAnalysis* software (version 4.0) by Bruker. For each compound/peptide the mass-charge ratio is indicated along with the intensity expressed by relative percentage. As far as addressable all deconvoluted ESI mass peaks and high-resolution (HR) ESI mass peaks are given for the target peptides.

Determination of the concentration of the diazomethane solution A defined volume of the diazomethane solution was diluted in absolute ether (~50 mL) and underlaid with water. Benzoic acid[i] (1.30 g, 10.6 mmol) and phenolphthalein were added and the solution was stirred for 5 min at 0 °C before the excess of benzoic acid was back titrated with 0.2 M KOH (aq). Based on the used volume of diazomethane and KOH and the amount of benzoic acid the concentration of the diazomethane solution can be determined.

$$c = \frac{n(\text{Benzoic acid}) - c(\text{KOH}) \cdot V(\text{KOH})}{V(\text{Diazomethane})} \tag{10.1}$$

[i] the benzoic acid must be in an excess to the diazomethane, which is seen by the vanishing of the yellow color

11 Chromatographic Methods

Thin Layer Chromatography In the case of the thin layer chromatography silica gel 60 F_{254} plates from Merck KGaA (Darmstadt, Germany) were used. Spots were detected by UV deletion at 254 nm or by immersion of the plates in immersion solution and subsequent drying.

Flash Chromatography The package material for the flash chromatography was silica gel 60 (Merck KGaA, Darmstadt, Germany) with a particle size of 0.063–0.02 mm. All columns were packed with an excess (with respect to the crude compound) of a suspension of silica gel and the appropriate eluent. The crude product was loaded on the column adsorbed on silica gel or as a concentrated solution in an appropriate solvent system. The purification was performed at an overpressure between 0.5–1 bar.

High Performance Liquid Chromatography (HPLC) All preparative and semi-preparative purifications were carried out on a *ÄKTA basic 10* system by Amersham Pharmacia Biotech (Umeå, Sweden) utilized with a *P-900* high pressure pump and a *UV-900* detector. For the detection of the peptides three different wavelength at 254, 300 and 464 nm were observed if not otherwise mentioned. The used solvent systems are:

The employed columns were listed below. The *Vydac 208TP* was purchased from HiChrom (Leicestershire, United Kingdom) and the *MN Nucleodur 100* is from Macherey-Nagel (Düren, Germany).

Column 1 Vydac 208TP, C-8, 250 × 10 mm, 300 Å, 5 µm

Column 2 MN Nucleodur 100 , C-18, 250 × 21 mm, 5 µm

The solvent systems for all preparative and semi-preparative runs were

Solvent A: Water + 0.1 % TFA

Solvent B: Acetonitrile/Water (80:20, *v/v*) + 0.1 % TFA

All analytical measurements were performed on a UHPLC *Ultimate3000* from Thermo Fisher Scientific (Waltham, Massachusetts, United States of America). The used columns are listed below. The *Hypersil Gold C8* is from Thermo Fisher Scientific and the *ACE Excel 2 C18* is from Advanced Chromatography Technologies Ltd (ACE, Aberdeen, Scotland).

Column 3 Hypersil Gold C8, C-8, 100 × 2.1 mm

Column 4 ACE Excel 2 C18, C-18, 100 × 2.1 mm

The solvent systems for the analytical runs were

Solvent C: MeOH + 0.085 % TFA

Solvent D: MeCN + 0.085 % TFA

Solvent E: Water + 0.1 % TFA

The exact details to every run are provided by the product analytics. The flow rate for the preparative column was 10 mL min^{-1}, for semi-preparative column was 3 mL min^{-1} and 0.4 mL min^{-1} for the analytical runs.

Gel Filtration - Size Exclusion Chromatography (SEC) The Size Exclusion Chromatography was performed with a column (height: 19.5 mm, diameter: 6 mm) packed with *Sephadex^{TM} G-50 Fine* from Amersham Pharmacia Biotech AB (Little Chalfont, United Kingdom). The material was filled in as a suspension with PBS-buffer (20 mM in solution, 8.1 mM Na_2HPO_4, 1.5 mM KH_2PO_4, 136.9 mM NaCl, 2.7 mM KCl, pH = 7.4). The vesicle sample was eluted with the same buffer and the fraction with the vesicles was collected in a dark tube. The vesicles solution was diluted 1:10 before the measurement.

12 Spectroscopic Methods

Nuclear Magnetic Resonance (NMR) The NMR spectra were recorded using a *Unity 300*, *INOVA-500*, *Mercury-Vx 300* and *VNMRS-300* from VARIAN (Palo Alto, California, USA). The chemical shift is given in ppm and the scalar coupling constant ${}^{n}J_{\mathrm{x,y}}$ is given in Hertz (Hz), yet "n" describes the number of bonds between the coupling atoms (x,y). As an internal standard for the chemical shift the resonance signals of the deuterated solvents were used. The employed solvents are listed below (Tab. 12.1) and is indicated within each compound.

Table 12.1: Reference signal of the used deuterated solvents.

Deuterated solvents	^{1}H-NMR signal (ppm)	^{13}C-NMR signal (ppm)
Chloroform-d_1	7.24	77.23
Dimethyl sulfoxide-d_6	2.50	39.51

The temperature was 27 °C for $CDCl_3$ and 35 °C for DMSO – d_6.

UV/Vis Spectroscopy The UV/Vis measurements were used for the determination of the peptide concentration, the resin loading efficiency and the metal induced aggregation. For the last one, see for detailed information in the specific section.

The concentration was measured in solution (MeOH) using a black quartz cuvette from HELLMA ANALYTICS (Müllheim, Germany) with 10 mm light path. The used device was a *NanoDrop 2000c* (cuvette function) from THERMO SCIENTIFIC. The sample volume was 450 µL. To determine the concentration of the stock solution of the β^3-peptides a diluted solution with known dilution factor was made. Hence, the

absorption from NBD ($\lambda_{max} = 464$ nm, $\epsilon = 22000\ \mathrm{L\,mol^{-1}\,cm^{-1}}$) should be less than 1, if it was not that case another diluted solution was made. The concentration was calculated by the Lambert-Beer-Law

$$A = \epsilon \cdot c \cdot d \tag{12.1}$$

the variables are A = measured absorption, ϵ = molar extinction coefficient in $\mathrm{L\,mol^{-1}\,cm^{-1}}$, c = concentration in $\mathrm{mol\,L^{-1}}$ and d = path length in cm. As reference was used the pure solvent with a baseline correction at 750 nm.

Fluorescence Spectroscopy For all fluorescence measurements an *FP-8200* fluorospectrometer from Jasco (Tokyo, Japan) was used. The temperature was controlled by a peltier thermostat *ETC-272T* by Jasco which was connected to a *Thermo Haake WKL26* water recirculator from Thermo Electron Corp. (Watham, USA). During the measurements a quartz glass precision cell from Hellma Analytics (Mühlheim, Germany) with a light path of 10 mm for the excitation and 4 mm for the emission was used. For the data acquisition and analysis was used the software *Spectra Manager* (version 1.54.03) provided by the manufacture. The Ex and Em wavelength are shown in the table (Tab. 12.2) below. The general device settings are given in the table (Tab. 12.3).

Table 12.2: Excitation and Emission wavelength of different FRET and self-quenching fluorophores.

Used type of fluorophores	Ex wavelength [nm]	Em wavelength [nm]
NBD	464	537
Lissamine rhodamine B	570	589
Sulforhodamin B	567	583
Oregon Green™ 488 DHPE	488	526
Texas Red™ DHPE	595	610

For the binding-assay between the peptides and model membranes and the leakage-assay the temperature was set to 25 °C.

Table 12.3: Used parameters for the fluorescence analysis of the synthesized β-peptides.

Parameter	Binding-assay	Leakage-assay	Peptide coordination
Measurement range [s]		0 - 43200	
Photometric mode		Em intensity	
Em Bandwidth [nm]		5.0	
Ex Bandwidth [nm]		5.0	
Response [s]		0.5	
Stirring speed [rpm]		700	
Sensitivity	medium	low	medium
Data interval [s]	60	30	60
Intensity normalization		off	
Blank correction		off	
Auto gain		off	

Circular dichroism (CD) spectroscopy CD measurements were performed on a Jasco *J-1500* (Tokyo, Japan) spectropolarimeter equipped with a Jasco *PTC510* temperature control unit. The temperature was set at 20 °C and controlled in the cell holder. The sample cell was flushed during each measurement with nitrogen and a 1.0 mm Suprasil® QS quartz glass cuvette from Hellma Analytics (Müllheim, Germany) was used. In the following table are listed the used parameters and solvents.

Table 12.4: Used parameters for the CD analysis of the synthesized β-peptides.

Parameter	MeOH	TFE	Buffer	H_2O
Measurement range [nm]		250 - 180		
Data mode		CD & Absorption		
Bandwidth [nm]		1.0		
Response [s]		1.0		
Scanning speed [nm min^{-1}]		50		
Accumulations		5		

continued on the next page

continued from previous page

Parameter	MeOH	TFE	Buffer	H_2O
Data pitch [nm]		0.5		
CD scale [mdeg / dOD]		200/1.0		
D.I.T. [s]		1.0		

13 Standard Operating Procedures (SOPs)

13.1 Synthesis of *N*-protected d-β^3-Amino acid

13.1.1 Synthesis of the diazo ketone[196, 233]

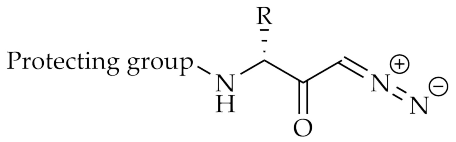

The synthesis of the diazo ketone is based on the procedure by Guichard *et al.* The *N*-protected D-α-amino acid (1.00 eq) was dissolved under an inert gas atmosphere in dry THF (4.70 mL mmol^{-1}) and cooled to 0 °C. NEt_3 (1.10 eq) and isobutylchloroformiate
(1.10 eq) were successively added under continued cooling. After 30 min stirring at constant temperature diazomethane (0.60–0.80 M[i] in Et_2O, 2.00 eq) was added under exclusion of light. The reaction mixture was allowed to warm to rt and stirred for 4 h, after which the solution was quenched with glacial acid (0.30 mL mmol^{-1}). The quenched mixture was taken up in aqueous 6 % $NaHCO_3$ (100 mL) and extracted with EtOAc (3 × 100 mL). The combined organic extracts were washed successively with Brine (100 mL) and saturated aqueous NH_4Cl (100 mL), dried over

[i]for each batch the concentration of the diazomethane solution was checked

$MgSO_4$ and the solvent was removed under reduced pressure to yield the respective diazomethane as a yellow oil or colorless solid. If the oil or solid had other colors (brown - red) the crude product was purified by flash column chromatography (SiO_2, *n*-pentane/EtOAc 1:1, *v/v*). If not otherwise stated the crude product was used without further purification and a quantitative yield.

13.1.2 Synthesis of the *N*-protected d-β³-Amino acid

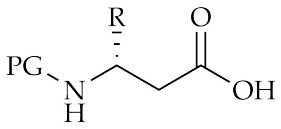

Path A[196, 233] Following a modified proceeding from Guichard *et al.* the diazo ketone was dissolved in a mixture of THF/Water (6.05 mL mmol^{-1}, 9:1, *v/v*) and under exclusion of light silver benzoate (0.10 eq) was added. After 2 h in an ultrasonic bath the organic phase was removed under reduced pressure and water (~50 mL) was added. The water phase was acidified with 1 M HCl to pH = 2-3 and extracted with EtOAc (3 × 100 mL). The combined organic phases were dried over $MgSO_4$ and the solvent was removed under reduced pressure. Precipitation and filtration of the crude product from EtOAc in cold *n*-pentane (-18 °C) yielded the desired product.

Path B[172] After a procedure from Patil *et al.* the diazo ketone (1.00 eq) was dissolved in 1,4-dioxane/H_2O (10.2 mL mmol^{-1}, 2:1, *v/v*) and mixed with silver benzoate (0.10 eq). The reaction mixture was irradiated in a domestic microwave oven (60 s, 470 watt), afterwards the organic part of the solvent mixture was removed under reduced pressure and the remaining solvent was diluted with water (~50 mL). The water phase was acidified with 1 M HCl to pH = 2-3 and extracted with EtOAc (3 × 100 mL). The combined organic phases were dried over $MgSO_4$and the solvent was removed under reduced pressure. Precipitation and filtration of the

crude product from EtOAc in cold *n*-pentane (-18 °C) yielded the desired product.

13.2 Peptide Synthesis

13.2.1 Loading of the first amino acid on the resin

The first amino acid is coupled after the SOP for the Manual SPPS.

13.2.2 Determination of the resin loading[234]

In a volumetric flask the dry resin (~5 mg) and a DBU/DMF mixture (2 mL, 2 vol.-%) was added. The flask was mechanically shaken for 30 min and then filled up to 10 mL with acetonitrile. This stock solution was again diluted by the ratio 1:12.5 to 25 mL with acetonitrile. A reference sample was made in the same manner. For both probes the absorption at 304 nm was measured. The resin loading can finally calculate by the following equation

$$\rho_{\text{resin}} \left[\text{mmol g}^{-1}\right] = \frac{A_{\text{sample}} - A_{\text{blank}} \cdot V \cdot f}{m_{\text{resin}} \cdot d \cdot \epsilon} \tag{13.1}$$

A is the absorption value by 304 nm for the sample and blank probe, V is the volume of the stock solution, f is the dilution factor, d is the path length of the cell (1 cm) and ϵ is the molar extinction coefficient of dibenzofulvene at 304 nm (ϵ = 7624 $\text{L mol}^{-1}\,\text{cm}^{-1}$).

13.2.3 Manual microwave assisted SPPS[233, 235]

The manual microwave assisted solid phase peptide synthesis (SPPS) was performed at a *Discover SPS microwave synthesizer* from CEM (Kamp-Lindtfort, Germany). The resin was transferred into a Becton Dickinson (BD; Heidelberg, Germany) *discardit II* syringe equipped with a polyethylene (PE) frit and swollen for 2 h in DMF. A NovaPEG Rink Amide LL resin ($\rho_{resin} = 0.18\,mmol\,g^{-1}$) was used for all synthesized β-peptides. The β-peptides were synthesized using the following cycle.

1. **Swelling**
   Swelling of the resin in DMF for 2 h

2. **Deprotection I**
   The *N*-terminal Fmoc-protecting group was removed microwave assisted (25 W, 50 °C, 30 s) with DMF/piperidine (8:2, *v*/*v*)

3. **Washing**
   The resin was washed with DMF (5×)

4. **Deprotection II**
   The *N*-terminal Fmoc-protecting group was microwave assisted (35 W, 65 °C, 3 min) removed with DMF/piperidine (8:2, *v*/*v*)

5. **Washing**
   The resin was washed with MeOH and DMF (10× each)

6. **Double coupling**
   The required amino acid (4.0 eq) was activated with HATU/HOAt (each 4.0 eq, 0.5 M in DMF) and DIPEA (8.0 eq, 2 M in NMP). The coupling reaction was carried out under microwave irradiation (35 W, 65 °C, 15 min), if not otherwise stated each amino acid was coupled twice. Between each coupling step the resin was washed (3×) with NMP

7. **Washing**
   The resin was washed with DMF (10×)

8. **Capping** The free amino groups were capped under microwave irradiation (35 W, 65 °C, 3 min) with Ac_2O/DMF (8:2, v/v)

9. **Washing**
   The resin was washed with MeOH and DMF (10× each)

The steps (2) til (9) were repeated until the desired peptide was completed.

13.2.4 Post synthetic peptide modifications

After synthesizing the peptide backbone after **SOP 13.2.3** the peptide backbone was modified on resin after the following procedures.

13.2.4.1 Alloc deprotection[236]

The swollen resin was vice rinsed to DCM and mechanically shaken for 30 min in DCM. The wet resin was suspended in a few milliliters of DCM and phenylsilane ($PhSiH_3$, 15.0 eq) was added. After one minute tetrakis(triphenylphosphine)palladium(0) (TPP palladium(0), 0.25 eq) was added and heated by microwave irradiation (20 W, 38 °C, 5min). The process was repeated for a complete deprotection of the allyl protecting group. Between the deprotection steps the resin was washed with DCM (3×). After the successful deprotection the resin was washed with DCM and DMF (10×each).

13.2.4.2 Mtt deprotection[237]

The swollen resin was vice rinsed to DCM and mechanically shaken for 30 min in DCM. Afterwards, the deprotection cocktail consisting of DCM/HFIP/TFE/TIS (6.5:2:1:0.5, $v/v/v/v$, 2 mL g^{-1} resin) was added to the resin and it was shaken mechanically for 1 h. After deprotection the resin was washed with DCM (10×) and the reaction completeness was checked. Therefore, a small sample of the washed resin was placed in a glass vial and mixed with 1 % TFA in DCM. Immediately occurring

of a yellow color from the 4-Methyltrityl (Mtt) cation shows an incomplete deprotection. In this case the deprotection was repeated and the resin was shaken with a new portion of the deprotection solution for 30 min.

13.2.4.3 Manual Cholestamine coupling

The swollen resin (in DMF) was mixed with a solution of COMU (8.00 eq) and DIPEA (16.0 eq) in DMF (1 mL) to activate the free carboxy group on the resin. The suspended resin was mechanically shaken til a deep red color occurred (~5 min). Cholestamine solved in as little as possible DCM was added in another sample vial and added to the prepared resin. The reaction mixture was mechanically shaken for 1 h at rt and washed with DMF, MeOH and DCM (10× each).

13.2.4.4 Manual coupling of the Recognition Unit

The manual coupling of the recognition unit follows the same routine as described in the procedure for the microwave assisted SPPS-steps **SOP 13.2.3** (6) til (9). The equivalents were doubled when two recognition units were incorporated.

13.2.5 Cleavage of the peptides from the resin[237–239]

For the cleavage of the peptides and the final deprotection of the remaining protecting groups, the resin dried was overnight or used wet from washing with DCM. For the cleavage/deprotection the resin was mixed with TFA/H_2O/TIS (95:2.5:2.5, *v/v/v*), vigorously shaken for 2 h and the final reaction mixture was concentrated under a steam of nitrogen. The crude peptide was precipitated from cold (-20 °C) Diethyl- or *tert*-Butyl methyl ether. The precipitation was centrifuged (9000 rpm, 20 min, -5 °C), washed with ether (5×) and dried overnight under reduced pressure.

13.2.6 *N*-terminal modification of the β-peptides with 4-Chloro-7-nitrobenzo-2-oxa-1,3-diazol (NBD-Cl)

For the *N*-terminal modification of the peptides was the terminal Fmoc protecting group after **SOP 13.2.3** (2) till (5) removed. The fluorophore (5.00 eq) was dissolved together with diisopropylethylamine (DIPEA, 20.0 eq) in DMF and mixed with the resin. Under exclusion of light the suspension was mechanically shaken overnight. The resin was washed with DMF and DCM (10× each) and dried overnight under reduced pressure or the peptide was direct cleaved from the resin after **SOP 13.2.5**.

13.3 Preparation of Large Unilamellar Vesicles (LUVs)[75]

The Large Unilamellar Vesicles (LUVs) were made by rehydration of a prepared lipid film. To obtain such a lipid film a desired amount of lipid (10 mg) was dissolved in $CHCl_3$ (1 mL) and stored on ice. Based on this stock solution a defined volume was transferred into small glass tubes and the organic solvent was removed at elevated temperatures (~40 °C) under a steam of nitrogen. If necessary, lipids marked with a fluorophore were added to each sample before the organic solvent was removed. To fully dry the lipid films, the films were stored under reduced pressure at 40 °C. Films with incorporated marked lipids were stored additionally under exclusion of light.

For the rehydration of a lipid film a defined volume of H_2O or PBS buffer was added and the resulting suspension was shaken for at least 2 h. After this time the samples were vortexed (1 min) and incubated (4 min) in five cycles to obtain a milky suspension. This suspension was extruded 21× through a polycarbonate membrane, with pore sizes between 100 and 400 nm, using an Avestin *Liposofast mini extruder* (Ottawa, Canada). The poly diversity of the clear solution was checked.

13.3.1 Binding Assay

For the binding assay between the model membrane and the β-peptide DOPC respectively DMPC was used as lipid material. The DOPC/DMPC was mixed with 1,2-dimyristoyl-*sn*-glycero-3-phosphoethanolamine-*N*-(lissamine rhodamine B sulfonyl) (0.75 mol-%), the peptide-lipid ratio was 1:300, with a sample volume of 1 mL and a peptide concentration of 4 µmol. The lipid film was rehydrated in 1 mL of PBS Puffer and extruded with a pore size of 100 nm for the polycarbonate membrane. The peptide was added after the extrusion respectively during the measurement.

13.3.2 Leakage Assay[240, 241]

In the measurements for the leakage assay to check the membrane activity of the peptides, DOPC was used without any further marked lipid material. The peptide-lipid ratio was 1:50 up to 1:500, with a sample volume of 1 mL and a peptide concentration of 4 µmol. The lipid film was rehydrated in 1 mL of a sulforhodamine B-PBS Puffer solution (20 mM) and extruded with a pore size of 100 nm for the polycarbonate membrane. After extrusion of the vesicle suspension, the filled vesicles were separated from the remaining sulforhodamine B solution via Size Exclusion Chromatography (SEC) as described in **SOP 11**. The peptide was added after the extrusion respectively during the measurement.

14 Synthesis

14.1 Synthesis of β^3-amino acid Building Blocks

14.1.1 (*R*)-3-(Fluorenylmethyloxycarbonylamino)-7-((*tert*-butoxycarbonyl)amino)heptanoic acid (4)

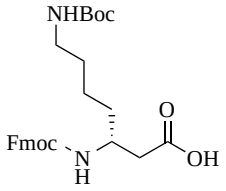

$C_{27}H_{34}N_2O_6$
[482.6]
4

On the basis of **SOP 13.1.1** and **SOP 13.1.2** (Path A) Fmoc-D-Lys(Boc)-OH (7.00 g, 14.9 mmol, 1.00 eq) was used as starting material converted to the final product **4** (5.10 g, 10.6 mmol, 75 %) as a pale yellow solid.

^{1}H-NMR (300 MHz, DMSO-d_6): δ [ppm] = 1.36 (d, $^3J_{H,H}$ = 1.8 Hz, 15 H, CH_3-Boc, γ-,δ-, ϵ-CH_2), 2.34 (t, $^4J_{H,H}$ = 6.3 Hz, 2 H, ζ-CH_2), 2.88 (q, $^4J_{H,H}$ = 6.6 Hz, 2 H, α-CH_2), 3.76 (m, 1 H, β-CH), 4.21 (d, $^3J_{H,H}$ = 6.4 Hz, 1 H, Fmoc-C$\underline{H}$), 4.29 (m, 2 H, Fmoc-C$\underline{H}$2), 6.68 (s, 1 H, NH), 7.14 (d, $^3J_{H,H}$ = 8.6 Hz, 1 H, NH), 7.32 (tt, $^3J_{H,H}$ = 7.4 Hz, $^4J_{H,H}$ = 1.4 Hz, 2 H, Fmoc-CH_{Ar}), 7.41 (td, $^3J_{H,H}$ = 7.5, 1.2 Hz,

2 H, Fmoc-CH_{Ar}), 7.68 (t, $^{3}J_{H,H}$ = 7.5, 2.3, 1.2 Hz, 2 H, Fmoc-CH_{Ar}), 7.88 (d, $^{3}J_{H,H}$ = 7.6, 1.0 Hz, 2 H, Fmoc-CH_{Ar}).

$^{13}C\{^{1}H\}$-NMR (126 MHz, DMSO-d_6): δ [ppm] = 20.71, 22.71, 28.26, 29.20, 33.85, 46.77, 47.88, 59.69, 65.13, 77.16, 119.91, 125.03, 126.88, 127.41, 140.54, 143.64, 143.79, 155.38, 172.28.

ESI-MS (MeOH) *m/z* (rel %) = 483.2 $[M+H]^+$ (10), 505.2 $[M+Na]^+$ (100), 987.5 $[2M+Na]^+$ (92).

HR-MS (ESI) $C_{27}H_{34}N_2O_6$ $[M+H]^+$ *m/z* = calc.: 483.2490, found: 483.2489.
$[M+Na]^+$ *m/z* = calc.: 505.2309, found: 505.2307.

14.1.2 (*R*)-3-(Fluorenylmethyloxycarbonylamino)-7-((diphenyl(*p*-tolyl)methyl)amino)heptanoic acid (5)

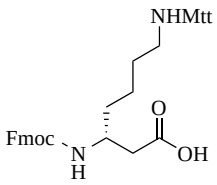

$C_{42}H_{42}N_2O_4$
[638.8]
5

On the basis of **SOP 13.1.1** and **SOP 13.1.2** (Path A) Fmoc-D-Lys(Mtt)-OH (2.00 g, 3.22 mmol, 1.00 eq) was used as starting material converted to the final product **5** (1.82 g, 2.85 mmol, 89 %) as a colorless solid.

^{1}H-NMR (300 MHz, DMSO-d_6): δ [ppm] = 1.10 – 1.49 (m, 6 H, γ-,δ-, ϵ-CH_2), 1.88 – 2.07 (m, 2 H, ζ-C$\underline{H}_2$), 2.23 (s, 3 H, C$\underline{H}_3$-Mtt), 2.28 – 2.41 (m, 2 H, α-C$\underline{H}_2$), 3.70 – 3.84 (m, 1 H, β-C$\underline{H}$), 4.12 – 4.37 (m, 3 H, Fmoc-C$\underline{H}$, Fmoc-C$\underline{H}_2$), 7.00 – 7.45 (m, 18 H, Fmoc-CH_{Ar}, Mtt-CH_{Ar}), 7.59 – 7.70 (m, 2 H, Fmoc-CH_{Ar}), 7.81 – 7.91 (m, 2 H, Fmoc-CH_{Ar}).

^{13}C{^{1}H}-NMR (126 MHz, DMSO-d_6): δ [ppm] = 20.52, 23.38, 29.96, 34.33, 43.32, 46.83, 47.88, 59.71, 64.94, 70.00, 119.88, 124.96, 126.80, 127.38, 128.03, 128.16, 134.72, 140.43, 143.52, 143.80, 146.24, 155.31, 172.17.

ESI-MS (MeOH) *m/z* (rel %) = 639.3 $[M+\mathrm{H}]^+$ (100).

HR-MS (ESI) $C_{42}H_{42}N_2O_4$ $[M+\mathrm{H}]^+$ *m/z* = calc.: 639.3217, found: 639.3220.
$[M+\mathrm{Na}]^+$ *m/z* = calc.: 661.3037, found: 661.3038.

14.1.3 (*S*)-3-(Fluorenylmethyloxycarbonylamino)-4-methylpentanoic acid (6)

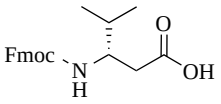

$C_{21}H_{23}NO_4$
[353.4]
6

On the basis of **SOP 13.1.1** and **SOP 13.1.2** (Path A) Fmoc-D-Val-OH (10.7 g, 29.5 mmol, 1.00 eq) was used as starting material converted to the final product **6** (8.25 g, 23.5 mmol, 80 %) as a colorless solid.

^{1}H-NMR (300 MHz, DMSO-d_6): δ [ppm] = 0.65 – 0.92 (m, 6 H, C$\underline{\mathrm{H}}_3$–CH–C$\underline{\mathrm{H}}_3$), 1.61 – 1.82 (m, 1 H, γ-C$\underline{\mathrm{H}}$), 2.35 (qd, $^{4}J_{\mathrm{H,H}}$ = 15.4, 6.9 Hz, 2 H, α-C$\underline{\mathrm{H}}_2$), 3.60 – 3.86 (m, 1 H, β-C$\underline{\mathrm{H}}$), 4.14 – 4.38 (m, 3 H, Fmoc-C$\underline{\mathrm{H}}$, Fmoc-C$\underline{\mathrm{H}}_2$), 7.17 (d, $^{3}J_{\mathrm{H,H}}$ = 9.0 Hz, 1 H, NH), 7.25 – 7.52 (m, 4 H, Fmoc-$\mathrm{CH_{Ar}}$), 7.65 – 7.72 (m, 2 H, Fmoc-$\mathrm{CH_{Ar}}$), 7.87 (m, 2 H, Fmoc-$\mathrm{CH_{Ar}}$).

^{13}C{^{1}H}-NMR (126 MHz, DMSO-d_6): δ [ppm] = 18.06, 18.88, 31.79, 36.77, 46.84, 53.06, 65.18, 119.96, 125.12, 126.94, 127.50, 140.56, 143.65, 143.83, 155.51, 172.67.

ESI-MS (MeOH) *m/z* (rel %) = 376.2 $[M+\mathrm{Na}]^+$ (100), 729.3 2 $[M+\mathrm{Na}]^+$ (34).

HR-MS (ESI) $C_{21}H_{23}NO_4$ $[M+H]^+$ m/z = calc.: 354.1700, found: 354.1699.
$[M+Na]^+$ m/z = calc.: 376.1519, found: 376.1517.

14.2 Recognition Unit for metal induced Aggregation

14.2.1 5-(4'-Methyl-[2,2'-bipyridin]-4-yl)pentanenitrile (30)

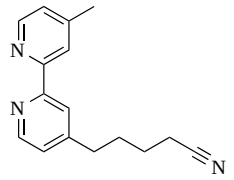

$C_{16}H_{17}N_3$
[251.3]
30

Dry THF (50 mL) was placed under an inert gas atmosphere in a schlenk flask and cooled to -78 °C. LDA (2.00 M in *n*-hexane, 19.5 mmol, 9.77 mL, 1.20 eq) was added and stirred for 15 min at -78 °C. 4,4'-Dimethyl-2,2'-bipyridine (3.00 g, 16.3 mmol, 1.00 eq) dissolved in THF (30 mL) was slowly added and stirred for additional 2 h at -78 °C. Afterwards, 4-Bromobutyronitrile (2.65 g, 17.9 mmol, 1.78 mL, 1.10 eq) dissolved in THF (5 mL) was added to the reaction mixture at -78 °C. The reaction mixture was allowed to warm up to 0 °C over 3 h and stirred at rt overnight. In order to quench the reaction, water (50 mL) was added in small amounts followed by extraction with EtOAc (3 × 100 mL). The combined organic phases were dried over $MgSO_4$ and the solvent was removed under reduced pressure. Flash column chromatography (SiO_2, *n*-pentane/EtOAc 2:1, *v/v* + 3 vol.-% NEt_3) yielded the desired product **30** (2.69 g, 10.7 mmol, 66 %) as yellow oil.

^{1}H-NMR (300 MHz, Chloroform-d_1): δ [ppm] = 1.63 – 1.73 (m, 2 H, -CH_2–C$\underline{H}_2$–$(CH_2)_2$-CN), 1.78 – 1.88 (m, 2 H, -$(CH_2)_2$–C$\underline{H}_2$–CH_2-CN), 2.33 (t, $^3J_{H,H}$ = 7.0 Hz, 2 H,

-$(CH_2)_3$-C<u>H</u>$_2$-CN), 2.40 (s, 3 H, C<u>H</u>$_3$), 2.71 (t, $^3J_{H,H}$ = 7.5 Hz, 2 H, -C<u>H</u>$_2$–$(CH_2)_3$-CN), 7.08 – 7.11 (m, 2 H, BiPy-CH), 8.18 – 8.21 (m, 2 H, BiPy-CH), 8.50 (d, $^3J_{H,H}$ = 5.0 Hz, 1 H, BiPy-CH), 8.54 (d, $^3J_{H,H}$ = 5.0 Hz, 1 H, BiPy-CH).

^{13}C{^{1}H}-NMR (126 MHz, Chloroform-d_1): δ [ppm] = 16.85, 20.98, 24.71, 29.00, 34.34, 119.17, 120.92, 121.84, 123.52, 124.56, 147.98, 148.73, 149.01, 150.95, 155.63, 156.17.

ESI-MS (MeOH) *m/z* (rel %) = 252.2 $[M+H]^+$ (100), 274.1 $[M + Na]^+$ (6).

HR-MS (ESI) $C_{16}H_{17}N_3$ $[M + H]^+$ *m/z* = calc.: 252.1495, found: 252.1504.
$[M + Na]^+$ *m/z* = calc.: 274.1315, found: 274.1310.

14.2.2 5-(4'-Methyl-[2,2'-bipyridin]-4-yl)pentanoic acid (26)

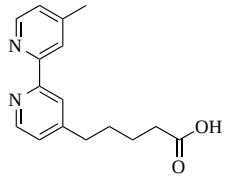

$C_{16}H_{18}N_2O_2$
[270.3]
26

5-(4'-methyl-[2,2'-bipyridin]-4-yl)pentanenitrile (**30**) (**14.2.1**) (1.23 g, 4.89 mmol, 1.00 eq) was dissolved in conc. HCl (15 mL) and heated to reflux over night. The cooled solution was neutralized with 6 M aqueous NaOH, extracted with $CHCl_3$ (4 × 50 mL) and the combined organic phases were dried over $MgSO_4$. Removal of the organic phase under reduced pressure yielded the product **26** (1.30 g, 4.80 mmol, quant.) as a pink solid.

^{1}H-NMR (300 MHz, Chloroform-d_1): δ [ppm] = 1.61 – 1.84 (m, 4 H, -CH_2–C<u>H</u>$_2$–C<u>H</u>$_2$–CH_2-CO_2H), 2.36 (t, $^3J_{H,H}$ = 7.0 Hz, 2 H, -$(CH_2)_3$–C<u>H</u>$_2$-CO_2H), 2.45 (s, 3 H, C<u>H</u>$_3$), 2.73 (t,

$^{3}J_{H,H}$ = 7.3 Hz, 2 H, -C$\underline{H}_2$–$(CH_2)_3$-CO_2H), 7.18 – 7.23 (m, 2 H, BiPy-CH), 8.11 – 8.33 (m, 2 H, BiPy-CH), 8.52 – 8.63 (m, 2 H, BiPy-CH).

$^{13}C\{^{1}H\}$-NMR (126 MHz, Chloroform-d_1): δ [ppm] = 21.29, 24.22, 29.32, 33.70, 34.98, 122.23, 123.14, 124.55, 125.25, 147.43, 148.15, 150.47, 153.51, 153.79, 176.96.

ESI-MS (MeOH) *m/z* (rel %) = 269.1 $[M - H]^-$ (100), 539.3 $[2M$ - $H]^-$ (40), 271.2 $[M + H]^+$ (100).

HR-MS (ESI) $C_{16}H_{18}N_2O_2$ $[M + H]^+$ *m/z* = calc.: 271.1441, found: 271.1448.
$[M - H]^-$ *m/z* = calc.: 269.1296, found: 269.1297

14.2.3 2-(4'-Methyl-[2,2'-bipyridin]-4-yl)acetic acid (27)

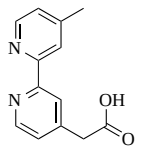

$C_{13}H_{12}N_2O_2$
[228.3]
27

Dry THF (15 mL) was placed under an inert gas atmosphere in a schlenk flask and cooled to -78 °C. LDA (2.00 M in *n*-hexane, 16.8 mmol, 8.40 mL, 1.20 eq) was added and stirred for 15 min at -78 °C. 4,4'-Dimethyl-2,2'-bipyridine (2.60 g, 14.0 mmol, 1.00 eq) dissolved in THF (50 mL) was slowly added and stirred for additional 2 h at -78 °C. The reaction solution was mixed with dry ice (in excess) and stirred overnight at rt. Diethyl ether (70 mL) was added and the resulting solution was extracted with 3 M aqueous NaOH (3 × 130 mL). The combined aqueous phases were neutralized with H_2SO_4, the volume was reduced under reduced pressure and the resulting residue was lyophilized. To remove the excess of Na_2SO_4 the residue was taken up in MeOH and filtered. Flash column chromatography (SiO_2, DCM/MeOH 3:1, *v/v*) yielded the desired product **27** (2.24 g, 9.83 mmol, 70 %) as a pink solid.

^{1}H-NMR (500 MHz, DMSO-d_6): δ [ppm] = 2.54 (s, 3 H, CH_3), 3.16 (s, 2 H, -C$\underline{H}_2$-CO_2H), 7.59 – 7.71 (m, 2 H, BiPy-CH), 8.51 – 8.56 (m, 2 H, BiPy-CH), 8.60 – 8.79 (m, 2 H, BiPy-CH).

^{13}C{^{1}H}-NMR (126 MHz, DMSO-d_6): δ [ppm] = 21.25, 48.55, 123.51, 127.11, 146.18, 147.89, 170.94.

14.3 Cholestamin as Lipid anchor

14.3.1 4-(*tert*-butyl) 1-cholesterol-(((9*H*-fluoren-9-yl)methoxy)carbonyl)-l-aspartate (23)

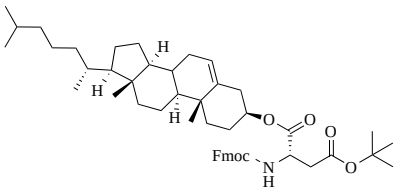

$C_{50}H_{69}NO_6$
[780.1]
23

Under an inert gas atmosphere Fmoc-L-Asp(OtBu)-OH (3.00 g, 7.29 mmol, 1.00 eq) was dissolved in dry DCM (25 mL), cholesterol (2.96 g, 7.66 mmol, 1.05 eq) in dry DCM (30 mL) together with DMAP (90.0 mg, 72.9 mmol, 0.10 eq) were added. A solution of DCC (1.50 g, 7.29 mmol, 1.00 eq) in dry DCM (20 mL) was slowly added and the reaction mixture was stirred for 2 d at rt. The resulting solution was filtered off and flash column chromatography (SiO_2, *n*-pentane/EtOAc 5:1, *v*/*v*) yielded the desired product **23** (3.61 g, 4.63 mmol, 64 %) as a colorless solid.

^{1}H-NMR (300 MHz, Chloroform-d_1): δ [ppm] = 0.66 – 1.62 (m, 43 H, Cholesterol), 1.74 – 2.06 (m, 8 H, Cholesterol), 2.24 – 2.35 (m, 2 H, Cholesterol), 2.69 – 3.00 (m,

3 H, α-C<u>H</u>–β-C<u>H</u>$_2$), 4.17 – 4.47 (m, 3 H, Fmoc-C<u>H</u>, Fmoc-C<u>H</u>$_2$), 7.21 – 7.44 (m, 4 H, Fmoc-CH_{Ar}), 7.53 – 7.64 (m, 2 H, Fmoc-CH_{Ar}), 7.70 – 7.79 (m, 2 H, Fmoc-CH_{Ar}).

^{13}C{^{1}H}-NMR (126 MHz, Chloroform-d_1): δ [ppm] = 11.83, 18.69, 19.27, 20.99, 22.52, 22.77, 23.79, 24.24, 24.91, 25.60, 27.62, 27.96, 28.03, 28.17, 31.80, 31.85, 33.91, 35.73, 36.13, 36.52, 36.86, 37.78, 37.84, 39.46, 39.66, 42.25, 47.05, 49.01, 49.92, 50.59, 56.06, 56.58, 60.26, 67.12, 75.48, 76.65, 76.91, 77.16, 81.59, 119.77, 122.73, 124.93, 124.99, 126.86, 127.49, 139.11, 141.05, 141.07, 143.53, 143.73, 155.73, 169.71, 169.98.

ESI-MS (MeOH) *m/z* (rel %) = 802.5 $[M + Na]^+$ (100).

HR-MS (ESI) $C_{50}H_{69}NO_6$ $[M + Na]^+$ *m/z* = calc.: 802.5017, found: 802.4992.

14.3.2 (3*S*)-3-(Fluorenylmethyloxycarbonylamino)-4-cholesterol-4-oxobutanoic acid (20)

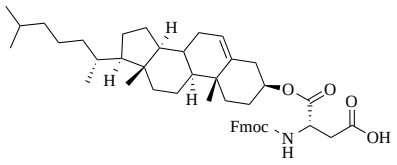

$C_{46}H_{61}NO_6$
[724.0]
20

The ester **23** (**14.3.1**) (1.75 g, 2.24 mmol, 1.00 eq) was dissolved in DCM (7 mL) under an inert gas atmosphere and subsequently TES (1.82 mL, 11.2 mmol, 5.00 eq) and TFA (2.23 mL, 29.1 mmol, 13.0 eq) were added. The reaction mixture was stirred for 24 h at rt and the organic solvent was removed under reduced pressure. Flash column chromatography (SiO_2, DCM/MeOH 40:1 + 0.1 % AcOH, *v/v*) yielded the desired product **20** (1.53 g, 2.11 mmol, 94 %) as a yellow oil.

^{1}H-NMR (300 MHz, DMSO-d_6): δ [ppm] = 0.74 – 2.00 (m, 42 H, Cholesterol), 2.18 – 2.33 (m, 2 H, Cholesterol), 2.51 – 2.80 (m, 2 H, Cholesterol), 3.11 – 3.46 (m, 2 H, β-C$\underline{H}_2$), 4.17 – 4.56 (m, 4 H, Fmoc-C$\underline{H}$, α-C$\underline{H}$, Fmoc-C$\underline{H}_2$), 7.24 – 7.47 (m, 4 H, Fmoc-CH_{Ar}), Fmoc-C$\underline{H}_2$), 7.65 – 7.79 (m, 2 H, Fmoc-CH_{Ar}), 7.83 – 7.93 (m, 2 H, Fmoc-CH_{Ar}), 12.36 (s, 1 H, COOH).

^{13}C{^{1}H}-NMR (126 MHz, DMSO-d_6): δ [ppm] = 11.59, 18.49, 18.83, 20.48, 22.30, 22.55, 23.12, 24.35, 25.25, 27.11, 27.28, 27.65, 31.24, 31.29, 33.24, 35.06, 35.57, 35.97, 36.28, 37.31, 38.84, 39.02, 39.11, 39.19, 39.35, 39.44, 39.52, 39.61, 39.78, 39.94, 40.02, 41.76, 47.41, 49.30, 55.48, 55.98, 119.85, 121.93, 124.90, 126.78, 127.37, 140.46, 143.47, 155.53, 170.16, 171.06.

ESI-MS (MeOH) *m/z* (rel %) = 746.4 $[M + \mathrm{Na}]^+$ (100).

14.3.3 Cholesterol methanesulfonate (24)

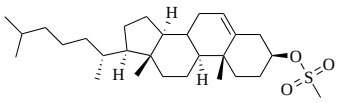

$C_{28}H_{48}O_3S$
[464.7]
24

Cholesterol (10.0 g, 25.9 mmol, 1.00 eq) was dissolved under an inert gas atmosphere in dry DCM (100 mL) mixed with NEt_3 (5.40 mL, 39.0 mmol, 1.50 eq). Afterwards, methanesulfonylchloride (3.10 mL, 40.1 mmol, 1.55 eq) in dry DCM (10 mL) was added at 0 °C and stirred for 16 h at rt. The organic solvent was removed under reduced pressure, the residue was taken up in DCM (in minimum amounts of) and the product was precipitated by addition of cold methanol. This step was repeated once again. Filtration of the precipitation yielded the product **24** (10.9 g, 23.4 mmol, 90 %) as a colorless solid.

^{1}H-NMR (300 MHz, Chloroform-d_1): δ [ppm] = 0.68 (s, 6 H, Cholesterol), 0.79 – 1.62 (m, 29 H, Cholesterol), 1.70 – 2.08 (m, 6 H, Cholesterol), 2.32 – 2.60

(m, 2 H, Cholesterol), 3.35 (s, 3 H, $-SO_3-C\underline{H}_3$), 5.30 – 5.46 (m, 2 H, Cholesterol).

$^{13}C\{^1H\}$-NMR (126 MHz, Chloroform-d_1): δ [ppm] = 12.11, 18.97, 19.61, 21.32, 23.04, 24.53, 28.23, 28.25, 28.46, 32.01, 32.13, 32.18, 35.99, 36.00, 37.11, 37.42, 38.92, 38.98, 39.73, 40.02, 42.54, 50.42, 55.75, 56.38, 56.98, 76.91, 77.16, 77.41, 80.50, 121.64, 140.94.

ESI-MS (MeOH) *m/z* (rel %) = 487.3 $[M + Na]^+$ (36), 946.7 $[2\,M + NH_4]^+$ (84), 1416.0 $[3\,M + Na]^+$ (100).

HR-MS (ESI) $C_{28}H_{48}O_3S$ $[M + Na]^+$ *m/z* = calc.: 487.3216, found: 487.3209.
$[2\,M + NH_4]^+$ *m/z* = calc.: 946.6987, found: 946.6937.
$[3\,M + Na]^+$ *m/z* = calc.: 1415.9865, found: 1415.9808.

14.3.4 Cholesterol azide (25)

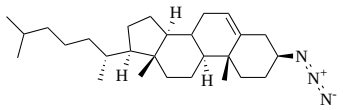

$C_{27}H_{45}N_3$
[411.7]
25

$TMSN_3$ (1.25 mL, 9.47 mmol, 1.10 eq) was added under an inert gas atmosphere to a solution of **24** (**14.3.3**) (4.00 g, 8.61 mmol, 1.00 eq) in dry DCM (40 mL). Afterwards, $BF_3 \cdot OEt_2$ (2.17 mL, 17.2 mmol, 2.00 eq) was added and stirred for 3 h at rt. To quench the mixture, it was poured into an aqueous NaOH solution (6 M) and the aqueous phase was extracted with DCM (3 ×100 mL). The combined organic phases were dried over $MgSO_4$ and the solvent was removed under reduced pressure. The resulting residue was dissolved in *n*-pentane and filtered through a short glas frit filled with a silica pad. Removing the organic solvent yielded the desired product **25** (2.90 g, 7.05 mmol, 82 %) as a colorless solid.

^{1}H-NMR (300 MHz, Chloroform-d_1): δ [ppm] = 0.57 – 1.68 (m, 32 H, Cholesterol), 1.74 – 2.09 (m, 5 H, Cholesterol), 2.23 – 2.34 (m, 2 H, Cholesterol), 3.12 – 3.29 (m, 1 H, Cholesterol), 5.37 – 5.40 (m, 1 H, Cholesterol).

^{13}C{^{1}H}-NMR (126 MHz, Chloroform-d_1): δ [ppm] = 11.94, 18.80, 19.35, 21.08, 22.63, 22.88, 23.91, 24.34, 28.01, 28.07, 28.28, 31.88, 31.93, 35.83, 36.25, 36.66, 37.64, 38.21, 39.57, 39.78, 42.36, 50.15, 56.19, 56.75, 61.18, 122.44, 139.73.

ESI-MS (MeOH) *m/z* (rel %) = 411.4 [*M*] (100).

HR-MS (ESI) $C_{27}H_{45}N_3$ [*M*] *m/z* = calc.: 411.3613, found: 411.3618.

14.3.5 Cholestamine (15)

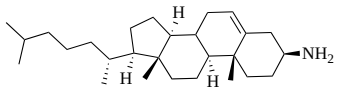

$C_{27}H_{47}N$
[385.7]
15

$LiAlH_4$ (350 mg, 9.00 mmol, 1.31 eq) was added in small portions (5 ×) to a solution of **25** (**14.3.4**) (2.90 g, 7.05 mmol, 1.00 eq) in dry Et_2O (30 mL) at 0 °C. The resulting mixture was stirred at 0 °C for 30 min, allowed to warm to rt and stirred for additional 2 h. The excess of $LiAlH_4$ was removed by addition of cold H_2O and the product was extracted with EtOAc (3 × 100 mL). The combined organic phases were dried over $MgSO_4$ and removing of the organic phase solvent yielded the product **15** (1.67 g, 4.33 mmol, 62 %) as a colorless solid.

^{1}H-NMR (300 MHz, Chloroform-d_1): δ [ppm] = 0.41 – 2.29 (m, 45 H, Cholesterol, –N$\underline{H}_2$), 2.50 – 2.72 (m, 1 H, Cholesterol), 5.20 – 5.44 (m, 1 H, Cholesterol).

ESI-MS (MeOH) *m/z* (rel %) = 369.4 $[M + H - NH_3]^+$ (70), 386.4 $[M + H]^+$ (100), 771.8 $[2\,M + H]^+$ (9).

HR-MS (ESI) $C_{27}H_{47}N$ [*M*] *m/z* = calc.: 386.3781, found: 386.3785.

14.4 Alternative Anchor Spacer

14.4.1 (*R*)-4-(Allyloxy)-1-carboxy-4-oxobutan-1-aminium chloride (17)

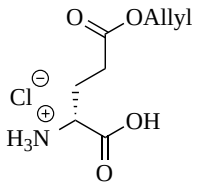

$C_8H_{14}ClNO_4$
[223.7]
17

D-Glutamic acid (1.00 g, 6.80 mmol, 1.00 eq) was suspended in allyl alcohol (35 mL) under an inert gas atmosphere. TMSCl (2.73 mL, 21.8 mmol, 3.2 eq) was added and the resulting suspension was stirred for 18 h. The clear solution was cooled to 0 °C and the desired product **17** (742 mg, 3.32 mmol, 49 %) was precipitated from cold diethyl ether and collected by centrifugation.

^{1}H-NMR (300 MHz, Deuterium oxide): δ [ppm] = 2.32 (h, $^3J_{H,H}$ = 7.4 Hz, 2 H, CH−C$\underline{H}_2$-CH_2−O^-), 2.72 (td, $^3J_{H,H}$ = 7.3, 1.4 Hz, 2 H, CH−CH_2−C$\underline{H}_2$−O-), 4.16 (t, $^3J_{H,H}$ = 6.7 Hz, 1 H, α−CH), 4.68 (dt, $^3J_{H,H}$ = 5.7, 1.5 Hz, 2 H, −O−C$\underline{H}_2$−CH=CH_2), 5.24 – 5.46 (m, 2 H, −O−CH_2−CH=C$\underline{H}_2$), 5.91 – 6.13 (m, 1 H, −O−CH_2−C$\underline{H}$=CH_2).

^{13}C{^{1}H}-NMR (126 MHz, Deuterium oxide): δ [ppm] = 27.75, 32.52, 54.99, 68.88, 121.31, 134.54, 174.02, 176.63.

ESI-MS (MeOH) *m/z* (rel %) = 188.1 $[M - Cl]^+$ (100), 210.1 $[M + H]^+$ (7), 375.2 $[2\,M - 2\,Cl]^+$ (1), 397.2 $[2\,M + Na - 2\,Cl]^+$ (2).

HR-MS (ESI) $C_8H_{14}ClNO_4$ $[M - Cl]^+$ *m/z* = calc.: 188.0917, found: 188.0914.
$[M + Na]^+$ *m/z* = calc.: 210.0737, found: 210.0739.

14.4.2 (*R*)-2-(Fluorenylmethyloxycarbonylamino)-5-(allyloxy)-5-oxopentanoic acid (18)

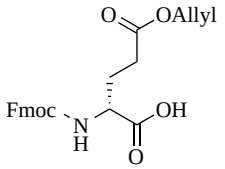

$C_{23}H_{23}NO_6$
[409.4]
18

17 (**14.4.1**) (700 mg, 3.14 mmol, 1.00 eq) was dissolved in H_2O (25 mL), cooled to 0 °C and K_2CO_3 (650 mg, 4.71 mmol, 1.50 eq) was added in small portions. Fmoc−Cl (890 mg. 3.46 mmol, 1.10 eq) in 1,4-dioxane (25 mL) was added at 0 °C and stirred for 4 h. After that H_2O (20 mL) was added, the organic phase was removed under reduced pressure and the aqueous phase was washed with diethyl ether (2 ×50 mL). The remaining aqueous phase was acidified with 6 M aqueous HCl to pH = 2 and extracted with diethyl ether (3 ×50 mL). The combined organic phases were dried over $MgSO_4$ and the solvent was removed under reduced pressure. The product **18** (1.06 g, 2.58 mmol, 82 %) was yielded as a yellow oil without further purification.

^{1}H-NMR (300 MHz, DMSO-d_6): δ [ppm] = 1.77 – 2.15 (m, 2 H, CH−C$\underline{H}_2$−CH_2−O-), 2.43 (td, $^3J_{H,H}$ = 7.1, 6.3, 2.7 Hz, 2 H, CH−CH_2−C$\underline{H}_2$−O-), 4.03 (td, $^3J_{H,H}$ = 9.1, 4.9 Hz, 1 H, α−CH), 4.17 – 4.35 (m, 3 H, Fmoc-C$\underline{H}$, Fmoc-C$\underline{H}_2$), 4.54 (dq, $^3J_{H,H}$ = 5.5, 2.6, 2.1 Hz, 2 H, −O−C$\underline{H}_2$−CH=CH_2), 5.14 – 5.36 (m, 2 H, −O−CH_2−CH=C$\underline{H}_2$), 5.91 (ddt, $^3J_{H,H}$ = 17.2, 10.7, 5.4 Hz, 1 H, −O−CH_2−C$\underline{H}$=CH_2), 7.26 – 7.47 (m, 4 H, Fmoc-CH_{Ar}), 7.58 – 7.92 (m, 4 H, Fmoc-CH_{Ar}).

^{13}C{^{1}H}-NMR (126 MHz, DMSO-d_6): δ [ppm] = 26.09, 30.04, 46.66, 52.92, 63.75, 64.31, 65.58, 66.28, 117.44, 119.88, 119.90, 125.04, 126.87, 127.44, 132.47, 132.48, 140.52, 143.63, 155.92, 171.60, 173.07.

ESI-MS (MeOH) *m/z* (rel %) = 410.2 $[M+H]^+$ (49), 427.2 $[M+NH_4]^+$ (26), 432.1 $[M+Na]^+$ (100), 448.1 $[M+K]^+$ (17).

HR-MS (ESI) $C_{23}H_{23}NO_6$ $[M+H]^+$ m/z = calc.: 410.1598, found: 410.1597.
$[M+NH_4]^+$ m/z = calc.: 427.1864, found: 427.1860.
$[M+Na]^+$ m/z = calc.: 432.1418, found: 432.1416.
$[M+K]^+$ m/z = calc.: 448.1157, found: 448.1147.

14.4.3 Allyl (*R*)-4-(Fluorenylmethyloxycarbonylamino)-6-diazo-5-oxohexanoate (19)

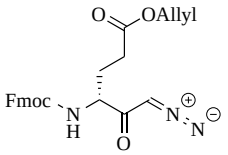

$C_{24}H_{23}N_3O_5$
[433.5]
19

On the basis of **SOP 13.1.1** Fmoc-D-Glu(OAllyl)-OH **18** (**14.4.2**) (1.08 g, 2.60 mmol, 1.00 eq) was used as starting material converted to the product **19** (quant. yield) as a yellow oil.

ESI-MS (MeOH) m/z (rel %) = 456.2 $[M+Na]^+$ (100), 889.3 $[M+Na]^+$ (9).

HR-MS (ESI) $C_{24}H_{23}N_3O_5$ $[M+Na]^+$ m/z = calc.: 456.1530, found: 456.1534.
$[M+K]^+$ m/z = calc.: 472.1269, found: 472.1291.

14.4.4 (*R*)-3-(Fluorenylmethyloxycarbonylamino)-6-(allyloxy)-6-oxohexanoic acid (7)

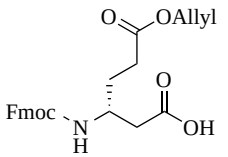

$C_{24}H_{25}NO_6$
[423.5]
7

On the basis of **SOP 13.1.2** (Path A) **19** (**14.4.3**) (2.00 g, 3.22 mmol, 1.00 eq) was converted to the final product **7** (1.55 g, 3.66 mmol, 70 %) as a colorless solid.

^{1}H-NMR (300 MHz, DMSO-d_6): δ [ppm] = 1.52 – 1.87 (m, 2 H, CH – C$\underline{H}_2$ – CH_2 – O-), 1.95 – 2.04 (m, 2 H, CH – CH_2 – C$\underline{H}_2$ – O-), 2.20 – 2.49 (m, 2 H, β – CH_2), 3.74 – 3.89 (m, 1 H, α – CH), 4.09 – 4.41 (m, 3 H, Fmoc-C$\underline{H}$, Fmoc-C$\underline{H}_2$), 4.53 (dt, $^3J_{H,H}$ = 5.4, 1.5 Hz, 2 H, –O – C$\underline{H}_2$ – CH=CH_2), 5.11 – 5.36 (m, 2 H, –O – CH_2 – CH=C$\underline{H}_2$), 5.84 – 5.97 (m, 1 H, –O – CH_2 – C$\underline{H}$=CH_2), 7.15 – 7.55 (m, 4 H, Fmoc-CH_{Ar}), 7.55 – 7.73 (m, 2 H, Fmoc-CH_{Ar}), 7.80 – 8.01 (m, 2 H, Fmoc-CH_{Ar}), 12.18 (s, 1 H, COO$\underline{H}$).

^{13}C{^{1}H}-NMR (126 MHz, DMSO-d_6): δ [ppm] = 18.29, 29.31, 30.06, 40.09, 46.73, 47.31, 64.16, 65.04, 117.36, 119.82, 124.89, 126.77, 127.32, 132.48, 140.47, 143.53, 143.69, 155.28, 171.85, 171.87.

ESI-MS (MeOH) *m/z* (rel %) = 446.2 $[M+Na]^+$ (100), 869.3 $[2\,M+Na]^+$ (22).

HR-MS (ESI) $C_{24}H_{25}NO_6$ $[M+H]^+$ *m/z* = calc.: 424.1755, found: 424.1752.
$[M+Na]^+$ *m/z* = calc.: 446.1574, found: 446.1578.

14.5 *trans*-2-((Fluorenylmethyloxycarbonylamino))-cyclohexane-1-carboxylic acid (31)

14.5.1 o

ctan-8-one]7-azabicyclo[4.2.0]octan-8-one (**33**)[183–185]

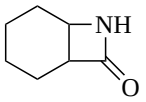

$C_7H_{11}NO$
[125.2]
33

Cyclohexen (25.0 mL, 247 mmol, 1.00 eq) was dissolved in DCM (70 mL) and cooled to 0 °C. Chlorosulfonyl Isocyanate (CSI) (21.4 mL, 247 mmol, 1.00 eq) in DCM (24 mL) was added dropwise. The reaction solution was stirred at 0 °C for 1 h and for additional 3 d at rt. The resulting β-lactam was used without any further purification. The mixture was cooled, carefully quenched with cold H_2O (50 mL) and added dropwise to a cold aqueous Na_2SO_3 solution (15.5 g in 200 mL H_2O, 124 mmol, 0.50 eq). The pH was kept constant between 5 and 7 with the usage of NaOH. After 1 h stirring at 0 °C the aqueous phase was extracted with EtOAc (4 × 100 mL). The combined organic phases were dried over $MgSO_4$ and removing of the organic phase yielded the product **33** (19.8 g, 158 mmol, 64 %) as a colorless solid.

^{1}H-NMR (300 MHz, DMSO-d_6): δ [ppm] = 1.21 – 1.80 (m, 8 H, Cyclo.-H), 2.95 – 3.12 (m, 1 H, CH), 3.62 – 3.68 (m, 1 H, CH), 7.97 (s, 1 H, NH).

^{13}C{^{1}H}-NMR (126 MHz, DMSO-d_6): δ [ppm] = 16.60, 18.74, 19.49, 25.22, 27.31, 41.72, 42.15, 44.92, 46.61, 48.84, 54.09.

ESI-MS (MeOH) *m/z* (rel %) = 126.1 $[M+H]^+$ (100).

HR-MS (ESI) $C_7H_{11}NO$ $[M-H]^-$ *m/z* = cal.: 124.0768, found: 124.0764.
$[M+H]^+$ *m/z* = cal.: 126.0913, found: 126.0917.
$[M+Na]^+$ *m/z* = cal.: 148.0733, found: 148.0733.

14.5.2 (1*S*,2*R*)-2-aminocyclohexane-1-carboxylic acid hydrochloride (34)[183–185]

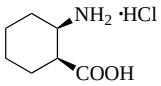

$C_7H_{14}ClNO_2$
[179.6]
34

33 (**14.5.1**) (19.8 g, 158 mmol, 1.00 eq) was dissolved in HCl (6 M, 200 mL), after 45 min another portion of conc. HCl (50 mL) was added and stirred o/n at rt. The solvent was removed under reduced pressure, precipitation from cold acetone yielded the product **34** (11.0 g, 61.5 mmol, 39 %) as colorless solid. This step was repeated one more time with the filtrate for a second crop (6.04 g, 33.6 mmol, 21 %).

^{1}H-NMR (300 MHz, DMSO-d_6): δ [ppm] = 1.27 – 1.37 (m, 3 H, Cyclo.-H), 1.63 – 1.73 (m, 4 H, Cyclo.-H), 1.94 – 2.04 (m, 1 H, Cyclo.-H), 2.85 – 2.97 (m, 1 H, CH), 3.17 – 3.40 (m, 1 H, CH), 8.11 (s, 3 H, NH_3-7), 12.67 (s, 1 H, COOH-8).

^{13}C{^{1}H}-NMR (126 MHz, DMSO-d_6): δ [ppm] = 21.85, 25.73, 26.09, 42.04, 49.51, 177.50.

ESI-MS (MeOH) *m/z* (rel %) = 142.1 $[M-H]^-$ (14), 144.1 $[M+H]^+$ (100).

HR-MS (ESI) $C_7H_{13}NO_2$ $[M-H-HCl]^-$ *m/z* = cal.: 142.0874, found: 142.0875.
$[M+H-HCl]^+$ *m/z* = cal.: 144.1019, found: 144.1021.

14.5.3 (1*S*,2*R*)-2-((*tert*-butoxycarbonyl)amino)cyclohexane-1-carboxylic acid (35)[182]

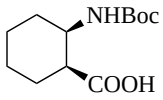

$C_{12}H_{21}NO_4$
[243.3]
35

The starting material **34** (**14.5.2**) (11.0 g, 61.5 mmol, 1.00 eq) was dissolved in 1,4-dioxane/water (130 mL, 5:8 *v/v*) at 0 °C and K_2CO_3 (17.0 g, 123 mmol, 2.00 eq) was added. A pre-cooled (0 °C) solution of Boc_2O (20.1 g, 92.2 mmol, 1.50 eq) in 1,4-dioxane (25 mL) was added dropwise, the reaction solution was stirred at 0 °C for 1 h and at rt o/n. The solution was diluted with H_2O (50 mL) and extracted with EtOAc (2 × 100 mL). The combined organic phases were back extracted with saturated aqueous $NaHCO_3$-solution (3 × 100 mL). The combined aqueous phases were acidified with 1 M HCl to pH 2-3 and extracted with EtOAc (3 × 100 mL). The combined organic phases were dried over $MgSO_4$, the volume was concentrated under reduced pressure to yield the product **35** (14.8 g, 60.6 mmol, 99 %) as a colorless solid.

^{1}H-NMR (300 MHz, Chloroform-d_1): δ [ppm] = 1.16 – 1.68 (m, 16 H, Cyclo.-H, Boc-CH_3), 1.78 – 1.88 (m, 1 H, Cyclo.-H), 2.49 – 2.65 (m, 1 H, CH), 3.79 – 3.93 (m, 1 H, CH), 6.48 (d, $^3J_{H,H}$ = 8.8 Hz, 1 H, NH), 12.01 (s, 1 H, COOH).

^{13}C{^{1}H}-NMR (126 MHz, Chloroform-d_1): δ [ppm] = 22.53, 24.37, 27.51, 28.45, 29.96, 44.89, 49.34, 79.52, 155.37, 179.29.

ESI-MS (MeOH) *m/z* (rel %) = 266.1 $[M+Na]^+$ (61), 282.1 $[M+K]^+$ (100).

HR-MS (ESI) $C_{12}H_{21}NO_4$ $[M+Na]^+$ *m/z* = calc.: 266.1363, found: 266.1367.
$[M+K]^+$ *m/z* = calc.: 282.1102, found: 282.1106.

14.5.4 (1*S*,2*R*)-2-((*tert*-butoxycarbonyl)amino)cyclohexane-1-carboxymethyl ester (36)[182]

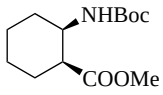

$C_{13}H_{23}NO_4$
[257.3]
36

Based on **35** (**14.5.3**) (14.8 g, 60.6 mmol, 1.00 eq) as dissolved in DCM (190 mL), cooled to 0 °C and subsequently it was added MeOH (3.70 mL, 60.6 mmol, 1.00 eq), DMAP (1.48 g, 12.2 mmol, 0.20 eq) and DCC (12.5 g, 60.6 mmol, 1.00 eq) in DCM (90 mL). The reaction solution was stirred for 30 min at 0 °C and o/n at rt. The precipitation was filtered off and the volume of the organic phase was removed under reduced pressure. Flash column chromatography (SiO_2, *n*-pentane/EtOAc 5:1, *v/v*) yielded the desired product **36** (11.8 g, 45.7 mmol, 75 %) as a colorless solid.

^{1}H-NMR (300 MHz, Chloroform-d_1): δ [ppm] = 1.22 – 1.52 (m, 13 H, Cyclo.-H, Boc-CH_3), 1.57 – 1.79 (m, 4 H, Cyclo.-H), 1.95 – 2.05 (m, 1 H, Cyclo.-H), 2.78 (q, $^3J_{H,H}$ = 4.6 Hz, 1 H, CH), 3.69 (s, 3 H, CO_2CH_3), 3.78 – 3.90 (m, 1 H, CH), 5.30 (s, 1 H, NH).

^{13}C{^{1}H}-NMR (126 MHz, Chloroform-d_1): δ [ppm] = 22.58, 23.74, 26.8, 28.36, 29.81, 44.81, 49.11, 51.57, 79.11, 155.08, 174.25.

ESI-MS (MeOH) *m/z* (rel %) = 258.2 $[M+H]^+$ (26), 280.2 $[M+Na]^+$ (100).

HR-MS (ESI) $C_{13}H_{23}NO_4$ $[M+H]^+$ *m/z* = calc.: 258.1700, found: 258.1701.
$[M+Na]^+$ *m/z* = calc.: 280.1519, found: 280.1521.
$[M+K]^+$ *m/z* = calc.: 296.1259, found: 296.1260.

14.5.5 (1*R*,2*R*)-2-((*tert*-butoxycarbonyl)amino)cyclohexane-1-carboxymethyl ester (37)[182]

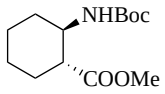

$C_{13}H_{23}NO_4$
[257.3]
37

Under an inter gas atmosphere sodium (541 mg, 23.5 mmol, 1.10 eq) was dissolved in methanol (50 mL) and was mixed with **36** (**14.5.4**) (5.50 g, 21.4 mmol, 1.00 eq) in MeOH (25 mL). The resulting solution was stirred for 5 h under reflux and at rt o/n. The reaction was stopped by adding aqueous saturated NH_4Cl-solution (10 mL) and the organic solvent was reduced. The resulting precipitation was filtered off and recrystallizing from *n*-heptane yielded the product **37** (3.10 g, 12.1 mmol, 52 %) as a colorless solid.

^{1}H-NMR (300 MHz, Chloroform-d_1): δ [ppm] = 1.11 – 1.50 (m, 12 H, Cyclo.-H, Boc-CH_3), 1.54 – 1.79 (m, 2 H, Cyclo.-H), 1.84 – 1.97 (m, 1 H, CH), 1.95 – 2.11 (m, 1 H, Cyclo.-H), 2.22 (td, $^4J_{H,H}$ = 11.2, $^3J_{H,H}$ = 3.7 Hz, 1 H, -C<u>H</u>–CO_2CH_3), 3.48 (s, 1 H, -C<u>H</u>–NHBoc), 3.67 (s, 3 H, -$CO_2C\underline{H}_3$), 4.47 (s, 1 H, NH).

^{13}C{^{1}H}-NMR (126 MHz, Chloroform-d_1): δ [ppm] = 24.48, 24.80, 28.40, 28.54, 33.13, 50.07, 51.23, 51.81, 79.21, 155.03, 174.54.

ESI-MS (MeOH) *m/z* (rel %) = 258.2 $[M+H]^+$ (43), 280.2 $[M+Na]^+$ (100), 296.1 $[M+K]^+$ (5).

HR-MS (ESI) $C_{13}H_{23}NO_4$ $[M+H]^+$ *m/z* = calc.: 258.1700, found: 258.1694.
$[M+Na]^+$ *m/z* = calc.: 280.1519, found: 280.1516.
$[M+K]^+$ *m/z* = calc.: 296.1259, found: 296.1253.

14.5.6 (1*R*,2*R*)-2-((*tert*-butoxycarbonyl)amino)cyclohexane-1-carboxylic acid (38)[182]

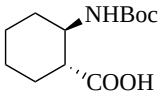

$C_{12}H_{21}NO_4$
[243.3]
38

In H_2O/MeOH (100 mL, 1:3 *v/v*) **37** (**14.5.5**) (4.01 g, 15.6 mmol, 1.00 eq) was dissolved, mixed with NaOH (1.90 g, 82.7 mmol, 5.30 eq) and stirred o/n at rt. The reaction mixture was concentrated under reduced pressure and a pH of 2–3 was set with conc. HCl, followed by an extraction with EtOAc (3 × 200 mL) and the combined organic phases were dried over $MgSO_4$. Removing of the solvent under reduced pressure yielded the product **38** (3.71 g, 15.2 mmol, 99 %) as colorless solid.

^{1}H-NMR (300 MHz, DMSO-d_6): δ [ppm] = 1.03 – 1.44 (m, 12 H, Cyclo.-H, Boc-CH_3), 1.54 – 1.94 (m, 4 H, Cyclo.-H), 2.19 (td, $^4J_{H,H}$ = 11.3 Hz, $^3J_{H,H}$ = 3.7 Hz, 1 H, -C<u>H</u>–CO_2CH_3), 3.28 – 3.50 (m, 1 H, -C<u>H</u>–NHBoc), 6.71 (d, $^3J_{H,H}$ = 9.0 Hz, 1 H, NH), 11.96 (s, 1 H, COOH).

^{13}C{^{1}H}-NMR (126 MHz, DMSO-d_6): δ [ppm] = 24.18, 24.46, 28.23, 28.68, 32.24, 48.27, 50.23, 77.34, 154.47, 175.19.

ESI-MS (MeOH) *m/z* (rel %) = 242.1 $[M-H]^-$ (77), 266.1 $[M+Na]^+$ (100).

HR-MS (ESI) $C_{12}H_{21}NO_4$ $[M-H]^-$ *m/z* = calc.: 242.1398, found: 242.1399.
$[M+Na]^+$ *m/z* = calc.: 266.1363, found: 266.1367.

14.5.7 (1*R*,2*R*)-2-aminocyclohexane-1-carboxylic acid (39)[182]

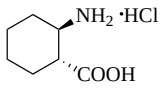

$C_7H_{14}ClNO_2$
[179.6]
39

The amino acid **38** (**14.5.6**) (3.71 g, 15.2 mmol) was dissolved in HCl in 1,4-dioxane (4 M, 42 mL) and mixed with conc. HCl (10 mL). The solution was stirred o/n at rt until the deprotection was complete. The solvent was removed under reduced pressure and yielded the desired product **39** without further purification (2.73 g, 15.2 mmol, quant.) as a green solid.

^{1}H-NMR (300 MHz, DMSO-d_6): δ [ppm] = 1.08 – 1.48 (m, 4 H, Cyclo.-H), 1.58 – 1.76 (m, 2 H, Cyclo.-H), 1.94 – 2.08 (m, 2 H, -C<u>H</u>–CO_2H), 2.39 – 2.50 (m, 1H), 3.08 – 3.21 (m, 1 H, -C<u>H</u>–NH_2), 8.13 (s, 3 H, NH), 12.82 (s, 1 H, COOH).

^{13}C{^{1}H}-NMR (126 MHz, DMSO-d_6): δ [ppm] = 23.59, 24.57, 28.60, 29.48, 46.10, 50.23, 174.93.

ESI-MS and **HR-MS (ESI)** of (1*R*,2*R*)-2-aminocyclohexane-1-carboxylic acid hydrochloride are similar to *cis*-2-aminocyclohexane-1-carboxylic acid hydrochloride, see **14.5.2**.

14.5.8 (1*R*,2*R*)-2-(Fluorenylmethyloxycarbonylamino)cyclohexane-1-carboxylic acid (31)[182]

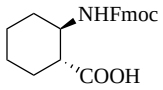

$C_{22}H_{23}NO_4$
[365.4]
31

The hydrochloride salt **39** (**14.5.7**) (2.73 g, 19.1 mmol, 1.00 eq) was dissolved in H_2O (70 mL) and mixed with $NaHCO_3$ (3.21 g, 38.2 mmol, 2.00 eq). The reaction solution was cooled to 0 °C, Fmoc-OSu (7.09 g, 21.0 mmol, 1.10 eq) in 1,4-dioxane (90 mL) was added dropwise and stirred for 1 h at constant temperature. Afterwards, the solution was stirred o/n at rt. Than HCl (1 M) was added to set a pH of 1 and extracted with EtOAc (5 × 150 mL). The combined organic phases were dried over $MgSO_4$ and removing of the volatile components yielded the crude product. The final product **31** was verified by MS, but could not be purified.

ESI-MS (MeOH) *m/z* (rel %) = 366.2 $[M-H]^-$ (14), 388.2 $[M]$ (100).

HR-MS (ESI) $C_{22}H_{23}NO_4$ $[M+H]^+$ *m/z* = calc.: 366.1700, found: 366.1694.
$[M+Na]^+$ *m/z* = calc.: 388.1519, found: 388.1512.

14.5.9 (*R*)-2-((1-phenylethyl)amino)cyclohex-1-ene-1-carboxylic acid ethyl ester (42)[186]

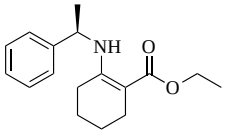

$C_{17}H_{23}NO_2$
[273.4]
42

Ethyl 2-oxocyclohexanecarboxylate (21.5 g, 20.0 mL, 126 mmol, 1.00 eq), (*R*)-α-Methylbenzylamine (17.6 g, 16.5 mL, 145 mmol, 1.15 eq) and *p*-toluenesulfonic acid (1.10 g, 6.39 mmol, 0.05 eq) were dissolved in toluene (150 mL) and heated to reflux at a water separator for 5.5 h. The organic phase was washed with aqueous saturated $NaHCO_3$ solution (3 × 50 mL), dried over $MgSO_4$ and the organic solvent was removed under reduced pressure. The product **42** (quant.) was yielded as a yellow oil and used without further purification.

^{1}H-NMR (300 MHz, Chloroform-d_1): δ [ppm] = 1.32 (t, $^3J_{H,H}$ = 7.1 Hz, 3 H, $CH_2C\underline{H}_3$), 1.40 – 1.62 (m, 7 H, Cyclo.-H, $CHCH_3$), 1.89 – 2.06 (m, 1 H, Cyclo.-H), 2.29 (td, $^3J_{H,H}$ = 2.3, 5.8, 6.3 Hz, 3 H, Cyclo.-H), 4.20 (qd, $^3J_{H,H}$ = 1.4, 7.1 Hz, 2 H, $C\underline{H}_2CH_3$), 4.66 (quint., $^3J_{H,H}$ = 7.0 Hz, 1 H, $C\underline{H}CH_3$), 7.22 – 7.45 (m, 5 H, Aromat.-H), 9.42 (d, $^3J_{H,H}$ = 7.8 Hz, 1 H, $N\underline{H}$).

^{13}C{^{1}H}-NMR (126 MHz, Chloroform-d_1): δ [ppm] = 14.69, 22.21, 22.60, 23.82, 25.37, 26.64, 51.99, 58.71, 90.55, 125.29, 126.79, 128.21, 145.85, 159.07, 170.95.

ESI-MS (MeOH) *m/z* (rel %) = 274.2 $[M+H]^+$ (100), 296.2 $[M+Na]^+$ (67).

HR-MS (ESI) $C_{17}H_{23}NO_2$ $[M+H]^+$ *m/z* = calc.: 274.1802, found: 274.1801.
$[M+Na]^+$ *m/z* = calc.: 296.1621, found: 296.1620.

14.5.10 (1*S*)-2-(((*R*)-1-phenylethyl)amino)cyclohexane-1-carboxylic acid ethyl ester (43)[186]

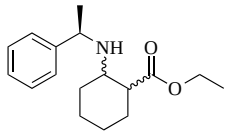

$C_{17}H_{25}NO_2$
[275.4]
43

Under an inert gas atmosphere isobutyric acid (209 g, 220 mL, 2.37 mmol, 18.8 eq) was cooled to 0 °C mixed with $NaBH_4$ (13.8 g, 0.37 mol, 2.9 eq), which was added in three portions and stirred for 30 min. **42** (**14.5.9**) (40.6 g, 0.13 mol, 1.00 eq) was added dropwise as a solution in toluene (70 mL) and stirred for additional 1.5 h at 0 °C. Another portion of $NaBH_4$ (3.40 g, 90.0 mmol, 0.70 eq) was added and the reaction mixture was stirred o/n at rt. To quench the excess of $NaBH_4$ H_2O (200 mL) was added and with NaOH the pH was set to 10. The reaction mixture was extracted with EtOAc (4 × 250 mL), the combined organic phases were dried over $MgSO_4$ and the volatile components were removed under reduced pressure. Flash column chromatography (SiO_2, *n*-pentane/EtOAc + 1 % AcOH 5:1, *v/v*) yielded the desired product **43** (14.0 g, 50.8 mmol, 40 %) as a yellow oil.

^{1}H-NMR (300 MHz, Chloroform-d_1): δ [ppm] = 1.04 – 1.98 (m, 15 H, Cyclo.-H, $CH_2C\underline{H}_3$, $CHC\underline{H}_3$), 2.70 – 2.92 (m, 2 H, Cyclo.-H), 3.89 (q, $^3J_{H,H}$ = 6.5 Hz, 1 H, $C\underline{H}CH_3$), 4.18 (q, $^3J_{H,H}$ = 7.2 Hz, 2 H, $C\underline{H}_2$CH3), 7.15 – 7.42 (m, 5 H, Aromat.-H).

ESI-MS (MeOH) *m/z* (rel %) = 276.2 $[M+H]^+$ (100), 298.2 $[M+Na]^+$ (11).

HR-MS (ESI) $C_{17}H_{25}NO_2$ $[M+H]^+$ *m/z* = calc.: 276.1958, found: 276.1966.
$[M+Na]^+$ *m/z* = calc.: 298.1778, found: 298.1779.

14.5.11 (1*R*,2*S*)-2-(ethoxycarbonyl)-*N*-((*R*)-1-phenylethyl)cyclohexan-1-aminium bromide (44)[186]

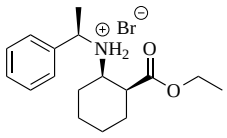

$C_{17}H_{26}BrNO_2$
[356.3]
44

43 (**14.5.10**) (14.0 g, 50.8 mmol, 1.00 eq) was dissolved in EtOAc (150 mL) under an inert gas atmosphere and cooled to 0 °C. The solution was mixed dropwise with HBr in propionic acid (17.0 g, 13.0 mL, 63.2 mmol, 1.20 eq), stirred for 1 h at 0 °C and stored o/n at -20 °C. The resulting precipitate was collected by filtration, washed with cold EtOAc and dried under reduced pressure. The crude product was recrystallized from MeCN and stored o/n at -20 °C for complete precipitation. The volume of the filtrate was reduced and stored o/n at -20 °C for a second crop. The product **44** (8.50 g, 23.9 mmol, 47 %) was yielded as a colorless solid.

^{1}H-NMR (300 MHz, Chloroform-d_1): δ [ppm] = 1.00 – 1.23 (m, 2 H, Cyclo.-H), 1.27 (t, $^3J_{H,H}$ = 7.1 Hz, 3 H, $CH_2C\underline{H}_3$), 1.44 – 1.89 (m, 3 H, Cyclo.-H), 1.89 (d, $^3J_{H,H}$ = 6.8 Hz, 3 H, $CHC\underline{H}_3$), 2.21 – 2.43 (m, 2 H,Cyclo.-H), 3.08-3.27 (m, 1 H, H-1), 3.36 – 3.45 (m, 1 H, H-2), 4.11 – 4.32 (m, 2 H, $C\underline{H}_2CH_3$), 4.38 (td, $^3J_{H,H}$ = 7.1, 5.6 Hz, 1 H, $C\underline{H}CH_3$), 7.30 – 7.47 (m, 3 H, Aromat.-H), 7.67 – 7.79 (m, 2 H, Aromat.-H), 9.20 (br. d, 2 H, $N\underline{H}_2$).

^{13}C{^{1}H}-NMR (126 MHz, Chloroform-d_1): δ [ppm] = 14.05, 19.89, 21.81, 24.25, 25.66, 27.15, 39.90, 56.23, 56.51, 62.09, 127.74, 129.46, 135.88, 174.01.

ESI-MS (MeOH) *m/z* (rel %) = 276.2 $[M - Br]^+$, 665.4 $[2\,M - Br + Na]^+$.

HR-MS (ESI) $C_{17}H_{26}NO_2Br$ $[M - Br]^+$ *m/z* = calc.: 276.1958, found: 276.1959.

14.5.12 (1*S*,2*R*)-2-(((*R*)-1-phenylethyl)amino)cyclohexane-1-carboxylic acid ethyl ester (45)[186]

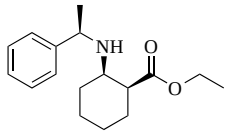

$C_{17}H_{25}NO_2$
[275.4]
45

44 (**14.5.11**) (7.48 g, 21.0 mmol, 1.00 eq) was dissolved in aqueous saturated $NaHCO_3$ (100 mL) solution and extracted with *tert*-butyl methyl ether (5 × 200 mL). The combined organic phases were dried over $MgSO_4$ and removing of the volatile components yielded the product **45** (5.37 g, 19.5 mmol, 93 %) as a colorless oil.

^{1}H-NMR (300 MHz, Chloroform-d_1): δ [ppm] = 1.04 – 1.98 (m, 15 H, Cyclo.-H, $CH_2C\underline{H}_3$, $CHC\underline{H}_3$), 2.70 – 2.92 (m, 2 H, Cyclo.-H), 3.89 (q, $^3J_{H,H}$ = 6.5 Hz, 1 H, $C\underline{H}CH_3$), 4.18 (q, $^3J_{H,H}$ = 7.2 Hz, 2 H, $C\underline{H}_2$CH3), 7.15 – 7.42 (m, 5 H, Aromat.-H).

ESI-MS (MeOH) *m/z* (rel %) = 276.2 $[M+H]^+$ (100), 298.2 $[M+Na]^+$ (11).

HR-MS (ESI) $C_{17}H_{25}NO_2$ $[M+H]^+$ *m/z* = calc.: 276.1958, found: 276.1966.
$[M+Na]^+$ *m/z* = calc.: 298.1778, found: 298.1779.

14.5.13 (1*R*,2*R*)-2-(((*R*)-1-phenylethyl)amino)cyclohexane-1-carboxylic acid ethyl ester (46)[186]

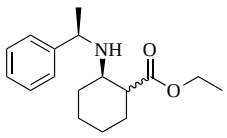

$C_{17}H_{25}NO_2$
[275.4]
46

Under an inert gas atmosphere dry EtOH (100 mL) was mixed in small portions with Na (3.30 g, 144 mmol, 7.40 eq) and a solution of **45** (**14.5.12**) (5.37 g, 19.5 mmol, 1.00 eq) in dry EtOH (25 mL) was added. The reaction mixture was heated to reflux o/n and the volatile components were removed under reduced pressure. The residue was taken up in a small amount of fresh EtOH and mixed with aqueous saturated NaCl-solution. The mixture was extracted with EtOAc (4 × 100 mL), the combined organic phases were dried over $MgSO_4$ and the solvent was removed under reduced pressure. The residue was taken up in DCM and filtered through

a pad of silica gel and eluted with *n*-pentane/EtOAc (3:1, *v*/*v*). Removing of the solvent under reduced pressure yielded the product **46** (3.43 g, 12.5 mmol, 64 %) as a yellow oil.

^{1}H-NMR (300 MHz, Chloroform-d_1): δ [ppm] = 1.04 – 1.98 (m, 15 H, Cyclo.-H, $CH_2C\underline{H}_3$, $CHC\underline{H}_3$), 2.70 – 2.92 (m, 2 H, Cyclo.-H), 3.89 (q, $^3J_{H,H}$ = 6.5 Hz, 1 H, $C\underline{H}CH_3$), 4.18 (q, $^3J_{H,H}$ = 7.2 Hz, 2 H, $C\underline{H}_2CH3$), 7.15 – 7.42 (m, 5 H, Aromat.-H).

ESI-MS (MeOH) *m*/*z* (rel %) = 276.2 $[M+H]^+$ (100), 298.2 $[M+Na]^+$ (11).

HR-MS (ESI) $C_{17}H_{25}NO_2$ $[M+H]^+$ *m*/*z* = calc.: 276.1958, found: 276.1966.
$[M+Na]^+$ *m*/*z* = calc.: 298.1778, found: 298.1779.

14.5.14 (1*R*,2*R*)-2-(ethoxycarbonyl)-N-((R)-1-phenylethyl)cyclohexan-1-aminium chloride (47)[186]

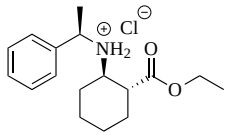

$C_{17}H_{26}ClNO_2$
[311.9]
47

In EtOAc (12 mL) **46** (**14.5.13**) (3.43 g, 12.5 mmol, 1.00 eq) was dissolved and cooled to 0 °C. Under stirring was added HCl in 1,4-dioxane (4 M, 3.74 mL, 15.0 mmol, 1.20 eq) and stored at -20 °C o/n. The precipitate was collected by filtration, dried under reduced pressure and recrystallized from MeCN. The solution was stored o/n at -20 °C o/n and the product **47** (2.68 g, 8.60 mmol, 69 %) was obtained by filtration as a colorless solid.

^{1}H-NMR (300 MHz, Chloroform-d_1): δ [ppm] = 0.80 – 0.99 (m, 1 H, Cyclo.-H), 1.05 – 1.24 (m, 2 H, Cyclo.-H), 1.27 (t, $^3J_{H,H}$ = 7.1 Hz, 3 H, $CH_2C\underline{H}_3$), 1.45 – 1.82

(m, 4 H, Cyclo.-H), 1.89 (d, $^{3}J_{H,H} = 6.9$ Hz, 3 H, CHC$\underline{H}_3$), 2.07 – 2.23 (m, 1 H, H-1), 3.04 – 3.12 (m, 2 H, Cyclo.-H, C$\underline{H}$CH$_3$), 4.11 – 4.34 (m, 2 H, C$\underline{H}_2$CH$_3$), 4.48 – 4.64 (m, 1 H, H-2), 7.26 – 7.47 (m, 3 H, Aromat.-H), 7.69 – 7.83 (m, 3 H, Aromat.-H), 9.82 (br. d, 2 H, N$\underline{H}_2$).

^{13}C{^{1}H}-NMR (126 MHz, Chloroform-d_1): δ [ppm] = 14.19, 20.71, 23.94, 24.16, 29.46, 30.13, 46.03, 56.68, 59.56, 61.31, 128.47, 128.91, 129.00, 136.68, 174.11.

ESI-MS (MeOH) m/z (rel %) = 276.2 $[M - \mathrm{Cl}]^+$, 298.2 $[M - \mathrm{HCl} + \mathrm{Na}]^+$.

HR-MS (ESI) $C_{17}H_{26}NO_2$ $[M - \mathrm{H}]^+$ m/z = calc.: 276.1958, found: 276.1959.

14.5.15 (1*R*,2*R*)-2-(((*R*)-1-phenylethyl)amino)cyclohexane-1-carboxylic acid (48)[186]

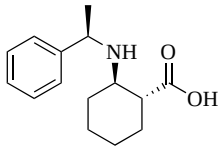

$C_{15}H_{21}NO_2$
[247.3]
48

47 (**14.5.14**) (3.10 g, 9.95 mmol, 1.00 eq) was dissolved in THF/EtOH/H_2O (100 mL, 2:1:1 $v/v/v$), cooled to 0 °C mixed with LiOH (1.96 g, 46.7 mmol, 4.70 eq) in H_2O (20 mL) and stirred o/n at rt. Removing of the volatile components under reduced pressure yielded the product **48** (2.46 g, 9.95 mmol, 100 %).

^{1}H-NMR (300 MHz, DMSO-d_6): δ [ppm] = 0.91 – 1.58 (m, 11 H, Cyclo.-H, CHC$\underline{H}_3$), 1.73 – 1.88 (m, 2 H, Cyclo.-H), 2.52 – 2.63(m, 1 H, Cyclo.-H), 3.73 (q, $^{3}J_{H,H} = 6.5$ Hz, 1 H, C$\underline{H}$CH$_3$), 7.04 – 7.40 (m, 5 H, Aromat.-H).

^{13}C{^{1}H}-NMR (126 MHz, DMSO-d_6): δ [ppm] = 29.38, 30.11, 40.11, 46.77, 47.34, 64.25, 64.38, 65.08, 117.45, 119.91, 119.93, 124.98, 126.83, 126.85, 127.40, 132.56, 140.54, 143.76, 155.35, 171.99.

ESI-MS (MeOH) m/z (rel %) = 248.2 $[M + \mathrm{H}]^+$ (100).

HR-MS (ESI) $C_{15}H_{21}NO_2$ $[M-H]^+$ m/z = calc.: 248.1645, found: 248.1641.
$[M+Na]^+$ m/z = calc.: 270.1465, found: 270.1464.

14.5.16 (1*R*,2*R*)-2-aminocyclohexane-1-carboxylic acid (39)[182]

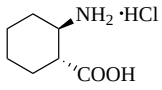

$C_7H_{14}ClNO_2$
[179.6]
39

Under an inert gas atmosphere **48** (**14.5.15**) (2.46 g, 9.94 mmol, 1.00 eq) was dissolved in MeOH (200 mL), mixed with Pd/C (10 %, 2.10 g, 19.8 mmol, 2.00 eq) and ammonium formate (3.13 g, 49.7 mmol, 5.00 eq). The reaction mixture was heated to reflux for 2.5–3 h until completion of the reaction. The solution was filtered over a pad of celite and the organic solvent was removed under reduced pressure to yield the product **39** (1.42 g, 9.94 mmol, 100 %) as a colorless solid.

^{1}H-NMR (300 MHz, DMSO-d_6): δ [ppm] = 1.08 – 1.48 (m, 4 H, Cyclo.-H), 1.58 – 1.76 (m, 2 H, Cyclo.-H), 1.94 – 2.08 (m, 2 H, -C<u>H</u>–CO_2H), 2.39 – 2.50 (m, 1H), 3.08 – 3.21 (m, 1 H, -C<u>H</u>–NH_2), 8.13 (s, 3 H, NH), 12.82 (s, 1 H, COOH).

^{13}C{^{1}H}-NMR (126 MHz, DMSO-d_6): δ [ppm] = 23.59, 24.57, 28.60, 29.48, 46.10, 50.23, 174.93.

ESI-MS and **HR-MS (ESI)** of (1*R*,2*R*)-2-aminocyclohexane-1-carboxylic acid hydrochloride are similar to *cis*-2-aminocyclohexane-1-carboxylic acid hydrochloride, see **14.5.2**.

14.5.17 (1*R*,2*R*)-2-(Fluorenylmethyloxycarbonylamino)cyclohexane-1-carboxylic acid (31)[182]

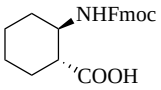

$C_{22}H_{23}NO_4$
[365.4]
31

39 (**14.5.16**) (1.40 g, 9.94 mmol, 1.00 eq) was dissolved in acetone/H_2O (300 mL, 2:1, *v*/*v*) cooled to 0 °C, $NaHCO_3$ (8.40 g, 99.4 mmol, 10.0 eq) and Fmoc-OSu (3.40 g, 9.95 mmol, 1.00 eq) were subsequently added. The reaction solution was stirred at 0 °C for 1 h and at rt o/n. The organic solvent was removed under reduced pressure and H_2O (50 mL) was added. The aqueous phase was mixed with diethyl ether (100 mL), stirred for 1 h and the organic phase was extracted with saturated aqueous $NaHCO_3$ (3 × 75 mL). The combined aqueous phases were acidified with 1 M HCl and extracted with EtOAc (3 × 100 mL). Removing of the volatile compounds could not yield the product **31**.

14.6 Alternative Recognition Binding Site

14.6.1 (*R*)-2-(Fluorenylmethyloxycarbonylamino)-3-amino-propanoic acid (10)[242]

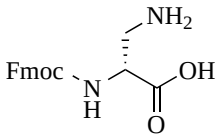

$C_{18}H_{18}N_2O_4$
[326.4]
10

Fmoc-D-Asn-OH **9** (10.0 g, 28.2 mmol, 1.00 eq) was suspended in EtOAc/MeCN/H_2O (250 mL, 2:2:1 *v/v/v*) and cooled to 0 °C. At 0 °C PIDA (10.9 g, 33.9 mmol, 1.20 eq) was added, the suspension was stirred for 3 h at 0 °C and for 4 h at rt. The resulting precipitation was filtered off and the filtrate was stored o/n at -20 °C for a second crop of the product **10** (5.23 g, 16.0 mmol, 57 %) as a colorless solid.

^{1}H-NMR (300 MHz, DMSO-d_6): δ [ppm] = 2.77 – 3.10 (m, 2 H, β-CH_2), 3.65 – 3.88 (m, 1 H, α-CH), 4.20 – 4.37 (m, 3 H, Fmoc-CH_2, Fmoc-CH), 6.81 (d, $^3J_{H,H}$ = 6.4 Hz, 1 H, NH), 7.20 – 7.50 (m, 4 H, Fmoc-CH_{Ar}), 7.69 (d, $^3J_{H,H}$ = 7.4 Hz, 2 H, Fmoc-CH_{Ar}), 7.80 – 7.91 (m, 2 H, Fmoc-CH_{Ar}).

ESI-MS (MeOH) *m/z* (rel %) = 327.1 $[M+H]^+$ (100), 349.1 $[M+Na]^+$ (37).

HR-MS (ESI) $C_{18}H_{18}N_2O_4$ $[M+H]^+$ *m/z* = calc.: 327.1338, found: 327.1337.
$[M+Na]^+$ *m/z* = calc.: 349.1160, found: 349.1162.

14.6.2 (*R*)-2-(Fluorenylmethyloxycarbonylamino)-3-((diphenyl(*p*-tolyl)methyl)amino)propanoic acid (11)[243]

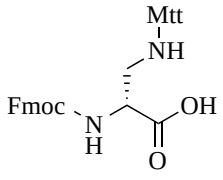

$C_{38}H_{34}N_2O_4$
[582.7]
11

Starting with **10** (**14.6.1**) (1.00 g, 3.10 mmol, 1.00 eq) suspended in DCM (15 mL) and cooled to 0 °C Et_3N (850 µL, 6.10 mmol, 2.00 eq) was added. The solution was mixed with Mtt−Cl (1.20 g, 4.00 mmol, 1.30 eq), stirred at 0 °C for 1 h and at rt o/n. The reaction mixture was quenched by addition of MeOH (15 mL) and the organic phase was removed under reduced pressure. Flash column chromatography (SiO_2, DCM/MeOH + 1 % AcOH 30:1, *v/v*) yielded the desired product **11** (1.40 g, 2.40 mmol, 78 %) as a colorless solid.

^{1}H-NMR (300 MHz, DMSO-d_6): δ [ppm] = 2.19 – 2.36 (m, 6 H, Mtt-CH_3, α-CH, β-CH_2), 4.11 – 4.36 (m, 2 H, Fmoc-CH_2), 6.30 (s, 1 H, NH), 6.97 – 7.48 (m, 24 H, Fmoc-CH_{Ar}, Mtt-CH_{Ar}), 7.62 – 7.75 (m, 1 H, Fmoc-CH_{Ar}), 7.83 – 7.94 (m, 1 H, Fmoc-CH_{Ar}).

^{13}C{^{1}H}-NMR (126 MHz, DMSO-d_6): δ [ppm] = 20.54, 46.62, 69.85, 80.31, 119.93, 125.01, 125.12, 125.91, 126.36, 126.66, 126.87, 127.26, 127.44, 127.50, 127.54, 127.56, 127.63, 127.87, 127.95, 128.00, 128.11, 128.13, 128.16, 128.22, 128.25, 128.70, 135.44, 137.13, 140.51, 143.60, 144.70, 147.72, 172.54.

ESI-MS (MeOH) *m/z* (rel %) = 583.3 $[M+H]^+$ (29), 605.3 $[M+Na]^+$ (100).

HR-MS (ESI) $C_{38}H_{34}N_2O_4$ $[M+H]^+$ *m/z* = calc.: 583.2591, found: 583.2584.
$[M+Na]^+$ *m/z* = calc.: 605.2411, found: 605.2409.

14.6.3 (*S*)-3-(Fluorenylmethyloxycarbonylamino)-4-((diphenyl(*p*-tolyl)methyl)amino)butanoic acid (8)

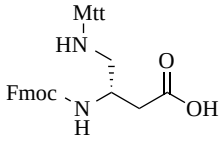

$C_{39}H_{36}N_2O_4$

[596.7]

8

The reaction was performed based on **SOP 13.1.1** and **SOP 13.1.2** (Path A) and **11** (**14.6.2**) (5.00 g, 8.58 mmol, 1.00 eq) was used as starting material. Unfortunately, the desired product **8** was not obtained based on a unwanted side reaction.

14.6.4 (*R*)-2-(Fluorenylmethyloxycarbonylamino)-3-((*tert*-butoxycarbonyl)amino)propanoic acid (13)[244]

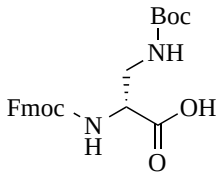

$C_{23}H_{26}N_2O_6$

[426.5]

13

Starting with **10** (**14.6.1**) (2.00 g, 6.13 mmol, 1.00 eq) suspended in H_2O (40 mL), cooled to 0 °C and mixed with $NaHCO_3$ (1.03 g, 12.3 mmol, 2.00 eq) Boc_2O (1.61 g, 7.35 mmol, 1.20 eq) in 1,4-dioxane (20 mL) was added dropwise. The resulting solution was stirred o/n at rt before H_2O (20 mL) was added. The aqueous phase

was washed with Et_2O (1 × 50 mL) acidified with 1 M HCl and extracted with EtOAc (3 × 100 mL). The combined organic phases were dried over $MgSO_4$ and the excess of organic solvent was removed under reduced pressure. The product **13** (1.70 g, 4.00 mmol, 65 %) was obtained without further purification as yellow oil.

^{1}H-NMR (300 MHz, DMSO-d_6): δ [ppm] = 1.37 (s, 9 H, CH_3-Boc), 3.21 – 3.36 (m, 2 H, β-CH_2), 4.01 – 4.14 (m, 1 H, α-CH), 4.16 – 4.34 (m, 3 H, Fmoc-CH, Fmoc-CH_2), 6.83 (t, $^3J_{H,H}$ = 6.0 Hz, 1 H, Fmoc-NH), 7.28 – 7.51 (m, 5 H, Fmoc-CH_{Ar}, Boc-NH), 7.71 (d, J = 7.4 Hz, 2 H, Fmoc-CH_{Ar}), 7.89 (d, $^3J_{H,H}$ = 7.5 Hz, 2 H, Fmoc-CH_{Ar}).

^{13}C{^{1}H}-NMR (126 MHz, DMSO-d_6): δ [ppm] = 28.17, 41.14, 46.60, 54.08, 65.68, 66.30, 77.96, 119.97, 125.06, 126.93, 127.49, 140.54, 143.59, 143.62, 155.44, 155.75, 171.79.

ESI-MS (MeOH) *m/z* (rel %) = 449.2 $[M+Na]^+$ (100).

HR-MS (ESI) $C_{23}H_{26}N_2O_6$ $[M+H]^+$ *m/z* = calc.: 427.1864, found: 427.1854.
$[M+Na]^+$ *m/z* = calc.: 449.1683, found: 449.1685.

14.6.5 (*S*)-3-(Fluorenylmethyloxycarbonylamino)-4-aminobutanoic acid (14)

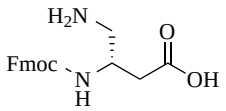

$C_{19}H_{20}N_2O_4$
[340.4]
14

The reaction was performed based on **SOP 13.1.1** and **SOP 13.1.2** (Path A) **13** (**14.6.4**) (1.70 g, 3.99 mmol, 1.00 eq) was converted to the corresponding β^3-amino acid as a colorless solid, which was used without further purification. The β^3-amino acid was suspended in 1,4-dioxane (5 mL), mixed with HCl in 1,4-dioxane

(4 M, 5 mL) and stirred for 2 h at rt. The reaction mixture was diluted with H_2O (10 mL) and the volatile components were removed under reduced pressure. The aqueous phase was washed with diethyl ether (2 × 15 mL) and lyophilized. The product **14** (1.36 g, 4.00 mmol, quant.) was obtained without further purification.

^{1}H-NMR (300 MHz, DMSO-d_6): δ [ppm] = 2.80 – 3.03 (m, 2 H, γ-CH_2), 3.28 – 3.51 (m, 2 H, α-CH_2), 3.93 – 4.15 (m, 1 H, β-CH), 4.20 – 4.34 (m, 3 H, Fmoc-CH_2, Fmoc-CH), 7.30 – 7.50 (m, 5 H, Fmoc-CH_{Ar}, Fmoc-NH), 7.75 (d, 2 H, $^3J_{H,H} = 7.5$ Hz, Fmoc-CH_{Ar}), 7.90 – 8.01 (m, 2 H, Fmoc-CH_{Ar}).

ESI-MS (MeOH) *m/z* (rel %) = 341.2 $[M + H]^+$ (100).

HR-MS (ESI) $C_{19}H_{20}N_2O_4$ $[M + H]^+$ *m/z* = calc.: 341.1495, found: 341.1494.

14.6.6 (*S*)-3-(Fluorenylmethyloxycarbonylamino)-4-((diphenyl(*p*-tolyl)methyl)amino)butanoic acid (8)

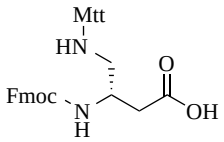

$C_{39}H_{36}N_2O_4$
[596.7]
8

Starting with **14** (**14.6.5**) (1.00 g, 2.94 mmol, 1.00 eq) suspended in DCM (15 mL) and cooled to 0 °C Et_3N (815 µL, 5.88 mmol, 2.00 eq) was added. The solution was mixed with Mtt–Cl (1.12 g, 3.82 mmol, 1.30 eq), stirred at 0 °C for 1 h and at rt o/n. The reaction mixture was quenched by addition of MeOH (15 mL) and the organic phase was removed under reduced pressure. The product **8** could not be isolated or verified by ESI-MS.

14.7 β-peptide Synthesis

14.7.1 Synthesis of P-49

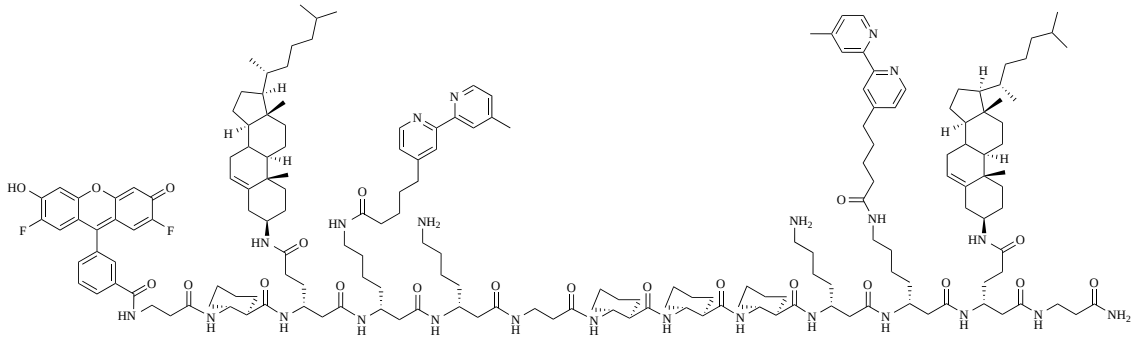

49

The peptide backbone was synthesized after **SOP 13.2.3** on a 100 µmol (500 mg resin) scale. All amino acids were coupled twice with the exception of *trans*-ACHC-OH (**14.5.8**) this amino acid was coupled three times. The post synthetic modifications were carried out after **SOP 13.2.4.1**, **13.2.4.3**, **13.2.4.2** and **13.2.4.4**. The fluorophore Oregon Green 488 (100 mg, 250 µmol, 2.50 eq) was coupled with HATU (32.7 mg, 250 µmol, 2.50 eq), HOAt (91.3 mg, 250 µmol, 2.50 eq) and DIPEA (86.0 µl, 500 µmol, 5.00 eq) at rt o/n. The final peptide was cleaved after **SOP 13.2.5** to yield the crude peptide as a green solid. The purification was done on a semipreparative scale to yield a green solid.

HPLC (semipreparative, gradient: 70 → 100 % B in 30 min, λ: 488, 300, 254 nm): t_R = 32.7 min.

ESI-MS (MeOH) *m/z* (rel %) = 636.2 $[M+H]^{5+}$ (3), 795.0 $[M+H]^{4+}$ (100), 1059.7 $[M+H]^{3+}$ (52), 1589.0 $[M+H]^{2+}$ (7).

HR-MS (ESI) $C_{183}H_{266}F_2N_{24}O_{21}$ $[M+H]^{5+}$ *m/z* = calc.: 636.2176, found: 636.2178.
$[M+H]^{4+}$ *m/z* = calc.: 795.0202, found: 795.0207.
$[M+H]^{3+}$ *m/z* = calc.: 1059.6912, found: 1059.6914.

$[M + \mathrm{H}]^{2+}$ m/z = calc.: 1589.0332, found: 1589.0328.

14.7.2 Synthesis of P-60

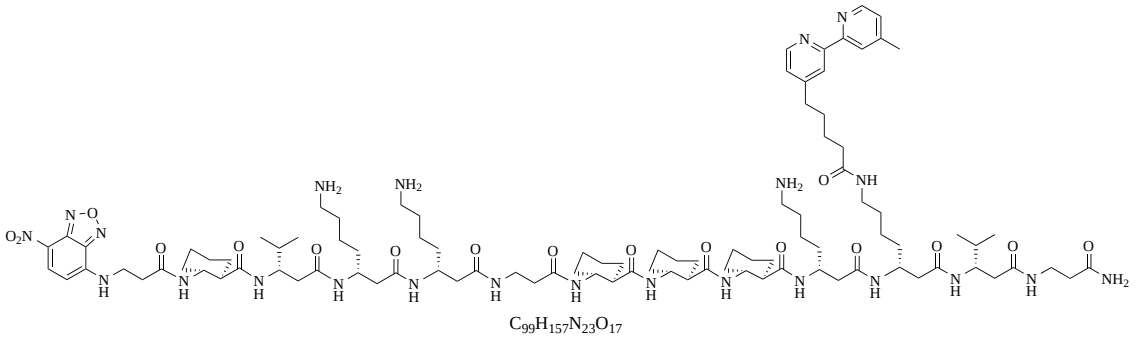

60

The peptide backbone was synthesized after **SOP 13.2.3** on a 40 µmol (200 mg resin) scale. All amino acids were coupled twice with the exception of *trans*-ACHC-OH (**14.5.8**) these amino acid was coupled three times. The post synthetic modifications were carried out after **SOP 13.2.4.2**, **13.2.4.4** and **13.2.6**. The final peptide was cleaved after **SOP 13.2.5** to yield the crude peptide as a green solid. The purification was done on a semipreparative scale to yield a green solid.

HPLC (semipreparative, gradient: 50 → 70 % B in 30 min, λ: 464, 300, 254 nm): t_R = 8.62 min.

ESI-MS (MeOH) m/z (rel %) = 486.3 $[M+\mathrm{H}]^{4+}$ (76), 648.1 $[M+\mathrm{H}]^{3+}$ (100), 971.6 $[M+\mathrm{H}]^{2+}$ (13).

HR-MS (ESI) $\mathrm{C_{99}H_{157}N_{23}O_{17}}$ $[M + \mathrm{H}]^{4+}$ m/z = calc.: 486.3112, found: 486.3115.
$[M + \mathrm{H}]^{3+}$ m/z = calc.: 648.0792, found: 648.0797.
$[M + \mathrm{H}]^{2+}$ m/z = calc.: 971.6151, found: 971.6150.

14.7.3 Synthesis of P-61

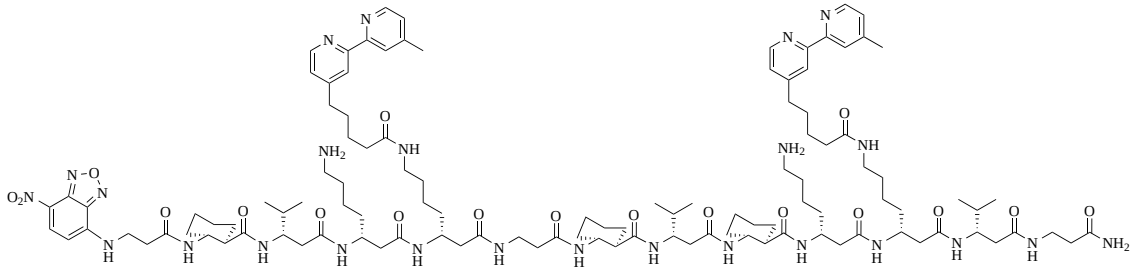

$C_{114}H_{173}N_{25}O_{18}$
[2181.8]

61

The peptide backbone was synthesized after **SOP 13.2.3** on a 40 μmol (200 mg resin) scale. All amino acids were coupled twice with the exception of *trans*-ACHC-OH (**14.5.8**) these amino acid was coupled three times. The post synthetic modifications were carried out after **SOP 13.2.4.2**, **13.2.4.4** and **13.2.6**. The final peptide was cleaved after **SOP 13.2.5** to yield the crude peptide as a green solid. The purification was done on a semipreparative scale to yield a green solid.

HPLC (semipreparative, gradient: 50 → 70 % B in 30 min, λ: 464, 300, 254 nm): t_R = 20.0 min.

ESI-MS (MeOH) *m/z* (rel %) = 546.4 $[M + H]^{4+}$ (76), 728.2 $[M + H]^{3+}$ (100), 1091.7 $[M + H]^{2+}$ (32).

HR-MS (ESI) $C_{114}H_{173}N_{25}O_{18}$ $[M + H]^{4+}$ *m/z* = calc.: 546.3428, found: 546.3431.
$[M + H]^{3+}$ *m/z* = calc.: 728.1213, found: 728.1216.
$[M + H]^{2+}$ *m/z* = calc.: 1091.6783, found: 1091.6783.

14.7.4 Synthesis of P-50

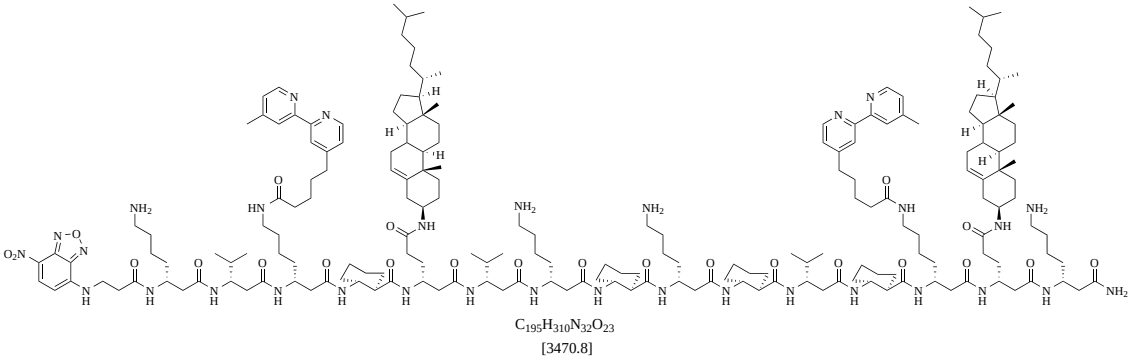

50

The peptide backbone was synthesized after **SOP 13.2.3** on a 40 µmol (200 mg resin) scale. All amino acids were coupled twice with the exception of *trans*-ACHC-OH (**14.5.8**) these amino acid was coupled three times. The post synthetic modifications were carried out after **SOP 13.2.4.1**, **13.2.4.3**, **13.2.4.2**, **13.2.4.4** and **13.2.6**. The final peptide was cleaved after **SOP 13.2.5** to yield the crude peptide as a green solid. The purification was done on a semipreparative scale to yield a green solid.

HPLC (analytically, gradient: 55 → 95 % D in 15 min, λ: 464, 300, 254 nm): t_R = 10.1 min.

ESI-MS (MeOH) *m/z* (rel %) = 579.5 $[M+H]^{6+}$ (34), 695.2 $[M+H]^{5+}$ (80), 868.7 $[M+H]^{4+}$ (100), 1157.9 $[M+H]^{3+}$ (33), 1736.4 $[M+H]^{2+}$ (5).

HR-MS (ESI) $C_{114}H_{173}N_{25}O_{18}$ $[M+H]^{6+}$ *m/z* = calc.: 579.4095, found: 579.4101.
$[M+H]^{5+}$ *m/z* = calc.: 695.0899, found: 695.0915.
$[M+H]^{4+}$ *m/z* = calc.: 868.6106, found: 868.6121.
$[M+H]^{3+}$ *m/z* = calc.: 1157.8117, found: 1157.8136.
$[M+H]^{2+}$ *m/z* = calc.: 1736.2139, found: 1736.2133.

14.7.5 Synthesis of P-51

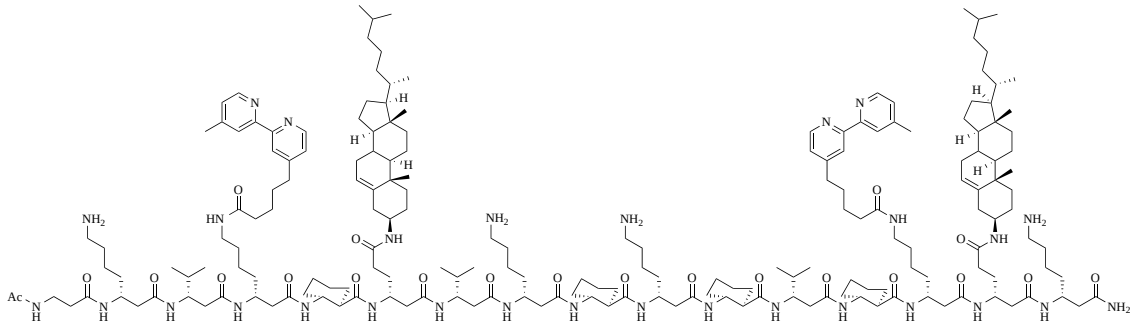

$C_{191}H_{311}N_{29}O_{21}$
[3349.8]

51

The peptide backbone was synthesized after **SOP 13.2.3** on a 28.5 µmol (150 mg resin) scale. All amino acids were coupled twice with the exception of *trans*-ACHC-OH (**14.5.8**) these amino acid was coupled three times. The post synthetic modifications were carried out after **SOP 13.2.4.1**, **13.2.4.3**, **13.2.4.2** and **13.2.4.4**. The final peptide was cleaved after **SOP 13.2.5** to yield the crude peptide as a colorless solid. The purification was done on a semipreparative scale to yield a colorless solid.

HPLC (analytically, gradient: 55 → 95 % C in 15 min, λ: 300, 254, 215 nm): t_R = 12.1 min.

ESI-MS (MeOH) *m/z* (rel %) = 559.2 $[M+H]^{6+}$ (34), 670.9 $[M+H]^{5+}$ (27), 838.4 $[M+H]^{4+}$ (100), 1117.5 $[M+H]^{3+}$ (69), 1680.8 $[M+H]^{2+}$ (4).

HR-MS (ESI) $C_{191}H_{311}N_{29}O_{21}$ $[M+H]^{6+}$ *m/z* = calc.: 559.2444, found: 559.2435.
$[M+H]^{5+}$ *m/z* = calc.: 670.8918, found: 670.8912.
$[M+H]^{4+}$ *m/z* = calc.: 838.3629, found: 838.3623.
$[M+H]^{3+}$ *m/z* = calc.: 1117.4815, found: 1117.4813.
$[M+H]^{2+}$ *m/z* = calc.: 1675.2169, found: 1675.2162.

14.7.6 Synthesis of P-52

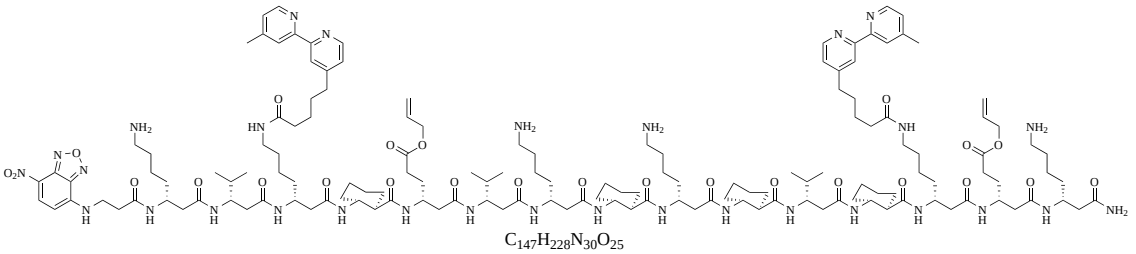

$C_{147}H_{228}N_{30}O_{25}$
[2815.6]

52

The peptide backbone was synthesized after **SOP 13.2.3** on a 67.0 µmol (334 mg resin) scale. All amino acids were coupled twice with the exception of *trans*-ACHC-OH (**14.5.8**) these amino acid was coupled three times. The post synthetic modifications were carried out after **SOP 13.2.4.2**, **13.2.4.4** and **13.2.6**. The final peptide was cleaved after **SOP 13.2.5** to yield the crude peptide as a green solid. The purification was done on a semipreparative scale to yield a green solid.

HPLC (semipreparative, gradient: 40 → 55 % B in 30 min, λ: 464, 300, 254 nm): t_R = 23.0 min.

ESI-MS (MeOH) *m/z* (rel %) = 563.9 $[M+H]^{5+}$ (77), 704.6 $[M+H]^{4+}$ (100), 939.2 $[M+H]^{3+}$ (24), 1408.2 $[M+H]^{2+}$ (3).

HR-MS (ESI) $C_{147}H_{228}N_{30}O_{25}$ $[M+H]^{6+}$ *m/z* = calc.: 470.1326, found: 470.1324.
$[M+H]^{5+}$ *m/z* = calc.: 563.9577, found: 563.9579.
$[M+H]^{4+}$ *m/z* = calc.: 704.6953, found: 704.6957.
$[M+H]^{3+}$ *m/z* = calc.: 939.2580, found: 939.2584.
$[M+H]^{2+}$ *m/z* = calc.: 1408.3834, found: 1408.3841.

14.7.7 Synthesis of P-53

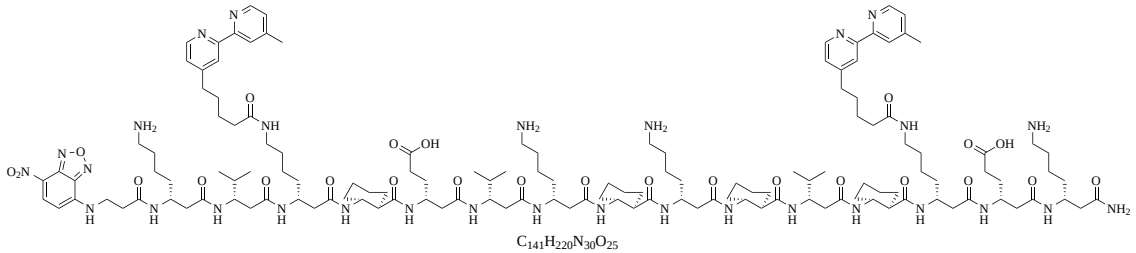

53

The peptide backbone was synthesized after **SOP 13.2.3** on a 9.50 µmol (50.0 mg resin) scale. All amino acids were coupled twice with the exception of *trans*-ACHC-OH (**14.5.8**) these amino acid was coupled three times. The post synthetic modifications were carried out after **SOP 13.2.4.1**, **13.2.4.2**, **13.2.4.4** and **13.2.6**. The final peptide was cleaved after **SOP 13.2.5** to yield the crude peptide as a green solid. The purification was done on a semipreparative scale to yield a green solid.

HPLC (semipreparative, gradient: 40 → 55 % B in 30 min, λ: 464, 300, 254 nm): t_R = 22.0 min.

ESI-MS (MeOH) *m/z* (rel %) = 547.9 $[M+H]^{5+}$ (61), 684.7 $[M+H]^{4+}$ (100), 912.6 $[M+H]^{3+}$ (35), 1368.4 $[M+H]^{2+}$ (6).

HR-MS (ESI) $C_{141}H_{220}N_{30}O_{25}$ $[M+H]^{6+}$ *m/z* = calc.: 456.7889, found: 456.7896.
$[M+H]^{5+}$ *m/z* = calc.: 547.9452, found: 547.9448.
$[M+H]^{4+}$ *m/z* = calc.: 684.6797, found: 684.6789.
$[M+H]^{3+}$ *m/z* = calc.: 912.5705, found: 912.5690.
$[M+H]^{2+}$ *m/z* = calc.: 1368.3521, found: 1368.3513.

14.7.8 Synthesis of P-54

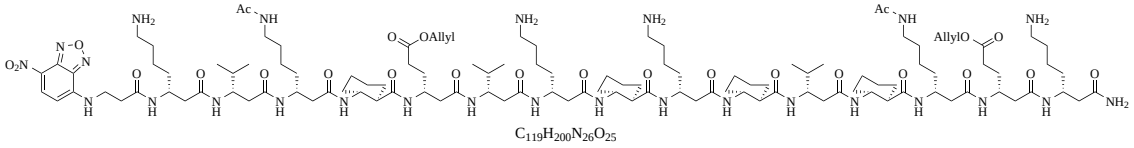

54

The peptide backbone was synthesized after **SOP 13.2.3** on a 9.50 µmol (50.0 mg resin) scale. All amino acids were coupled twice with the exception of *trans*-ACHC-OH (**14.5.8**) these amino acid was coupled three times. The post synthetic modifications were carried out after **SOP 13.2.4.2** (the free amino groups after the Mtt deprotection were capped) and **SOP 13.2.6**. The final peptide was cleaved after **SOP 13.2.5** to yield the crude peptide as a green solid. The purification was done on a semipreparative scale to yield a green solid.

HPLC (semipreparative, gradient: 40 → 55 % B in 30 min, λ: 464, 254, 215 nm): t_R = 20.0 min.

ESI-MS (MeOH) *m/z* (rel %) = 599.6 $[M + H]^{4+}$ (100), 799.2 $[M + H]^{3+}$ (71), 1198.3 $[M + H]^{2+}$ (11).

HR-MS (ESI) $C_{119}H_{200}N_{26}O_{25}$ $[M + H]^{6+}$ *m/z* = calc.: 470.1326, found: 470.1324.
$[M + H]^{5+}$ *m/z* = calc.: 563.9577, found: 563.9579.
$[M + H]^{4+}$ *m/z* = calc.: 599.6375, found: 599.6379.
$[M + H]^{3+}$ *m/z* = calc.: 799.1809, found: 799.1812.
$[M + H]^{2+}$ *m/z* = calc.: 1198.2677, found: 1198.2668.

14.7.9 Synthesis of P-55

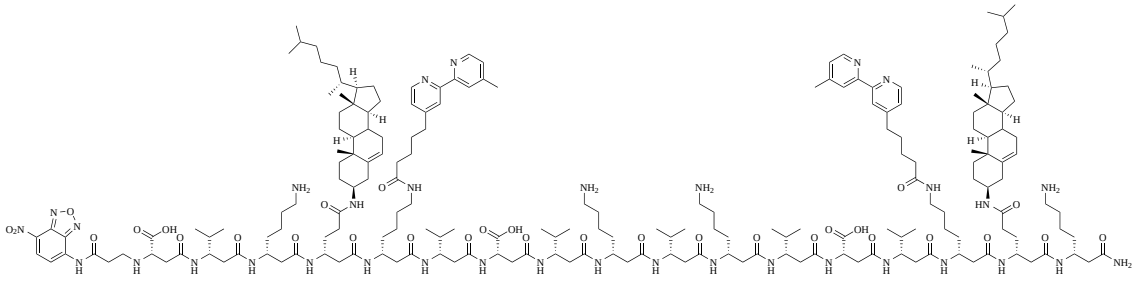

$C_{197}H_{314}N_{34}O_{31}$
[3654.9]

55

The peptide backbone was synthesized after **SOP 13.2.3** on a 40 µmol (200 mg resin) scale. All amino acids were coupled twice with the exception of *trans*-ACHC-OH (**14.5.8**) these amino acid was coupled three times. The post synthetic modifications were carried out after **SOP 13.2.4.1**, **13.2.4.3**, **13.2.4.2**, **13.2.4.4** and **13.2.6**. The final peptide was cleaved after **SOP 13.2.5** to yield the crude peptide as a green solid. The purification was done on a semipreparative scale to yield a green solid.

HPLC (semipreparative, gradient: 70 → 100 % B in 30 min, λ: 464, 300, 254 nm): t_R =23.3 min.

ESI-MS (MeOH) *m/z* (rel %) = 610.1 $[M+H]^{6+}$ (10), 731.9 $[M+H]^{5+}$ (81), 914.6 $[M+H]^{4+}$ (100), 1219.1 $[M+H]^{3+}$ (57), 1828.2 $[M+H]^{2+}$ (6).

HR-MS (ESI) $C_{197}H_{314}N_{34}O_{31}$ $[M+H]^{6+}$ *m/z* = calc.: 610.0756, found: 610.0751.
$[M+H]^{5+}$ *m/z* = calc.: 731.8893, found: 731.8895.
$[M+H]^{4+}$ *m/z* = calc.: 914.6098, found: 914.6105.
$[M+H]^{3+}$ *m/z* = calc.: 1219.1439, found: 1219.1446.
$[M+H]^{2+}$ *m/z* = calc.: 1828.2123, found: 1828.2103.

14.7.10 Synthesis of P-62

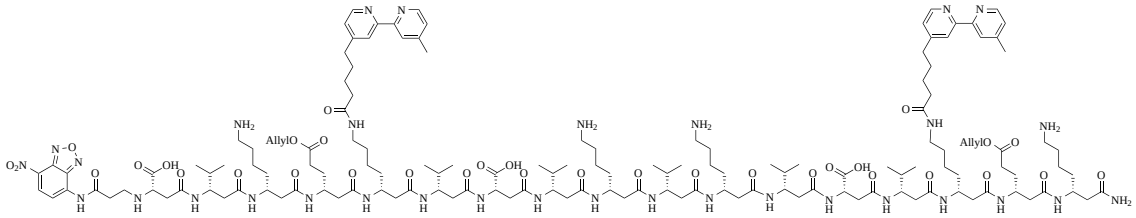

$C_{149}H_{232}N_{32}O_{33}$
[2999.7]

62

The peptide backbone was synthesized after **SOP 13.2.3** on a 40 μmol (200 mg resin) scale. All amino acids were coupled twice with the exception of *trans*-ACHC-OH (**14.5.8**) these amino acid was coupled three times. The post synthetic modifications were carried out after **SOP 13.2.4.2**, **13.2.4.4** and **13.2.6**. The final peptide was cleaved after **SOP 13.2.5** to yield the crude peptide as a green solid. The purification was done on a semipreparative scale to yield a green solid.

HPLC (semipreparative, gradient: 40 → 65 % B in 30 min, λ: 464, 300, 254 nm): t_R =13.3 min.

ESI-MS (MeOH) *m/z* (rel %) = 500.8 $[M+H]^{6+}$ (25), 600.8 $[M+H]^{5+}$ (79), 750.7 $[M+H]^{4+}$ (100), 1000.6 $[M+H]^{3+}$ (35), 1500.4 $[M+H]^{2+}$ (6).

HR-MS (ESI) $C_{149}H_{232}N_{32}O_{33}$ $[M+H]^{6+}$ *m/z* = calc.: 500.7988, found: 500.7974.
$[M+H]^{5+}$ *m/z* = calc.: 600.7571, found: 600.7562.
$[M+H]^{4+}$ *m/z* = calc.: 750.6945, found: 750.6938.
$[M+H]^{3+}$ *m/z* = calc.: 1000.5903, found: 1000.5889.
$[M+H]^{2+}$ *m/z* = calc.: 1500.3817, found: 1500.3795.

14.7.11 Synthesis of P-56

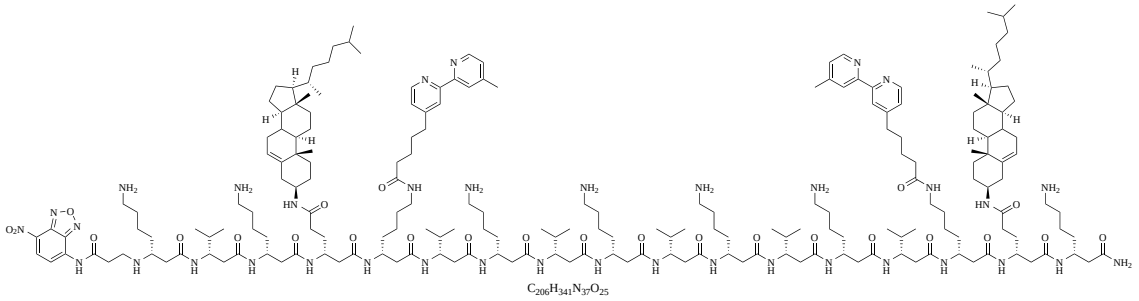

$C_{206}H_{341}N_{37}O_{25}$
[3736.2]

56

The peptide backbone was synthesized after **SOP 13.2.3** on a 40 μmol (200 mg resin) scale. All amino acids were coupled twice with the exception of *trans*-ACHC-OH (**14.5.8**) these amino acid was coupled three times. The post synthetic modifications were carried out after **SOP 13.2.4.1**, **13.2.4.3**, **13.2.4.2**, **13.2.4.4** and **13.2.6**. The final peptide was cleaved after **SOP 13.2.5** to yield the crude peptide as a green solid. The purification was done on a semipreparative scale to yield a green solid.

HPLC (semipreparative, gradient: 70 → 90 % B in 30 min, λ: 464, 300, 254 nm): t_R = 19.0 min.

ESI-MS (MeOH) *m/z* (rel %) = 633.9 $[M+H]^{6+}$ (45), 760.5 $[M+H]^{5+}$ (95), 950.4 $[M+H]^{4+}$ (100), 1266.9 $[M+H]^{3+}$ (15).

HR-MS (ESI) $C_{197}H_{314}N_{34}O_{31}$ $[M+H]^{6+}$ *m/z* = calc.: 623.6174, found: 623.6160.
$[M+H]^{5+}$ *m/z* = calc.: 748.1395, found: 748.1386.
$[M+H]^{4+}$ *m/z* = calc.: 934.9225, found: 934.9211.
$[M+H]^{3+}$ *m/z* = calc.: 1246.2276, found: 1246.2249.

14.7.12 Synthesis of P-57

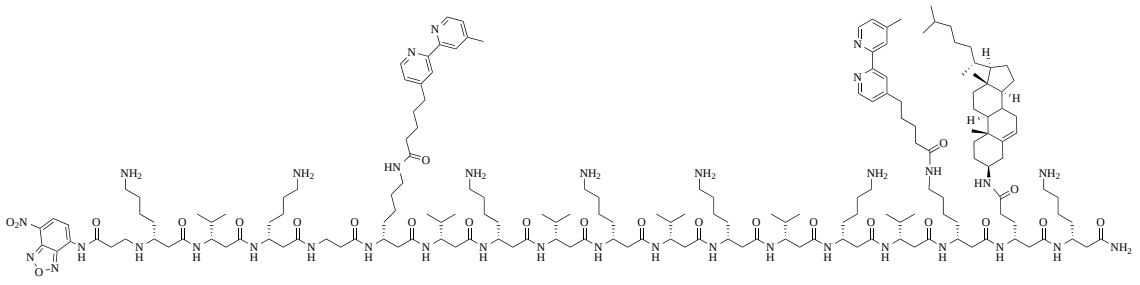

$C_{176}H_{292}N_{36}O_{24}$
[3296.50]

57

The peptide backbone was synthesized after **SOP 13.2.3** on a 40 µmol (200 mg resin) scale. All amino acids were coupled twice with the exception of *trans*-ACHC-OH (**14.5.8**) these amino acid was coupled three times. The post synthetic modifications were carried out after **SOP 13.2.4.1**, **13.2.4.3**, **13.2.4.2**, **13.2.4.4** and **13.2.6**. The final peptide was cleaved after **SOP 13.2.5** to yield the crude peptide as a green solid. The purification was done on a semipreparative scale to yield a green solid.

HPLC (semipreparative, gradient: 50 → 60 % B in 30 min, λ: 464, 300, 254 nm): t_R = 13.8 min.

ESI-MS (MeOH) *m/z* (rel %) = 471.9 $[M+H]^{7+}$ (40), 550.4 $[M+H]^{6+}$ (100), 660.3 $[M+H]^{5+}$ (90), 825.1 $[M+H]^{4+}$ (56), 1099.8 $[M+H]^{3+}$ (9).

HR-MS (ESI) $C_{176}H_{292}N_{36}O_{24}$ $[M+H]^{7+}$ *m/z* = calc.: 471.9044, found: 471.9037.
$[M+H]^{6+}$ *m/z* = calc.: 550.3873, found: 550.3870.
$[M+H]^{5+}$ *m/z* = calc.: 660.2633, found: 660.2631.
$[M+H]^{4+}$ *m/z* = calc.: 825.0773, found: 825.0777.
$[M+H]^{3+}$ *m/z* = calc.: 1099.7673, found: 1099.7672.

14.7.13 Synthesis of P-58

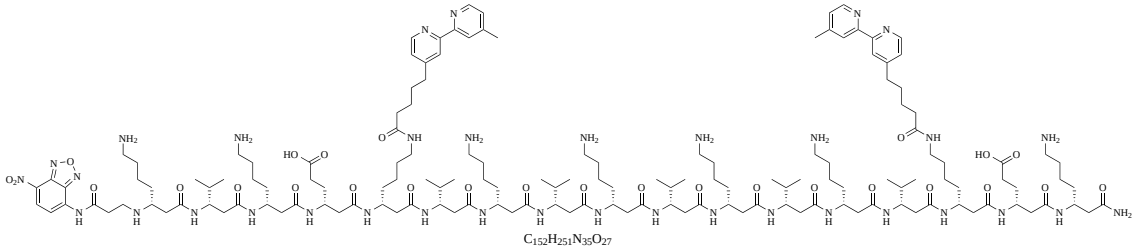

58

The peptide backbone was synthesized after **SOP 13.2.3** on a 40 μmol (200 mg resin) scale. All amino acids were coupled twice with the exception of *trans*-ACHC-OH (**14.5.8**) these amino acid was coupled three times. The post synthetic modifications were carried out after **SOP 13.2.4.1**, **13.2.4.2**, **13.2.4.4** and **13.2.6**. The final peptide was cleaved after **SOP 13.2.5** to yield the crude peptide as a green solid. The purification was done on a semipreparative scale to yield a green solid.

HPLC (semipreparative, gradient: 38 → 53 % B in 30 min, λ: 464, 300, 254 nm): t_R = 16.4 min.

ESI-MS (MeOH) *m/z* (rel %) = 441.0 $[M+H]^{7+}$ (42), 514.3 $[M+H]^{6+}$ (87), 617.0 $[M+H]^{5+}$ (100), 771.0 $[M+H]^{4+}$ (64), 1027.7 $[M+H]^{3+}$ (11).

HR-MS (ESI) $C_{152}H_{251}N_{35}O_{25}$ $[M+H]^{7+}$ *m/z* = calc.: 441.0073, found: 441.0068.
$[M+H]^{6+}$ *m/z* = calc.: 514.3406, found: 514.3401.
$[M+H]^{5+}$ *m/z* = calc.: 617.0073, found: 617.0070.
$[M+H]^{4+}$ *m/z* = calc.: 771.0073, found: 771.0073.
$[M+H]^{3+}$ *m/z* = calc.: 1027.6739, found: 1027.6735.

14.7.14 Synthesis of P-59

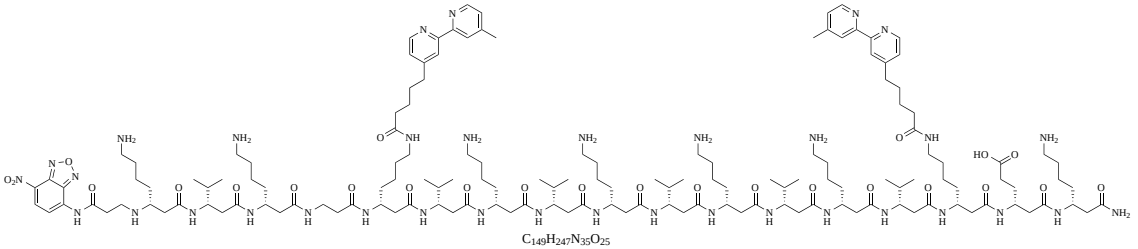

$C_{149}H_{247}N_{35}O_{25}$
[2928.8]

59

The peptide backbone was synthesized after **SOP 13.2.3** on a 40 µmol (200 mg resin) scale. All amino acids were coupled twice with the exception of *trans*-ACHC-OH (**14.5.8**) these amino acid was coupled three times. The post synthetic modifications were carried out after **SOP 13.2.4.1**, **13.2.4.2**, **13.2.4.4** and **13.2.6**. The final peptide was cleaved after **SOP 13.2.5** to yield the crude peptide as a green solid. The purification was done on a semipreparative scale to yield a green solid.

HPLC (semipreparative, gradient: 38 → 45 % B in 30 min, λ: 464, 300, 254 nm): t_R = 17.6 min.

ESI-MS (MeOH) *m/z* (rel %) = 425.0 $[M+H]^{7+}$ (40), 495.7 $[M+H]^{6+}$ (40), 594.6 $[M+H]^{5+}$ (100), 743.0 $[M+H]^{4+}$ (90), 990.3 $[M+H]^{3+}$ (56).

HR-MS (ESI) $C_{152}H_{251}N_{35}O_{25}$ $[M+H]^{7+}$ *m/z* = calc.: 424.9998, found: 424.9995.
$[M+H]^{6+}$ *m/z* = calc.: 495.6652, found: 495.6650.
$[M+H]^{5+}$ *m/z* = calc.: 594.5968, found: 594.5965.
$[M+H]^{4+}$ *m/z* = calc.: 742.9942, found: 742.9937.
$[M+H]^{3+}$ *m/z* = calc.: 990.3231, found: 990.3218.

Appendices

A CD-Spectra

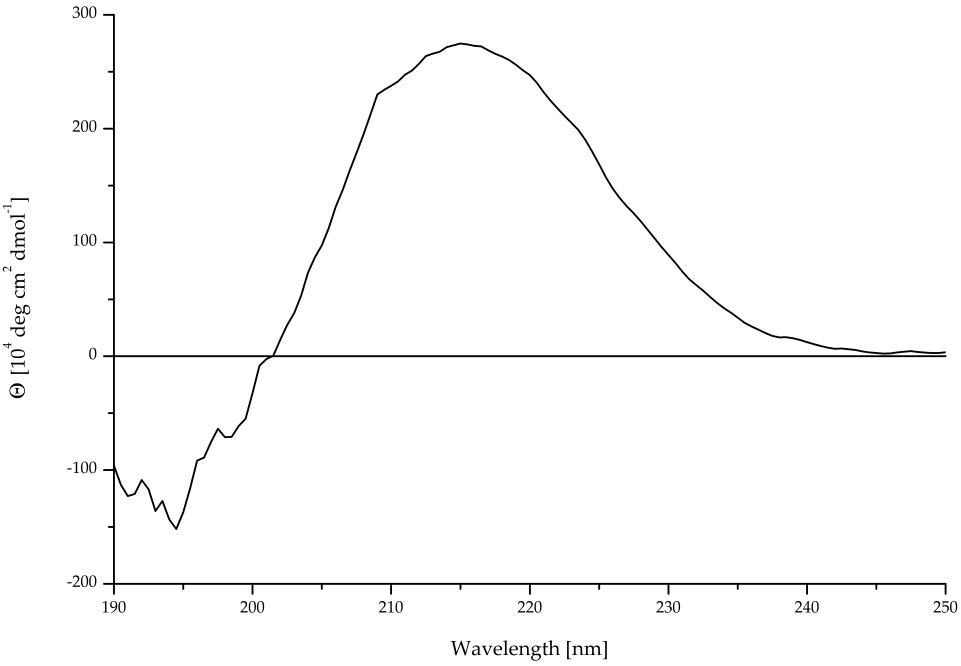

Figure A.1: CD-spectra of **P-49** in MeCN (c = 10.4 μM).

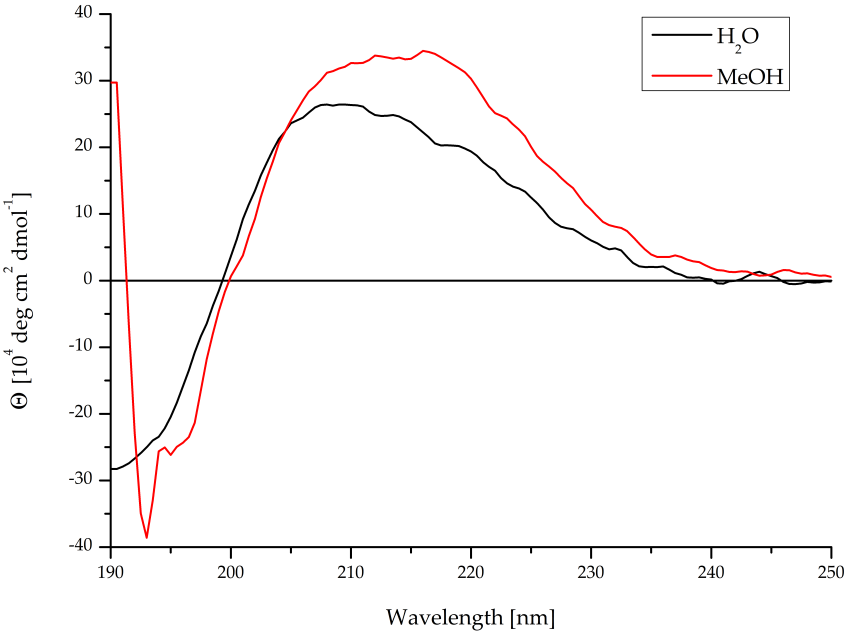

Figure A.2: CD-spectra of **P-60** in different solvent systems (c = 16.0 µM).

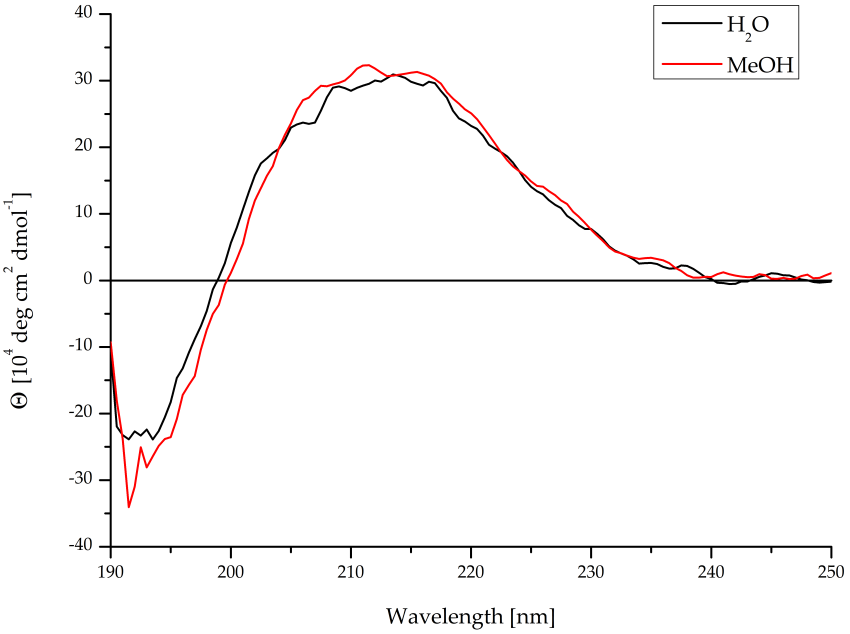

Figure A.3: CD-spectra of **P-61** in different solvent systems (c = 16.0 µM).

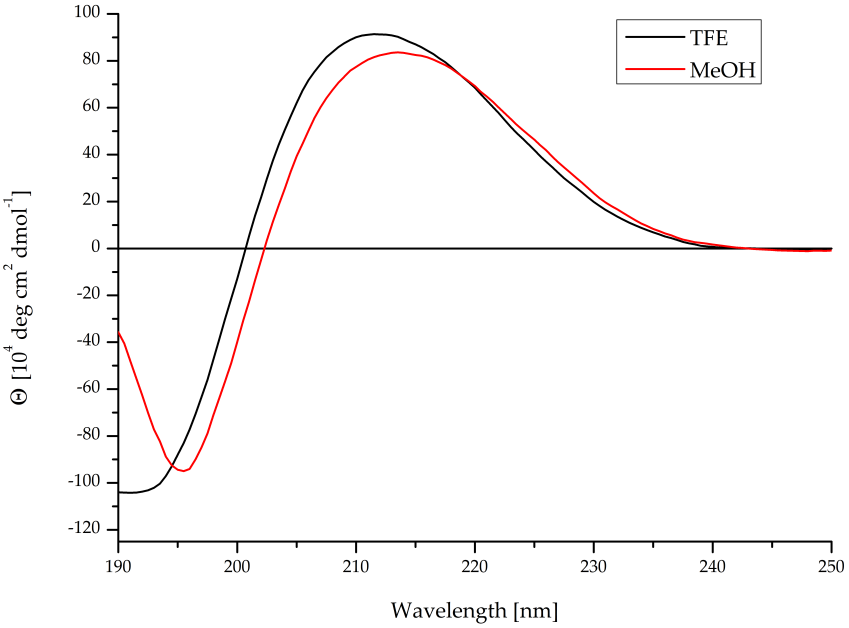

Figure A.4: CD-spectra of **P-50** in different solvent systems (c = 15.9 µM).

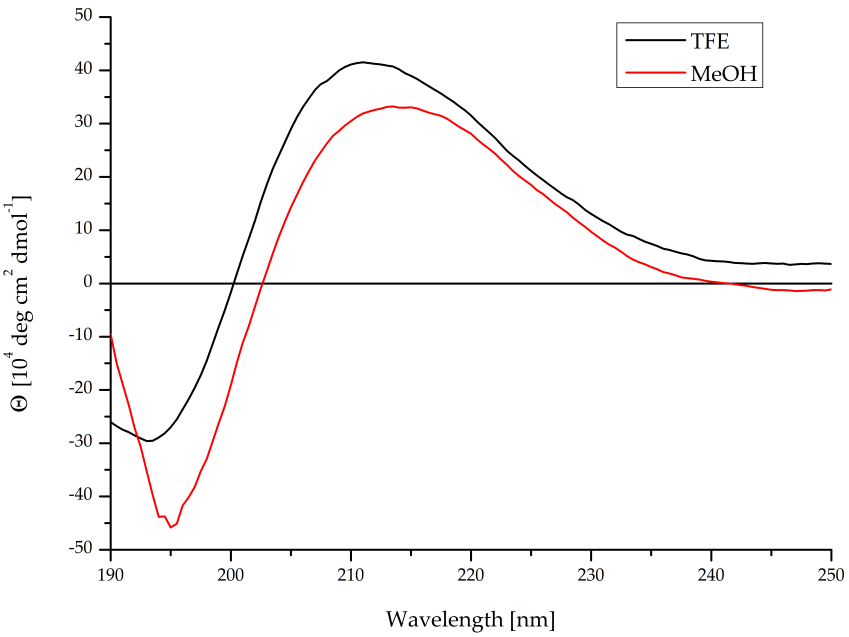

Figure A.5: CD-spectra of **P-51** in different solvent systems (c = 20.8 µM).

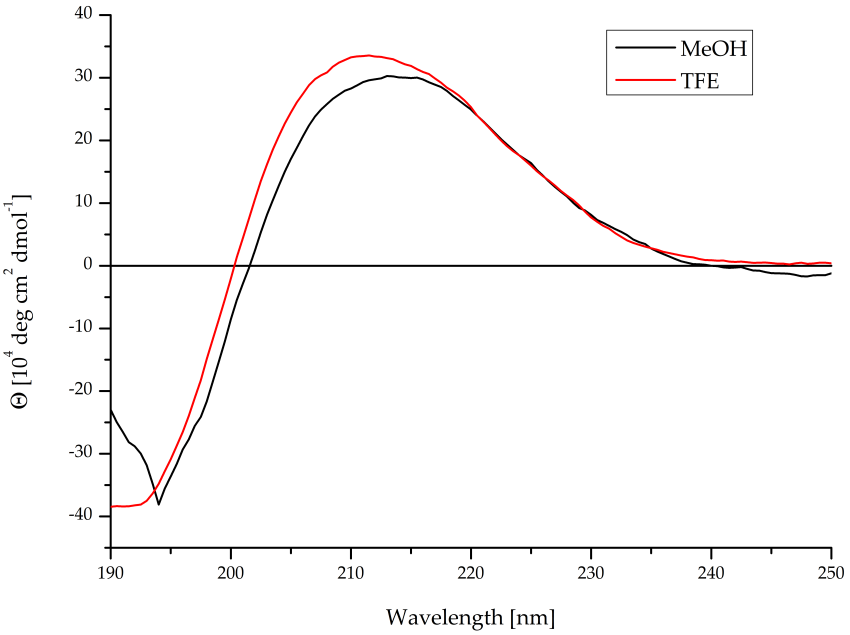

Figure A.6: CD-spectra of **P-52** in different solvent systems (c = 15.9 µM).

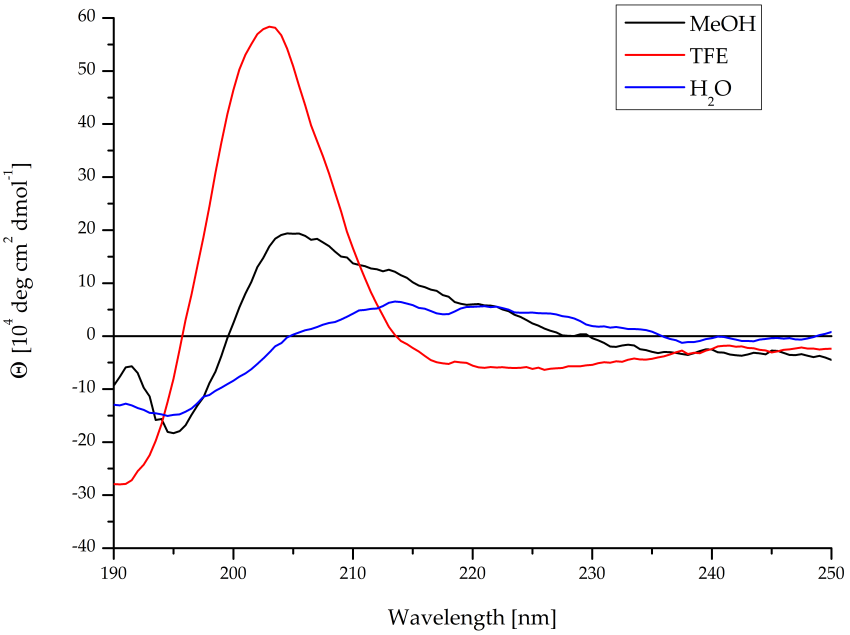

Figure A.7: CD-spectra of **P-55** in different solvent systems (c = 30.0 µM).

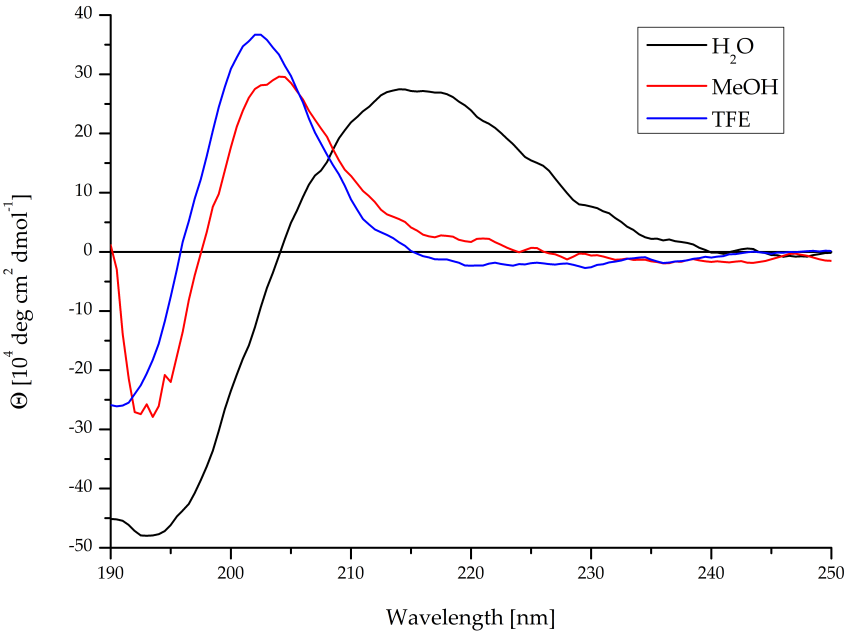

Figure A.8: CD-spectra of **P-62** in different solvent systems (c = 30.0 µM).

B Metal induced aggregation

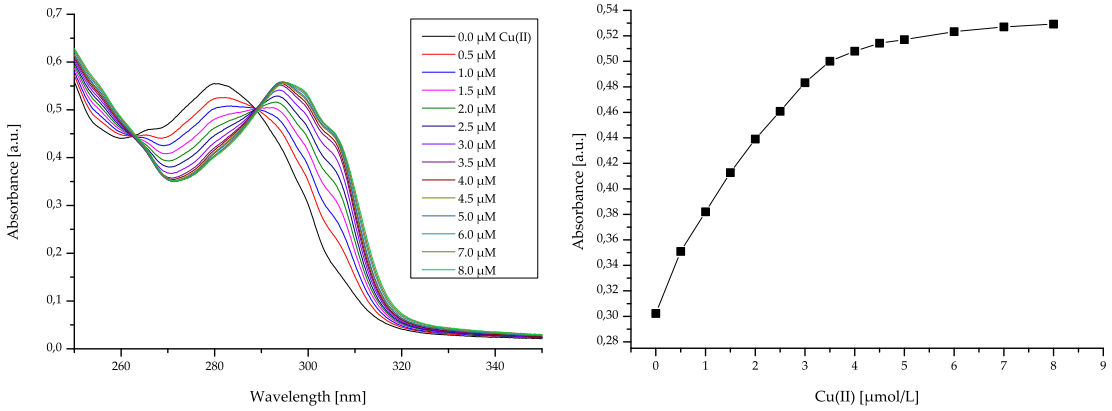

(a) Plot of the change in the absorption of **P-49** (8 µM) during the metal titration of $Cu(ClO_4)_2$ (250 µM) in MeOH.

(b) Plot of the absorption values at 300 nm against their corresponding Cu(II) concentration.

Figure B.1: UV/Vis analysis of **P-49** (8 µM) in MeOH with $Cu(ClO_4)_2$.

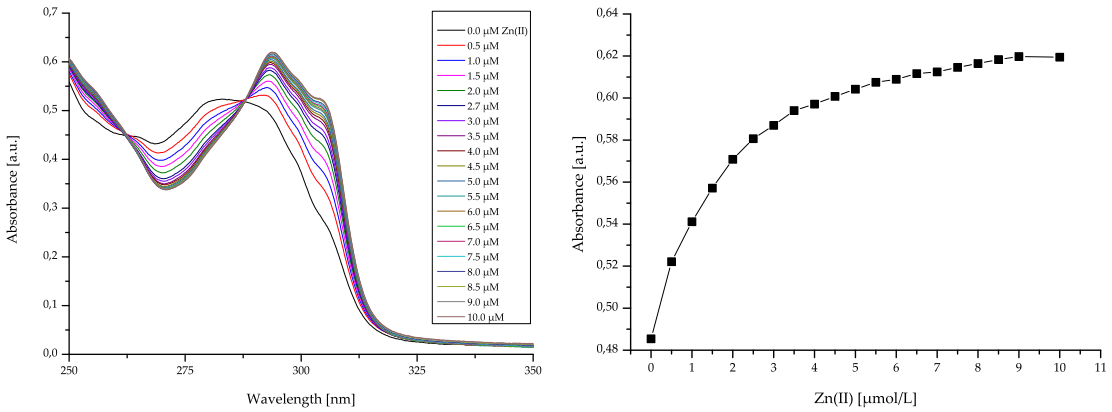

(a) Plot of the change in the absorption of **P-49** (8 µM) during the metal titration of $ZnBr_2$ (250 µM) in MeOH.

(b) Plot of the absorption values at 300 nm against their corresponding Cu(II) concentration.

Figure B.2: UV/Vis analysis of **P-49** (8 µM) in MeOH with $ZnBr_2$.

C Binding on the surface

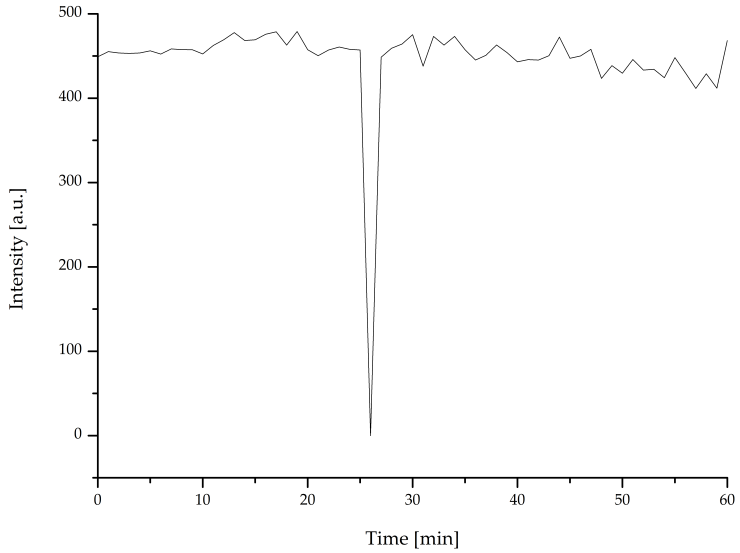

Figure C.1: Peptide coordination with a peptide-lipid-ratio of 1:50, 100 nm DOPC vesicles, a fluorescence label of 1.5 mole-% and **P-51** was incorporated after method **I**.

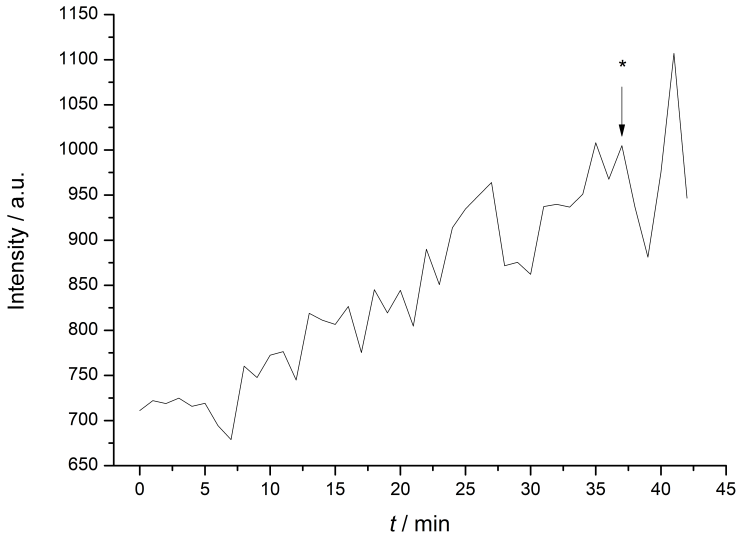

Figure C.2: Peptide coordination with a peptide-lipid-ratio of 1:50, 100 nm DOPC vesicles, a fluorescence label of 1.5 mole-% and **P-51** was incorporated after method **E**.

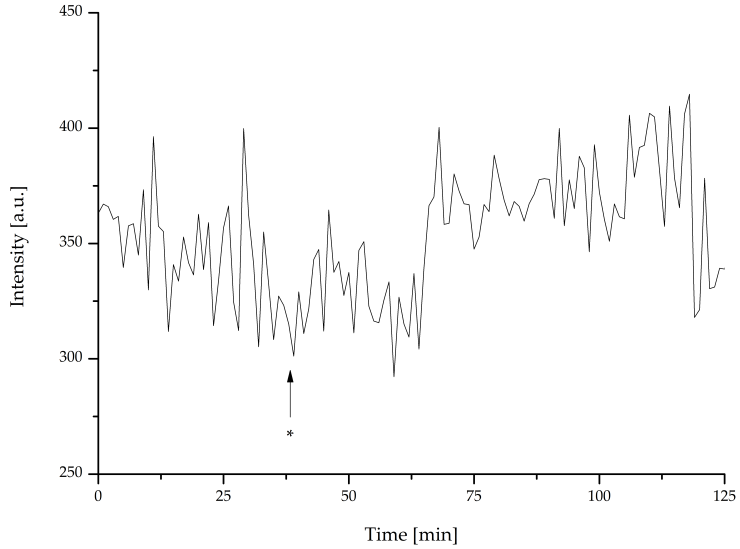

Figure C.3: Peptide coordination with a peptide-lipid-ratio of 1:50, 200 nm DOPC vesicles, a fluorescence label of 1.5 mole-% and **P-51** was incorporated after method **I**.

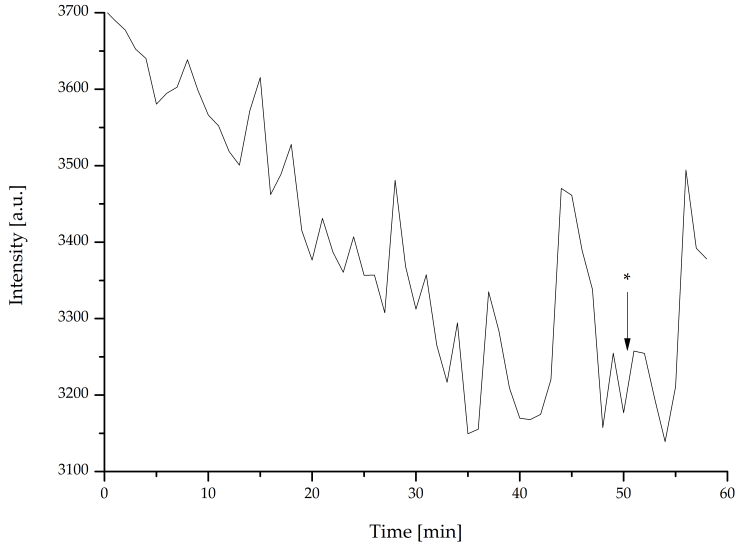

Figure C.4: Peptide coordination with a peptide-lipid-ratio of 1:50, 100 nm vesicle diameter, a fluorescence label of 0.2 mole-% and the peptide was incorporated after extrusion (**E**).

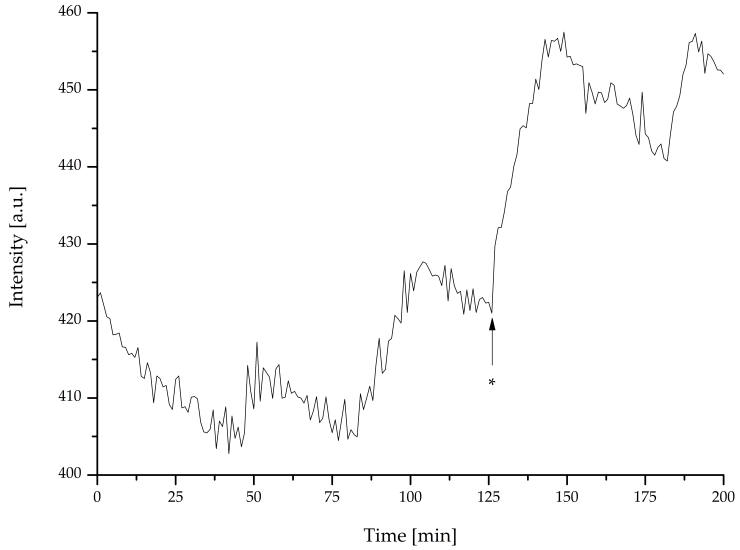

Figure C.5: Peptide coordination with a peptide-lipid-ratio of 1:50, 400 nm DOPC vesicles, a fluorescence label of 1.5 mole-% and **P-51** was incorporated after method **I**.

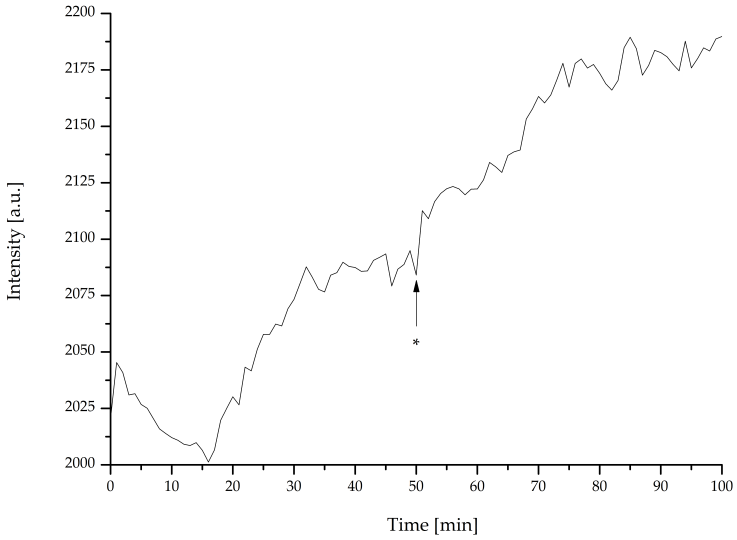

Figure C.6: Peptide coordination with a peptide-lipid-ratio of 1:50, 400 nm DOPC vesicles, a fluorescence label of 0.2 mole-% and **P-51** was incorporated after method **I**.

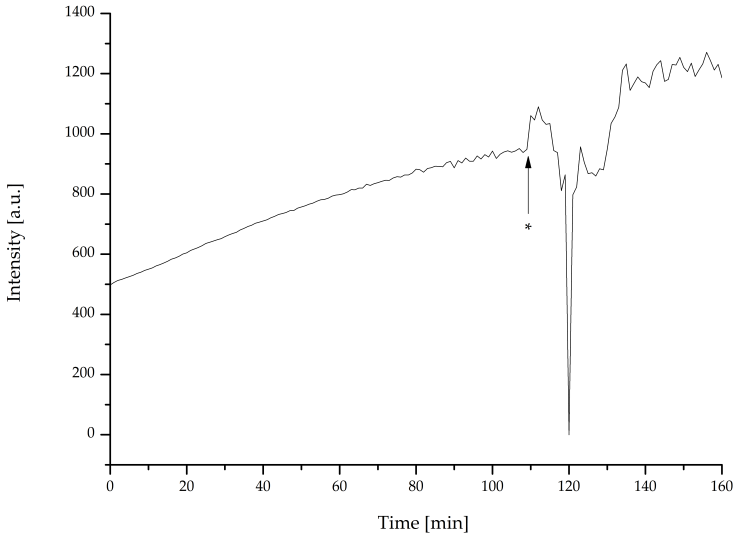

Figure C.7: Peptide coordination with a peptide-lipid-ratio of 1:50, 200 nm DOPC vesicles, a fluorescence label of 1.5 mole-% and **P-51** was incorporated after method **E**.

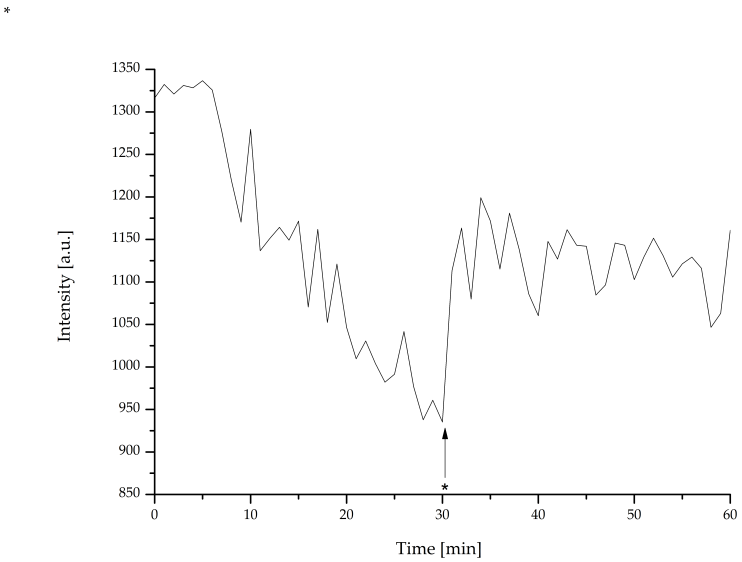

Figure C.8: Peptide coordination with a peptide-lipid-ratio of 1:50, 400 nm DOPC vesicles, a fluorescence label of 1.5 mole-% and **P-51** was incorporated after method **E**.

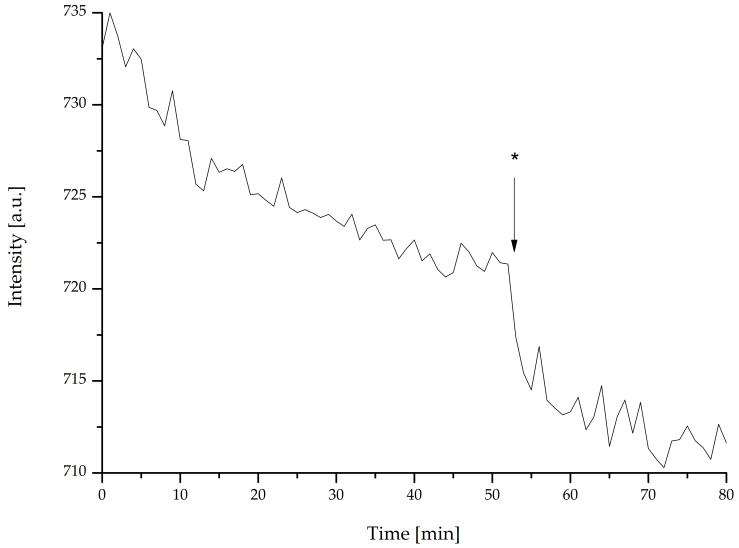

Figure C.9: Peptide coordination with a peptide-lipid-ratio of 1:50, 200 nm DOPC vesicles, a fluorescence label of 0.2 mole-% and **P-51** was incorporated after method **I**.

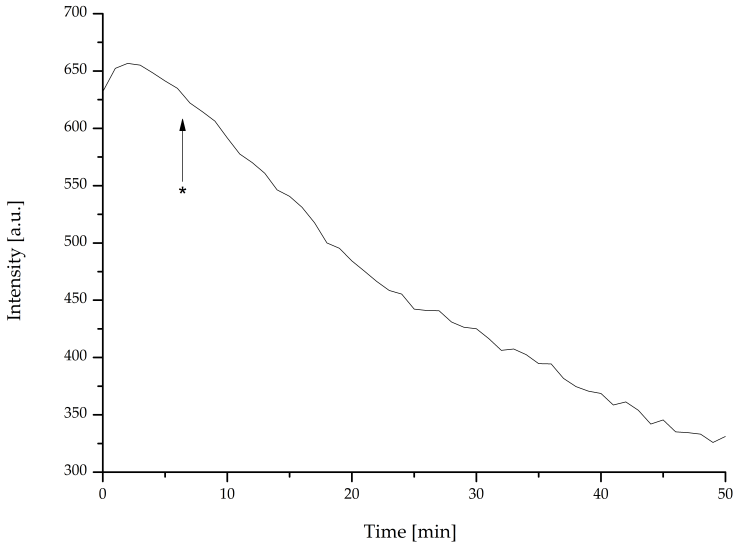

Figure C.10: Peptide coordination with a peptide-lipid-ratio of 1:50, 200 nm DOPC vesicles, a fluorescence label of 0.2 mole-% and **P-51** was incorporated after method **I**.

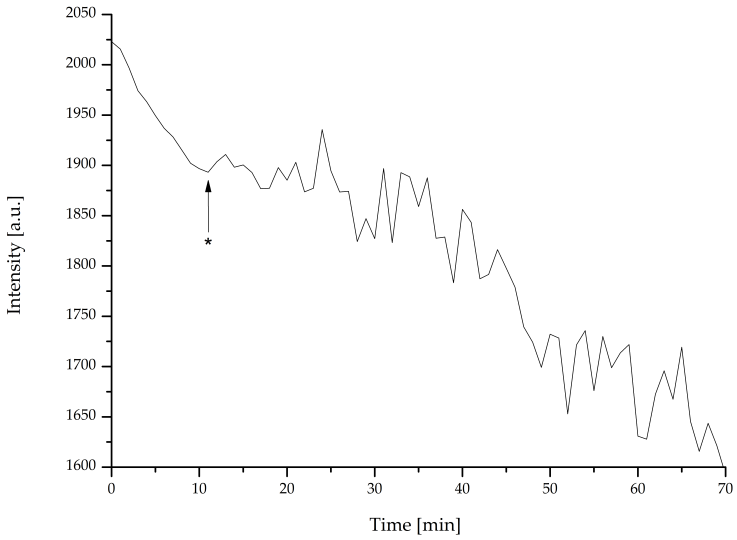

Figure C.11: Peptide coordination with a peptide-lipid-ratio of 1:50, 100 nm DOPC vesicles, a fluorescence label of 0.2 mole-% and **P-51** was incorporated after method **E**.

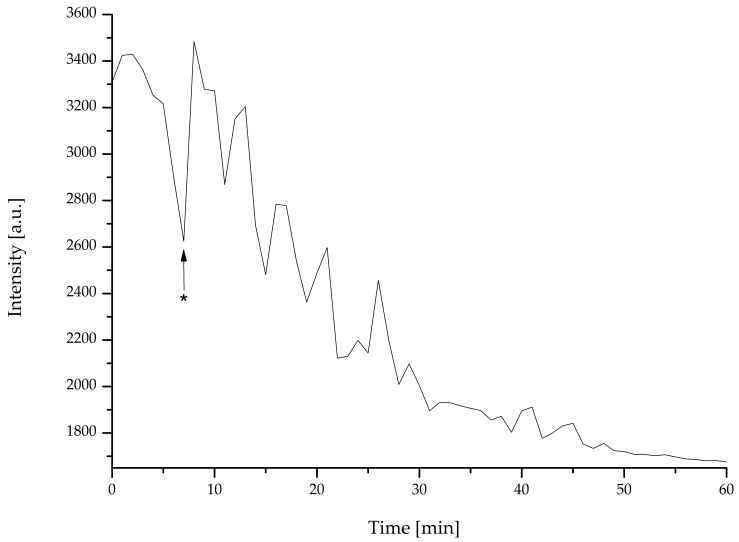

Figure C.12: Peptide coordination with a peptide-lipid-ratio of 1:50, 200 nm DOPC vesicles, a fluorescence label of 0.5 mole-% and **P-51** was incorporated after method **I**.

D Leakage-assay

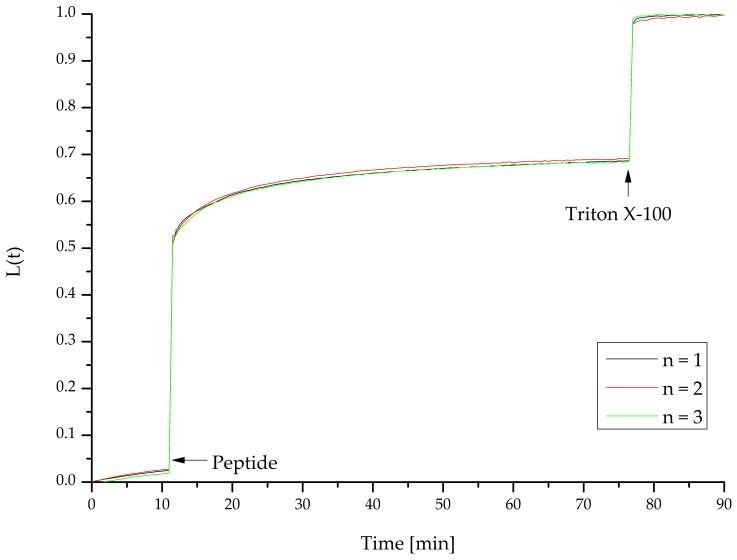

Figure D.1: Leakage-assay with a peptide/lipid ratio of 1:300, the β-peptide **P-51** is solved in TFE/buffer (25 µL, 4:1, v/v). The β-peptide is added after 11 min and Triton X-100 is added after 77 min.

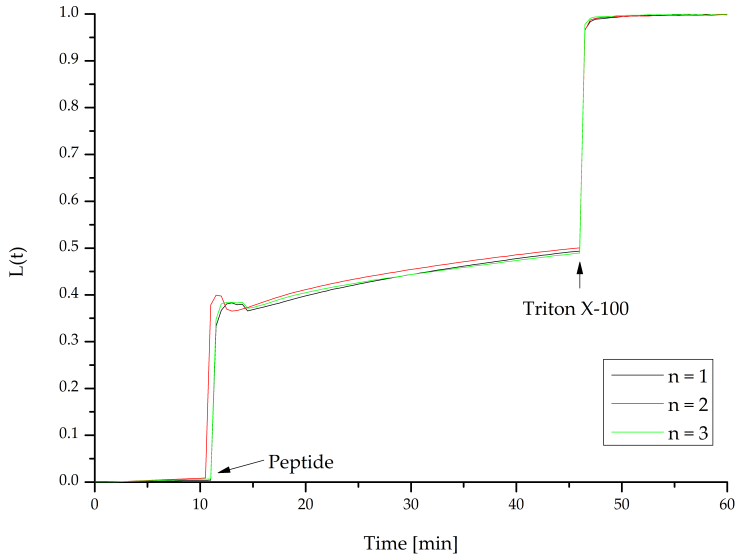

Figure D.2: Leakage-assay with a peptide/lipid ratio of 1:500, the β-peptide **P-51** is solved in TFE/buffer (25 µL, 4:1, v/v). The β-peptide is added after 11 min and Triton X-100 is added after 46 min.

AA	amino acid
Ac	acetyl
Ac_2O	acetic anhydride
ACHC	trans-2-aminocyclohexanecarboxlyic acid
All	allyl ether
AMP	antimicrobial peptides
aq	aqueous
BD	Benton Dickinson
Boc	tert-butoxycarbonyl
CD	circular dichroism
$CHCl_3$	chloroform
Chol	cholesterol
COMU	(1-cyano-2-ethoxy-2-oxoethylidenaminooxy)dimethylaminomorpholino-carbenium hexafluorophosphate
CPP	cell penetrating peptides
DBU	1,8-diazabicyclo[5.4.0]undec-7-ene
DCC	N,N'-dicyclohexylcarbodiimide
DCM	dichloromethane
DHPC	1,2-dihexanoyl-sn-glycero-3-phosphocholine
DIPEA	N,N-diisopropylethylamine
DLS	dynamic light scattering
DMAP	4-dimethylaminopyridine
DMF	dimethylformamide
DMPC	1,2-dimyristoyl-sn-glycero-3-phosphocholine
DMSO	dimethyl sulfoxide
DOPC	1,2-dioleoyl-sn-glycero-3-phosphocholine
EDT	1,2-ethanedithiole
EE	ethyl acetate
eq	equivalents
ESI	electrospray ionization
EtOAc	ethyl acetate
EtOH	ethanol
Et2O	diethyl ether
Fmoc	fluorenylmethoxycarbonyl

FRET	Förster resonance energy transfer
HATU	1-(bis(dimethylamino)methylene)-1H-1,2,3-triazolo[4,5-b]-pyridinium 3-oxide hexafluorophosphate
HFIP	hexafluoroisopropanol
HOAt	1-hydroxy-7-azabenzotriazole
HPLC	high performance liquid chromatography
HR	high resolution
IR	infrared
J	coupling constant
LUV	large unilamellar vesicle
MeCN	acetonitrile
MeOH	methanol
MLV	multilamellar vesicle
MS	mass spectrometry
MSK	membrane skeleton
MST	microscale thermophoresis
MTT	4-methyltrityl
MW	microwave
m/z	mass-to-charge ratio
NBD	7-nitrobenz-2-oxa-1,3-diazol-4-yl
NEt_3	triethylamine
NMP	N-methyl-2-pyrrolidone
NMR	nuclear magnetic resonance spectroscopy
prep.	preparative
Rhod	lissamine rhodamine B
RP	reverse-phase
rpm	rounds per minute
rt	room temperature
sat.	saturated
SOP	standard operating protocol
SPPS	solid-phase peptide synthesis
SRB	sulforhodamine B
SUV	small unilamellar vesicle
TFA	trifluoroacetic acid

THF	tetrahydrofuran
TLC	thin layer chromatography
TMS	trimethylsilan
TRIS	tris(hydroxymethyl)aminomethane
U-HPLC	ultra-high performance liquid chromatography
UV	ultraviolet
Vis	visible
v/v	volume-to-volume ratio

Bibliography

[1] A. L. Lehninger et al., *Prinzipien der Biochemie*, 2. Aufl., Studienausg, Spektrum Akad. Verl, Heidelberg, **1998**.

[2] C. Hackenberger, *Chemie in unserer Zeit* **2006**, *40*, 174–183.

[3] Y. Guo, S. Pogodin, V. A. Baulin, *J. Chem. Phys.* **2014**, *140*, 174903.

[4] J. A. Killian, T. K. M. Nyholm, *Curr Opin Struct Biol* **2006**, *16*, 473–479.

[5] M. Rueping et al., *Chem. Eur. J.* **2004**, *10*, 1607–1615.

[6] L. K. Tsou, C. D. Tatko, M. L. Waters, *J. Am. Chem. Soc.* **2002**, *124*, 14917–14921.

[7] E. M. Sletten, C. R. Bertozzi, *Angewandte Chemie International Edition* **2009**, *48*, 6974–6998.

[8] H.-D. Arndt et al., *Angewandte Chemie International Edition* **2002**, *41*, 4062–4065.

[9] M. Pelay-Gimeno et al., *Angewandte Chemie International Edition* **2015**, *54*, 8896–8927.

[10] A. Holt, J. A. Killian, *Eur Biophys J* **2010**, *39*, 609–621.

[11] M. R. R. de Planque, J. A. Killian, *Mol Membr Biol* **2003**, *20*, 271–284.

[12] A. Elofsson, G. von Heijne, *Annu Rev Biochem* **2007**, *76*, 125–140.

[13] G. von Heijne, *J Intern Med* **2007**, *261*, 543–557.

[14] J. M. Berg et al., *Stryer Biochemie*, 8. Aufl. 2018, Springer Spektrum, Berlin, Heidelberg, **2018**.

[15] U. Koert, *Angewandte Chemie* **1997**, *109*, 1922–1923.

[16] D. H. Appella et al., *J. Am. Chem. Soc.* **1999**, *121*, Publisher: American Chemical Society, 2309–2310.

[17] P. I. Arvidsson, M. Rueping, D. Seebach, *Chem. Commun.* **2001**, Publisher: The Royal Society of Chemistry, 649–650.

[18] D. Seebach, D. F. Hook, A. Glättli, *Biopolymers* **2006**, *84*, 23–37.

[19] T. L. Raguse, J. R. Lai, S. H. Gellman, *J. Am. Chem. Soc.* **2003**, *125*, 5592–5593.

[20] C. Kaes, A. Katz, M. W. Hosseini, *Chem. Rev.* **2000**, *100*, 3553–3590.

[21] H. Ishida, M. Kyakuno, S. Oishi, *Biopolymers* **2004**, *76*, 69–82.

[22] S.-i. Yusa, *International Journal of Polymer Science* **2012**, *2012*, 1–10.

[23] J. D. Hartgerink et al., *J. Am. Chem. Soc.* **1996**, *118*, 43–50.

[24] Y.-S. Wang et al., *European Polymer Journal* **2007**, *43*, 43–51.

[25] T. Förster, *Annalen der Physik* **1948**, *437*, 55–75.

[26] E. A. Jares-Erijman, T. M. Jovin, *Nat Biotechnol* **2003**, *21*, 1387–1395.

[27] S. Arumugam, P. Bassereau, *Essays in Biochemistry* **2015**, *57*, (Ed.: I. Parmryd), 109–119.

[28] S. J. Singer, G. L. Nicolson, *Science* **1972**, *175*, 720–731.

[29] T. S. van Zanten, S. Mayor, *F1000Res* **2015**, *4*, 1380.

[30] S. J. Singer in *Structure and Function of Biological Membranes*, (Ed.: L. I. Rothfield), Academic Press, **1971**, pp. 145–222.

[31] S. H. Richardson, H. O. Hultin, D. E. Green, *Proc Natl Acad Sci U S A* **1963**, *50*, 821–827.

[32] D. Haldar, K. Freeman, T. S. Work, *Nature* **1966**, *211*, 9–12.

[33] E. D. Kiehn, J. J. Holland, *Proc Natl Acad Sci U S A* **1968**, *61*, 1370–1377.

[34] D. E. Green et al., *Proceedings of the National Academy of Sciences* **1968**, *60*, 277–284.

[35] J. Lenard, *Biochemistry* **1970**, *9*, 1129–1132.

[36] B. Ke, *Archives of Biochemistry and Biophysics* **1965**, *112*, 554–561.

[37] D. F. Wallach, P. H. Zahler, *Proceedings of the National Academy of Sciences* **1966**, *56*, 1552–1559.

[38] J. Lenard, S. J. Singer, *Proceedings of the National Academy of Sciences* **1966**, *56*, 1828–1835.

[39] J. K. Blasie, C. R. Worthington, *Journal of Molecular Biology* **1969**, *39*, 417–439.

[40] D. Bownds, A. C. Gaide-Huguenin, *Nature* **1970**, *225*, 870–872.

[41] D. M. Engelman, *Nature* **2005**, *438*, 578–580.

[42] J. Yu, D. A. Fischman, T. L. Steck, *J. Supramol. Struct.* **1973**, *1*, 233–248.

[43] S. N. Ahmed, D. A. Brown, E. London, *Biochemistry* **1997**, *36*, 10944–10953.

[44] B. D. A, R. J. K, *Cell (Cambridge Mass.)* **1992**, *68*, 533–544.

[45] G van Meer et al., *The Journal of Cell Biology* **1987**, *105*, 1623–1635.

[46] A. Pralle et al., *Journal of Cell Biology* **2000**, *148*, 997–1008.

[47] R. Varma, S. Mayor, *Nature* **1998**, *394*, 798–801.

[48] S Thomas et al., *Molecular Immunology* **2004**, *41*, 399–409.

[49] Z. Korade, A. K. Kenworthy, *Neuropharmacology* **2008**, *55*, 1265–1273.

[50] L. J. Pike, *Journal of Lipid Research* **2006**, *47*, 1597–1598.

[51] E. Sezgin et al., *Nat Rev Mol Cell Biol* **2017**, *18*, 361–374.

[52] K. Simons, E. Ikonen, *Nature* **1997**, *387*, 569 –572.

[53] J. Fan, M. Sammalkorpi, M. Haataja, *FEBS Letters* **2010**, *584*, 1678–1684.

[54] L. A. Bagatolli, O. G. Mouritsen, *Front. Plant Sci.* **2013**, *0*, DOI `10.3389/fpls.2013.00457`.

[55] D. Lingwood, K. Simons, *Science* **2010**, *327*, 46–50.

[56] K. Jacobson, O. G. Mouritsen, R. G. W. Anderson, *Nat Cell Biol* **2007**, *9*, 7–14.

[57] A. C. S. Alves et al., *CMC* **2018**, *25*, 2082–2104.

[58] J. M. Sanderson, *Org. Biomol. Chem.* **2005**, *3*, 201–212.

[59] A. Bangham, M. Standish, J. Watkins, *Journal of Molecular Biology* **1965**, *13*, 238–IN27.

[60] F Szoka, D Papahadjopoulos, *Annu. Rev. Biophys. Bioeng.* **1980**, *9*, 467–508.

[61] A. Akbarzadeh et al., *Nanoscale Res Lett* **2013**, *8*, 102.

[62] K. Shashi, K. Satinder, B. Parashar, *International Research Journal of Pharmacy* **2012**, *3*.

[63] A. Wagner, K. Vorauer-Uhl, *Journal of Drug Delivery* **2011**, *2011*, 1–9.

[64] S. S. Chrai, R. Murari, I. Ahmad, **2001**, *14*, 10–14.

[65] T. M. Allen, *Drugs* **1997**, *54*, 8–14.

[66] S. K. Sahoo, V. Labhasetwar, *Drug Discovery Today* **2003**, *8*, 1112–1120.

[67] A. Gabizon et al., *Journal of Controlled Release* **1998**, *53*, 275–279.

[68] A Sharma, *International Journal of Pharmaceutics* **1997**, *154*, 123–140.

[69] M. J. Hope et al., *Biochimica et Biophysica Acta (BBA) - Biomembranes* **1985**, *812*, 55–65.

[70] N. F. Morales-Penningston et al., *Biochim Biophys Acta* **2010**, *1798*, 1324–1332.

[71] Y.-H. M. Chan, S. G. Boxer, *Current Opinion in Chemical Biology*, Model systems/Biopolymers **2007**, *11*, 581–587.

[72] G. Sessa, G. Weissmann, *Journal of Lipid Research* **1968**, *9*, 310–318.

[73] D. Papahadjopoulos, N. Miller, *Biochimica et Biophysica Acta (BBA) - Biomembranes* **1967**, *135*, 624–638.

[74] D. Papahadjopoulos, J. Watkins, *Biochimica et Biophysica Acta (BBA) - Biomembranes* **1967**, *135*, 639–652.

[75] R. C. MacDonald et al., *Biochimica et Biophysica Acta (BBA) - Biomembranes* **1991**, *1061*, 297–303.

[76] H. Hub, U. Zimmermann, H. Ringsdorf, *FEBS Letters* **1982**, *140*, 254–256.

[77] S. Kolusheva, T. Shahal, R. Jelinek, *Biochemistry* **2000**, *39*, 15851–15859.

[78] S. Galdiero et al., *IJMS* **2013**, *14*, 18758–18789.

[79] J.-J. Jung et al., *Bioscience Reports* **2012**, *32*, 383–391.

[80] M. Koch, M. Holt, *Biochimica et Biophysica Acta (BBA) - Molecular and Cell Biology of Lipids*, Lipids and Vesicular Transport **2012**, *1821*, 1114–1132.

[81] S. Galdiero, *Protein and Peptide Letters* **2009**, *16*, 711–711.

[82] A. Falanga et al., *Protein and Peptide Letters* **2009**, *16*, 751–759.

[83] E. M. A. R. B. Castanho, *Membrane Active Peptides: Methods and Results on Structure and Function*, first Edition, International University Line, La Jolla, Calif, **2010**.

[84] *Cell-Penetrating Peptides: Processes and Applications*, 0th ed., (Ed.: U. Langel), CRC Press, **2002**.

[85] S. Yamaguchi et al., *Biochemistry* **2002**, *41*, 9852–9862.

[86] J. M. Ageitos et al., *Biochemical Pharmacology*, Antibiotics - Meeting the Challenges of 21st Century Health Care: Part I **2017**, *133*, 117–138.

[87] S. Galdiero et al., *CDM* **2012**, *13*, 93–104.

[88] I. D. Alves et al., *Biochimica et Biophysica Acta (BBA) - Biomembranes*, Delivery of Therapeutic Molecules: **2010**, *1798*, 2231–2239.

[89] E. Koren, V. P. Torchilin, *Trends in Molecular Medicine* **2012**, *18*, 385–393.

[90] N. Kamei et al., *Therapeutic Delivery* **2013**, *4*, 315–326.

[91] S. R. MacEwan, A. Chilkoti, *WIREs Nanomedicine and Nanobiotechnology* **2013**, *5*, 31–48.

[92] K. A. Brogden, *Nat Rev Microbiol* **2005**, *3*, 238–250.

[93] F. Guilhelmelli et al., *Frontiers in Microbiology* **2013**, *4*, 353.

[94] A. Hollmann et al., *Frontiers in Chemistry* **2018**, *6*, 204.

[95] J. Oreopoulos et al., *Biophysical Journal* **2010**, *98*, 815–823.

[96] K. El Kirat, S. Morandat, Y. F. Dufrêne, *Biochimica et Biophysica Acta (BBA) - Biomembranes*, A Surface View on Membrane Structure, Dynamics and Applications **2010**, *1798*, 750–765.

[97] A. J. García-Sáez et al., *Biophysical Journal* **2007**, *93*, 103–112.

[98] R. Volinsky et al., *Biochimica et Biophysica Acta (BBA) - Biomembranes*, Membrane Biophysics of Antimicrobial Peptides **2006**, *1758*, 1393–1407.

[99] K. Lohner, E. J. Prenner, *Biochimica et Biophysica Acta (BBA) - Biomembranes* **1999**, *1462*, 141–156.

[100] T. Pott et al., *Chemistry and Physics of Lipids* **2001**, *109*, 209–223.

[101] J.-F. Faucon et al., *Biochimica et Biophysica Acta (BBA) - Biomembranes* **1995**, *1234*, 235–243.

[102] D. Seebach, J. Gardiner, *Acc. Chem. Res.* **2008**, *41*, 1366–1375.

[103] D. Seebach, A. K. Beck, D. J. Bierbaum, *Chemistry & Biodiversity* **2004**, *1*, 1111–1239.

[104] G. R. Marshall, F. Ballante, *Drug Development Research* **2017**, *78*, 245–267.

[105] S. H. Gellman, *Accounts of Chemical Research* **1998**, *31*, 173–180.

[106] T. Hintermann, D. Seebach, *CHIMIA International Journal for Chemistry* **1997**, *51*, 244–247.

[107] D. Seebach, J. L. Matthews, *Chemical Communications* **1997**, 2015–2022.

[108] J. Podlech, D. Seebach, *Angewandte Chemie International Edition in English* **1995**, *34*, 471–472.

[109] R. P. Cheng, S. H. Gellman, W. F. DeGrado, *Chemical Reviews* **2001**, *101*, 3219–3232.

[110] P. Balaram, *Biopolymers* **2010**, *94*, 733–741.

[111] R. W. Hooft, C. Sander, G. Vriend, *Bioinformatics* **1997**, *13*, 425–430.

[112] D. Seebach et al., *Helvetica Chimica Acta* **1996**, *79*, 913–941.

[113] D. H. Appella et al., *J. Am. Chem. Soc.* **1996**, *118*, 13071–13072.

[114] J. Applequist et al., *J. Am. Chem. Soc.* **1998**, *120*, 4891–4892.

[115] J. M. Fernández-Santín et al., *Nature* **1984**, *311*, 53–54.

[116] D. H. Appella et al., *Nature* **1997**, *387*, 381–384.

[117] N. Rathore, S. H. Gellman, J. J. de Pablo, *Biophysical Journal* **2006**, *91*, 3425–3435.

[118] J. M. Fernandez-Santin et al., *Macromolecules* **1987**, *20*, 62–68.

[119] F. López-Carrasquero, C. Alemán, S. Muñoz-Guerra, *Biopolymers* **1995**, *36*, 263–271.

[120] D. H. Appella et al., *J. Am. Chem. Soc.* **1999**, *121*, 7574–7581.

[121] D. Seebach et al., *Helv. Chim. Acta* **1998**, *81*, 932–982.

[122] D. Seebach et al., *Helvetica Chimica Acta* **2000**, *83*, 34–57.

[123] D. Seebach et al., *Helvetica chimica acta* **1996**, *79*, 2043–2066.

[124] K. A. Bode, J. Applequist, *Macromolecules* **1997**, *30*, 2144–2150.

[125] P. J. Halling, *Journal of Chemical Technology & Biotechnology* **1995**, *62*, 105–105.

[126] M. R. Lockett et al., *Angewandte Chemie International Edition* **2013**, *52*, 7714–7717.

[127] B. Breiten et al., *J. Am. Chem. Soc.* **2013**, *135*, 15579–15584.

[128] I. Cosic, *IEEE Transactions on Biomedical Engineering* **1994**, *41*, 1101–1114.

[129] J. J. Lavigne, E. V. Anslyn, *Angewandte Chemie International Edition* **2001**, *40*, 3118–3130.

[130] T. Šmejkal, B. Breit, *Angew. Chem. Int. Ed.* **2008**, *47*, 311–315.

[131] G. De Santis et al., *Angew. Chem. Int. Ed. Engl.* **1996**, *35*, 202–204.

[132] C. B. Aakeröy, A. M. Beatty, B. A. Helfrich, *Angewandte Chemie International Edition* **2001**, *40*, 3240–3242.

[133] Y. Kubo et al., *Angew. Chem. Int. Ed.* **2003**, *42*, 2036–2040.

[134] S. K. Kim et al., *J. Am. Chem. Soc.* **2004**, *126*, 16499–16506.

[135] M. D. Cohen et al., *J. Chem. Soc. Perkin Trans. 2* **1973**, 1095.

[136] F. D. Lewis et al., *J. Am. Chem. Soc.* **1988**, *110*, 1261–1267.

[137] P. L. Egerton et al., *J. Am. Chem. Soc.* **1981**, *103*, 3859–3863.

[138] D. M. Bassani et al., *J. Am. Chem. Soc.* **2000**, *122*, 8795–8796.

[139] F. Blau, *Monatshefte für Chemie* **1889**, *10*, 375–388.

[140] M. Lieberman, T. Sasaki, *J. Am. Chem. Soc.* **1991**, *113*, 1470–1471.

[141] M. R. Ghadiri, C. Soares, C. Choi, *J. Am. Chem. Soc.* **1992**, *114*, 825–831.

[142] T. Koide et al., *J. Am. Chem. Soc.* **2002**, *124*, 9388–9389.

[143] H. Ishida et al., *ChemBioChem* **2006**, *7*, 1567–1570.

[144] H. Rensmo, S. Lunell, H. Siegbahn, *Journal of Photochemistry and Photobiology A: Chemistry* **1998**, *114*, 117–124.

[145] N. A. Uhlich et al., *Chem. Commun.* **2009**, 6237–6239.

[146] A. A. McCarthy, *Chemistry & Biology* **2005**, *12*, 499–501.

[147] A. M. Ginsberg, B. O. King, R. G. Roeder, *Cell* **1984**, *39*, 479–489.

[148] R. S. Brown, C. Sander, P. Argos, *FEBS Letters* **1985**, *186*, 271–274.

[149] E. H. Cox, G. L. McLendon, *Current Opinion in Chemical Biology* **2000**, *4*, 162–165.

[150] M. S. Lee et al., *Science* **1989**, *245*, 635–637.

[151] R. E. Klevit, J. R. Herriott, S. J. Horvarth, *Proteins: Structure Function and Bioinformatics* **1990**, *7*, 215–226.

[152] J. H. Laity, B. M. Lee, P. E. Wright, *Current Opinion in Structural Biology* **2001**, *11*, 39–46.

[153] T. Saski, M. Lieberman, *Tetrahedron* **1993**, *49*, 3677–3689.

[154] D. Jaque, F. Vetrone, *Nanoscale* **2012**, *4*, 4301.

[155] D. Wöhrle, M. W. Tausch, W.-D. Stohrer, *Photochemie: Konzepte, Methoden, Experimente*, im Kolophon: Milton Keynes: Lightning Source, 2010, Wiley-VCH, Weinheim, **2010**.

[156] G. G. Stokes, *Philosophical Transactions of the Royal Society of London* **1852**, *142*, 463–562.

[157] J. F. W. Herschel, *Philosophical Transactions of the Royal Society of London* **1845**, *135*, 143–145.

[158] J. R. Lakowicz, *Principles of Fluorescence Spectroscopy*, Springer Science & Business Media, **2013**.

[159] A. Jablonski, *Nature* **1933**, *131*, 839–840.

[160] R. B. Sekar, A. Periasamy, *J Cell Biol* **2003**, *160*, 629–633.

[161] P. G. Wu, L. Brand, *Analytical Biochemistry* **1994**, *218*, 1–13.

[162] C. G. dos Remedios, M. Miki, J. A. Barden, *J Muscle Res Cell Motil* **1987**, *8*, 97–117.

[163] H. Sahoo, *Journal of Photochemistry and Photobiology C: Photochemistry Reviews* **2011**, *12*, 20–30.

[164] H. Sahoo, P. Schwille, *ChemPhysChem* **2011**, *12*, 532–541.

[165] L Stryer, *Annu. Rev. Biochem.* **1978**, *47*, 819–846.

[166] J. Szöllosi, S. Damjanovich, L. Mátyus, *Cytometry* **1998**, *34*, 159–179.

[167] M. R. Linder, S. Steuer, J. Podlech, *Org. Synth.* **2002**, *79*, 154.

[168] F. Arndt, B. Eistert, *Berichte der deutschen chemischen Gesellschaft (A and B Series)* **1935**, *68*, 200–208.

[169] T. Ye, M. A. McKervey, *Chem. Rev.* **1994**, *94*, 1091–1160.

[170] W. E. Bachmann, W. S. Struve in *Organic Reactions*, John Wiley & Sons, Ltd, **2011**, pp. 38–62.

[171] A. M. Brückner et al., *Angewandte Chemie* **2003**, *115*, 4532–4536.

[172] G.-R. Vasanthakumar, B. S. Patil, V. V. Suresh Babu, *Lett Pept Sci* **2002**, *9*, 207–209.

[173] B. Neises, W. Steglich, *Angew. Chem. Int. Ed. Engl.* **1978**, *17*, 522–524.

[174] Q. Sun, S. Cai, B. R. Peterson, *Organic Letters* **2009**, *11*, 567–570.

[175] A. Štimac, J. Kobe, *Carbohydrate research* **2000**, *324*, 149–160.

[176] K. El Akri et al., *Bioorganic & Medicinal Chemistry Letters* **2007**, *17*, 6656–6659.

[177] C. W. Shoppee, G. H. R. Summers, *Journal of the Chemical Society (Resumed)* **1952**, 3361–3374.

[178] E. M. Kosower, S. Winstein, *J. Am. Chem. Soc.* **1956**, *78*, 4347–4354.

[179] S. Winstein, E. M. Kosower, *Journal of the American Chemical Society* **1959**, *81*, 4399–4408.

[180] D. Chouikhi et al., *Chemistry – A European Journal* **2012**, *18*, 12698–12704.

[181] D. Li, D. L. Elbert, *The Journal of Peptide Research* **2002**, *60*, 300–303.

[182] J. Caroen et al., *Tetrahedron* **2016**, *72*, 148–160.

[183] J. M. Dener et al., *Org. Process Res. Dev.* **2001**, *5*, 445–449.

[184] E. Nativ, P. Rona, *Israel Journal of Chemistry* **1972**, *10*, 55–58.

[185] E. J. Moriconi, W. C. Crawford, *J. Org. Chem.* **1968**, *33*, 370–378.

[186] M. Schinnerl et al., *Eur. J. Org. Chem.* **2003**, *2003*, 721–726.

[187] K. Hioki et al., *Synthesis* **2006**, *2006*, 1931–1933.

[188] F. Fülöp, *Chem. Rev.* **2001**, *101*, 2181–2204.

[189] In *Comprehensive Organic Name Reactions and Reagents*, John Wiley & Sons, Inc., Hoboken, NJ, USA, **2010**, conrr411.

[190] D. H. Appella et al., *J. Org. Chem.* **2000**, *65*, Publisher: American Chemical Society, 4766–4769.

[191] J. B. Merrifield, *J. Am. Chem. Soc.* **1963**, *85*, 2149–2154.

[192] B. Marglin, R. B. Merrifield, *J. Am. Chem. Soc.* **1966**, *88*, 5051–5052.

[193] P. Chakraborty, U. Diederichsen, *Chemistry – A European Journal* **2005**, *11*, 3207–3216.

[194] C.-D. Chang, J. Meienhofer, *International Journal of Peptide and Protein Research* **1978**, *11*, 246–249.

[195] E. Atherton et al., *J. Chem. Soc. Chem. Commun.* **1978**, 537–539.

[196] G. Guichard, S. Abele, D. Seebach, *Helvetica Chimica Acta* **1998**, *81*, 187–206.

[197] X. Daura et al., *Eur Biophys J* **2003**, *32*, 661–670.

[198] X. Daura et al., *Chemistry – A European Journal* **1997**, *3*, 1410–1417.

[199] J. R. Allison, M. Müller, W. F. van Gunsteren, *Protein Science* **2010**, *19*, 2186–2195.

[200] S. M. Kelly, T. J. Jess, N. C. Price, *Biochimica et Biophysica Acta (BBA) - Proteins and Proteomics* **2005**, *1751*, 119–139.

[201] S. Kelly, N. Price, *CPPS* **2000**, *1*, 349–384.

[202] D. F. Rane et al., *Tetrahedron Letters* **1993**, *34*, 3201–3204.

[203] H. Onuki, K. Tachibana, N. Fusetani, *Tetrahedron Letters* **1993**, *34*, 5609–5612.

[204] L. Yang et al., *Tetrahedron Letters* **1993**, *34*, 7035–7038.

[205] M. A. Ondetti, S. L. Engel, *J. Med. Chem.* **1975**, *18*, 761–763.

[206] K. Iizuka et al., *J. Chem. Soc. Chem. Commun.* **1989**, 1678–1680.

[207] N. J. Greenfield, *Nat Protoc* **2006**, *1*, 2876–2890.

[208] K. Kaur et al., *Biochimica et Biophysica Acta (BBA) - Proteins and Proteomics* **2008**, *1784*, 658–665.

[209] N. Abdul-Manan, J. F. Hinton, *Biochemistry* **1994**, *33*, 6773–6783.

[210] F. D. Sonnichsen et al., *Biochemistry* **1992**, *31*, 8790–8798.

[211] Y. Hamuro, J. P. Schneider, W. F. DeGrado, *J. Am. Chem. Soc.* **1999**, *121*, 12200–12201.

[212] M. Biner et al., *J. Am. Chem. Soc.* **1992**, *114*, 5197–5203.

[213] K. Ozutsumi, T. Kawashima, *Inorganica Chimica Acta* **1991**, *180*, 231–238.

[214] Z. Setifi et al., *Acta Crystallogr C Struct Chem* **2014**, *70*, 465–469.

[215] M. Becke-Goehring, *Angew. Chem.* **1963**, *75*, 391–391.

[216] R. P. Cheng, S. L. Fisher, B. Imperiali, *J. Am. Chem. Soc.* **1996**, *118*, 11349–11356.

[217] J. H. Espenson, *Chemical kinetics and reaction mechanisms*, *Vol. 102*, New York: McGraw-Hill, **1995**.

[218] J. S. Renny et al., *Angew. Chem. Int. Ed.* **2013**, *52*, 11998–12013.

[219] Y. L. Loukas, *Journal of Pharmacy and Pharmacology* **1997**, *49*, 944–948.

[220] J. Tate, M. Jones, *Journal of Inorganic and Nuclear Chemistry* **1960**, *12*, 241–251.

[221] K. Adachi, H. Watarai, *Chem. Eur. J.* **2006**, *12*, 4249–4260.

[222] T. Doiuchi, Y. Minoura, *Macromolecules* **1978**, *11*, 270–274.

[223] I. Krossing, I. Raabe, *Angew. Chem. Int. Ed.* **2004**, *43*, 2066–2090.

[224] A. J. Situ et al., *J. Phys. Chem. B* **2018**, *122*, 1185–1194.

[225] M. R. R. d. Planque et al., *J. Biol. Chem.* **1999**, *274*, 20839–20846.

[226] A. J. de Jesus, T. W. Allen, *Biochimica et Biophysica Acta (BBA) - Biomembranes* **2013**, *1828*, 864–876.

[227] D. M. Pahlke, U. Diederichsen, *J. Pept. Sci.* **2016**, *22*, 636–641.

[228] U. Rost, C. Steinem, U. Diederichsen, *Chem. Sci.* **2016**, *7*, 5900–5907.

[229] C. Peters et al., *Proc Natl Acad Sci U S A* **2004**, *101*, 8531–8536.

[230] N. N. Nalivaeva, A. J. Turner in *Handbook of Neurochemistry and Molecular Neurobiology: Neural Lipids*, (Eds.: A. Lajtha, G. Tettamanti, G. Goracci), Springer US, Boston, MA, **2009**, pp. 353–372.

[231] A. S. Achalkumar, R. J. Bushby, S. D. Evans, *Soft Matter* **2010**, *6*, 6036–6051.

[232] E. Rideau et al., *Chem. Soc. Rev.* **2018**, *47*, 8572–8610.

[233] P. Arvidsson, J. Frackenpohl, D. Seebach, *HCA* **2003**, *86*, 1522–1553.

[234] M. Gude, J. Ryf, P. D. White, *Lett Pept Sci* **2002**, *9*, 203–206.

[235] B. Blankemeyer-Menge, M. Nimtz, R. Frank, *Tetrahedron Letters* **1990**, *31*, 1701–1704.

[236] K. R. Wilson et al., *Journal of Peptide Science* **2016**, DOI 10.1002/psc.2910.

[237] Calbiochem-Novabiochem Corp., *Novabiochem catalog & peptide synthesis handbook*, Calbiochem-Novabiochem Corp., San Diego, CA, **2010**.

[238] H. Choi, J. Aldrich, *International Journal of Peptide and Protein Research* **2009**, *42*, 58–63.

[239] D. S. King, C. G. Fields, G. B. Fields, *International Journal of Peptide and Protein Research* **2009**, *36*, 255–266.

[240] A. I. Sorochkina et al., *Biochimica et Biophysica Acta (BBA) - Biomembranes* **2013**, *1828*, 2428–2435.

[241] A. Ladokhin, W. Wimley, S. White, *Biophysical Journal* **1995**, *69*, 1964–1971.

[242] L.-h. Zhang et al., *J. Org. Chem.* **1997**, *62*, 6918–6920.

[243] B Sax et al., *Peptide research* **1992**, *5*, 245–6.

[244] Andrew G. Myers, James L. Gleason, *Org. Synth.* **1999**, *76*, 57 –76.

Acknowledgements

I would like to thank Prof. Dr. Ulf Diederichsen in a very special way for the extremely interesting and challenging topic, the freedom to fully involve myself in the topic and always to be able to rely on the support and experience of Mr. Diederichsen.

I would also like to thank Prof. Dr. Manuel Alcarazo for taking on the role of Reviewer at short notice and for his support even though I am not directly part of the Alcarazo working group. I would also like to thank Prof. Dr. Claudia Steinem for deciding at short notice to be my new second Reviewer.

Furthermore, I would like to thank all other members of my examination board Prof. Dr. Jörg Enderlein, Prof. Dr. Kai Tittmann, Prof. Dr. Konrad Koszinowski and Prof. Dr. Marina Bennati.

I would like to thank Dr. Holm Frauendorf and the whole team of the central analytics, as well as Dr. Michael John and the "NMR department" for the countless mass as well as NMR spectra and the constant helpfulness in case of questions or problems.

My thanks also go to the heart and soul of AK Diederichsen Aoife Neville and Angela Heinemann. Without your support and your assistance, not only in the organizational concerns, the entire group would be missing something.

To my current and former colleagues in AK Diederichsen and especially to those from laboratory 108, Dr. Ulrike Rost, Dr. Denis Michael Pahlke, Dr. Martin Kloos, Atida Nasufovska, Dr. Julia Schneider, Dr. Janine Wegner, Dr. Marta Anna Cal and Iryna Portnova. I would like to thank for the good and productive working

atmosphere. A special thanks goes to Denis, Martin and Ulrike without you this would have been impossible!

A big thank you also goes to the tireless souls who helped me with proofreading: Dr. Martin Kloos, Dr. Ulrike Rost and Iryna Portnova.

A big thank you also goes to my Bachelor students, without your help the work would not be where it is today. I would also like to thank you for the experience I was able to gain. My thanks go to Tim Gniech, Lydia Beyer and Malte Schlüter.

Finally, I would like to thank my friends and family, without whose support this would not have been possible. A special thank you goes out to my favorite sister, Caroline, without you my life would be less stressful, but even less meaningful.